

Copyright  
by  
Stephanie Leigh Foster  
2021

**The Dissertation Committee for Stephanie Leigh Foster Certifies that this is the  
approved version of the following dissertation:**

**Elucidating Mechanisms of Immunity to Nipah Virus Infection  
through Generation of Attenuated Viruses  
and a Single-Cycle Vectored Vaccine**

**Committee:**

---

Thomas W. Geisbert, Ph.D., Chair

---

Chad E. Mire, Ph.D.

---

Tian Wang, Ph.D.

---

Katharine N. Bossart, Ph.D.

---

Christopher C. Broder, Ph.D.

---

Dean, Graduate School

**Elucidating Mechanisms of Immunity to Nipah Virus Infection  
through Generation of Attenuated Viruses  
and a Single-Cycle Vectored Vaccine**

**by**

**Stephanie Leigh Foster, B.S.**

**Dissertation**

Presented to the Faculty of the Graduate School of  
The University of Texas Medical Branch  
in Partial Fulfillment  
of the Requirements  
for the Degree of

**Doctor of Philosophy**

**The University of Texas Medical Branch  
December 2021**

## **Dedication**

I dedicate this dissertation to my mother, Julia Foster, for her unwavering support and valuable advice over the years as I have pursued a challenging and demanding scientific career.

## Acknowledgements

First and foremost, I would like to thank my advisor, Thomas W. Geisbert, Ph.D., for his mentorship and for the opportunity to do exciting and relevant research as a member of his laboratory. I am grateful to Chad E. Mire, Ph.D., without whose mentorship and training these projects could not have been completed. Thank you to Christopher C. Broder, Ph.D., Katharine N. Bossart, Ph.D., and Tian Wang, Ph.D., for their depth of knowledge of NiV vaccines, animal models, and immunity, which have made these projects immeasurably better. I could not have completed my training without mentorship from Robert W. Cross, M.P.H., Ph.D., Viktoriya Borisevich, M.D., Ph.D., and Krystle Agans. Thank you to current and former Geisbert lab members Benjamin Satterfield, M.D., Ph.D., Abhishek Prasad, Ph.D., Courtney Woolsey, Ph.D., Kevin Melody, M.S., Ph.D., Sergio Rodriguez, M.S., Ph.D., Dylan M. Johnson, M.S., Ph.D., Teresa Sorvillo, Ph.D., Corri Levine, M.S., M.P.H., Karla A. Fenton, D.V.M., Ph.D., Joan Geisbert, Daniel Deer, Natalie Dobias, Brittany Fransaw, and Kira Zapalac for technical guidance, illuminating discussions, and experimental support. I am immensely grateful to Corey May Fulton, D.V.M., Ph.D., Corri Levine, M.S., M.P.H., Sarah van Tol, M.S., Adam Hage, M.S., and Megan Mears for their friendship, support, and guidance throughout this process—I would not have made it through without you. Thank you to my mother for her unwavering belief that I could do this, and to Vern Huang, M.D., for his love, support, and encouragement throughout the journey.

**Elucidating Mechanisms of Immunity to Nipah Virus Infection  
through Generation of Attenuated Viruses  
and a Single-Cycle Vectored Vaccine**

Publication No. \_\_\_\_\_

Stephanie Leigh Foster, Ph.D.

The University of Texas Medical Branch, 2021

Supervisor: Thomas W. Geisbert, Ph.D.

Nipah virus (NiV) is an emerging paramyxovirus that has caused outbreaks with high case-fatality rates in South and Southeast Asia. Mechanisms of NiV virulence are poorly understood, and there is no licensed vaccine nor treatment. Accessory proteins produced from the NiV P gene through co-transcriptional gene editing (V and W) inhibit multiple molecules in the type-I interferon (IFN-I) induction and response pathways to modulate the host innate immune response to NiV infection. Previously, ferrets infected with a recombinant NiV (rNiV) lacking V survived an otherwise lethal NiV challenge via an unknown mechanism. Mutation of the V gene of the related canine distemper virus prevented binding of V protein to melanoma differentiation-associated protein 5 (MDA5) and attenuated virulence in an otherwise lethal ferret model. The NiV V-MDA5 binding site and the effects of blocking this interaction on virulence were previously unknown. The work described here identified amino acid I414 in NiV V as a critical residue for binding to MDA5 through co-immunoprecipitation/western blot and IFN- $\beta$  dual luciferase reporter assays in a plasmid overexpression system. Subsequently, rNiV lacking the ability to bind to MDA5 and signal transducer and activator of transcription 1 (STAT1) were recovered, characterized in cell culture with and without IFN-I pretreatment, and used in an experimental infection model in ferrets. Interestingly, 25% of ferrets infected with the rNiV lacking V survived challenge with a higher virus dose than in previous studies, while 75% of ferrets infected with a rNiV lacking the ability to bind to MDA5 and STAT1 survived. These experiments identified MDA5 and STAT1 together as important targets for NiV virulence. Additionally, previous NiV vaccine candidates have shown efficacy against NiV challenge in a variety of animal models, but no virus-vectored vaccines have been tested for efficacy shortly prior to challenge, as in an outbreak scenario. Therefore, a vesicular stomatitis virus-vectored NiV vaccine was rescued and tested in African green monkeys. Animals were protected from lethal challenge with NiV when the vaccine was given seven or three days prior. The vaccine is non-replicative and yet works rapidly in a single dose with no adjuvants. Combined, the experiments described here will advance understanding of NiV virulence and development of effective vaccines against this deadly infection.

## TABLE OF CONTENTS

List of Tables .....	x
List of Figures .....	xi
List of Abbreviations .....	xv
Chapter 1: Introduction .....	21
Nipah virus is an emerging human pathogen.....	21
Nipah virus is a pathogenic paramyxovirus within the genus <i>Henipavirus</i> .....	21
NiV outbreaks have been identified throughout South and Southeast Asia .....	21
Ecology and epidemiology of NiV .....	22
Signs and symptoms of NiV disease in humans .....	24
Molecular virology of NiV .....	26
NiV is genetically related to other paramyxoviruses of importance to animal and human health .....	26
The NiV genome contains six open reading frames encoding nine proteins .....	27
The specific NiV receptors are highly conserved among mammals and are expressed on a wide variety of cells .....	30
NiV is a potent inhibitor of the interferon response .....	32
Viral RNA in cell cytoplasm is detected by retinoic acid-inducible gene I- like receptors.....	32
Type-I IFNs act in an autocrine and paracrine fashion to induce an antiviral state in cells .....	33
Henipaviruses are known inhibitors of IFN induction and response .....	34
Animal models of NiV disease .....	36
Diverse mammals are susceptible to NiV infection and disease .....	36
Syrian golden hamster model.....	38
Ferret model .....	39
AGM model .....	41
Vaccines in development for NiV .....	42
There is no clinically licensed vaccine to prevent NiV disease .....	42
HeV-sG glycoprotein subunit vaccine .....	44

VSV-vectored vaccines.....	44
Questions to be addressed here.....	46
Current understanding of NiV RLR evasion .....	46
Current progress toward development of a NiV vaccine.....	47
Gaps in knowledge.....	48
Study hypotheses .....	50
Chapter 2: A Single Point Mutation in NiV V Abrogates Binding to MDA5 and Partially Restores IFN- $\beta$ Induction by MDA5 in Plasmid-Based Protein Overexpression Studies.....	51
Introduction.....	51
Methods .....	53
Plasmids .....	53
Cell culture.....	54
Co-immunoprecipitation/western blots.....	54
IFN- $\beta$ luciferase reporter assays .....	57
Minigenome luciferase reporter assays.....	58
Statistics .....	60
Results.....	60
A single amino acid facilitated NiV <sub>M</sub> V binding to MDA5 and conferred inhibited MDA5-induced IFN- $\beta$ production.....	60
Unlike MeV, NiV <sub>M</sub> did not use the same interface for binding to LGP2 as for MDA5 .....	78
Point mutations are not likely to inhibit viral replication in full-length rNiV .....	78
Discussion.....	81
Chapter 3: Abrogation of V Binding to MDA5 and STAT1 Using Recombinant NiV <sub>M</sub> Mutants Reveals Moderate Increases in Interferon Sensitivity <i>in vitro</i> and Ferret Survival <i>in vivo</i> .....	85
Introduction.....	85
Methods .....	87
Plasmids .....	87
Cloning to produce full-length pNiV <sub>M</sub> plasmids encoding designed mutations in V.....	87
Cell culture.....	89

Recovery and amplification of rNiV <sub>M</sub> containing designed mutations in V	90
.....	90
Determination of rNiV <sub>M</sub> growth kinetics.....	94
Animal Studies.....	94
Animal handling and procedures .....	94
Blood collection, processing, and hematology .....	95
Tissue collection and processing .....	96
Determination of viral load by plaque assay and RT-qPCR.....	97
Statistics .....	98
Results.....	98
Full-length rNiV <sub>M</sub> containing MDA5- and STAT1-binding mutations were rescued by reverse genetics.....	98
Rescued rNiV <sub>M</sub> containing MDA5-binding mutations grew to slightly lower peak titers in IFN-competent cells and IFN-incompetent cells pretreated with IFN .....	99
A rNiV <sub>M</sub> encoding mutations designed to prevent binding to MDA5 and STAT1 exhibited reduced lethality in the ferret model .....	103
Discussion.....	113
<b>Chapter 4: A Single-Dose, Single-Cycle, VSV-Vectored Vaccine Protects African Green Monkeys when Given Shortly Prior to Nipah Virus Bangladesh Challenge .....</b>	<b>118</b>
Introduction.....	118
Methods .....	120
Cell culture.....	120
Cloning to produce the full-length pVSV-ΔG-NiV <sub>B</sub> G plasmid .....	120
Recovery, amplification, and characterization of the G*-rVSV-ΔG-NiV <sub>B</sub> G vaccine .....	121
Immunofluorescence assays.....	124
Animal Studies.....	125
Animal handling and procedures .....	125
Blood collection and processing .....	126
Tissue collection and processing .....	127
Determination of viral load by plaque assay and RT-qPCR.....	128
NiV <sub>B</sub> plaque reduction neutralization tests .....	129

NiV-specific enzyme-linked immunosorbent assays.....	129
Results.....	129
The G*-rVSV-ΔG-NiV <sub>B</sub> G vaccine grew to high titers in cell culture and expressed the NiV <sub>B</sub> G protein.....	129
The G*-rVSV-ΔG-NiV <sub>B</sub> G vaccine protected AGMs from lethal NiV disease when given shortly prior to challenge with NiV <sub>B</sub> .....	133
Surviving AGMs vaccinated with the G*-rVSV-ΔG-NiV <sub>B</sub> G vaccine developed NiV-specific humoral immune responses .....	144
Discussion.....	148
Chapter 5: Conclusions .....	153
Previous understanding of NiV inhibition of RLRs .....	153
Contributions to understanding of NiV inhibition of RLRs made here.....	153
1. The single amino acid I414 is necessary for NiV V binding to MDA5, but additional amino acids are likely involved in binding to LGP2 .....	153
2. Blocking of viral inhibition of MDA5 alone was not sufficient to attenuate rNiV <sub>M</sub> <i>in vitro</i> or <i>in vivo</i> .....	154
3. Together, MDA5 and STAT1 are important mediators of NiV virulence .....	156
Previous progress toward a NiV vaccine for emergency use .....	156
Contributions toward a rapid-acting NiV vaccine .....	157
1. The G*-rVSV-ΔG-NiV <sub>B</sub> G vaccine protected 100% of AGMs from NiV <sub>B</sub> when given seven days prior to challenge and 67% of AGMs when given three days prior to challenge .....	157
2. Survivors vaccinated with G*-rVSV-ΔG-NiV <sub>B</sub> G mounted a NiV-specific humoral response.....	158
References.....	160

## List of Tables

<b>Table 3-1: rNiV<sub>M</sub> constructs cloned and recovered to abrogate MDA5 and STAT1 binding.....</b>	<b>88</b>
<b>Table 3-2: Clinical disease and findings in ferrets after experimental infection with rNiV<sub>M</sub>.....</b>	<b>109</b>
<b>Table 4-1: Clinical disease and findings in AGMs vaccinated seven days prior to experimental infection with NiV<sub>B</sub>.....</b>	<b>138</b>
<b>Table 4-2: Clinical disease and findings in AGMs vaccinated three days prior to experimental infection with NiV<sub>B</sub>.....</b>	<b>139</b>

## List of Figures

<b>Figure 1-1: <i>Pteropus</i> bat geographic range and location of henipavirus outbreaks</b> .....	23
<b>Figure 1-2: NiV genome, proteins, and viral structure</b> .....	28
<b>Figure 2-1: NiV minigenome luciferase reporter system</b> .....	59
<b>Figure 2-2: The HA-NiV<sub>M</sub> V protein and 10-alanine scanning mutants used in plasmid overexpression studies</b> .....	62
<b>Figure 2-3: All NiV<sub>M</sub> alanine scanning mutants demonstrate reduced MDA5 and LGP2 binding</b> .....	63
<b>Figure 2-4: Secondary structure of the NiV<sub>M</sub> V CTD and residues potentially involved in binding to MDA5</b> .....	64
<b>Figure 2-5: Alignment of V CTDs of relevant paramyxoviruses and of RLRs in mammals and birds</b> .....	66
<b>Figure 2-6: Point mutants made in the pCAGGS-HA-NiV<sub>M</sub> V expression plasmid</b> .....	68
<b>Figure 2-7: NiV<sub>M</sub> E411 and W416 point mutants did not demonstrate reduced MDA5 binding</b> .....	69
<b>Figure 2-8: Point mutants exhibited a reduced ability to inhibit IFN-<math>\beta</math> in an NF-<math>\kappa</math>B- independent manner at lower concentrations</b> .....	70

<b>Figure 2-9: Sequence of three-alanine scanning mutants in pCAGGS-HA-NiV<sub>M</sub> V expression plasmids</b> .....	71
<b>Figure 2-10: NiV<sub>M</sub> V alanine scanning mutants of three amino acids each revealed nuances of MDA5 binding</b> .....	72
<b>Figure 2-11: NiV<sub>M</sub> V alanine scanning mutants of three amino acids each exhibited a reduced ability to inhibit IFN-<math>\beta</math> in an NF-<math>\kappa</math>B-independent manner at lower concentrations</b> .....	74
<b>Figure 2-12: Additional point mutations made in the pCAGGS-HA-NiV<sub>M</sub> V expression plasmid</b> .....	75
<b>Figure 2-13: I414A point mutants lose the ability to bind to MDA5 in a co-IP/western blot assay</b> .....	76
<b>Figure 2-14: NiV<sub>M</sub> V I414A point mutants exhibited a reduced ability to inhibit IFN-<math>\beta</math> in an NF-<math>\kappa</math>B-independent manner at moderate concentrations</b> .....	77
<b>Figure 2-15: The I414A point mutant was not sufficient to prevent binding to LGP2 in a co-IP/western blot assay</b> .....	79
<b>Figure 2-16: NiV<sub>M</sub> V point mutants did not indicate decreased viral transcription/translation in a minigenome luciferase assay</b> .....	80
<b>Figure 3-1: Recovery of rNiV<sub>M</sub> full-length constructs</b> .....	91
<b>Figure 3-2: rNiV<sub>M</sub>-induced CPE on Vero 76 cells</b> .....	92

<b>Figure 3-3: Viral growth kinetics of rNiV<sub>M</sub> with MDA5- and STAT1-binding mutations in Vero 76 cells and HEK293T cells.....</b>	<b>101</b>
<b>Figure 3-4: Study design for ferrets challenged with rNiV<sub>M</sub> .....</b>	<b>104</b>
<b>Figure 3-5: Survival curve for ferrets challenged with rNiV<sub>M</sub>.....</b>	<b>105</b>
<b>Figure 3-6: NiV<sub>M</sub> genomes detected by RT-qPCR in ferrets challenged with rNiV<sub>M</sub> .....</b>	<b>111</b>
<b>Figure 4-1: Recovery of rVSV-ΔG-NiV<sub>B</sub> G virions.....</b>	<b>122</b>
<b>Figure 4-2: The rVSV-ΔG-NiV<sub>B</sub> G-GFP and rVSV-ΔG-NiV<sub>B</sub> G genomes.....</b>	<b>130</b>
<b>Figure 4-3: The G*-rVSV-ΔG-NiV<sub>B</sub> G construct expresses NiV<sub>B</sub> G protein .....</b>	<b>132</b>
<b>Figure 4-4: Study designs for experimental challenge studies in AGMs .....</b>	<b>134</b>
<b>Figure 4-5: Survival curves following challenge of vaccinated AGMs with NiV<sub>B</sub> .....</b>	<b>135</b>
<b>Figure 4-6: Respiratory rates following challenge of AGMs with NiV<sub>B</sub> .....</b>	<b>140</b>
<b>Figure 4-7: Viremia in vaccinated AGMs after challenge with NiV<sub>B</sub> .....</b>	<b>142</b>
<b>Figure 4-8: NiV<sub>B</sub> genomic RNA detected in vaccinated AGMs after challenge with NiV<sub>B</sub> .....</b>	<b>143</b>
<b>Figure 4-9: PRNT<sub>50</sub> results for AGMs vaccinated prior to challenge with NiV<sub>B</sub> .....</b>	<b>145</b>

**Figure 4-10: Detection of NiV-specific IgM and IgG binding antibodies in AGMs vaccinated prior to challenge with NiV<sub>B</sub>.....147**

## List of Abbreviations

6FAM	6-Carboxyfluorescein
AAALAC	Association for Assessment and Accreditation of Lab Animal Care
AAV	Adeno-Associated Virus
AGM	African Green Monkey
ALP	Alkaline Phosphatase
ALT	Alanine Aminotransferase
ANOVA	Analysis of Variance
AST	Aspartate Aminotransferase
ATCC	American Type Culture Collection
ATP(ase)	Adenosine Triphosphate(ase)
BHK	Baby Hamster Kidney
BSA	Bovine Serum Albumin
BSL	Biosafety Level
BUN	Blood Urea Nitrogen
°C	Degrees Celsius
CARD	Caspase Recruitment Domain
Cat. No.	Catalog Number
CD	Cluster of Differentiation
cDNA	Complementary Deoxyribonucleic Acid
CDV	Canine Distemper Virus
CedV	Cedar Virus
CFR	Case-Fatality Rate

CNS	Central Nervous System
CO <sub>2</sub>	Carbon Dioxide
CPE	Cytopathic Effect
CRE	Creatinine
CRP	C-Reactive Protein
CTD	C-Terminal Domain
DMEM	Dulbecco's Modified Eagle Medium
DNA	Deoxyribonucleic Acid
dpi	Days Post-Infection
dsRNA	Double-Stranded Ribonucleic Acid
EBOV	Zaire Ebolavirus
EBOV GP	Zaire Ebolavirus Attachment Glycoprotein
EDTA	Ethylenediaminetetraacetic Acid
ELISA	Enzyme-Linked Immunosorbent Assay
EM	Electron Microscopy
FBS	Fetal Bovine Serum
g	Gram
GEq	Genome Equivalent
GFP	Green Fluorescent Protein
GGT	Gamma Glutamyltransferase
GhV	Ghana Virus
GNL	Galveston National Laboratory
HA	Hemagglutinin

HBSS	Hank's Balanced Salt Solution
HCl	Hydrochloric Acid
HEK	Human Embryonic Kidney
HeV	Hendra Virus
HeV-sG	Soluble Hendra Virus Attachment Glycoprotein
hpi	Hours Post-Infection
HRP	Horseradish Peroxidase
IACUC	Institutional Animal Care and Use Committee
IDT	Integrated DNA Technologies, Incorporated
IFA	Immunofluorescence Assay
IFIT	Interferon-Induced Protein with Tetratricopeptide Repeats
IFN	Interferon
Ig	Immunoglobulin
IKK $\epsilon$	Inhibitor of NF- $\kappa$ B Kinase Subunit Epsilon
i.m.	Intramuscular(ly)
i.n.	Intranasal(ly)
Inc.	Incorporated
i.p.	Intraperitoneal(ly)
IP	Immunoprecipitation
IRF	Interferon Regulatory Factor
ISG	Interferon-Stimulated Gene
i.t.	Intratracheal(ly)
LGP2	Laboratory of Genetics and Physiology 2

LOD	Limit of Detection
M	Molar (Moles Per Liter)
mAb	Monoclonal Antibody
MAVS	Mitochondrial Antiviral Signaling Protein
MDA5	Melanoma Differentiation-Associated Protein 5
MEM	Minimum Essential Medium
MeV	Measles Virus
mg	Milligram
mL	Milliliter
mM	Millimolar (Millimoles Per Liter)
MOI	Multiplicity of Infection
MojV	Mòjiāng Virus
mRNA	Messenger Ribonucleic Acid
MuV	Mumps Virus
μg	Microgram
μL	Microliter
NaCl	Sodium Chloride
NEB	New England Biolabs
NF-κB	Nuclear Factor Kappa-Light-Chain-Enhancer of Activated B Cells
ng	Nanogram
NHP	Nonhuman Primate
NiV	Nipah Virus
NiV <sub>B</sub>	Nipah Virus Bangladesh Strain

NiV <sub>M</sub>	Nipah Virus Malaysia Strain
NTD	N-Terminal Domain
ORF	Open Reading Frame
PAGE	Polyacrylamide Gel Electrophoresis
PAMP	Pathogen-Associated Molecular Pattern
PBMC	Peripheral Blood Mononuclear Cell
pBS	pBluescript
PBS	Phosphate-Buffered Saline
PCR	Polymerase Chain Reaction
PFU	Plaque-Forming Unit
PIV5	Parainfluenza Virus 5
PP1	Protein Phosphatase 1
PRNT	Plaque Reduction Neutralization Test
PVDF	Polyvinylidene Fluoride
RIG-I	Retinoic Acid-Inducible Gene I
RIPA	Radioimmunoprecipitation Assay
RLR	Retinoic Acid-Inducible Gene I-Like Receptor
RNA	Ribonucleic Acid
rNiV	Recombinant Nipah Virus
RNP	Ribonucleoprotein
RPM	Revolutions Per Minute
RT-(q)PCR	Reverse Transcriptase (Quantitative) Polymerase Chain Reaction
rVSV	Recombinant Vesicular Stomatitis Virus

SDS	Sodium Dodecyl Sulfate
SEM	Standard Error of the Mean
SeV	Sendai Virus
STAT	Signal Transducer and Activator of Transcription
TAMRA	Tetramethylrhodamine
TBK1	TANK-Binding Kinase 1
TBS(T)	Tris-Buffered Saline (with Tween™ 20)
TCID <sub>50</sub>	Median Tissue Culture Infectious Dose
TRIM25	Tripartite Motif-Containing Protein 25
USA	United States of America
UTMB	University of Texas Medical Branch
VLP	Virus-Like Particle
VSV	Vesicular Stomatitis Virus
WCL	Whole Cell Lysate
w/v	Weight/Volume

## Chapter 1: Introduction

### NIPAH VIRUS IS AN EMERGING HUMAN PATHOGEN

#### **Nipah virus is a pathogenic paramyxovirus within the genus *Henipavirus***

Nipah virus (NiV) is a causative agent of severe, often fatal acute encephalitis and respiratory disease with outbreaks identified in South and Southeast Asia. NiV first emerged in 1998, resulting in an outbreak of acute encephalitis among pig farmers and abattoir workers in Malaysia and Singapore<sup>1,2</sup>. Electron microscopy (EM), serological testing, and genomic sequencing determined that NiV was a novel member of the virus family *Paramyxoviridae*, closely related to Hendra virus (HeV)<sup>1,3,4</sup>. Subsequently, NiV was categorized in the new genus *Henipavirus* along with HeV, which first emerged in Australia in 1994 as a highly lethal respiratory disease of racehorses<sup>5-7</sup>. Cedar virus (CedV), Ghana virus (GhV), and Mòjiāng virus (MojV) are more recently identified members of the genus, first detected in Australia, Ghana, and China, respectively<sup>8-10</sup>. CedV was isolated as a live virus from a bat in Australia in 2009<sup>8</sup>. GhV was detected as a full-length ribonucleic acid (RNA) genome isolated from a bat in Ghana in 2009, while MojV genomic RNA was isolated from a rat in China in 2012<sup>9,10</sup>. Live virus has not been isolated for GhV nor MojV. Of the members of the *Henipavirus* genus, HeV and NiV have caused outbreaks of human disease, while CedV appears to be apathogenic.

#### **NiV outbreaks have been identified throughout South and Southeast Asia**

NiV was first isolated and characterized as clinically and epidemiologically distinct from the closely related HeV in March 1999 from a patient from the village of Sungai Nipah, Malaysia<sup>11</sup>. The patient was part of the first identified outbreak of NiV, which occurred in 1998 and 1999 among pig farmers in Malaysia and abattoir workers in Singapore who came into contact with infected pigs and subsequently developed acute encephalitis<sup>1,2</sup>. Nearly 300 people were infected, and approximately 40% of them

succumbed to NiV disease<sup>12</sup>. In 2001, a similar virus caused a small outbreak in Bangladesh, although this time, no intermediate host was identified<sup>13</sup>. The infections were traced to the consumption of raw date palm sap or to close contact with infected patients, and small outbreaks have continued to occur in Bangladesh and eastern India nearly annually<sup>14-16</sup>. In 2014, an outbreak was identified in the Philippines, this time spreading from horses to humans<sup>17</sup>. A small portion of the viral nucleoprotein was sequenced and found to be identical to the viral strain that caused the outbreak in Malaysia and Singapore and distinct from the strain causing outbreaks in India and Bangladesh<sup>17</sup>. Eventually, these two strains of NiV came to be known as NiV Malaysia strain (NiV<sub>M</sub>) and NiV Bangladesh strain (NiV<sub>B</sub>)<sup>18</sup>. Most recently, NiV<sub>B</sub> has caused outbreaks in the southwest Indian state of Kerala; an outbreak in 2018 caused 21 deaths out of 23 identified cases<sup>19</sup>. This region is geographically distant from the previous NiV<sub>B</sub> outbreaks in India, which occurred near its border with Bangladesh, but the range of the bats that carry NiV extends throughout India (**Figure 1-1**).

### **Ecology and epidemiology of NiV**

The wildlife reservoir of NiV is pteropid fruit bats, which have a large geographic range from Asia to Australia to Africa (**Figure 1-1**)<sup>13,20</sup>. These bats exhibit no clinical signs of NiV disease, and a sizable percentage of tested bats from multiple species were found to have serologic evidence of prior infection<sup>21-23</sup>. The wide host range of pteropid bats and the fact that henipaviral RNA and/or virus has been isolated from bats from West Africa to East Asia to Australia underscore that the risk of further outbreaks of henipaviral disease is very high. A NiV isolate from a pteropid bat in Cambodia has been recently characterized<sup>24</sup>. The molecular and clinical features of the virus isolate were intermediate between the NiV<sub>M</sub> and NiV<sub>B</sub> strains, meaning other, highly pathogenic strains may exist and could cause future outbreaks<sup>24</sup>.

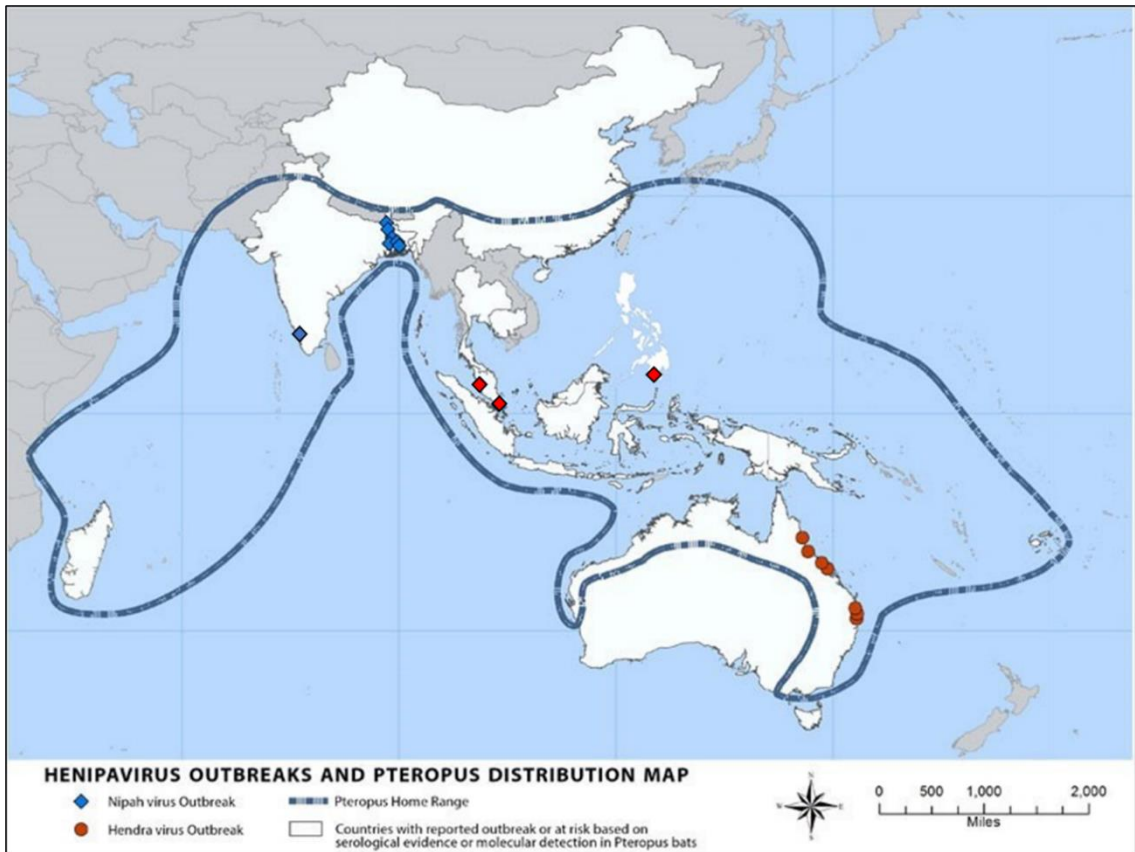


**Figure 1-1: *Pteropus* bat geographic range and location of henipavirus outbreaks**

The geographic range of pteropid fruit bats is shown inside the blue dashed line. Outbreaks of NiV<sub>B</sub> disease are shown as blue diamonds (India and Bangladesh), outbreaks of NiV<sub>M</sub> disease are shown as red diamonds (Malaysia, Singapore, and the Philippines), and outbreaks of HeV disease are shown as orange circles (Australia). Countries in white have reported outbreaks of human disease and/or serological/genetic evidence of henipavirus exposure in tested bats. However, all areas within the *Pteropus* host range are at risk for future outbreaks of henipavirus disease. Modified from the Centers for Disease Control and Prevention (<https://www.cdc.gov/vhf/nipah/outbreaks/distribution-map.html>).

In the case of NiV<sub>M</sub>, human infections usually result from contact with an intermediate animal host. The first identified outbreak spread to humans from infected pigs, which exhibited more upper respiratory clinical signs than humans and therefore served as ideal amplifying hosts<sup>12</sup>. The pigs were infected by bats roosting in fruit trees above their pens, which dropped fruit and excretions containing NiV<sub>M</sub> into the pig enclosures; over one million pigs were culled to bring the outbreak under control<sup>1,12</sup>. In the Philippines, humans had contact with infected horses<sup>17</sup>. No direct evidence of human-to-human transmission of NiV<sub>M</sub> has been found, although some of the cases in the 2014 Philippines outbreak had no identified epidemiologic links other than to infected patients<sup>17</sup>, and nosocomial transmission has been suggested as the cause of a subclinical NiV<sub>M</sub> infection in a nurse who treated NiV patients during the original Malaysia outbreak<sup>25</sup>. Furthermore, the theoretical transmissibility of NiV<sub>M</sub> has been demonstrated in hamsters and ferrets<sup>26,27</sup>.

Contrary to NiV<sub>M</sub>, outbreaks of NiV<sub>B</sub> have been linked to direct human contact with bats (without an intermediate host) or consumption of raw date palm sap, which can be contaminated with bat saliva or urine<sup>14,15,28</sup>. Furthermore, person-to-person transmission is a feature of NiV<sub>B</sub> outbreaks, with transmission occurring to those in close contact with infected patients, such as caregivers in a home or hospital setting<sup>16</sup>. The 2018 outbreak of NiV<sub>B</sub> in Kerala, India, identified a wildlife source only for the index case, with all remaining cases infected through contact with other patients in hospital settings<sup>19,29</sup>.

### **Signs and symptoms of NiV disease in humans**

NiV can cause severe acute encephalitis, respiratory distress, and diffuse vasculitis in infected patients. The disease begins with a flulike prodromic phase four to 18 days after exposure to the fluids or tissues of an infected human or animal, with fever, headache, and reduced consciousness the most common clinical findings among

symptomatic patients<sup>12,13,30,31</sup>. NiV disease can worsen to severe, progressive encephalitis, with central nervous system (CNS) manifestations such as areflexia, segmental myoclonus, and seizures common<sup>12,30,31</sup>. Brain stem involvement and older age are associated with poor prognosis<sup>12,31</sup>. Many patients have respiratory involvement, with cough and dyspnea common and progression to atypical pneumonia and severe acute respiratory distress syndrome possible<sup>2,13,19</sup>. Target cells for NiV include endothelial cells of the respiratory system and CNS, which can lead to diffuse systemic vasculitis and invasion of other body systems, including the blood vessels of the heart and kidneys<sup>30</sup>. Most hematologic and clinical chemistry values remain normal throughout the clinical course of disease, with a minority of patients exhibiting thrombocytopenia, leukopenia, or elevated liver enzymes<sup>4,12</sup>.

NiV<sub>M</sub> primarily causes neurological and systemic disease, with fewer respiratory symptoms observed in patients compared to NiV<sub>B</sub> patients, although atypical pneumonia and influenza-like illness have been recorded in outbreaks of NiV<sub>M</sub><sup>2,17</sup>. Case-fatality rates (CFRs) for outbreaks of NiV<sub>M</sub> have been between 40 and 50% for identified cases<sup>12,17</sup>.

Shortness of breath and other acute respiratory symptoms are common in patients with NiV disease caused by NiV<sub>B</sub><sup>13,19,32</sup>. Compared to NiV<sub>M</sub>, outbreaks of NiV<sub>B</sub> have featured clear patterns of person-to-person transmission and higher CFRs<sup>16,32</sup>. However, it is unknown whether this difference is caused by genetic differences between the two strains or by social and behavioral differences between NiV<sub>M</sub> and NiV<sub>B</sub> case-patients and caregivers<sup>16,32</sup>. Cases in Bangladesh have been associated with community leaders with large social networks and with care provided by family members instead of medical staff, while NiV patients in Malaysia were more likely to receive mechanical ventilation and other intensive treatments<sup>16,32</sup>. However, the recent outbreak of NiV<sub>B</sub> in Kerala was associated with transmission in a hospital among medical staff<sup>19,29</sup>. Transmission of NiV<sub>B</sub> between people is highly associated with contact with the saliva or respiratory secretions of a NiV patient<sup>32</sup>, and NiV<sub>B</sub> has been shown to induce higher levels of virus in the

respiratory secretions of ferrets than NiV<sub>M</sub><sup>33</sup>. Outbreaks of NiV<sub>B</sub> typically have a CFR of 75 to 80%, although higher CFRs have been reported<sup>19,32</sup>. The reasons for the difference in CFRs between strains are not understood.

During the initial outbreak of NiV<sub>M</sub>, it was reported that two of 11 cases (15%) of primary NiV infection in Singapore abattoir workers were asymptomatic<sup>34</sup>. Subsequently, 89 additional cases were identified by positive serology in individuals with reported mild symptoms or no symptoms, increasing the apparent mild to asymptomatic infection rate to about 25% for NiV<sub>M</sub><sup>35</sup>. Approximately 3% of patients with recognized asymptomatic initial infections and 7.5% of those who recovered from acute encephalitis experienced late-onset or relapsed neurologic disease<sup>35</sup>. The majority of cases of relapsed encephalitis occurred from a few months to about two years following acute NiV infection, but two cases were observed in 2003, four years later<sup>36-38</sup>. The longest reported recrudescence of NiV encephalitic disease is 11 years after acute infection<sup>39</sup>. Recrudescence of henipavirus encephalitis was first noted in the second fatal human case of HeV infection 13 months after initial acute disease<sup>40,41</sup>. Furthermore, fatigue and neurological symptoms may persist for months after acute NiV disease in at least 20% of patients<sup>12,42</sup>. Relapse encephalitis can cause ongoing encephalopathy, neurological abnormalities detectable by magnetic resonance imaging, and depression and mood disorders, as well as recurrence of common symptoms such as fever, headache, seizures, and coma<sup>35,42,43</sup>.

## **MOLECULAR VIROLOGY OF NiV**

### **NiV is genetically related to other paramyxoviruses of importance to animal and human health**

As previously discussed, NiV is classified as a member of the viral family *Paramyxoviridae* and the genus *Henipavirus* based on its morphological, genetic, and serological characteristics<sup>1,3,4,6</sup>. Therefore, NiV is closely related to viruses associated with significant human and animal morbidity and mortality. Other paramyxoviruses of

importance to human health include measles virus (MeV), mumps virus (MuV), and the human parainfluenza viruses<sup>44</sup>. Paramyxoviruses of agricultural and wildlife health importance include canine distemper virus (CDV), Newcastle disease virus, and rinderpest virus<sup>44</sup>.

### **The NiV genome contains six open reading frames encoding nine proteins**

NiV is a negative-sense, single-stranded RNA virus with a genome 18,246 (in the case of NiV<sub>M</sub>) or 18,252 (NiV<sub>B</sub>) nucleotides in length—much larger than most other paramyxoviruses—that is fully encapsidated by the NiV nucleoprotein<sup>18,45</sup>. These genome lengths are divisible by six because, like other paramyxoviruses, NiV obeys the rule of six, so each nucleoprotein subunit encapsidates exactly six nucleotides of viral genome, forming a helical nucleocapsid<sup>45</sup>. The organization of the negative-sense NiV genome is shown in **Figure 1-2A**. Genes are transcribed in the order shown from left to right, resulting in gradient transcription in which more N messenger RNAs (mRNAs) and fewer L mRNAs are produced compared to the other genes because the polymerase pauses at each intergenic region and can dissociate from the genome<sup>46</sup>.

The open reading frames (ORFs) shown in **Figure 1-2A** produce the structural proteins of the NiV virion when transcribed faithfully<sup>3,6</sup>. The N ORF encodes the nucleoprotein (N), which encapsidates the viral RNA genome, as discussed above<sup>45</sup>. The P ORF encodes the phosphoprotein (P), which is an essential polymerase cofactor mediating the interaction between the encapsidated genome and the L polymerase<sup>45</sup>. The M ORF encodes the matrix protein (M), which lines the inside of the viral envelope and is essential for viral particle assembly and budding of nascent virions<sup>47-49</sup>. The F and G ORFs encode the trimeric fusion (F) glycoprotein and the tetrameric attachment (G) glycoprotein, respectively, which are the oligomeric spike glycoproteins protruding from the surface of the NiV virion<sup>50,51</sup>. The F protein is a class I fusion glycoprotein that mediates a pH-independent membrane fusion event between the virion and host cell

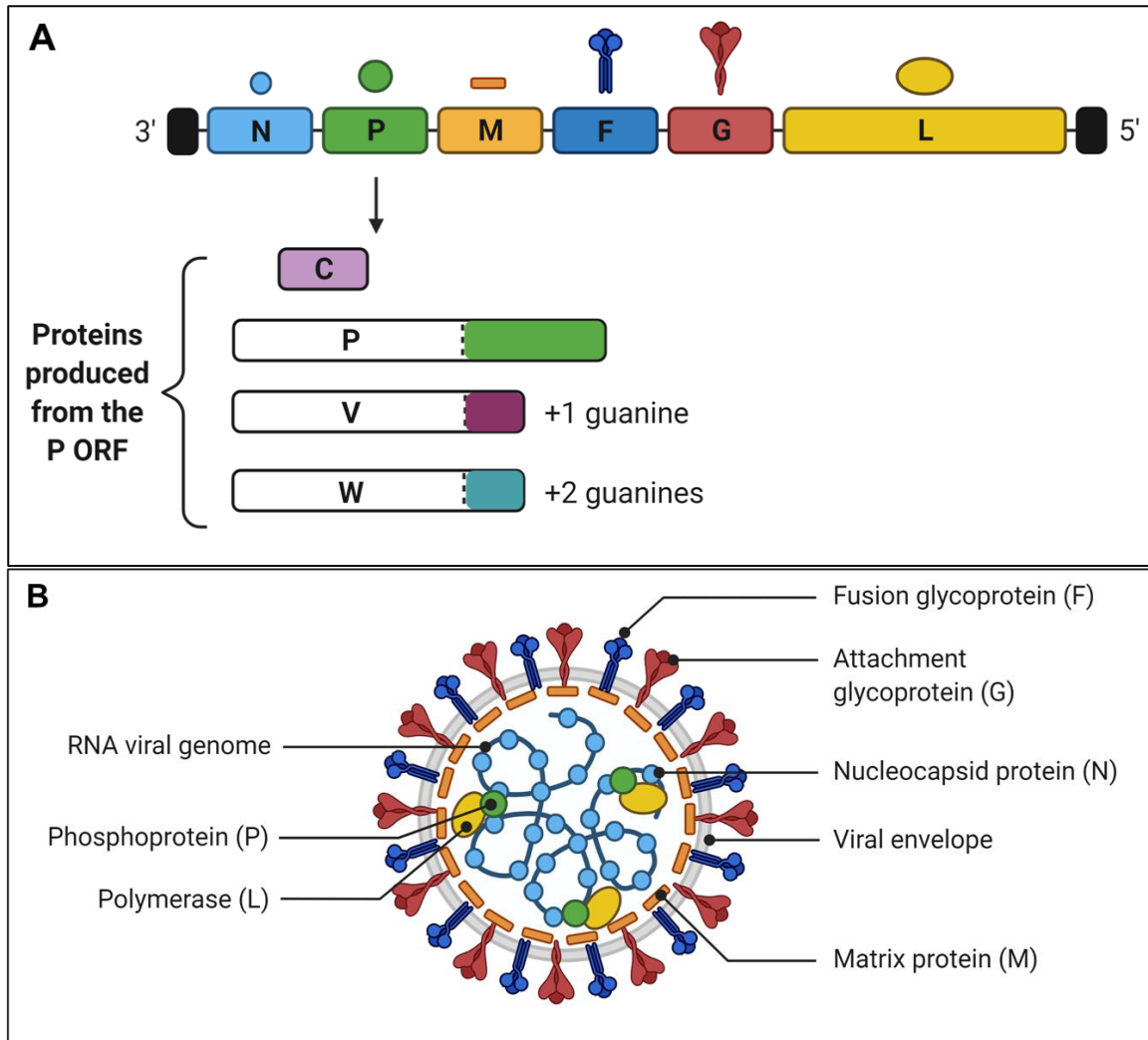


**Figure 1-2: NiV genome, proteins, and viral structure**

(A) Organization of the NiV genome and proteins produced from its ORFs. The six ORFs of the NiV genome are shown in order from 3' to 5'; intergenic regions are shown as black lines, and the 3' and 5' genomic leader and trailer sequences are shown as black boxes at the beginning and end of the genome. Structural proteins produced are shown above each ORF; colors and shapes correspond to those in (B). Nonstructural proteins produced from the P ORF are shown below the genome. Faithful transcription of the ORF produces the P protein, which is essential for viral replication (shown in white and green). Stuttering of the polymerase at the co-transcriptional gene editing site (shown as a dashed line within P, V, and W) inserts untemplated guanine residues and causes a frameshift resulting in the production of V protein (in the +1 frame, shown in white and magenta) and W protein (in the +2 frame, shown in white and turquoise). The shared NTDs of these proteins are shown in white, while the unique CTDs are shown in green, magenta, or turquoise. The C protein (shown in lavender) is produced from an alternative start codon in a different frame compared to the NTD of the P, V, and W proteins, so it shares no amino acid homology with the other proteins. (B) A diagram of the structure of the NiV virion. The viral envelope derived from the cellular plasma membrane, the RNA genome, and the structural proteins shown in (A) are visible. Figure created with BioRender.com.

during infection through a conformational rearrangement of the F trimer involving insertion of the protein's fusion peptide into the host cell membrane and the subsequent formation of the post-fusion conformation referred to as the six-helix bundle<sup>50-53</sup>. The G glycoprotein binds to the cellular membrane-expressed ligands ephrin-B2 and ephrin-B3, which serve as the NiV viral entry receptors<sup>54-56</sup>. The binding of G to ephrin-B2 or -B3 initiates a specific interaction between G and the pre-fusion form of F, subsequently triggering the conformational change in F and the merge of the virion and host cell membranes<sup>57-59</sup>. Both the F and G proteins are required for viral entry<sup>50,51</sup>. The L ORF encodes the large subunit of the viral RNA-dependent RNA polymerase (L), which, together with the P protein and the N-encapsidated RNA genome, comprise the ribonucleoprotein (RNP) complex<sup>45</sup>. The M protein traffics through multiple cellular compartments during infection to facilitate the packaging of the RNP complex into the nascent virion, which obtains a phospholipid membrane envelope derived from the infected cell and studded with the F and G surface proteins upon viral budding (**Figure 1-2 B**)<sup>47,49,60</sup>. Like other paramyxoviruses, NiV viral particles are roughly spherical to pleomorphic in shape and of varying size, with a distinctive herringbone structure to the nucleocapsid visible under EM<sup>1,60</sup>.

Besides the structural proteins listed above and shown in **Figures 1-2A** and **1-2B**, the P ORF of NiV encodes additional nonstructural proteins with immunomodulatory functions<sup>3,61</sup>. The P ORF contains a conserved uracil- and cytosine-rich mRNA editing site at which the polymerase stutters and can insert additional untemplated guanines during transcription<sup>62,63</sup>. This co-transcriptional gene editing results in the production of the V protein (when  $3n+1$  additional guanines are added) and the W protein ( $3n+2$  additional guanines)<sup>3,64</sup>. Most paramyxoviruses produce these edited transcripts, but NiV edits its P gene at a higher rate than paramyxoviruses of other genera and can add up to 11 additional guanine residues to each transcript<sup>64,65</sup>. Additionally, translation from alternative start codons near the 5' end of P/V/W transcripts results in the production of

the C protein<sup>3</sup>. Importantly, the C protein is out of frame compared to the P/V/W proteins and therefore shares no amino acid homology with them (**Figure 1-2A**)<sup>61</sup>. Similarly, the V and W proteins share the amino acid sequence of P in their N-terminal domains (NTDs) upstream of the gene editing site, but the frameshift induced by the untemplated guanine residues results in C-terminal domains (CTDs) of these proteins which share no amino acid homology with the CTD of the P protein (**Figure 1-2A**)<sup>63,65</sup>. The NiV P, V, W, and C proteins can antagonize host antiviral responses, as shown using plasmid overexpression experiments in cell lines and in small animal models<sup>61,66–70</sup>.

### **The specific NiV receptors are highly conserved among mammals and are expressed on a wide variety of cells**

The cellular entry receptors for NiV have been identified as the receptor tyrosine kinases ephrin-B2 and ephrin-B3, which are critical for the formation of neurons and blood vessels and for the migration of neuronal dendrites and endothelial cells<sup>54–56,71,72</sup>. Binding to ephrin-B2 or -B3 by the G protein of NiV prompts a conformational change in the F protein that promotes fusion of the cell and viral membranes and release of the RNP complex into the cytoplasm<sup>50,51,59</sup>.

Ephrin-B2 is widely expressed on the surface of endothelial cells throughout the vascular system and in the cortex and epithelial cells of the brain, as well as cells in the placenta, spleen, and the lining of lymph nodes and smooth muscle cells in small arteries<sup>59,71–73</sup>. Ephrin-B3 is mostly restricted to expression on cells in the CNS, especially neurons and endothelial cells in the brain and spinal cord<sup>52,56,72–74</sup>. Together, the distribution of ephrin-B ligand expression on these cell types explains the tropism of NiV—pathology is noted in endothelial cells, small arteries, the brain, and lymphoid tissues<sup>30</sup>, leading to the diffuse vasculitis and systemic symptoms characteristic of NiV disease<sup>56,57,72</sup>. After primary infection of lymphoid tissues, it has been suggested that NiV viremia leads to dissemination throughout the body and secondary infection of endothelial cells, leading to increased vascular permeability which allows invasion of the

CNS and direct infection and death of neurons and glial cells<sup>72,75,76</sup>. Vertical transmission of NiV has been noted in an infected cat, and high expression of ephrin-B2 in the placenta during development could explain this phenomenon<sup>72,77</sup>.

Although acute necrosis of lymphoid tissue is a feature of NiV pathology, human lymphocytes have not been shown to be permissive to productive NiV infection and do not express ephrin-B2 nor -B3 at the transcript level<sup>78</sup>. Therefore, infection of the cells lining the spleen and lymph nodes which do express ephrin-B2 would be a better explanation of the characteristic lymphoid pathology<sup>71,72</sup>. However, it has been shown that lymphocytes can contribute to systemic dissemination of NiV in the hamster model, perhaps due to basal levels of expression of ephrin-B ligands on their surface<sup>78</sup>.

The ephrin-B ligands are highly conserved among mammalian species, which partially explains the much broader host range of henipaviruses compared to other paramyxoviruses, which are generally host-restricted<sup>59,71</sup>. A wide variety of wild and domesticated mammalian species can be naturally infected with NiV, including bats, pigs, cats, dogs, goats, horses, and humans<sup>1,13,17,20,32</sup>. Therefore, a variety of small and large animal models for NiV disease have been developed to investigate NiV pathogenesis and immune responses and to test vaccines and therapeutics, including hamsters, ferrets, guinea pigs, nonhuman primates (NHPs), pigs, and cats<sup>75,79-86</sup>. Interestingly, however, mouse ephrin-B2 and -B3 function equally to ephrins from natural NiV hosts as receptors for NiV<sup>74</sup>, even though wild-type mice are not permissive to systemic NiV infection<sup>75,87,88</sup>. These results indicate an additional, later mechanism of inhibiting NiV replication in mice or a downregulation of the ephrins at the protein level<sup>73,74</sup>. In conclusion, the tropism of NiV for the vasculature and the nervous system, as well as the wide host range of henipaviruses among mammalian species, is explained in part by the broad functions, widespread expression, and evolutionary conservation of the ephrin-B2 and -B3 cellular receptors.

## **NIIV IS A POTENT INHIBITOR OF THE INTERFERON RESPONSE**

### **Viral RNA in cell cytoplasm is detected by retinoic acid-inducible gene I-like receptors**

The retinoic acid-inducible gene I (RIG-I)-like receptors (RLRs) are a family of cytosolic proteins that detect viral RNA in the cytoplasm of infected cells<sup>89</sup>. The RLRs are pattern recognition receptors that are responsible for detecting pathogen-associated molecular patterns (PAMPs), such as non-self RNA, within cells<sup>90</sup>. There are three sensors within the RLR family: RIG-I, melanoma differentiation-associated protein 5 (MDA5), and laboratory of genetics and physiology 2 (LGP2)<sup>91-94</sup>. These proteins are DExD/H-box helicases with adenosine triphosphatase (ATPase) activity<sup>89,95</sup>. RIG-I and MDA5 contain caspase recruitment domains (CARDs) near their N-termini that interact with homologous CARDs on the mitochondrial membrane antiviral signaling (MAVS; also known as VISA, IPS-1, and Cardif) adaptor protein on the outer mitochondrial membrane after the RLRs bind viral RNA<sup>96-100</sup>. This interaction causes a signaling cascade in which the kinases inhibitor of nuclear factor kappa-light-chain-enhancer of activated B cells (NF- $\kappa$ B) kinase subunit epsilon (IKK $\epsilon$ ) and TANK-binding kinase 1 (TBK1) are activated, which in turn phosphorylate the transcription factors interferon regulatory factor (IRF)3 and IRF7<sup>101-103</sup>. Activated IRF3 and IRF7 translocate to the nucleus, where they bind to promoter elements within the genome that upregulate the expression of type-I interferons (IFNs), including IFN- $\alpha$  and IFN- $\beta$ , as well as antiviral proinflammatory cytokines<sup>101,102</sup>.

RIG-I and MDA5 bind different ligands and can have overlapping and distinct roles during viral infections<sup>104,105</sup>. RIG-I is thought to preferentially bind to short double-stranded (ds)RNA and RNA that is 5'-triphosphorylated, while MDA5 is thought to bind to long dsRNA<sup>106</sup>. These nucleic acid species are not common in eukaryotic cells undergoing normal metabolism, so the RLRs are sensors responsible for early detection of infection with a pathogen<sup>90</sup>.

LGP2 lacks the CARDs that allow binding to MAVS, so it can bind RNA but cannot induce the signaling cascade that leads to IFN production<sup>104</sup>. Depending on the inducer used (e.g., viruses known to induce strong IFN responses such as Sendai virus (SeV) or artificial dsRNA mimetics such as poly(I:C)) and the system under study (cell type, primary or continuous cells, infectious agent, etc.), the function of LGP2 as a positive or negative regulator of RLR signaling varies<sup>101,107</sup>. For example, susceptibility to picornaviruses (which are known to be primarily sensed by MDA5 rather than RIG-I in infected cells) of cells lacking LGP2 was found to be higher than wild-type cells, indicating a positive regulatory effect of LGP2 on MDA5 for these viruses<sup>108</sup>. A similar positive effect of LGP2 on MDA5 has been observed for paramyxoviruses<sup>109</sup>. Conversely, it was recently reported that LGP2 can block tripartite motif-containing protein 25 (TRIM25)-mediated ubiquitination of RIG-I, which is a necessary step in the activation of RIG-I-mediated signaling<sup>110</sup>. Interestingly, this inhibitory mechanism mirrors the recently identified mechanism by which NiV V inhibits TRIM25-mediated activation of RIG-I<sup>111</sup>.

### **Type-I IFNs act in an autocrine and paracrine fashion to induce an antiviral state in cells**

The type-I IFNs expressed by upregulation of the IFN production pathway are released from the cell and can act on the same cell (autocrine) or on other cells (paracrine) to induce an antiviral state<sup>112,113</sup>. IFN binds to its receptor on the cell surface, which activates the tyrosine kinases Janus kinase 1 and tyrosine kinase 2 through phosphorylation<sup>112,114</sup>. These kinases phosphorylate signal transducer and activator of transcription (STAT)1 and STAT2, which form an activated heterodimer that translocates to the nucleus<sup>112-114</sup>. The STAT1/STAT2 heterodimer binds to promoter elements known as IFN-sensitive response elements to upregulate expression of interferon-stimulated genes (ISGs) encoding antiviral functions<sup>112,114</sup>. ISGs include genes that can directly inhibit viral replication, such as 2',5'-oligoadenylate synthetase 1, which activates the

enzyme RNase L to degrade viral RNA, thus directly inhibiting viral replication<sup>115</sup>. Other ISGs can sequester viral products and prevent their interactions and functions, such as interferon-induced protein with tetratricopeptide repeats (IFIT)1, which binds to and sequesters RNA with a triphosphate group on the 5' end<sup>116</sup>, and ISG15, which is a posttranslational modification similar to ubiquitin that conjugates to viral proteins and prevents downstream functions<sup>117</sup>. IFIT2 (also known as ISG54) can promote apoptosis of infected cells to prevent further viral spread<sup>118</sup>. In summary, the IFN signaling pathway is a vital part of the innate immune system, capable of responding to viral infections within minutes and directly inhibiting or destroying viral PAMPs<sup>112</sup>. Thus, viruses often encode mechanisms of inhibiting its activity<sup>112</sup>.

### **Henipaviruses are known inhibitors of IFN induction and response**

Paramyxoviruses are well-known and well-characterized inhibitors of both the IFN production and IFN signaling pathways. Most of these functions are attributed to the accessory P gene products, which have IFN-inhibitory functions and are produced by nearly every identified paramyxovirus<sup>61,119</sup>. A wide variety of paramyxoviruses can evade IFN production by directly inhibiting RNA binding by MDA5<sup>120,121</sup> and by inhibiting downstream signal transduction by preventing activation of IKK $\epsilon$ <sup>122</sup> or nuclear translocation of IRF3<sup>123</sup>. Additionally, paramyxoviruses can inhibit the type-I IFN response by directly antagonizing STAT1 and STAT2, as discussed below.

Each genus of paramyxoviruses has a unique mechanism of inhibiting IFN signaling by targeting STAT1 and STAT2. Rubulaviruses target the STATs for proteasomal degradation<sup>124</sup>, morbilliviruses prevent translocation of activated STAT1 and STAT2 to the nucleus<sup>125</sup>, and henipaviruses sequester both STAT1 and STAT2 into high-molecular weight complexes in the cytoplasm or nucleus so that they cannot be used for signaling<sup>126,127</sup>. The binding sites for STAT1 and STAT2 are on the shared NTD of the NiV P/V/W proteins, so all three proteins are capable of inhibiting IFN signaling in this

manner<sup>128</sup>. The location of the STAT-binding domains within the NTD of P/V/W is unique to henipaviruses among the paramyxoviruses—other genera evade STAT function through the CTD of the V protein<sup>113</sup>. The V CTD is highly conserved among all paramyxoviruses, including NiV and HeV, but the NTD of the henipaviruses is unique, sharing no amino acid homology with the V NTDs of other members of the viral family<sup>113</sup>. Therefore, the henipaviruses evolved a unique mechanism for inhibition of STAT function<sup>113</sup>. There is some evidence that the N protein of henipaviruses may be able to recapitulate this STAT sequestration function<sup>129</sup>, a conservation of IFN-inhibitory capacity which is also unique among the paramyxoviruses.

In addition to inhibiting STAT function, the V proteins of paramyxoviruses are well-characterized inhibitors of MDA5. The unique CTD of paramyxoviral V proteins binds to MDA5 within its helicase domain and therefore prevents it from binding to viral RNA<sup>130</sup>. This innate immune evasion mechanism will be discussed in detail in Chapter 2. Interestingly, paramyxoviral V proteins can bind the helicase domains of MDA5 and LGP2 but not RIG-I<sup>131</sup>, although there is some evidence they can bind to RIG-I through its CARDs, instead<sup>111</sup>. NiV W protein also inhibited the IFN production pathway in common continuous cell lines used in the laboratory, in which its nuclear localization signal causes its accumulation in the nucleus<sup>123,132</sup>. When localized to the nucleus, W prevented nuclear accumulation of phosphorylated IRF3 by inhibiting an activator of IRF3 signaling upstream of TBK1<sup>123</sup>. However, W has been found in the cytoplasm in primary endothelial cells, which are NiV target cells, so further elucidation of these innate immune evasion mechanisms in relevant cell types is needed<sup>64,133</sup>.

## ANIMAL MODELS OF NiV DISEASE

### **Diverse mammals are susceptible to NiV infection and disease**

As a result of the evolutionary conservation of the cellular receptors ephrin-B2 and ephrin-B3, a wide variety of mammals, including humans, bats, pigs, cats, dogs, goats, and horses are documented natural hosts of NiV; other species may also be susceptible<sup>1,13,17,20,32</sup>. Animals that have been subjected to experimental NiV infection to develop models that recapitulate human NiV disease or investigate NiV pathology and immune responses include mice, guinea pigs, ferrets, Syrian golden hamsters, cats, pigs, squirrel monkeys, cynomolgus macaques, and African green monkeys (AGMs)<sup>75,79–86</sup>.

Small animals that have been subjected to experimental NiV infection include mice, guinea pigs, Syrian golden hamsters, and ferrets<sup>75,81,82</sup>. Immunocompetent mice were not susceptible to NiV disease and developed only subclinical respiratory infections following intranasal (i.n.) or intraperitoneal (i.p.) NiV inoculation<sup>75,87,88</sup>. Conversely, mice lacking type-I IFN signaling capacity developed encephalitis and lethal NiV disease when infected by the same routes, and wild-type and immunocompromised mice alike succumbed to NiV disease following intracerebral infection<sup>88</sup>. Guinea pigs developed vasculitis and endothelial syncytia following i.p. infection with NiV, but clinical illness was mild (transient fever and weight loss), and only a proportion of inoculated animals developed clinical or histopathological signs of infection<sup>75,82</sup>. In guinea pigs, i.n. infection was non-productive, and animals failed to develop respiratory nor CNS lesions<sup>75,82</sup>. Therefore, neither mice nor guinea pigs are reliable small animal models of NiV disease<sup>134</sup>. The best-characterized small animal models are hamsters and ferrets, which will be discussed in detail below.

Experimental infections of cats and pigs have been used to characterize NiV pathology using defined doses and inoculation routes in these natural hosts<sup>80,83,84</sup>. Pigs inoculated via subcutaneous or oral routes developed respiratory clinical signs with detectable NiV in the upper respiratory tract, and they could transmit the virus to nearby

pigs, consistent with reported cases in Malaysia and Singapore<sup>83,84</sup>. Neurological disease was less common, but invasion of the CNS in affected animals was confirmed by antigen staining and presence of viral RNA<sup>83,84</sup>. Syncytia and vasculitis were rare<sup>83,84</sup>. Cats infected via the subcutaneous route or i.n. universally developed severe respiratory disease, nearly always necessitating euthanasia<sup>80,84</sup>. Viral RNA was detectable in the respiratory tract and in the brain; syncytia were present in the endothelium<sup>80,84</sup>. Vertical transmission and infection of the fetus was observed in one animal<sup>77</sup>. Cats, therefore, represent a viable model for therapeutic testing, although encephalitis was not observed in these animals<sup>134</sup>. Accordingly, a subunit vaccine for NiV based on a soluble version of the HeV G attachment glycoprotein (HeV-sG) was successfully tested in the feline model, in which it mediated protection from NiV challenge<sup>80,135</sup>.

NHPs that have been investigated as models for human NiV disease include squirrel monkeys, cynomolgus macaques, and AGMs<sup>79,85,86</sup>. Only a proportion of experimentally infected squirrel monkeys developed mild clinical illness following i.n. infection, and more severe disease with detectable viral RNA in tissues occurred only in animals infected by the intravenous route<sup>85</sup>. Vasculitis and brain pathology were not evident<sup>85</sup>. Similarly, cynomolgus macaques developed only mild clinical illness following challenge with NiV<sub>B</sub> and subclinical illness after challenge with NiV<sub>M</sub> via the i.n. and intratracheal (i.t.) routes, with no pathological lesions consistent with NiV infection<sup>86</sup>. These animals developed robust neutralizing NiV-specific antibodies, and they were predicted to have robust T-cell and B-cell responses based on transcriptomic profiling<sup>86</sup>. On the other hand, AGMs challenged with the same dose and via the same route as in the study in macaques reproducibly developed respiratory and neurological signs and diffuse vasculitis consistent with human NiV disease, so this model will be discussed further below<sup>79,136</sup>.

### **Syrian golden hamster model**

The Syrian hamster model is one of the most commonly used animal models of NiV disease. Experimentally infected animals develop severe respiratory disease, neurological lesions, and endothelial syncytia representative of human NiV disease. However, clinical outcomes can be inconsistent and vary by route and dose. In one study, hamsters inoculated with a dose of NiV as low as 100 plaque-forming units (PFU) i.p. and as high as  $10^6$  PFU i.n. developed neurological signs and succumbed to NiV disease by nine days post-challenge via the i.p. route and by 15 days post-infection (dpi) via the i.n. route<sup>75</sup>. However, hamsters infected with a similar dose of NiV i.p. or i.n. in a different study developed severe acute respiratory disease and succumbed by day five post-challenge, while animals given a lower dose by either route developed neurological signs and more systemic spread of the infection through the endothelium before succumbing by 12 dpi<sup>137</sup>. Blood chemistry analysis provided further support of two different phenotypes of NiV infection in hamsters, one associated with respiratory disease and the other with neurological disease, although neither dose nor route was obviously correlated with which phenotype was observed<sup>138</sup>. Comparisons of NiV<sub>M</sub> and NiV<sub>B</sub> isolates as challenge inocula underscored the inconsistency of disease in this model. One study found that NiV<sub>M</sub> was more pathogenic than NiV<sub>B</sub> when administered i.p., with earlier viral replication and death in animals infected with NiV<sub>M</sub><sup>139</sup>. However, another study found that NiV<sub>B</sub> caused more severe respiratory lesions in hamsters shortly after oronasal infection<sup>140</sup>.

Despite inconsistencies in clinical outcome, hamsters have been used for a wide variety of studies investigating NiV pathogenesis, therapeutics, and vaccines, as they are relatively simple to house and handle. Contributions of the NiV nonstructural proteins to virulence were investigated, and a role for the C protein in inhibition of proinflammatory cytokine induction was described<sup>69,70</sup>. A mechanism for systemic dissemination in which NiV can attach to leukocytes without directly infecting them was identified<sup>78</sup>, and a

mechanism by which NiV may invade the CNS directly from the respiratory tract via the olfactory bulb was detailed<sup>141</sup>. The plausibility of transmission via date palm sap and via direct contact with infected secretions was demonstrated in a controlled laboratory setting with infected hamsters<sup>26,142</sup>. The capacity of small molecules such as poly(I:C), heparin, favipiravir, and griffithsin to protect hamsters from lethal NiV challenge was described<sup>143–146</sup>, and the protective efficacy of vaccinia-vectored, adeno-associated virus (AAV)-vectored, adenovirus-vectored, MeV-vectored, vesicular stomatitis virus (VSV)-vectored, virus-like particle (VLP)-based, and mRNA-based vaccines in the hamster model was demonstrated<sup>147–154</sup>. Therefore, the Syrian golden hamster is a popular and well-characterized small animal model of NiV disease, although a more clinically consistent model using a more relevant infection route would be desirable.

### **Ferret model**

Ferrets are the preferred small animal model for research on influenza and other respiratory viruses because their respiratory tracts are anatomically similar to those of humans, they express similar viral cellular receptors, and they have a similar gene expression distribution in tissues compared to humans<sup>155,156</sup>. As might be expected, experimental infection of ferrets with NiV has recapitulated the acute encephalitis, severe respiratory disease, and diffuse vasculitis characteristic of human infections<sup>81,134</sup>. Unlike the models discussed above, in which i.n. infection had variable pathogenicity, i.n. NiV infection in ferrets of doses 500 median tissue culture infectious dose (TCID<sub>50</sub>) and above caused severe disease requiring humane euthanasia<sup>81,157</sup>. Animals consistently developed clinical signs including depression, cough, dyspnea, hind limb paresis, ataxia, tremors, seizures, facial edema, nasal discharge, fever, and rash<sup>81,134,157</sup>. On necropsy, NiV-infected animals had vascular lesions, alveolar epithelial and endothelial syncytia, pulmonary edema and petechial hemorrhages on the lungs, congestion in blood vessels of the brain, and focal necrosis in numerous tissues<sup>67,81,134,157</sup>. NiV was isolated and viral

RNA was recovered from multiple fluids and tissues, and viral antigen was evident in vessels and organs throughout the body following immunohistochemical staining<sup>67,81,134,157</sup>.

Ferrets have been used to investigate NiV pathogenesis and transmission in order to answer questions about virulence using a relevant small animal model. The impacts of the NiV nonstructural proteins were investigated by infecting ferrets with recombinant NiV (rNiV) lacking the V, W, and/or C proteins, and infection with a rNiV lacking the V protein was found to be non-lethal in this model at a dose of 5,000 PFU i.n.<sup>67,68</sup>. Furthermore, impacts of evasion of the innate immune system by NiV were evaluated, as when a rNiV unable to bind to STAT1 caused delayed time to death following challenge with the same route and dose<sup>158</sup>. Ferrets were not shown to transmit NiV to cagemates without direct inoculation with respiratory secretions in a small study, although NiV<sub>B</sub> caused more shedding and a higher viral load in the respiratory tract than NiV<sub>M</sub><sup>27,33</sup>. These experiments showed that repeated, direct contact with respiratory secretions of late-stage infected patients is likely necessary for NiV transmission, providing a virological mechanism by which NiV<sub>B</sub> may cause outbreaks with person-to-person transmission in humans<sup>27</sup>.

Ferrets have also been used to evaluate the antibody therapies and vaccines against NiV that have proven most promising for control of this pathogen in humans. The potent cross-reactive neutralizing antibody m102.4, a human monoclonal antibody (mAb) capable of neutralizing both NiV and HeV<sup>159,160</sup>, fully protected ferrets from NiV challenge when administered 10 hours post-challenge<sup>81</sup>. The m102.4 antibody is approved for compassionate use in Australia and has been used following henipavirus exposures in 13 people; none of those treated developed signs of henipavirus disease<sup>161</sup>. Furthermore, the HeV-sG subunit vaccine, which is approved for use in horses in Australia to prevent HeV infection<sup>162</sup> and is currently in phase I clinical trials in humans<sup>163</sup>, was successfully tested in this model. Administration of two doses 20 days

apart protected ferrets from challenge 20 days post-boost, as well as more than 12 months later<sup>164</sup>. Protective efficacy of VSV-vectored NiV vaccine candidates against NiV<sub>M</sub> challenge was also demonstrated in ferrets<sup>165</sup>. Therefore, these small animals are reproducible and useful models of NiV infection that have helped to answer questions about human disease and test medical countermeasures that are now being administered to humans.

### **AGM model**

Although the ferret model of NiV disease is uniformly lethal, consistent, and faithfully recapitulates NiV disease in humans, NHP models of human NiV disease are essential for further testing of vaccine candidates. Experimental infection of AGMs with at least 2,500 PFU of NiV<sub>M</sub> via the i.t. and oral routes caused subjects to develop severe respiratory disease with neurological involvement, and endothelial syncytia and NiV antigen staining were present in many organs throughout the body, including in neurons in the brain stem<sup>79</sup>. Additional models involving experimental infection via the i.n. and aerosol routes were also developed<sup>136,166–170</sup>. Animals in these studies developed respiratory signs such as dyspnea and tachypnea, neurological signs such as seizures and ataxia, and widespread, diffuse vasculitis within small vessels following i.n. infection with as low as 2000 PFU of NiV<sup>79,134,171</sup>. There is evidence that the viral dose and route affect virulence in AGMs<sup>134</sup>. Viral RNA was recoverable from a variety of tissues, and NiV antigen staining revealed antigen presence in the tissues and vessels<sup>79,171</sup>. Disease in AGMs followed the course of severe human disease, and animals succumbed to NiV disease between six and 12 days following challenge<sup>79,171</sup>. On necropsy, infected AGMs had hemorrhaging and edema in the lungs, endothelial syncytia and widespread vasculitis, and congestion of the blood vessels in the brain<sup>79,134,171</sup>.

The development of the AGM model of NiV disease has allowed comparisons of virulence of the NiV<sub>M</sub> and NiV<sub>B</sub> strains, in-depth analyses of immune responses induced

by NiV, and further testing of promising therapeutics and vaccine candidates. Infection with NiV<sub>M</sub> was not uniformly lethal at doses as low as 400 PFU via the i.t. and aerosol routes<sup>79,168</sup>. On the other hand, challenge with NiV<sub>B</sub> was uniformly lethal, and testing with a uniform dose and route showed that NiV<sub>B</sub> was more virulent in AGMs than NiV<sub>M</sub><sup>136,172</sup>. The potent mAb m102.4 protected AGMs from both NiV<sub>M</sub> and NiV<sub>B</sub>, although treatment needed to be initiated sooner to protect AGMs from lethal outcome following NiV<sub>B</sub> challenge than NiV<sub>M</sub> challenge<sup>172,173</sup>. As in ferrets, the HeV-sG vaccine protected AGMs from NiV challenge in a single dose; furthermore, animals were protected in a window as short as one week between vaccination and challenge<sup>174,175</sup>. VSV-vectored vaccines tested in AGMs also demonstrated protective efficacy<sup>176,177</sup>. Experimental infections have identified cluster of differentiation (CD)8<sup>+</sup> T cells, effector memory T cells, NiV-specific immunoglobulin (Ig)M<sup>+</sup> B cells and antibodies, and NiV-specific neutralizing antibodies as possible mediators of survival in this model<sup>86,168</sup>. These findings correlate with a recent report of elevated activated CD8<sup>+</sup> T cells, B cells, and NiV-specific IgM and IgG in survivors of the recent NiV<sub>B</sub> outbreak in Kerala, further highlighting the relevance of the AGM model for answering questions about human NiV disease<sup>19</sup>.

## **VACCINES IN DEVELOPMENT FOR NIV**

### **There is no clinically licensed vaccine to prevent NiV disease**

While a veterinary vaccine for HeV has been approved for use in horses in Australia<sup>162</sup>, there are currently no clinically licensed specific treatments nor vaccines for NiV for livestock nor humans. However, a variety of approaches have been attempted, including VLPs, a HeV-sG subunit vaccine, and multiple viral vectors including poxviruses, adenoviruses, AAV, MeV, rabies virus, and VSV.

Plasmid overexpression of the matrix protein and surface glycoprotein(s) of a virus in mammalian cells causes the spontaneous self-assembly of VLPs that have the size and surface structure of infectious virus without the RNP complex inside<sup>178,179</sup>. These VLPs are therefore non-replicative and non-infectious<sup>153,179</sup>. Co-expression of NiV M, F, and G proteins was shown to produce VLPs that retained the structure, humoral immunogenicity, and innate immune response induction of wild-type virus, without any NiV genetic material<sup>178</sup>. Inoculation of mice with the NiV VLPs without adjuvant caused them to generate binding and neutralizing antibodies proportional to the VLP dose<sup>178</sup>. Furthermore, 100% of Syrian hamsters challenged with NiV following one or three doses of VLP vaccine with or without adjuvant survived to the study endpoint, although a significant proportion of animals in the adjuvant-only control groups also survived<sup>153</sup>. Nonetheless, these results demonstrated the feasibility and immunogenicity of VLPs as a vaccine for prevention of NiV disease.

Viral-vectored vaccine approaches have been attempted for NiV with a variety of vectors. These vaccines contain the backbone of a harmless virus and the F and/or G glycoprotein of NiV and have proven immunogenic and to have protective efficacy in animal models<sup>180</sup>. Two doses of an attenuated poxvirus containing NiV F, G or both given to hamsters, followed by challenge with NiV<sub>M</sub> i.p. three months later, were protective<sup>147</sup>, as was a canarypox vector containing NiV F, G or both given to pigs in two doses, followed by i.n. challenge with NiV<sub>M</sub> 28 days after boost<sup>181</sup>. A different poxvirus-vectored vaccine encoding either full-length NiV G or a soluble version lacking the transmembrane domain was immunogenic in mice lacking IFN signaling capacity, although no challenge with NiV was attempted<sup>182</sup>. Similarly, an AAV-vectored NiV G vaccine given to hamsters i.m. protected them from later challenge with NiV<sub>M</sub> i.p.<sup>148</sup>, and a chimpanzee adenovirus-vectored NiV<sub>B</sub> G vaccine protected hamsters from either NiV<sub>B</sub> or NiV<sub>M</sub> 28 days after a single dose<sup>150</sup>. NiV<sub>M</sub> G vaccines in MeV vaccine strain backbones protected hamsters and AGMs from i.p challenge with NiV<sub>M</sub> when given as a

two-dose regimen<sup>149</sup>. Finally, rabies-vectored vaccines have been assessed for immune responses in mice and pigs and were found to induce neutralizing and binding antibodies specific for NiV<sub>M</sub><sup>183–185</sup>. In short, NiV antigens within various viral vectors have been shown to be immunogenic and protective in multiple animal models, highlighting the efficacy and safety of these vaccination strategies<sup>180</sup>.

### **HeV-sG glycoprotein subunit vaccine**

The most advanced vaccine candidate for NiV, with a phase I clinical trial underway (clinical trial #NCT04199169), is the HeV-sG subunit vaccine<sup>163</sup>. A formulation of this vaccine has been approved for use in horses in Australia to prevent HeV disease and is marketed as Equivac® HeV by Zoetis, Incorporated (Inc.)<sup>162</sup>. Although the vaccine is based on HeV, it shows cross-protection against NiV<sup>80,164,174</sup>. The HeV-sG antigen was first developed in 2000 and was first tested as a vaccine antigen in the NiV feline model<sup>80,186</sup>. The vaccine protected cats from lethal NiV<sub>M</sub> challenge when given in two or three doses at least 21 days prior to NiV infection, even at doses as low as 5 µg<sup>80,135</sup>. Similarly, low doses of HeV-sG were protective against NiV<sub>B</sub> in ferrets when given in two doses 20 days or 14 months prior to challenge<sup>164</sup>, and vaccine doses as low as 10 µg protected AGMs from challenge with NiV<sub>M</sub> 21 days after the second dose<sup>174</sup>. More recently, studies have shown that one dose of the subunit vaccine is sufficient for protection of AGMs from lethal challenge with NiV<sub>B</sub>, and vaccination as close as one week before challenge mediates protection<sup>175</sup>. Therefore, the HeV-sG vaccine has demonstrated protective efficacy in relevant animal models of NiV disease at low doses and with short windows between vaccination and challenge, which are important characteristics for a vaccine used to control an ongoing outbreak of NiV disease.

### **VSV-vectored vaccines**

Recombinant VSV (rVSV) has been used as a vector to deliver NiV vaccines for over a decade<sup>187</sup>. Usually, the VSV G surface protein is replaced with a glycoprotein

from a pathogen of interest; the resulting constructs are called rVSV- $\Delta$ G vectors and are pseudotyped with the antigen of interest. Feasibility of the rVSV- $\Delta$ G vaccine platform has been previously demonstrated, as it was used to generate the rVSV-ZEBOV vaccine against Zaire ebolavirus (EBOV) which was crucial in ending the 2014 EBOV outbreak<sup>188,189</sup>. The rVSV-ZEBOV vaccine has been licensed in the USA and Europe under the name ERVEBO™ following demonstration of its safety and efficacy in clinical trials<sup>188</sup>.

Since the NiV genome encodes two surface proteins, F and G, which are both required for viral entry, rVSV- $\Delta$ G vectors encoding only one of these antigens must be complemented with the other surface protein or with the missing VSV G protein for amplification of viral stocks and can undergo only one cycle of replication. Co-transfection of rVSV- $\Delta$ G genomes containing either NiV F or NiV G into the same cells allows them to complement each other and produces single-cycle rVSV- $\Delta$ G viruses expressing both proteins on their surface<sup>190</sup>. Single-cycle rVSV- $\Delta$ G vectors encoding either NiV<sub>M</sub> F or G protected Syrian hamsters from challenge with NiV<sub>M</sub> when given 32 days prior to challenge<sup>151</sup>. Similarly, single-cycle rVSV- $\Delta$ G constructs encoding NiV<sub>B</sub> F, G, or both along with green fluorescent protein (GFP) protected ferrets from challenge with NiV<sub>M</sub> when given 28 days prior to challenge and induced strong neutralizing antibody responses<sup>165</sup>. The rVSV- $\Delta$ G-NiV<sub>B</sub> G-GFP construct from that study was given to AGMs 28 days prior to challenge and protected them from otherwise lethal doses of NiV<sub>B</sub><sup>191</sup>.

Another approach to combat the replication incompetence of rVSV- $\Delta$ G-NiV vectors is to co-express a NiV surface protein with another viral protein capable of viral entry on its own, such as the EBOV attachment glycoprotein (EBOV GP), within the rVSV- $\Delta$ G backbone. Such vectors containing NiV<sub>M</sub> F or G protected 100% of Syrian hamsters as well as AGMs when given 28 days (hamsters) or 29 days (AGMs) prior to challenge with NiV<sub>M</sub>, and protection could be passively transferred to naïve

hamsters<sup>152,176</sup>. These constructs also protected hamsters when given very close to challenge, although the influence of innate immune responses to either the vector or the EBOV antigen could not be distinguished from NiV-specific, adaptive immune responses to the vaccines<sup>192</sup>. Overall, rVSV-ΔG vaccine constructs are highly effective at protecting ferrets, Syrian hamsters, and AGMs from lethal challenge with either NiV<sub>M</sub> or NiV<sub>B</sub> in a single dose, whether replication-competent or single-cycle.

## QUESTIONS TO BE ADDRESSED HERE

### Current understanding of NiV RLR evasion

The ability of paramyxovirus V proteins to bind to and inhibit the function of MDA5 was first recognized more than 15 years ago among diverse paramyxoviral genera<sup>120</sup>. In plasmid overexpression studies, the MuV V CTD and NiV V CTD have been shown to be necessary and sufficient for binding to MDA5<sup>120,121</sup>. Furthermore, paramyxovirus V CTDs bind to LGP2 in the same helicase region as MDA5, disrupting RNA binding and ATPase activity<sup>130,131</sup>. Specific binding sites on the V protein and on MDA5 and LGP2 have been identified for MeV, parainfluenza virus 5 (PIV5), and CDV<sup>193–195</sup>.

Paramyxoviruses strongly inhibit induction of type-I IFNs, as shown through IFN-β luciferase reporter assays with V proteins and in an infection model with PIV5<sup>121,131</sup>. CDV that is unable to bind to MDA5 loses the ability to inhibit this pathway *in vitro*<sup>194</sup>. NiV V protein can inhibit IFN-β in a reporter assay when stimulated with MDA5, and expression plasmids containing mutations at the beginning of the CTD of the V protein demonstrate reduced ability to inhibit reporter activity<sup>196</sup>.

The ability of paramyxoviruses to inhibit RIG-I is poorly understood. Previous studies failed to find a direct interaction between V proteins and RIG-I, although a mechanism by which V bound to LGP2 and then the V-LGP2 complex bound to RIG-I to

inhibit its activity has been proposed<sup>131</sup>. What is certain is that paramyxovirus V proteins cannot bind to RIG-I through the same helicase domain used for MDA5 and LGP2 because of amino acid differences in the region important for binding<sup>195</sup>. However, one study provided evidence that NiV V and other paramyxovirus V proteins can bind to RIG-I directly through its CARDS<sup>111</sup>. This distinct mechanism prevented activation of RIG-I-mediated signaling by blocking the ability of TRIM25 to ubiquitinate RIG-I<sup>111</sup>. More research is needed to corroborate this mechanism of viral inhibition and to further characterize it.

The paramyxoviral genus most closely related to the henipaviruses is the *Morbillivirus* genus. CDV is a morbillivirus with a lethal ferret model of CDV disease, so it is closely related to NiV with a similar small animal model<sup>194</sup>. A recombinant CDV unable to bind to MDA5 was non-lethal in the otherwise lethal ferret model, lending credence to the hypothesis that MDA5 is an important mediator of virulence for NiV by providing *in vivo* data for a closely related virus in a very similar model<sup>194</sup>. Importantly, the mutation used to prevent MDA5 binding likely also prevented binding to LGP2, so distinct contributions of these two RLRs to CDV virulence could not be determined<sup>194</sup>.

### **Current progress toward development of a NiV vaccine**

At present, the most advanced NiV vaccine candidate is the HeV-sG subunit vaccine, which has been approved for use in horses in Australia and is in phase I clinical trials in humans<sup>162,163</sup>. This vaccine has been shown to work quickly to protect AGMs from NiV challenge with a single dose<sup>175</sup>, although the durability of these responses will need to be tested. The present formulation for human use includes Alum as an adjuvant to enhance immunogenicity.

Vaccines vectored with rVSV and encoding NiV F or G have been well-characterized and can induce immunity that can be passively transferred to naïve hamsters<sup>152</sup>. Fully replication-competent and single-cycle constructs have been developed

and tested in Syrian hamsters, ferrets, and AGMs<sup>152,165,176,191,192</sup>. Most studies have used NiV<sub>M</sub> as the challenge virus, although a more recent study found that one dose of a single-cycle rVSV encoding NiV<sub>B</sub> G given 28 days prior to challenge protected AGMs from a lethal dose of NiV<sub>B</sub><sup>191</sup>, which has been found to be more virulent in AGMs than NiV<sub>M</sub><sup>172</sup>. The construct used in that study required no adjuvants, but it encoded GFP in addition to NiV<sub>B</sub> G.

### **Gaps in knowledge**

The ability of paramyxoviruses to evade the innate immune response has been well-characterized for many species. However, NiV and HeV are recently emerged viruses with unprecedented virulence, lethality, and host range compared to previously identified paramyxoviruses. The shared NTD of the henipaviral P/V/W protein has unique IFN signaling inhibitory capacity and no homology to any known proteins<sup>113</sup>. Furthermore, the mechanism by which the NiV V CTD inhibits type-I IFN production has not been characterized. Therefore, contribution of evasion of the innate immune response to NiV virulence remains a significant gap in knowledge. A better understanding of the mechanisms by which NiV evades type-I IFN responses could help develop targeted therapeutics and countermeasures in the future.

Interactions of NiV V protein with MDA5 and LGP2 have been well-characterized *in vitro*, but these studies have been limited to biosafety level (BSL)-2 conditions with expression plasmids because of the lack of availability of BSL-4 facilities and the difficulty of performing molecular biology assays under BSL-4 conditions. These interactions have not been investigated with replicating virus nor in an animal model of NiV disease. Furthermore, the exact binding site on NiV V at which the interaction with MDA5 and LGP2 occurs has not been elucidated, although the interaction has been isolated to the unique CTD of the protein<sup>121</sup>. In this dissertation, efforts to determine the

specific binding site of MDA5 by NiV V will be detailed, and mutations designed to inhibit this binding were tested *in vitro* and *in vivo* under BSL-4 biocontainment.

NiV causes recurrent outbreaks with high CFRs, and large portions of Africa, Asia, and Oceania are at risk of future henipavirus outbreaks because they are within the geographic range of its reservoir hosts, pteropid bats (**Figure 1-1**)<sup>13,20,22,23</sup>. However, no countermeasures for the prevention or treatment of NiV disease are currently available, except for the human mAb m102.4, which is available for compassionate use following known exposures<sup>161</sup>. A vaccine to prevent NiV disease is urgently needed, and one that works quickly would be most advantageous for preventing transmission during an outbreak, where transmission often occurs in hospitals or from patients to their caregivers<sup>16,19,29</sup>.

The HeV-sG vaccine has been shown to protect AGMs from NiV challenge shortly after administration in one dose<sup>175</sup> and protected ferrets from NiV challenge more than a year following two doses<sup>164</sup>. However, the durability of the response to one dose has not been evaluated, and shorter times between vaccination and challenge than one week have not been tested. A rVSV-vectored NiV<sub>B</sub> G vaccine has been shown to be effective against challenge with NiV<sub>B</sub> in one dose when given 28 days prior to challenge<sup>191</sup>. However, this construct encodes a fluorescent reporter, which is not ideal for future clinical trials, and it has not been tested for efficacy at shorter timeframes between vaccination and challenge than 28 days. In an outbreak scenario, rapid efficacy would be crucial for controlling spread of NiV infection. Therefore, this dissertation will report the recovery of a rVSV construct lacking the GFP reporter, and protection of AGMs from challenge with NiV<sub>B</sub> seven days and three days after vaccination was demonstrated.

## **Study hypotheses**

**Hypothesis 1:** The first hypothesis investigated in this dissertation is that abolishment of binding to MDA5 by NiV V protein using specific point mutations will restore IFN induction *in vitro* and will attenuate rNiV<sub>M</sub> *in vivo*. This hypothesis is addressed in Chapters 2 and 3.

**Hypothesis 2:** The second hypothesis investigated in this dissertation is that administration of a single-dose, single-cycle, VSV-vectored vaccine shortly prior to challenge will induce immune responses and protect AGMs from lethal infection with NiV<sub>B</sub>. This hypothesis is discussed in Chapter 4.

## **Chapter 2: A Single Point Mutation in NiV V Abrogates Binding to MDA5 and Partially Restores IFN- $\beta$ Induction by MDA5 in Plasmid-Based Protein Overexpression Studies**

### **INTRODUCTION**

As discussed in Chapter 1, paramyxoviruses cause significant morbidity and mortality in humans and animals worldwide. The morbilliviruses MeV and CDV infect humans/NHPs and carnivores, respectively, while the closely related henipaviruses NiV and HeV can cause disease in humans, horses, pigs, dogs, cats, goats, and possibly cattle<sup>1,5,13,17,32</sup>. A lethal ferret model exists for CDV as well as for NiV, and these models allow the study of viral pathogenesis and the evaluation of vaccines and therapeutics, as they faithfully recapitulate disease in the carnivorous and human hosts, respectively<sup>81,197</sup>.

Binding to MDA5 to prevent its downstream signal transduction is a well-established immune evasion mechanism for paramyxoviruses. Paramyxovirus V proteins strongly inhibited induction of IFN- $\beta$ , as shown using luciferase reporter assays with plasmid overexpression<sup>120,121</sup> and in a PIV5 infection model<sup>131</sup>. Blocking binding to MDA5 restored the induction of IFN- $\beta$  in plasmid overexpression systems<sup>194,196</sup>. Furthermore, inhibition of binding to MDA5 by CDV V protein was sufficient to render the virus 100% non-lethal in an otherwise 100% lethal ferret model<sup>194</sup>. Multiple members of the family, including MeV, MuV, CDV, PIV5, NiV, and HeV have been shown to bind to MDA5 through the CTD of their V proteins<sup>120,121,130</sup>, and this binding strongly inhibited the ATPase activity of MDA5, as shown through ATP hydrolysis assays<sup>130</sup>. Therefore, the importance of this evasion mechanism to the virulence of paramyxoviruses has been well-established both *in vitro* and *in vivo*.

The binding site of MDA5 by NiV V protein has been previously isolated to the cysteine-rich CTD of the V protein<sup>121</sup>, but the exact binding site has not yet been

elucidated. Point mutations that prevent binding of MeV, CDV, and PIV5 V proteins to MDA5 have been found<sup>193–195</sup>; however, mutation of the putative binding domain of MDA5 in an attempt to find the NiV V-MDA5 binding site failed to inhibit NiV V binding in a plasmid-based protein overexpression system<sup>109,195</sup>. Importantly, knockout of the CTD of the V protein of NiV prevented binding to MDA5<sup>121</sup>, indicating that the NiV V-MDA5 binding site lies within the CTD.

Mutation of the CDV V protein to prevent MDA5 binding resulted in a marked loss of ability to control IFN- $\beta$  induction in a plasmid overexpression system<sup>194</sup>. Another study performed alanine scanning of the beginning of the NiV V CTD and found loss of IFN- $\beta$  inhibition similar to the results for CDV V for several mutations after induction with MDA5, but the specific binding site was not determined<sup>196</sup>. Therefore, the specific binding site of NiV V to MDA5 remains a significant gap in knowledge, and inhibition of this interaction could have profound effects on virulence in the lethal ferret model, as evidenced by results with CDV in ferrets<sup>194</sup>. Understanding mechanisms of virulence for NiV is essential for the development of medical countermeasures, and the V-MDA5 interaction is a promising antiviral drug target due to its universality among paramyxovirus V proteins<sup>198</sup>. Finding the specific NiV V binding site to MDA5 is the first step in evaluating viral inhibition of this cellular factor as a contributor to NiV virulence.

In this chapter, attempts to identify the specific binding site of NiV V to MDA5 using co-immunoprecipitation (IP)/western blot following plasmid overexpression in cell culture will be detailed. The NiV V mutations were evaluated *in vitro* for loss of ability to control IFN- $\beta$  induction using a luciferase reporter assay and for ability to bind to LGP2. Finally, V mutant expression plasmids were evaluated using a minigenome luciferase reporter assay to determine probable effects on viral transcription and replication.

## METHODS

### Plasmids

Expression plasmids encoding NiV<sub>M</sub> V protein with a hemagglutinin (HA) tag fused to the N-terminus were ordered from Mutagenex, Inc. (now Charm Gene Science, LLC; Dublin, Ohio, United States of America (USA)) in the pCAGGS backbone<sup>199</sup>. These plasmids encoded the V protein from NiV<sub>M</sub> clinical isolate UMMC1 (GenBank accession number AY029767) with alanine scanning mutations or point mutations for ascertaining the NiV<sub>M</sub> binding site to MDA5.

An expression plasmid encoding human MDA5, pUNO1-hMDA5 (Invivogen; San Diego, California, USA; catalog number (Cat. No.) puno1-hmda5) and an expression plasmid encoding human LGP2, pCMV-10-3xFLAG-LGP2 (a kind gift from Dr. Curt Horvath, currently at Northwestern University; Evanston, Illinois, USA; Addgene plasmid #58681; <http://n2t.net/addgene:58681>; RRID:Addgene 58681)<sup>200</sup> were purchased commercially and used for constitutive expression of MDA5 or LGP2 in transfected cells.

The reporter plasmids p125-Luc and p55-C1b-Luc were kind gifts from Dr. Takashi Fujita (currently at Kyoto University; Kyoto, Kyoto Prefecture, Japan). The p125-Luc reporter encoded the entire human IFN- $\beta$  gene 5' regulatory region driving the firefly luciferase gene, while the p55-C1b-Luc reporter encoded four IRF-binding motifs in tandem, also driving the firefly luciferase gene<sup>201</sup>.

The pNiV-MG-Luc minigenome plasmid and pTM1-HA-NiV<sub>M</sub> P helper plasmid were kind gifts from Dr. Christopher Basler (currently at Georgia State University; Atlanta, Georgia, USA). The pNiV-MG-Luc plasmid encoded the 3' leader and 5' trailer regulatory sequences of the NiV<sub>M</sub> genome flanking the firefly luciferase gene and driven by a bacteriophage T7 promoter, while the pTM1-HA-NiV<sub>M</sub> P helper plasmid encoded the NiV<sub>M</sub> P protein with an HA tag fused to its N-terminus in the pTM1 expression plasmid, also driven by a T7 promoter<sup>66</sup>. The helper plasmids pTM1-NiV<sub>M</sub> N and pTM1-

NiV<sub>M</sub> L were cloned by Dr. Benjamin Satterfield (currently at Mayo Clinic; Rochester, Minnesota, USA) and encoded the NiV<sub>M</sub> N and NiV<sub>M</sub> L genes in the pTM1 expression plasmid, driven by a T7 promoter<sup>67</sup>. The GenBank accession number for the NiV<sub>M</sub> leader and trailer sequences and the P, N, and L genes is AY029767.

### **Cell culture**

Human embryonic kidney (HEK) 293T cells are a highly transfectable, continuous cell line transformed by the simian vacuolating virus 40 large T antigen<sup>202</sup>. HEK293T cells (clone 17; American Type Culture Collection (ATCC); Manassas, Virginia, USA; Cat. No. CRL-11268) were maintained in high-glucose Dulbecco's Modified Eagle Medium (DMEM; Gibco; Waltham, Massachusetts, USA; Cat. No. 10566) supplemented with 10% heat-inactivated fetal bovine serum (FBS; Gibco; Cat. No. 10082), 1% penicillin/streptomycin solution (10,000 units/milliliter (mL) penicillin and 10,000 micrograms (µg)/mL streptomycin; Gibco; Cat. No. 15140), and 1% GlutaMAX<sup>TM</sup> Supplement (Gibco; Cat. No. 35050).

Baby hamster kidney (BHK) cells stably expressing bacteriophage T7 polymerase (BSR T7/5 cells) are a fast-growing, continuous cell line for the expression of proteins from plasmids containing T7 promoters in a vaccinia-free system<sup>203</sup>. BSR T7/5 cells were maintained in high-glucose DMEM supplemented with 10% heat-inactivated FBS, 1% penicillin/streptomycin solution, and 1% GlutaMAX<sup>TM</sup> Supplement and supplemented once per week with Geneticin<sup>TM</sup> Selective Antibiotic (G418 sulfate, 50 milligrams (mg)/mL; Gibco; Cat. No. 10131) at a final concentration of 1 mg/mL.

### **Co-immunoprecipitation/western blots**

HEK293T cells were seeded in 6-well plates to be 80 to 90% confluent for transfection the next day. Cells were transfected with 1.25 µg each of pUNO1-hMDA5 or pCMV-10-3xFLAG-LGP2 expression plasmid and pCAGGS-HA-NiV<sub>M</sub> V expression plasmid (with or without alanine scanning mutations or point mutations designed to

prevent binding to MDA5) using *TransIT*-LT1 transfection reagent (Mirus Bio; Madison, Wisconsin, USA; Cat. No. MIR 2300). Briefly, plasmids and transfection reagent (3 microliters ( $\mu\text{L}$ )/ $\mu\text{g}$  plasmid or 7.5  $\mu\text{L}$ /well) were added to OptiMEM<sup>TM</sup> I Reduced Serum Medium (Gibco; Cat. No. 31985-070) and incubated at room temperature according to the manufacturer's protocol. During incubation, growth media on the cells was changed to 2.5 mLs complete DMEM containing 5% FBS per well, and then transfection mix was added to cells.

At 24 hours post-transfection, cells were lysed with 400  $\mu\text{L}$ /well of Radioimmunoprecipitation Assay (RIPA) buffer (made in-house: 25 millimoles/liter (mM) Tris-hydrochloric acid (HCl), pH 7.5; 0.3 moles/liter (M) sodium chloride (NaCl); 1% NP-40 substitute; 1% sodium deoxycholate; 0.1% sodium dodecyl sulfate (SDS)), collected into an autoclave-sterilized 1.5-mL microcentrifuge tube (VWR; Radnor, Pennsylvania, USA; Cat. No. 89000-028), and centrifuged at maximum speed at 4 degrees Celsius ( $^{\circ}\text{C}$ ) for 20 minutes to remove insoluble material. Protein was quantified using a Pierce<sup>TM</sup> bicinchoninic acid Protein Assay Kit (Thermo Scientific; Waltham, Massachusetts, USA; Cat. No. PI23225).

For co-IP, 50  $\mu\text{g}$  of total protein per sample was incubated with 35  $\mu\text{g}$  of anti-HA agarose beads (Pierce<sup>TM</sup> HA-Tag IP/Co-IP Kit; Thermo Scientific; Cat. No. PI26180) at 4 $^{\circ}\text{C}$  for one hour and then prepared for SDS-polyacrylamide gel electrophoresis (PAGE) by washing ten times with Tris-buffered saline (TBS) containing 0.3M NaCl and 0.05% Tween<sup>TM</sup> 20 (Fisher Scientific; Waltham, Massachusetts, USA; Cat. No. BP337-500), then eluting in non-reducing sample buffer according to the manufacturer's protocol for the HA-Tag IP/Co-IP kit. Samples were then reduced with  $\beta$ -mercaptoethanol (MilliporeSigma; Burlington, Massachusetts, USA; Cat. No. M3148). Additionally, 5  $\mu\text{g}$  of whole cell lysate (WCL) per sample was treated with 5X Laemmli sample buffer containing  $\beta$ -mercaptoethanol (made-in house: 300 mM Tris-HCl, pH 6.8; 50% glycerol;

12.5%  $\beta$ -mercaptoethanol; 10% SDS weight/volume (w/v); 0.025% bromophenol blue) and heated to 95°C for five minutes to prepare for SDS-PAGE.

Equivalent volumes of IP samples and WCL samples were run on denaturing Mini-PROTEAN® TGX™ pre-cast 8-16% gradient polyacrylamide gels (Bio-Rad Laboratories; Hercules, California, USA; Cat. No. 4561106) with Precision Plus Western C standard (Bio-Rad Laboratories; Cat. No. 1610376) and then transferred to Power Blotter Select Polyvinylidene Fluoride (PVDF) Transfer Stacks (Thermo Scientific Invitrogen; Cat. No. PB5240) using the Power Blotter system (Thermo Scientific; Cat. No. PB0012). Membranes were blocked in TBS with Tween™ 20 (TBST; 100 mM Tris-HCl pH 7.5, 0.9% NaCl w/v, 0.1% Tween™ 20; all components Fisher Scientific; Cat. Nos. BP153-500, S271-1, and BP337-500, respectively) with 5% bovine serum albumin (BSA; Fisher Scientific; Cat. No. BP9706100). Membranes were incubated overnight at 4°C with either rabbit mAb against the HA tag (dilution 1:1,000; Cell Signaling Technology; Danvers, Massachusetts, USA; Cat. No. 3724S) or rabbit mAb against MDA5 or LGP2 (dilution 1:1,000; Cell Signaling Technology; Cat. Nos. 5321S and 12869S, respectively), each diluted in TBST with 5% BSA, followed by four washes in TBST. Membranes were then incubated with goat anti-rabbit IgG conjugated to horseradish peroxidase (HRP; dilution 1:5,000; Thermo Scientific Invitrogen; Cat. No. 31460) and Streptactin-HRP (dilution 1:10,000; Bio-Rad Laboratories; Cat. No. 1610380) diluted in TBST with 5% BSA for two hours at room temperature, followed by four washes in TBST. All membranes were incubated with SuperSignal™ West Pico PLUS Chemiluminescent Substrate (Thermo Scientific; Cat. No. 34580) for two minutes and imaged using the iBright™ FL1500 Imaging System (Thermo Scientific; Cat. No. A44241).

For each co-IP/western blot experiment, a duplicate SDS-PAGE gel was run but not transferred and then stained with SimplyBlue™ SafeStain (Thermo Scientific

Invitrogen; Cat. No. LC6065) according to manufacturer instructions to assess consistency of protein loading across wells.

Binding efficiency was evaluated by measuring the amount of MDA5 or LGP2 that co-immunoprecipitated with NiV<sub>M</sub> V wild-type or mutant proteins using densitometry assessed by ImageJ software (National Institutes of Health; Bethesda, Maryland, USA). Briefly, the amount of MDA5 or LGP2 for each well was normalized to the amount of HA-tagged NiV<sub>M</sub> V protein that was pulled down with the anti-HA agarose beads for the same well. Similarly, the total amount of MDA5 or LGP2 protein expressed in each well was normalized to the total amount of HA-tagged NiV<sub>M</sub> V protein expressed in each well. Values are presented as a percentage of wild-type V protein binding (normalized IP/normalized WCL), with wild-type V set to 100%. A representative blot of two replicates is shown in figures with error bars.

### **IFN- $\beta$ luciferase reporter assays**

The IFN- $\beta$  luciferase reporter assay protocol was modified from Guito, *et al*<sup>204</sup>. HEK293T cells were seeded in 48-well plates at a density of  $1 \times 10^5$  cells per well to be 80 to 90% confluent for transfection the next day. For each HA-tagged NiV<sub>M</sub> V plasmid (wild-type or mutant), six wells each were transfected with 160 nanograms (ng) per well (for initial experiments) or 2.5, 5, 10, 20, 40, and 80 ng per well (for titration experiments) of pCAGGS-HA-NiV<sub>M</sub> V, 20 ng per well of p125-Luc or p55-C1b-Luc firefly luciferase vector, and 0.67 ng per well of pGL4.74 *Renilla* luciferase expression plasmid (Promega; Madison, Wisconsin, USA; Cat. No. E6921) as a transfection control, using *TransIT-LT1*. Total plasmid amount was normalized with pHM-GFP GFP expression plasmid (Promega; Cat. No. E6421). Briefly, plasmids and transfection reagent (3  $\mu$ L/ $\mu$ g plasmid) were added to Opti-MEM<sup>TM</sup> I Reduced Serum Medium and incubated at room temperature. During incubation, growth media on the cells was changed to 250  $\mu$ L complete DMEM containing 5% FBS per well, and then transfection

mix was added to cells. At 18 hours post-transfection, triplicate wells of each NiV<sub>M</sub> V plasmid condition were induced with 120 ng per well of pUNO1-hMDA5 expression plasmid, or pHM-GFP as a transfection control, using *TransIT-LT1* as above. At 24 hours post-induction, cells were lysed with 65  $\mu$ L per well of 1X Passive Lysis Buffer (sold as a 5X solution by Promega; Cat. No. E1941 or part of the Dual Luciferase Reporter Assay system) according to manufacturer instructions. After a freeze/thaw cycle at -20°C, readings for firefly and *Renilla* luciferase were obtained using the Dual Luciferase Reporter Assay system (Promega; Cat. No. E1960) and the Cytation 5 plate reader (BioTek Instruments; Winooski, Vermont, USA; Cat. No. 1321022). The ratio of firefly to *Renilla* luciferase expression was calculated for each well, and then fold induction was expressed as the average of the ratio of triplicate wells induced with MDA5 over wells without induction.

### **Minigenome luciferase reporter assays**

A schematic of the minigenome luciferase reporter assay system is shown in **Figure 2-1**. BSR T7/5 cells were seeded in 24-well plates to be 80 to 90% confluent for transfection the next day. Cells in quadruplicate wells were transfected with 187.5 ng per well of pTM1-NiV<sub>M</sub> N<sub>wt</sub> helper plasmid, 100 ng per well of pTM1-NiV<sub>M</sub> L<sub>wt</sub> helper plasmid, 875 ng per well of pNiV-MG-Luc expressing firefly luciferase, 0.25 ng per well of pGL4.74 *Renilla* luciferase expression plasmid as a transfection control, and 0, 12.5, 25, 50, 100, or 200 ng per well of pTM1-HA-NiV<sub>M</sub> P wild-type or mutant plasmid, using *TransIT-LT1*. Total plasmid amount was normalized with pHM-GFP GFP expression plasmid. Briefly, plasmids and transfection reagent (3  $\mu$ L/ $\mu$ g plasmid) were added to Opti-MEM<sup>TM</sup> I Reduced Serum Medium and incubated at room temperature. During incubation, growth media on the cells was changed to 500  $\mu$ L complete DMEM containing 5% FBS per well, and then transfection mix was added to cells. At 24 hours post-transfection, cells were lysed with 100  $\mu$ L per well of 1X Passive Lysis Buffer

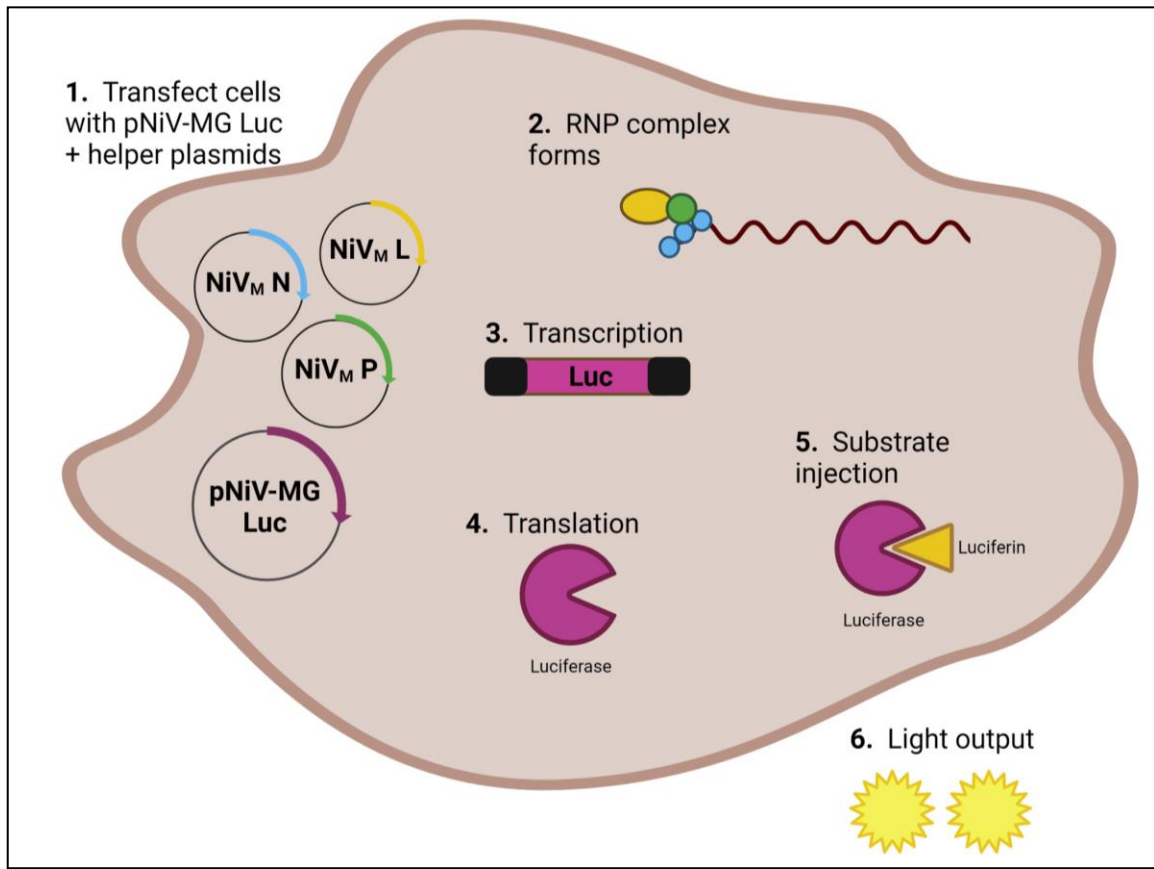


**Figure 2-1: NiV minigenome luciferase reporter system**

Diagram of the minigenome luciferase reporter assay in BSR T7/5 cells, which stably express bacteriophage T7 polymerase. **1.** Cells were transfected with the NiV minigenome luciferase plasmid and with helper plasmids encoding NiV<sub>M</sub> N, NiV<sub>M</sub> P, and NiV<sub>M</sub> L, all under the control of the T7 promoter. **2.** The helper plasmids were transcribed and translated to produce NiV<sub>M</sub> N, P, and L proteins; the NiV minigenome plasmid was transcribed to produce the minigenomic RNA encoding firefly luciferase flanked by the 3' leader and 5' trailer of the NiV<sub>M</sub> genome. Together, the proteins and RNA formed the RNP complex. **3.** The RNA genome was transcribed to produce mRNA encoding the minigenome luciferase construct. **4.** The mRNA was translated to produce firefly luciferase enzyme. **5.** Addition of luciferin substrate to the cells allowed luciferase to bind to the luciferin, which caused light to be produced (**6**), which was read using the Cytation 5 plate reader. Figure created using BioRender.com.

according to manufacturer instructions. After a freeze/thaw cycle at -20°C, readings for firefly and *Renilla* luciferase were obtained using the Dual Luciferase Reporter Assay system and Cytation 5 plate reader. Average values for quadruplicate wells were expressed as the ratio of firefly to *Renilla* for each condition.

### **Statistics**

For co-IP/western blot densitometry graphs, error bars represent the standard error of the mean (SEM) of two biological replicates. Statistical differences were calculated using Prism software (GraphPad Software; San Diego, California, USA) and represent comparisons to the wild-type NiV<sub>M</sub> V control by one-way analysis of variance (ANOVA). \*, P < 0.05; †, P < 0.01; ‡, P < 0.001 as compared to wild-type control by Dunnett's Multiple Comparison Test following one-way ANOVA.

For IFN-β luciferase reporter assays, error bars represent the SEM of three biological replicates. For minigenome luciferase reporter assays, error bars represent the SEM of four biological replicates. Statistical differences were calculated using Prism software and represent comparisons to the wild-type NiV<sub>M</sub> V (IFN-β reporter assays) or the wild-type NiV<sub>M</sub> P (minigenome assays) controls by two-way ANOVA. \*, P < 0.05; †, P < 0.01; ‡, P < 0.001 as compared to wild-type control by Bonferroni posttests following two-way ANOVA.

## **RESULTS**

### **A single amino acid facilitated NiV<sub>M</sub> V binding to MDA5 and conferred inhibited MDA5-induced IFN-β production**

Because previous efforts to ascertain the specific binding site of NiV to MDA5 were unsuccessful, plasmids encoding mutant V proteins with overlapping alanine scanning regions were designed in order to narrow down the specific binding site. Each plasmid replaced ten amino acids in the NiV<sub>M</sub> V CTD (amino acids 408-456, 49 amino

acids total) with alanine residues (**Figure 2-2**). These plasmids were ordered from Mutagenex, Inc. in the pCAGGS expression plasmid backbone<sup>199</sup> and contained an HA tag at the N-terminus of the V protein (**Figure 2-2A**). The plasmids were designed to allow the determination of the NiV<sub>M</sub> V binding site to MDA5 down to a resolution of five amino acids, as that was the magnitude of the overlap of the alanine residues across mutants.

**Figure 2-3A** shows the results of a co-IP/western blot assay to assess the binding of the alanine scanning mutants to overexpressed human MDA5 in HEK293T cells. A pCAGGS-HA empty vector plasmid and a plasmid encoding only the NTD of NiV<sub>M</sub> V were included as negative controls, while full-length, wild-type NiV<sub>M</sub> V protein as well as an acellular HA positive control included in the co-IP kit served as positive controls. Input blots in which WCL was probed with antibodies against HA or MDA5 were included to show equal loading of HA-tagged V protein and MDA5 overexpressed protein in each lane. Densitometry to quantify binding of each mutant to MDA5 as a percentage of binding of wild-type V protein to MDA5 is shown in **Figure 2-3B**. All alanine scanning mutants demonstrated decreased ability to bind to MDA5, particularly the first three mutants. However, a more specific binding site could not be determined based on these results. For LGP2, which is hypothesized to share the MDA5 binding site based on results for MeV<sup>130,193</sup>, the alanine scanning mutants showed a uniformly decreased ability to bind compared to wild-type NiV<sub>M</sub> V (**Figures 2-3C and 2-3D**).

The CTD of the paramyxoviral V protein has a highly ordered secondary structure, containing multiple  $\beta$ -sheets and anchored by seven conserved cysteine residues that bind two zinc ions<sup>193,196,205,206</sup>. A simple schematic of the NiV<sub>M</sub> V CTD is shown in **Figure 2-4A**, with the NiV<sub>M</sub> V amino acid positions of the conserved cysteine residues indicated. Clearly, the mutation of stretches of ten amino acids to alanine removed the anchoring cysteine residues and disrupted the secondary structure of the

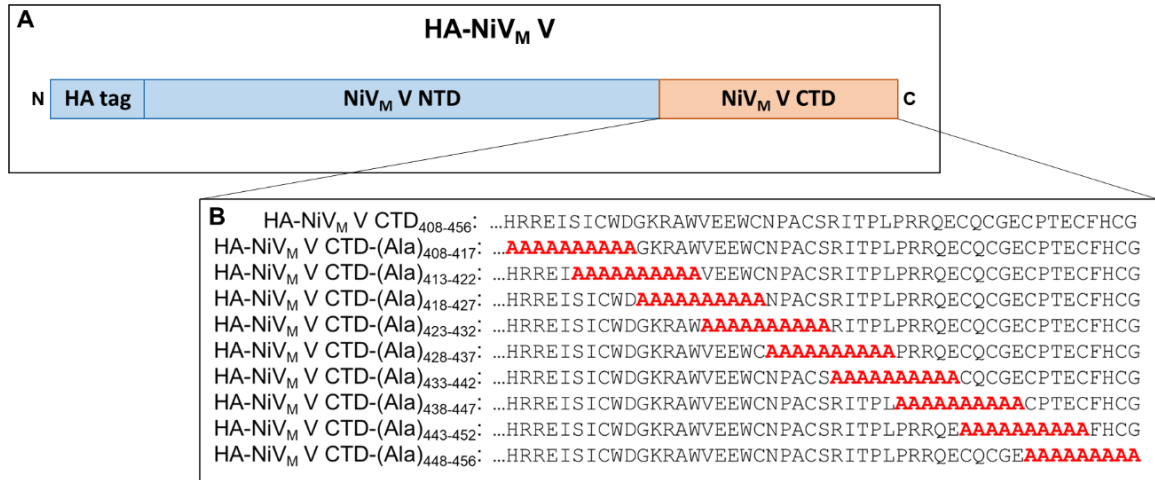


**Figure 2-2: The HA-NiV<sub>M</sub> V protein and 10-alanine scanning mutants used in plasmid overexpression studies**

**(A)** Schematic of the protein produced by the pCAGGS-HA-NiV<sub>M</sub> V expression plasmid. The N- and C-termini are indicated, and the domains of the HA-tagged V protein produced by expression of the plasmid are shown as boxes. The HA tag and the NTD of the V protein are shown in blue, while the unique CTD of the V protein is shown in pink.

**(B)** Amino acid sequences (one-letter codes) of the NiV<sub>M</sub> CTD only, indicating the residues replaced with alanine (represented by “Ala” in the name of each mutant and with red letters in the sequence) in each of the 10-alanine scanning mutants and their amino acid positions within the V protein. All numbers represent the amino acid position within the full-length NiV<sub>M</sub> V protein.

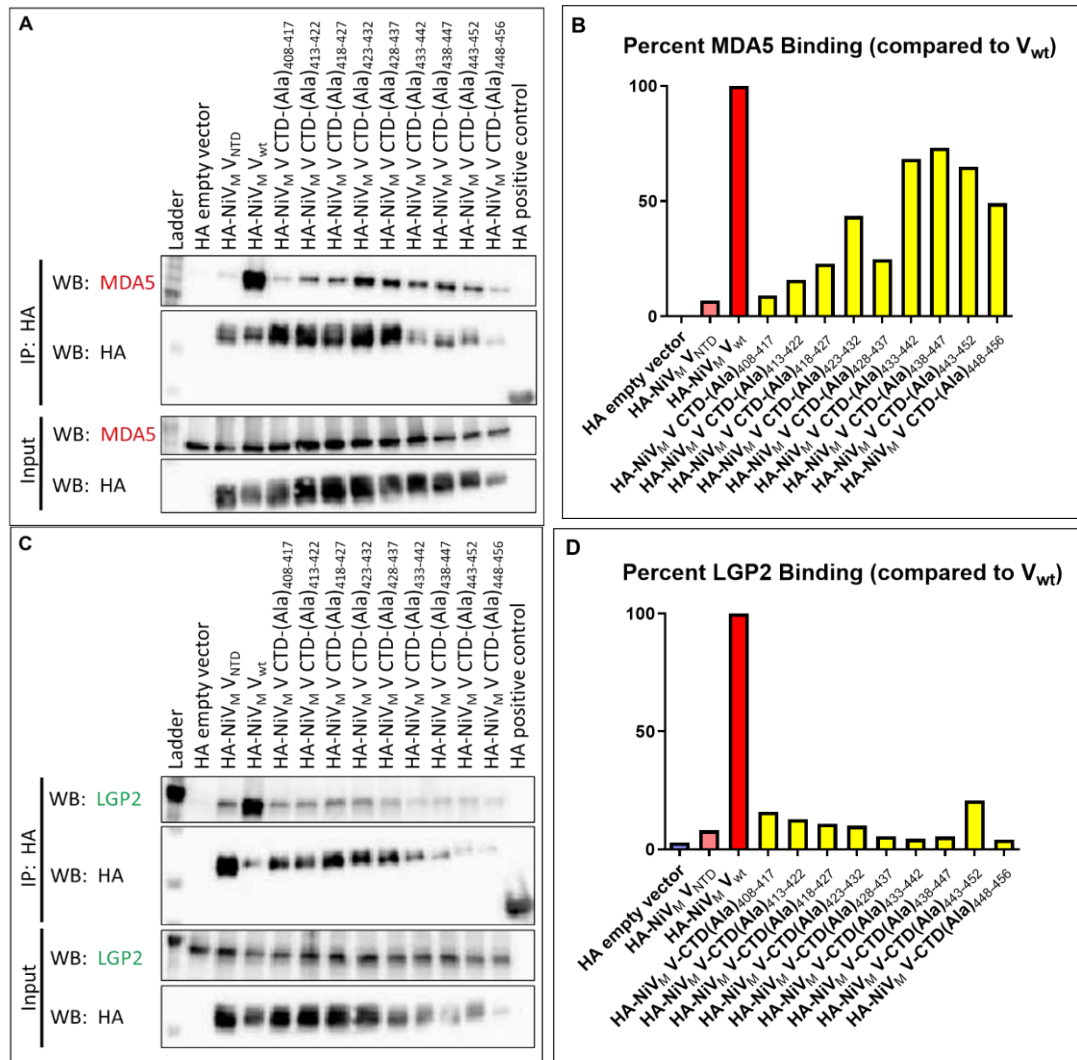


**Figure 2-3: All NiV<sub>M</sub> alanine scanning mutants demonstrate reduced MDA5 and LGP2 binding**

(Panels A and C) Co-IP/western blot results after pulldown of HA-tagged NiV<sub>M</sub> V proteins containing alanine scanning mutations and bound overexpressed (A) MDA5 or (C) LGP2. The first two lanes of each panel (an empty vector plasmid and a plasmid encoding only the NTD of NiV<sub>M</sub> V) serve as negative controls, while the third and thirteenth lanes of each panel (a plasmid encoding wild-type, full-length NiV<sub>M</sub> V and an acellular recombinant HA protein included with the co-IP kit) serve as positive controls. The bottom two WCL input blots in each panel demonstrate that approximately equal amounts of protein were loaded on each lane. MDA5 is visible at about 140 kDa, while LGP2 runs at around 80 kDa. The HA-tagged NiV<sub>M</sub> V proteins are 50 to 56 kDa, and the acellular positive control runs at around 37 kDa. (Panels B and D) Quantification of the results in panels (A) and (C) by densitometry. Panel (B) shows the amount of binding to MDA5 by each mutant, expressed as a ratio of the normalized IP fraction (MDA5/HA) to the normalized WCL fraction (MDA5/HA). Panel (D) shows the results of the same calculations for LGP2 binding. Wild-type NiV<sub>M</sub> V has been set to 100% for each panel, and all other lanes are expressed in relation to the wild-type lane.

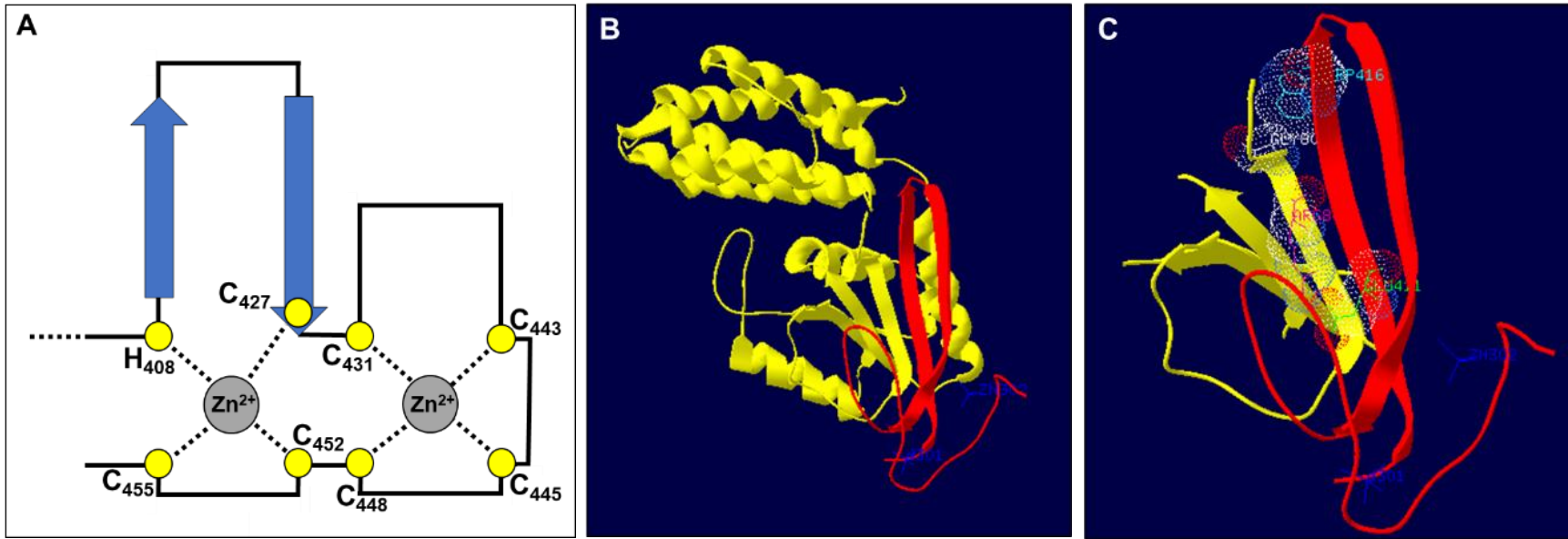


**Figure 2-4: Secondary structure of the NiV<sub>M</sub> V CTD and residues potentially involved in binding to MDA5**

(A) Schematic of the CTD of the NiV<sub>M</sub> V protein, with  $\beta$ -sheets indicated as blue arrows and conserved histidine (H) and cysteine (C) residues shown as yellow circles. The amino acid position of the conserved residues is given. The zinc ions bound by the NiV<sub>M</sub> V CTD are shown as grey circles. Figure modified from Li, *et al.*, *Cell* 2006 and Uchida, *et al.*, *Sci Rep* 2018<sup>196,205</sup>. (B) Ribbon diagram of the NiV<sub>M</sub> V CTD (shown in red) in complex with porcine MDA5 (shown in yellow), modified from Motz, *et al.*, *Science* 2013 (PDB ID 4I1S)<sup>193</sup>.  $\alpha$ -helices and  $\beta$ -sheets are indicated. (C) Close-up view of the interface between NiV<sub>M</sub> V and MDA5. Glutamic acid 411 on NiV<sub>M</sub> V is shown in lime green, and arginine 803 on MDA5 is shown in pink; the interaction of the negatively charged oxygen atoms (red dots) on GLU411 with the positively charged nitrogen atoms (blue dots) on ARG803 is visible. Tryptophan 416 on NiV<sub>M</sub> V is shown in cyan, and glycine 805 on MDA5 is shown in white; their Van der Waals radii (white dots) overlap. For panels (B) and (C), bound zinc ions are shown in blue and are labeled d301 and ZN302. Panels (B) and (C) were made using Swiss PDB Viewer software (<https://spdbv.vital-it.ch/>).

domain. Therefore, the degree of disruption of binding to MDA5 and LGP2 was similar across all the alanine scanning mutants, thus preventing the determination of a specific binding site. Instead, point mutations that could be involved in binding to MDA5 by NiV V were predicted. Swiss PDB Viewer (<https://spdbv.vital-it.ch/>) was used to thread the amino acid sequence of the NiV<sub>M</sub> V CTD onto a published crystal structure of the PIV5 V CTD in complex with MDA5<sup>193</sup>. No steric hindrance was observed after threading the NiV<sub>M</sub> V CTD residues onto the PIV5 V CTD structure, which was corroborated by recent experimental evidence that the secondary structure of the NiV V CTD recapitulates that of other paramyxoviruses<sup>206</sup>. **Figure 2-4B** shows ribbon diagrams of the NiV<sub>M</sub> V CTD (red) in complex with the MDA5 superfamily 2 ATPase domain (yellow). The  $\beta$ -sheets of the NiV<sub>M</sub> V CTD interleave with  $\beta$ -sheets in the ATPase domain and displace them. As shown in **Figure 2-4C**, a salt bridge is formed between a negatively charged glutamic acid (E, shown in lime green) on the V protein and a positively charged arginine (R, shown in pink) on MDA5. Also, there is a pocket formed by glycine (G, shown in white) on MDA5 into which a tryptophan (W, shown in cyan) on the V protein can fit; their Van der Waals radii overlap. These residues are conserved among paramyxoviruses, including NiV (**Figure 2-5A**) and among MDA5 and LGP2 in mammals and birds (**Figure 2-5B**), meaning they likely play a conserved role and making them attractive targets for investigation.

Importantly, vertebrate RIG-I has a leucine in place of arginine and a glutamic acid in place of glycine (**Figure 2-5B**), so it is unable to participate in the electrostatic interaction with glutamic acid on the V CTD and sterically hinders interaction with tryptophan<sup>193,195</sup>. NiV V is hypothesized to block RIG-I signaling via a distinct mechanism, either by binding to LGP2 and forming a complex which then interacts with RIG-I<sup>131</sup> or by interacting directly with the CARDS of RIG-I instead of the helicase domain<sup>111</sup>.



Based on the structure and interactions shown in **Figure 2-4C**, E411 and W416 of NiV<sub>M</sub> V were mutated to interrogate their ability to bind to MDA5. Expression plasmids encoding HA-tagged NiV<sub>M</sub> V protein with a combination of E411A and either W416S (polar) or W416L (nonpolar) mutations in the pCAGGS backbone were ordered from Mutagenex, Inc., as before (**Figure 2-6**). **Figure 2-7A** shows the results of a co-IP/western blot with these mutants. Surprisingly, the E411 and W416 mutations, singly or in combination with each other, did not cause a defect in binding to MDA5 by NiV<sub>M</sub> V, as shown in the densitometry in **Figure 2-7B**. However, an IFN- $\beta$  luciferase reporter assay was carried out to determine whether the point mutants exhibited a functional defect in IFN- $\beta$  induction. Interestingly, a dose-dependent effect on downstream induction of IFN- $\beta$  was observed for the point mutants; at low amounts of NiV<sub>M</sub> V, the mutant viral proteins partially lost the ability to inhibit the production of IFN- $\beta$  in an NF- $\kappa$ B-independent fashion (**Figure 2-8**).

Since mutations of E411 and W416 did not cause the expected defect in binding and marked loss of ability to inhibit IFN- $\beta$ , and because mutations of ten amino acids at a time disrupted the highly ordered secondary structure of the NiV<sub>M</sub> V CTD, smaller alanine scanning mutations were made in order to narrow down the binding site of MDA5 by NiV<sub>M</sub> V. Because the binding sites for the related paramyxoviruses MeV, CDV, and PIV5 were isolated to the beginning of the V CTD<sup>193,194</sup>, only the first 15 amino acids were mutated. This approach was corroborated by a study by Uchida, *et al.*, in which alanine scanning mutations of three amino acids each at the beginning of the NiV<sub>M</sub> V CTD caused a decrease in ability to inhibit IFN- $\beta$  induction after stimulation with MDA5<sup>196</sup>. Two sets of overlapping alanine scanning mutants were made, containing three amino acids each, offset by one amino acid, to increase the potential resolution to which the binding site could be detected (**Figure 2-9**). As before, plasmids containing the designed mutations were generated using site-directed mutagenesis by Mutagenex, Inc. and contained an N-terminal HA tag. As shown in **Figure 2-10**, two of the mutants

	<u>R<sub>409</sub></u>	<u>R<sub>410</sub></u>	<u>E<sub>411</sub></u>	<u>I<sub>412</sub></u>	<u>S<sub>413</sub></u>	<u>I<sub>414</sub></u>	<u>C<sub>415</sub></u>	<u>W<sub>416</sub></u>	<u>D<sub>417</sub></u>	<u>G<sub>418</sub></u>
HA-NiV <sub>M</sub> V <sub>409-418</sub> :	...aga	cgc	gaa	ata	tcc	atc	tgc	tgg	gac	gga...
HA-NiV <sub>M</sub> V <sub>E411A-1</sub> :	...aga	cgc	<u>A<sub>411</sub></u> gca	ata	tcc	atc	tgc	tgg	gac	gga...
HA-NiV <sub>M</sub> V <sub>E411A-2</sub> :	...aga	cgc	<u>A<sub>411</sub></u> gcg	ata	tcc	atc	tgc	tgg	gac	gga...
HA-NiV <sub>M</sub> V <sub>W416L</sub> :	...aga	cgc	gaa	ata	tcc	atc	tgc	<u>L<sub>416</sub></u> t <del>t</del> g	gac	gga...
HA-NiV <sub>M</sub> V <sub>W416S</sub> :	...aga	cgc	gaa	ata	tcc	atc	tgc	<u>S<sub>416</sub></u> t <del>t</del> g	gac	gga...
HA-NiV <sub>M</sub> V <sub>E411A-2/W416L</sub> :	...aga	cgc	<u>A<sub>411</sub></u> gcg	ata	tcc	atc	tgc	<u>L<sub>416</sub></u> t <del>t</del> g	gac	gga...
HA-NiV <sub>M</sub> V <sub>E411A-2/W416S</sub> :	...aga	cgc	<u>A<sub>411</sub></u> gcg	ata	tcc	atc	tgc	<u>S<sub>416</sub></u> t <del>t</del> g	gac	gga...

**Figure 2-6: Point mutants made in the pCAGGS-HA-NiV<sub>M</sub> V expression plasmid**

E411 and W416 point mutations made in the pCAGGS-HA-NiV<sub>M</sub> V expression plasmid are shown. Nucleotide sequences, split into codons, are shown in lowercase letters. One-letter codes of the amino acids encoded by the codons are shown in uppercase letters in black at the top of the chart. Changes made from wild-type NiV<sub>M</sub> V are indicated in red. All numbers represent the amino acid position within the full-length NiV<sub>M</sub> V protein.

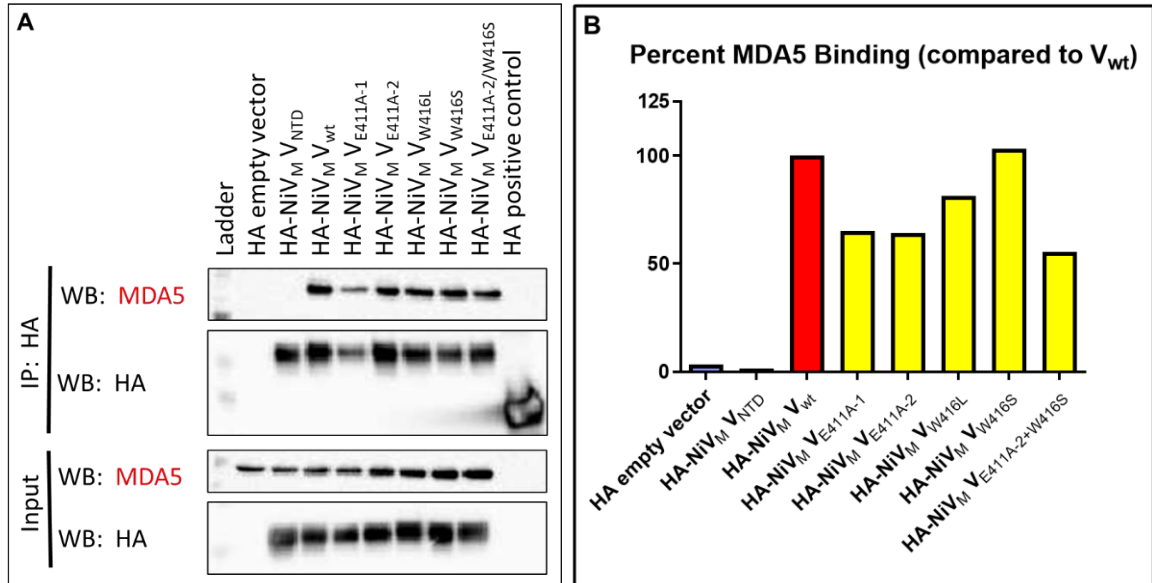


**Figure 2-7: NiV<sub>M</sub> E411 and W416 point mutants did not demonstrate reduced MDA5 binding**

(A) Co-IP/western blot results after pulldown of HA-tagged NiV<sub>M</sub> V proteins containing E411 and W416 point mutations and bound overexpressed MDA5. The second and third lanes (an empty vector plasmid and a plasmid encoding only the NTD of NiV<sub>M</sub> V) served as negative controls, while the fourth and tenth lanes (a plasmid encoding wild-type, full-length NiV<sub>M</sub> V and an acellular recombinant HA protein included with the co-IP kit) served as positive controls. The bottom two WCL input blots demonstrated that approximately equal amounts of protein were loaded on each lane. MDA5 is visible at about 140 kDa, the HA-tagged NiV<sub>M</sub> V proteins are 50 to 56 kDa, and the acellular positive control runs at around 37 kDa. (B) Quantification of the results in panel (A) by densitometry. The amount of binding to MDA5 by each mutant is expressed as a ratio of the normalized IP fraction (MDA5/HA) to the normalized WCL fraction (MDA5/HA). Wild-type NiV<sub>M</sub> V has been set to 100% for each panel, and all other lanes are expressed in relation to the wild-type lane.

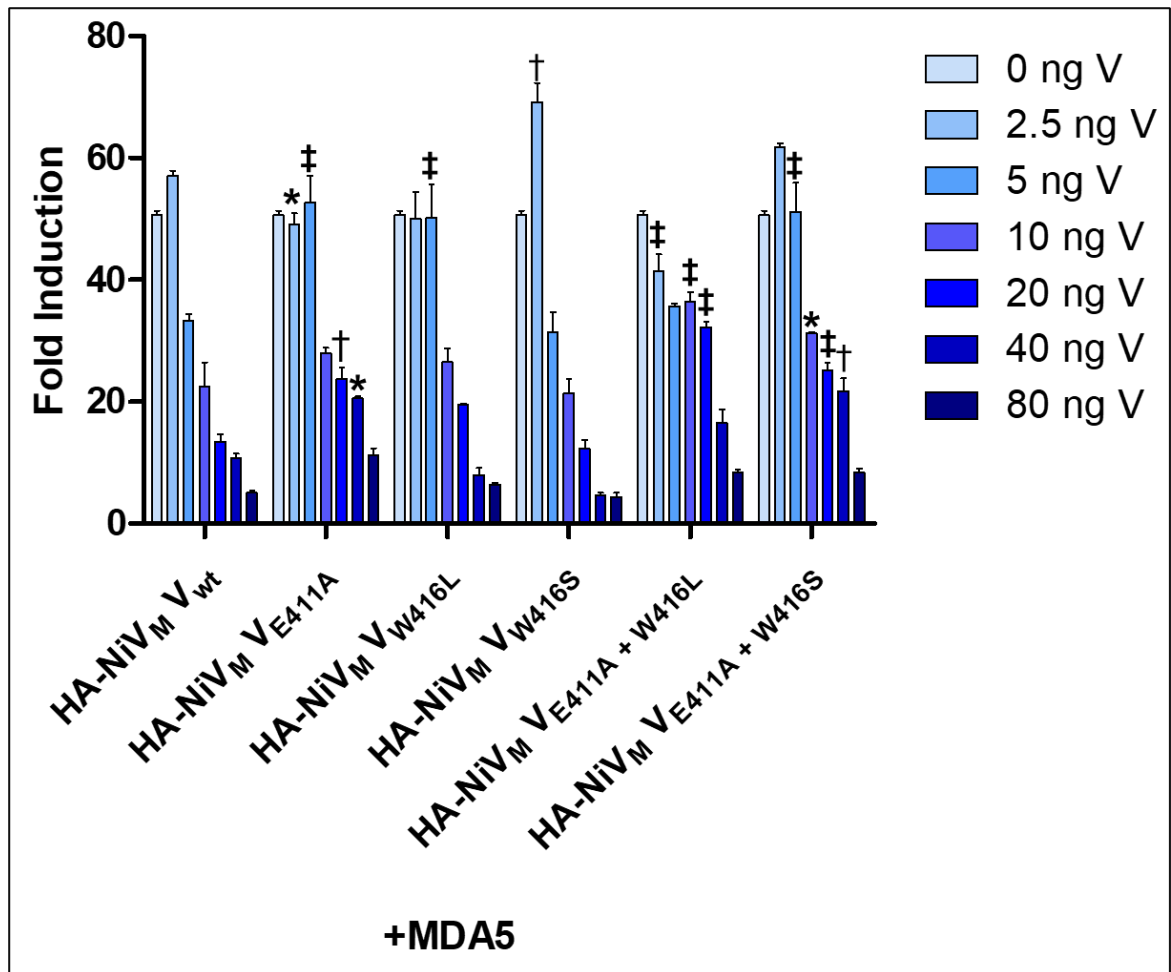


**Figure 2-8: Point mutants exhibited a reduced ability to inhibit IFN- $\beta$  in an NF- $\kappa$ B-independent manner at lower concentrations**

IFN- $\beta$  luciferase reporter assay results for the indicated amount of HA-tagged NiV<sub>M</sub> V expression plasmid per condition and a luciferase reporter encoding only the IRF3/IRF7 binding sites of the human IFN- $\beta$  promoter are shown. The HA-NiV<sub>M</sub> V<sub>wt</sub> condition served as a positive control of inhibition of IFN- $\beta$  by wild-type NiV<sub>M</sub> V protein. Values are expressed as fold induction of MDA5-induced samples compared to samples that were not induced with MDA5. Error bars represent the SEM for three replicates. \*, P<0.05; †, P<0.01; ‡, P<0.001 as compared to wild-type V control by Bonferroni posttests following two-way ANOVA.

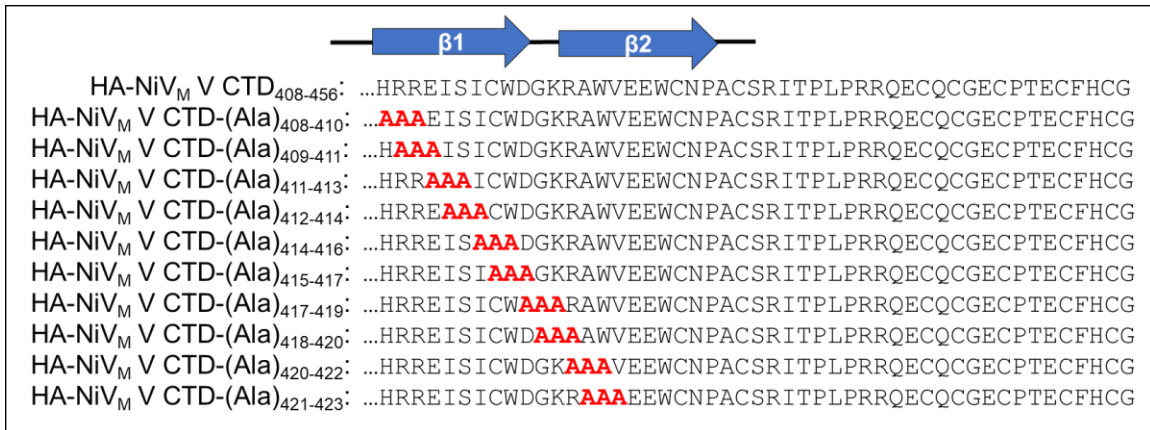


**Figure 2-9: Sequence of three-alanine scanning mutants in pCAGGS-HA-NiV<sub>M</sub> V expression plasmids**

Amino acid sequences (one-letter codes) of the NiV<sub>M</sub> V CTD only, indicating the residues replaced with alanine (represented by “Ala” in the name of each mutant and with red letters in the sequence) in each of the three-alanine scanning mutants and their amino acid positions within the V protein. All numbers represent the amino acid position within the full-length NiV<sub>M</sub> V protein. The β-sheets present in the NiV<sub>M</sub> V CTD are indicated as blue arrows.

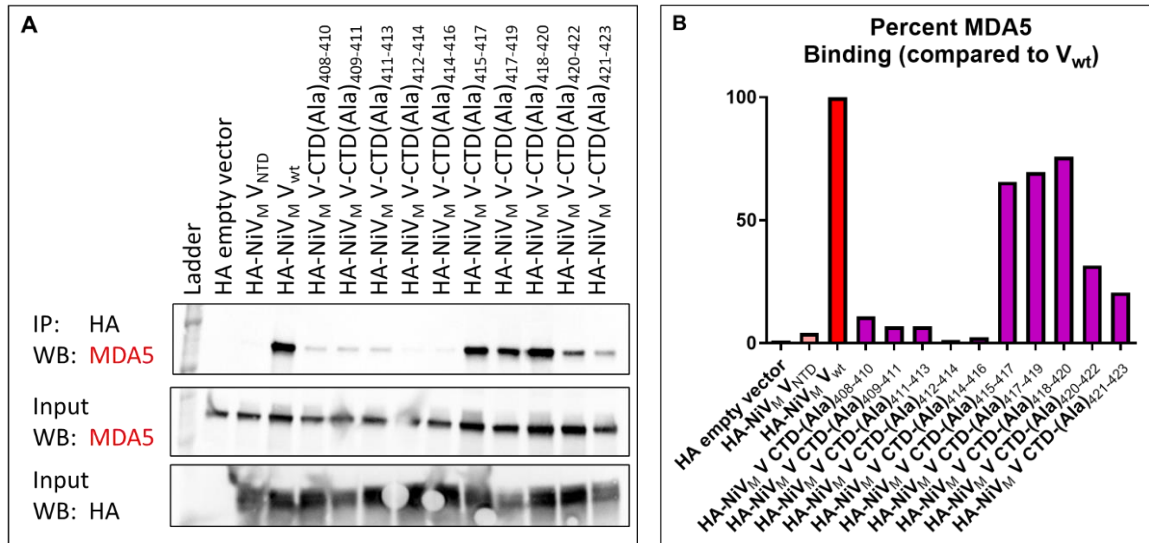


**Figure 2-10: NiV<sub>M</sub> V alanine scanning mutants of three amino acids each revealed nuances of MDA5 binding**

**(A)** Co-IP/western blot results after pulldown of HA-tagged NiV<sub>M</sub> V proteins containing alanine scanning mutations in the CTD along with bound overexpressed MDA5. The second and third lanes (an empty vector plasmid and a plasmid encoding only the NTD of NiV<sub>M</sub> V) served as negative controls, while the fourth lane (a plasmid encoding wild-type, full-length NiV<sub>M</sub> V) served as a positive control. The bottom two WCL input blots demonstrated that approximately equal amounts of protein were loaded on each lane. MDA5 is visible at about 140 kDa, and the HA-tagged NiV<sub>M</sub> V proteins are 50 to 56 kDa. **(B)** Quantification of the results in panel (A) by densitometry. The amount of binding to MDA5 by each mutant is expressed as a ratio of the normalized IP fraction (MDA5/HA) to the normalized WCL fraction (MDA5/HA). Wild-type NiV<sub>M</sub> V has been set to 100% for each panel, and all other lanes are expressed in relation to the wild-type lane.

demonstrated a near-complete defect in binding compared to wild-type NiV<sub>M</sub> V protein. The only amino acid shared by these two mutants was the isoleucine at amino acid position 414. Like the E411 and W416 point mutants, several of these alanine scanning mutants exhibited a partial loss of ability to inhibit NF-κB-independent IFN-β induction at moderate concentrations (**Figure 2-11**). Although only a few of the alanine scanning mutants were statistically significantly less able to inhibit IFN-β induction than the same amount of wild-type NiV<sub>M</sub> V plasmid, the mutants containing I414A trended toward a loss of ability to inhibit IFN-β induction as compared to wild-type NiV<sub>M</sub> V at moderate plasmid concentrations (**Figure 2-11**). These results corroborate those published previously, in which alanine scanning mutants near the beginning of the NiV<sub>M</sub> CTD were least able to inhibit downstream IFN-β induction; a construct including I414A in that study showed results comparable to the vector control<sup>196</sup>.

To further corroborate and characterize the necessity of I414 for NiV<sub>M</sub> V-MDA5 binding, expression plasmids encoding the I414A point mutation were generated. Again, Mutagenex, Inc. generated expression plasmids containing an N-terminal HA tag and either the I414A mutation in isolation or with E411A as a double mutant (**Figure 2-12**). As shown in **Figure 2-13**, the mutants recapitulate the near-complete defect in binding observed for the alanine scanning mutations. Therefore, I414 is critical for NiV<sub>M</sub> binding to MDA5. Moderate amounts of V proteins containing point mutations rendering them unable to bind to MDA5 exhibited a modest loss of ability to inhibit IFN-β induction in an NF-κB-independent manner (**Figure 2-14**). Again, these results corroborate previously published work, in which presence of the I414A mutation resulted in a complete loss of ability to inhibit IFN-β induction following stimulation with MDA5<sup>196</sup>. These experiments constitute the first description of the specific binding site of MDA5 by NiV V protein and the first characterization of the effect of binding on downstream signaling.

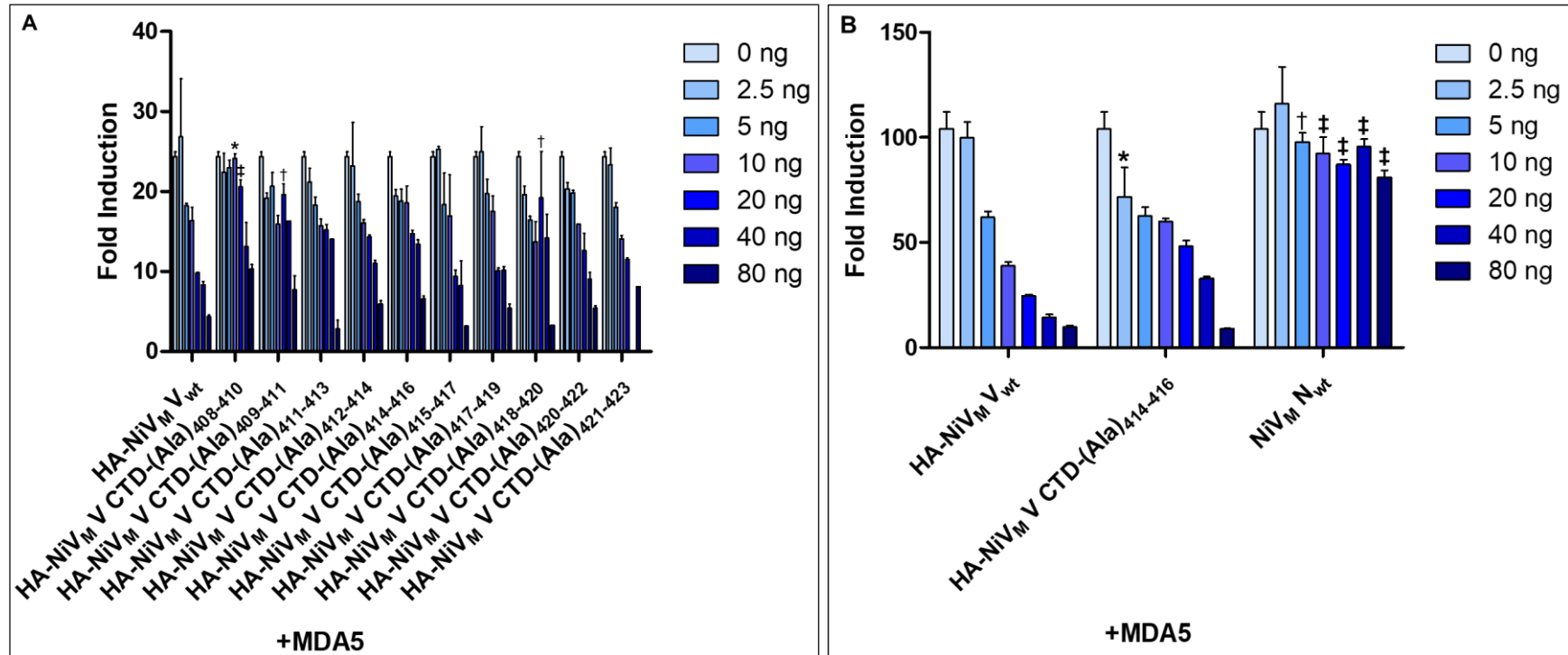


**Figure 2-11: NiV<sub>M</sub> V alanine scanning mutants of three amino acids each exhibited a reduced ability to inhibit IFN- $\beta$  in an NF- $\kappa$ B-independent manner at lower concentrations**

IFN- $\beta$  luciferase reporter assay results for the indicated amount of HA-tagged NiV<sub>M</sub> V expression plasmid per condition and a luciferase reporter encoding only the IRF3/IRF7 binding sites of the human IFN- $\beta$  promoter for (A) all alanine scanning mutants of three amino acids each and (B) a separate assay showing a representative mutant containing the I414A mutation as well as an additional control, NiV<sub>M</sub> N<sub>wt</sub>, which did not inhibit IFN- $\beta$  induction in this reporter assay. The HA-NiV<sub>M</sub> V<sub>wt</sub> condition served as a positive control of inhibition of IFN- $\beta$  by wild-type NiV<sub>M</sub> V protein. Values are expressed as fold induction of MDA5-induced samples compared to samples that were not induced with MDA5. Error bars represent the SEM for three replicates. \*, P<0.05; †, P<0.01; ‡, P<0.001 as compared to wild-type V control by Bonferroni posttests following two-way ANOVA.

	<u>R<sub>409</sub></u>	<u>R<sub>410</sub></u>	<u>E<sub>411</sub></u>	<u>I<sub>412</sub></u>	<u>S<sub>413</sub></u>	<u>I<sub>414</sub></u>	<u>C<sub>415</sub></u>	<u>W<sub>416</sub></u>	<u>D<sub>417</sub></u>	<u>G<sub>418</sub></u>
HA-NiV <sub>M</sub> V <sub>409-418</sub> :	...aga	cgc	gaa	ata	tcc	atc	tgc	tgg	gac	gga...
HA-NiV <sub>M</sub> V <sub>I414A</sub> :	...aga	cgc	gaa	ata	tcc	<u>A<sub>414</sub></u> <u>gct</u>	tgc	tgg	gac	gga...
HA-NiV <sub>M</sub> V <sub>E411A-2/I414A</sub> :	...aga	cgc	<u>A<sub>411</sub></u> <u>gcg</u>	ata	tcc	<u>A<sub>414</sub></u> <u>gct</u>	tgc	tgg	gac	gga...

**Figure 2-12: Additional point mutations made in the pCAGGS-HA-NiV<sub>M</sub> V expression plasmid**

Additional E411 and I414 point mutations made in the pCAGGS-HA-NiV<sub>M</sub> V expression plasmid are shown. Nucleotide sequences, split into codons, are shown in lowercase letters. One-letter codes of the amino acids encoded by the codons are shown in uppercase letters in black at the top of the chart. Changes made from wild-type NiV<sub>M</sub> V are shown in red. All numbers represent the amino acid position within the full-length NiV<sub>M</sub> V protein.

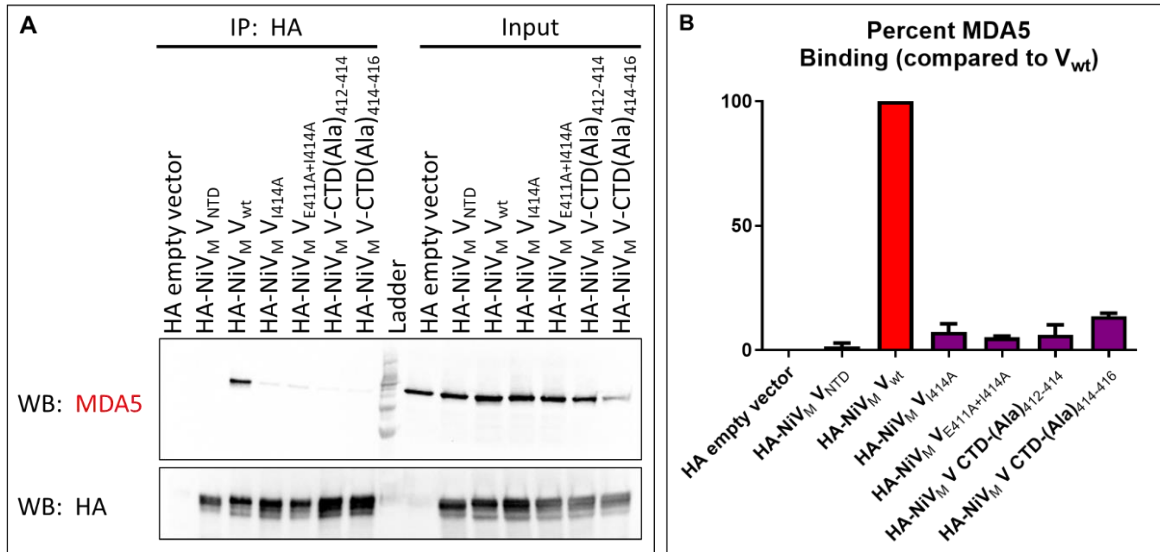


**Figure 2-13: I414A point mutants lose the ability to bind to MDA5 in a co-IP/western blot assay**

(A) Co-IP/western blot results after pulldown of HA-tagged NiV<sub>M</sub> V proteins containing point mutations designed to inhibit MDA5 binding along with bound overexpressed MDA5. The first and second lanes (an empty vector plasmid and a plasmid encoding only the NTD of NiV<sub>M</sub> V) served as negative controls, while the third lane (a plasmid encoding wild-type, full-length NiV<sub>M</sub> V) served as a positive control. The right half of the blot shows WCL to demonstrate that approximately equal amounts of protein were loaded on each lane. MDA5 is visible at about 140 kDa, and the HA-tagged NiV<sub>M</sub> V proteins are 50 to 56 kDa. (B) Quantification of the results in panel (A) by densitometry. The amount of binding to MDA5 by each mutant is expressed as a ratio of the normalized IP fraction (MDA5/HA) to the normalized WCL fraction (MDA5/HA). Wild-type NiV<sub>M</sub> V has been set to 100% for each panel, and all other lanes are expressed in relation to the wild-type lane. Error bars represent the SEM of two independent replicates.

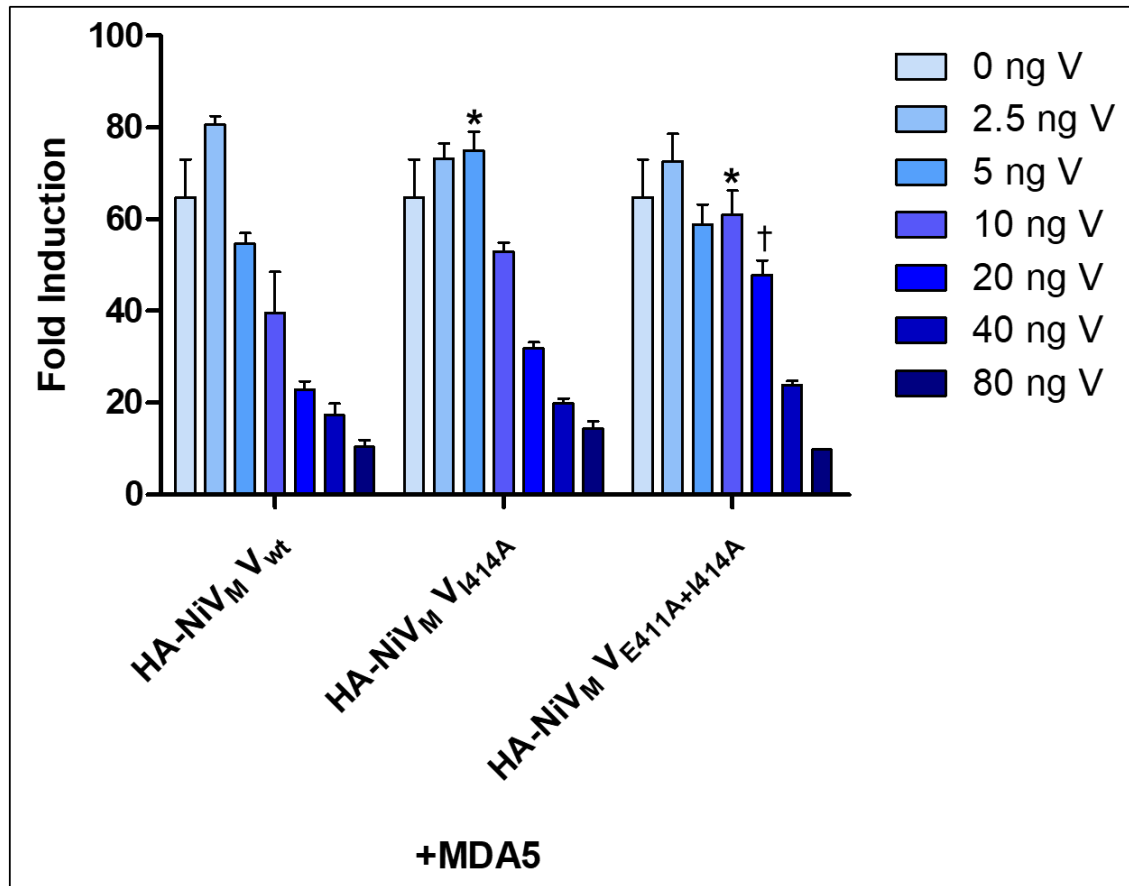


**Figure 2-14: NiV<sub>M</sub> V I414A point mutants exhibited a reduced ability to inhibit IFN- $\beta$  in an NF- $\kappa$ B-independent manner at moderate concentrations**

IFN- $\beta$  luciferase reporter assay results for the indicated amount of HA-tagged NiV<sub>M</sub> V expression plasmid per condition and a luciferase reporter encoding only the IRF3/IRF7 binding sites of the human IFN- $\beta$  promoter. The HA-NiV<sub>M</sub> V<sub>wt</sub> condition served as a positive control of inhibition of IFN- $\beta$  by wild-type NiV<sub>M</sub> V protein. Values are expressed as fold induction of MDA5-induced samples compared to samples that were not induced with MDA5. Error bars represent the SEM for three replicates. \*, P<0.05 as compared to wild-type V control by Bonferroni posttests following two-way ANOVA.

### **Unlike MeV, NiV<sub>M</sub> did not use the same interface for binding to LGP2 as for MDA5**

Because the mechanism of paramyxoviral inhibition of MDA5 and LGP2 is hypothesized to be shared<sup>130</sup>, the ability of the I414A mutation to prevent binding to LGP2 by NiV<sub>M</sub> V was evaluated. The results of a co-IP/western blot for LGP2 are shown in **Figure 2-15A**. Although the point mutation I414A appeared to reduce LGP2 binding compared to wild-type NiV<sub>M</sub> V, LGP2 remained detectable, unlike the more complete abrogation of MDA5 binding. Densitometry analysis, shown in **Figure 2-15B**, indicated that the point mutations appeared to inhibit binding by about 70%. Therefore, I414 appears to be a part of the NiV<sub>M</sub> V-LGP2 binding site, but there are likely other amino acids involved. Additional replicates are needed to confirm this result, although **Figure 2-15B** shows the mean and SEM of two replicates of this co-IP/western blot.

### **Point mutations are not likely to inhibit viral replication in full-length rNiV**

Because NiV V shares an ORF with P and W, nucleotide changes to V will also alter the sequence of P and W in the context of the complete viral genome. P is an essential, structural protein, and even small changes or deletions can have large impacts on viral replication depending on their location<sup>66</sup>. Therefore, checking for possible interference with viral transcription and translation using a minigenome luciferase assay was important before attempting to recover full-length rNiVs containing MDA5-binding mutations. This assay uses light output as a proxy for viral activity, so any differences between wild-type P protein and MDA5-binding mutant P protein could indicate that the mutations are deleterious to viral replication. Mutations that did not affect viral replication in the absence of innate immune signaling were necessary to prevent confounding effects of reduced viral replication from complicating analysis of differences in innate immune evasion function mediated by V protein.

The results of the minigenome reporter assays are shown in **Figure 2-16**. Paramyxoviruses require a precise ratio of N to P to L protein for efficient replication, so

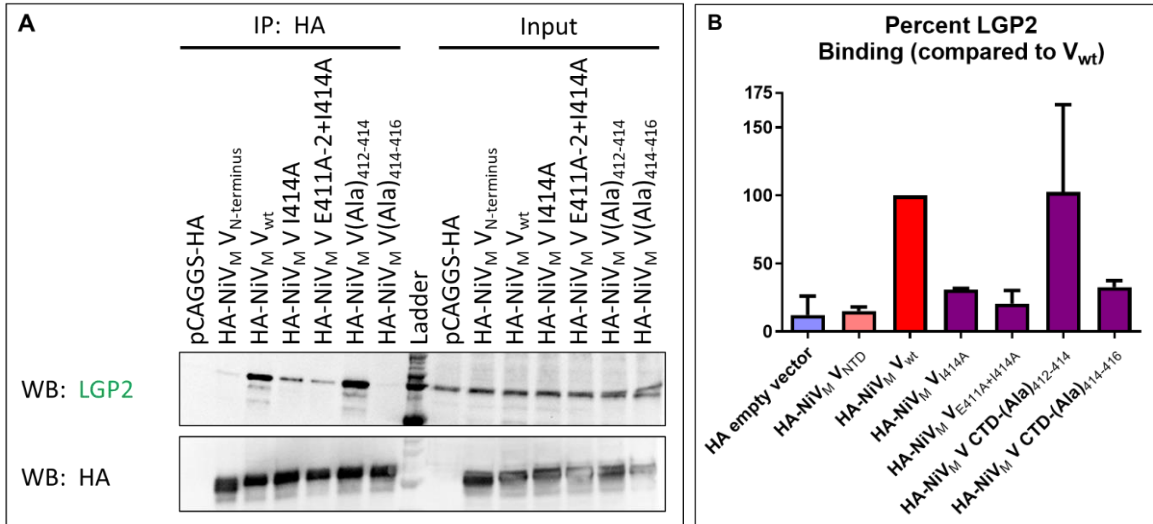


**Figure 2-15: The I414A point mutant was not sufficient to prevent binding to LGP2 in a co-IP/western blot assay**

**(A)** Co-IP/western blot results after pulldown of HA-tagged NiV<sub>M</sub> V proteins containing point mutations designed to inhibit MDA5 binding along with bound overexpressed LGP2. The first and second lanes (an empty vector plasmid and a plasmid encoding only the NTD of NiV<sub>M</sub> V) served as negative controls, while the third lane (a plasmid encoding wild-type, full-length NiV<sub>M</sub> V) served as a positive control. The right half of the blot shows WCL input to demonstrate that approximately equal amounts of protein were loaded on each lane. LGP2 is visible at around 80 kDa, and the HA-tagged NiV<sub>M</sub> V proteins are 50 to 56 kDa. **(B)** Quantification of the results in panel **(A)** by densitometry. The amount of binding to LGP2 by each mutant is expressed as a ratio of the normalized IP fraction (LGP2/HA) to the normalized WCL fraction (LGP2/HA). Wild-type NiV<sub>M</sub> V has been set to 100% for each panel, and all other lanes are expressed in relation to the wild-type lane. Error bars represent the SEM of two independent replicates.

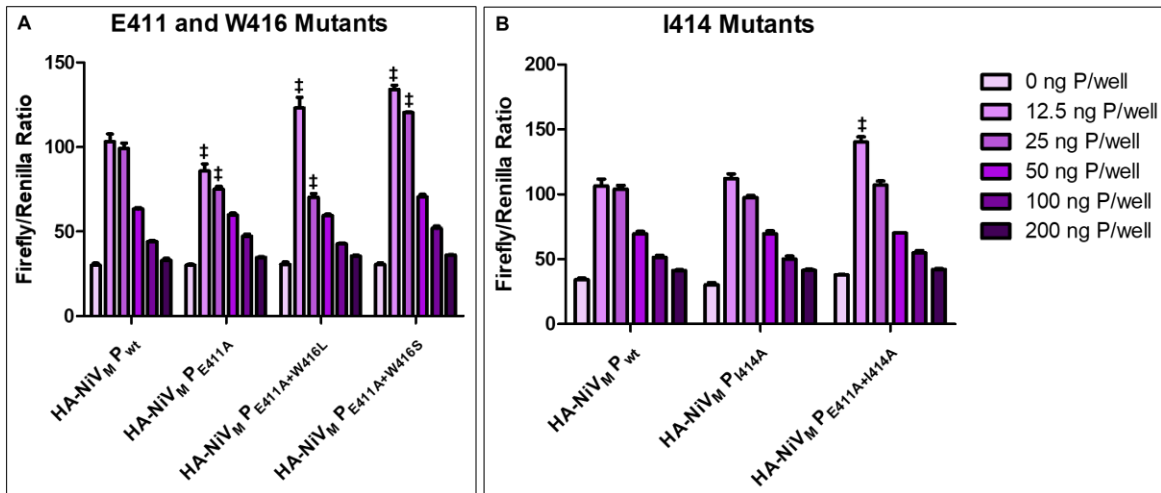


**Figure 2-16: NiV<sub>M</sub> V point mutants did not indicate decreased viral transcription/translation in a minigenome luciferase assay**

Minigenome luciferase assay results for (A) the E411 and W416 mutants and (B) the I414A mutants for indicated amounts of pCAGGS-HA-NiV<sub>M</sub> P. The HA-NiV<sub>M</sub> P<sub>wt</sub> condition served as a positive control of induction of minigenome expression by wild-type NiV<sub>M</sub> P protein. Values are expressed as the ratio of firefly (minigenome) luciferase expression to *Renilla* (basal transfection control) luciferase expression. Error bars represent the SEM of four replicates. ‡,  $P < 0.001$  as compared to wild-type P control by Bonferroni posttests following two-way ANOVA.

a range of amounts of P was included to optimize the ratio of RNP complex components. None of the point mutations tested caused a decrease in viral replication, and, in fact, the I414A mutation slightly increased light output in this BSL-2 reporter assay. Therefore, each set of mutations was carried forward to be investigated in the context of full-length rNiV, the recovery and testing of which *in vitro* and *in vivo* will be covered in Chapter 3.

## DISCUSSION

The V protein is a known immunomodulator and virulence factor for NiV which can interact with a wide variety of host molecules, including STAT1<sup>126</sup>, STAT2<sup>126</sup>, STAT4<sup>207</sup>, STAT5<sup>208</sup>, RIG-I<sup>111</sup>, LGP2<sup>130</sup>, polo-like kinase 1<sup>209</sup>, protein phosphatase 1 (PP1)<sup>210</sup>, UBX domain protein 1<sup>196</sup>, damage-specific deoxyribonucleic acid (DNA)-binding protein 1<sup>206</sup>, and MDA5<sup>121</sup>. Knockout of the unique CTD of NiV<sub>M</sub> V protein rendered the virus non-lethal in the ferret model<sup>67</sup>; however, the mechanism of NiV V-induced virulence has yet to be determined. Abolishment of binding to MDA5 by CDV V protein rendered that virus non-lethal in an otherwise 100% lethal ferret model<sup>194</sup>. Importantly, the binding site of MDA5 by NiV V was previously unknown but has been elucidated in the experiments described here, and, of additional importance, the point mutations that abolished MDA5 binding did not negatively affect viral replication according to a minigenome luciferase assay.

While it is likely that a protein with so many binding partners will be responsible for multiple functions during a NiV infection, the non-lethal effect shared by CDV lacking the ability to bind to MDA5<sup>194</sup> and NiV lacking the CTD of the V protein<sup>67</sup> in the ferret model made the MDA5 cellular factor an attractive target for further investigation. However, the CDV-infected ferrets and NiV-infected ferrets did still exhibit clinical signs during infection with the knockout or mutant viruses<sup>67,194</sup>. Therefore, the attenuating effect of interfering with MDA5 interaction did not render these viruses completely non-

pathogenic, but rather tempered their virulence to a degree that the euthanasia criteria were not reached. In addition, other immune-modulating proteins, such as C, P, and W, have also been shown to be involved in paramyxovirus-mediated virulence in animal models<sup>67-69</sup>. It is noteworthy that the henipavirus CedV cannot edit its mRNA to produce the V or W accessory proteins and, indeed, CedV is non-pathogenic in guinea pig, ferret, hamster, and AGM models of NiV and HeV disease<sup>8,211,Geisbert and Broder unpublished data</sup>, which may indicate a significant role for V and W in virulence. Some additional effects on pathogenicity could be attributed to differences in receptor usage, however, as CedV does not employ ephrin-B3 as a functional entry receptor<sup>212</sup>. Nonetheless, further investigation of the mechanism of virulence of the V protein is clearly warranted, and the interaction between V and MDA5 is a promising virus-host cellular relationship based on previous *in vivo* data in the ferret model<sup>67,194</sup>. Inhibition of MDA5 is conserved across all studied paramyxoviruses, which implies that it is critical for paramyxovirus virulence<sup>198</sup>. Accordingly, the interaction between V and MDA5 is an attractive target for antivirals which could have broad-spectrum activity across the *Paramyxoviridae* family<sup>198</sup>. However, MDA5 is part of a complex cellular signaling pathway with many other molecules involved in its function and regulation; prevention of binding to MDA5 by paramyxoviruses alone may not be sufficient to activate the type-I IFN production pathway and control viral replication<sup>210</sup>. Therefore, a multi-pronged approach with inhibition of multiple components of the NiV immune evasion response may be necessary to evaluate NiV virulence and for rational design of therapeutics.

The activity of RLRs must be tightly regulated to prevent unnecessary inflammation and autoimmunity, and, indeed, MDA5 has been shown to have an additional regulatory switch for activation upon binding of viral RNA<sup>213</sup>. The serine at position 88 is dephosphorylated by the host phosphatase PP1 upon PAMP binding, which frees MDA5 for binding to the CARDs of the MAVS adaptor protein<sup>210,213</sup>. A previous study using plasmid overexpression found that the MeV and NiV V CTDs bind to PP1

independently of binding to MDA5 and that the V-PP1 interaction serves as an additional check on MDA5 antiviral activity<sup>210</sup>. The binding site identified in this study for MeV V protein binding to PP1, RIWY, is not present in the NiV V CTD, so further investigation would be required to find and abrogate the NiV V-PP1 binding site. The redundancy of these two anti-MDA5 virulence mechanisms may explain the modest difference in reporter induction between wild-type NiV<sub>M</sub> and the MDA5 binding-deficient mutants generated in this study. Further investigation is needed to determine whether blocking of both binding sites would allow antiviral signaling through the MDA5 pathway and subsequent control of viral replication.

RIG-I and MDA5 recognize different RNA structures because of structural and regulatory differences between them. RIG-I recognizes 5'-triphosphorylated RNA and shorter dsRNA, while MDA5 recognizes longer dsRNA<sup>106</sup>. Because of the RNA species produced during infection, paramyxoviruses are thought to be primarily sensed by RIG-I upon infection of cells, while MDA5 is thought to be involved in recognition of picornaviruses<sup>105,214</sup>. However, studies have shown that MDA5 can work in tandem with RIG-I to sense paramyxoviruses such as MeV and SeV<sup>215,216</sup>. The interaction between paramyxoviruses and MDA5 has been well-defined and is highly conserved within the family<sup>121,130</sup>, while just one recent study has found a direct interaction between NiV V protein and RIG-I<sup>111</sup>. Previously, it was thought that paramyxoviruses were only able to inhibit RIG-I signaling through indirect interaction with LGP2 first, if at all<sup>131</sup>. However, the presence of two distinct mechanisms for inhibiting MDA5 specifically (direct binding to prevent ATPase activity and RNA binding, and prevention of activation through dephosphorylation), which are conserved among multiple genera of paramyxoviruses, suggests that MDA5 has significant antiviral activity against paramyxoviruses when not prevented from signaling. The mechanisms of RLR regulation and recognition of viral RNA are still poorly understood, especially in specific cell types and under specific conditions, so more investigation is clearly needed.

The apparent contradiction between the species that detects NiV genomic RNA (RIG-I) and the species that paramyxovirus nonstructural proteins strongly block (MDA5) is puzzling; however, there could be several explanations. NiV V protein strongly inhibited downstream induction of type-I IFNs when exogenous MDA5 was used as an inducer, as seen in the IFN- $\beta$  reporter assays in this chapter, so it is possible that blocking of one RLR is sufficient to control the host IFN response. Alternatively, it is possible that the mechanism by which paramyxoviruses inhibit MDA5 has been well-characterized but that there is a mechanism for inhibition of RIG-I that is just as important for paramyxovirus virulence that is just beginning to be appreciated<sup>111</sup>. A third possibility is that the RLRs are temporally regulated during viral infection and that inhibition of MDA5 is important during later stages of NiV infection. A temporal model of RNA sensing has been proposed for West Nile virus, in which RIG-I mediates early viral sensing and MDA5 late sensing<sup>217</sup>. Similar regulatory mechanisms may be involved in paramyxovirus infection, and additional experiments are needed to determine whether there is a temporal component to RLR sensing of NiV<sup>210</sup>.

Inhibition of MDA5 is an important virulence factor for NiV and other paramyxoviruses. However, prior to the studies detailed here, the specific binding site of MDA5 by the NiV nonstructural protein V was unknown. The experiments in this chapter detailed the discovery of the specific NiV V-MDA5 binding site, effects of mutations to the binding site on IFN- $\beta$  luciferase reporter assays and on minigenome luciferase reporter assays, and a preliminary investigation into whether the NiV V-MDA5 binding site is shared with the NiV V-LGP2 binding site. The next chapter will build on these findings by investigating the impact of mutations designed to inhibit MDA5 binding by NiV V on viral growth in cell culture and on pathogenicity in the ferret model of NiV disease.

# Chapter 3: Abrogation of V Binding to MDA5 and STAT1 Using Recombinant NiV<sub>M</sub> Mutants Reveals Moderate Increases in Interferon Sensitivity *in vitro* and Ferret Survival *in vivo*

## INTRODUCTION

As discussed in Chapter 1, the P gene products of paramyxoviruses inhibit the IFN production and signaling pathways to prevent the induction of antiviral responses in infected cells<sup>61,119</sup>. The nonstructural V protein was previously shown to bind to the cytoplasmic viral RNA sensor MDA5, but the specific binding site on NiV V was unknown<sup>121,195</sup>. Chapter 2 detailed the discovery of the NiV V-MDA5 specific binding site by co-IP/western blot, its effects on IFN- $\beta$  reporter induction *in vitro*, and verification that point mutations to abrogate MDA5 binding were not likely to affect viral replication through a minigenome luciferase reporter assay.

NiV infection fails to induce a strong type-I IFN response, as observed in human, porcine, and hamster primary cells<sup>211,218,219</sup>, Geisbert unpublished data. Furthermore, plasmid-based overexpression of the NiV V protein alone was sufficient to inhibit IFN- $\beta$  induction as evaluated using luciferase reporter assays (**Figures 2-8, 2-11, 2-14**)<sup>121,196</sup>. Blocking interactions of V with MDA5 and STAT1 restored induction of IFN- $\beta$  as observed using luciferase reporter assays<sup>158,194,196</sup>. Therefore, the observed IFN resistance of NiV is likely due to the interactions of V with components of the type-I IFN pathway.

The ferret model of NiV disease faithfully recapitulates the acute encephalitis, severe respiratory disease, and systemic vasculitis observed in human cases of NiV disease<sup>81,134</sup>. This model is 100% lethal at doses 5,000 TCID<sub>50</sub> and above given via the oronasal route and allows for the study of viral pathogenesis as well as the evaluation of the efficacy of antivirals and vaccines<sup>81,164,165</sup>. A lethal model of the closely related

morbillivirus CDV also exists<sup>197</sup>, and a recombinant CDV lacking the ability to bind to MDA5 was found to be non-lethal in challenged ferrets<sup>194</sup>.

Previous work with the NiV ferret model attempted to elucidate the distinct roles of the V, W, and C proteins in NiV virulence<sup>67,68</sup>. Importantly, the V protein was found to be a major determinant of NiV virulence, as 100% of ferrets challenged i.n. with 5,000 PFU of a rNiV unable to produce the V protein survived to the study endpoint<sup>67</sup>. The importance of the paramyxoviral V protein as a virulence factor has been previously established, as knockout of the V CTD of PIV5 allowed normal nuclear translocation of IRF3 and STAT1 to resume in cultured cells, thus allowing the IFN- $\beta$  production and IFN signaling normally strongly inhibited by PIV5 to proceed<sup>220</sup>. Furthermore, infection of established models of MeV disease with MeV lacking V protein led to reduced virulence and mortality and restricted viral spread in the brains of newborn transgenic mice, as well as less virus re-isolated from the lungs of cotton rats, as compared to intact MeV Edmonston strain<sup>221,222</sup>. In summary, the paramyxoviral V protein is an important virulence factor driving pathogenicity, but determinants of NiV V protein-induced virulence have yet to be elucidated.

In this chapter, further characterization of the NiV<sub>M</sub> V MDA5-binding mutants was carried out by cloning point mutations into full-length plasmids and using an established reverse genetics system to generate rNiV deficient in MDA5 binding. These mutations were tested alone or in combination with a previous mutation shown to abrogate binding to STAT1<sup>158</sup> to assess their effects on viral replication in IFN-competent and -incompetent cells, with and without exogenous IFN pretreatment. Previously, inhibition of STAT1 binding was shown to significantly delay time to death in the ferret model but not to change lethal outcome<sup>158</sup>, so the effects of MDA5 and STAT1 on virulence were assessed together in the experiments presented here. Study design and impacts on survival in the ferret model will be discussed in context with previous results.

## **METHODS**

### **Plasmids**

The genomic sequence used to generate full-length rNiVs for these experiments was the NiV<sub>M</sub> clinical isolate UMMC1 from the original outbreak in Malaysia (GenBank accession number AY029767). Antigenomic complementary DNA (cDNA) was amplified by reverse transcriptase (RT)-polymerase chain reaction (PCR) in three segments as previously described<sup>66</sup>: the pNiV<sub>M</sub> A segment comprised nucleotides 1 to 6780, the pNiV<sub>M</sub> B segment nucleotides 6780 to 10404, and the pNiV<sub>M</sub> C segment nucleotides 10404 to 18246. These segments allowed the introduction of designed mutations at specific points within the genome and were assembled into full-length antigenomic pNiV<sub>M</sub>-FL plasmids in the pSL1180 cloning vector with T7 promoter, T7 terminator, and hepatitis delta ribozyme sequences upstream and downstream of the antigenomic sequence<sup>66</sup>.

As described in Chapter 2, the pTM1-HA-NiV<sub>M</sub> P helper plasmid was a kind gift from Dr. Christopher Basler (currently at Georgia State University; Atlanta, Georgia, USA) and encoded the NiV<sub>M</sub> P protein with an HA tag fused to its N-terminus in the pTM1 expression plasmid, driven by a T7 promoter<sup>66</sup>. The helper plasmids pTM1-NiV<sub>M</sub> N and pTM1-NiV<sub>M</sub> L were cloned by Dr. Benjamin Satterfield (currently at Mayo Clinic; Rochester, Minnesota, USA) and encoded NiV<sub>M</sub> N and NiV<sub>M</sub> L genes in the pTM1 expression plasmid, driven by a T7 promoter<sup>67</sup>. The sequences for the helper plasmids were derived from NiV<sub>M</sub> isolate UMMC1 (GenBank accession number AY029767).

### **Cloning to produce full-length pNiV<sub>M</sub> plasmids encoding designed mutations in V**

Site-directed mutagenesis was used by Mutagenex, Inc. to create pNiV<sub>M</sub> A plasmids containing the point mutations listed in **Table 3-1** within the +1 frame of the P ORF (designed to abrogate binding to MDA5 by NiV<sub>M</sub> V). The wild-type pNiV<sub>M</sub> full-length plasmid was digested with SacII and MluI-HF restriction enzymes (New England

Nickname	MDA5-Binding Mutations	Genotype	Passage 2 Seed Stock Titer
rSLF8	E411A/W416S	rNiV <sub>M</sub> V E411A (gaa→gca) + W416S (tgg→tcg)	2.23×10 <sup>7</sup> PFU/mL
rSLF9		rNiV <sub>M</sub> V E411A (gaa→gcg) + W416S (tgg→tcg)	1.68×10 <sup>7</sup> PFU/mL
rSLF10		rNiV <sub>M</sub> V Y116E (tac→gag) + E411A (gaa→gcg) + W416S (tgg→tcg)	1.23×10 <sup>6</sup> PFU/mL
rSLF15	E411A/W416L	rNiV <sub>M</sub> V E411A (gaa→gca) + W416L (tgg→ttg)	1.63×10 <sup>7</sup> PFU/mL
rSLF16		rNiV <sub>M</sub> V E411A (gaa→gcg) + W416L (tgg→ttg)	1.25×10 <sup>7</sup> PFU/mL
rSLF17		rNiV <sub>M</sub> V Y116E (tac→gag) + E411A (gaa→gcg) + W416L (tgg→ttg)	8.25×10 <sup>5</sup> PFU/mL
rSLF32	E411A/I414A	rNiV <sub>M</sub> V I414A (atc→gct)	1.38×10 <sup>7</sup> PFU/mL
rSLF33		rNiV <sub>M</sub> V E411A (gaa→gcg) + I414A (atc→gct)	1.45×10 <sup>7</sup> PFU/mL
rSLF34		rNiV <sub>M</sub> V Y116E (tac→gag) + E411A (gaa→gcg) + I414A (atc→gct)	8.75×10 <sup>5</sup> PFU/mL

**Table 3-1: rNiV<sub>M</sub> constructs cloned and recovered to abrogate MDA5 and STAT1 binding**

Biolabs (NEB; Ipswich, Massachusetts, USA; Cat. Nos. R0157 and R3198, respectively) and purified by SDS-PAGE electroelution to generate vector plasmid appropriate for Gibson assembly<sup>223</sup>. Oligonucleotide PCR primers designed with large overhangs for Gibson assembly were ordered from Integrated DNA Technologies, Inc. (IDT; Coralville, Iowa, USA). Inserts were generated by PCR using the primers, pNiV<sub>M</sub> A plasmids containing designed mutations, and Platinum<sup>™</sup> SuperFi<sup>™</sup> DNA polymerase (Thermo Scientific Invitrogen; Cat. No. 12351) according to manufacturer instructions. Full-length pNiV<sub>M</sub> plasmids containing mutations designed to inhibit binding to MDA5 and STAT1 were assembled using the NEBuilder<sup>®</sup> HiFi DNA Assembly Cloning Kit (NEB; Cat. No. E5520S) according to manufacturer instructions. The following constructs were assembled: pNiV<sub>M</sub>-FL V E411A-1+W416S, pNiV<sub>M</sub>-FL V E411A-2+W416S, pNiV<sub>M</sub>-FL V Y116E+E411A-2+W416S, pNiV<sub>M</sub>-FL V E411A-1+W416L, pNiV<sub>M</sub> FL V E411A-2+W416L, pNiV<sub>M</sub>-FL V Y116E+E411A-2+W416L, pNiV<sub>M</sub>-FL V I414A, pNiV<sub>M</sub>-FL V E411A-2+I414A, and pNiV<sub>M</sub>-FL V Y116E+E411A-2+I414A (**Table 3-1**). The presence of designed mutations within each construct was confirmed by Sanger sequencing. Large cultures of *E. coli* transformed with each full-length pNiV<sub>M</sub> plasmid were grown, and DNA was extracted using the ZymoPURE II Plasmid Maxiprep kit (Zymo Research; Irvine, California, USA; Cat. No. D4203). Purified DNA was screened by restriction digest to ensure full-length plasmid was present before rNiV<sub>M</sub> rescue was attempted.

### **Cell culture**

Vero 76 cells (ATCC; Cat. No. CRL-1587) are a continuous cell line derived from the kidney of an AGM, and they are deficient in type-I IFN production<sup>224</sup>. Vero 76 cells were maintained in Eagle's Minimum Essential Medium (ATCC; Cat. No. 30-2003) supplemented with 10% heat-inactivated FBS, 1% penicillin/streptomycin solution (10,000 units/mL penicillin and 10,000 µg/mL streptomycin), and 1% GlutaMAX<sup>™</sup> Supplement.

BSR T7/5 cells<sup>203</sup> were maintained as described in Chapter 2.

HEK293T cells were maintained as described in Chapter 2.

### **Recovery and amplification of rNiV<sub>M</sub> containing designed mutations in V**

A schematic showing the process for recovery of mutant rNiV<sub>M</sub> constructs is shown in **Figure 3-1** and was carried out as described previously<sup>66</sup>. Briefly, BSR T7/5 cells were seeded in T75 tissue culture flasks and grown to confluence for transfection in suspension. Cells were transfected with 3.5 µg per well of each pNiV<sub>M</sub>-FL full-length clone containing designed mutations, 0.75 µg per well of pTM1-NiV<sub>M</sub> N expression plasmid, 0.1 µg per well of pTM1-NiV<sub>M</sub> P expression plasmid, and 0.4 µg per well of pTM1-NiV<sub>M</sub> L expression plasmid using *TransIT-LT1* transfection reagent. Plasmids and transfection reagent (3 µL per µg of plasmid DNA) were added to Opti-MEM<sup>TM</sup> I Reduced Serum Medium and incubated at room temperature. During incubation, cells were washed with phosphate-buffered saline (PBS) without calcium or magnesium (Thermo Scientific Gibco; Cat. No. 10010-049), trypsinized with 0.25% Trypsin-ethylenediaminetetraacetic acid (EDTA; made from 0.5% solution; Thermo Scientific Gibco; Cat. No. 15400-054), and resuspended in DMEM containing 10% FBS without G418. Cells were combined with transfection mix, mixed well by inversion, and plated into 6-well tissue culture plates and incubated at 37°C and 5% carbon dioxide (CO<sub>2</sub>) for 72 hours.

At 72 hours post-transfection, the cells were scraped off of the 6-well plates, freeze/thawed to disrupt the cells, clarified to remove cell debris, and used to infect Vero 76 cells in 6-well plates. The Vero cells were monitored for NiV cytopathic effect (CPE), which usually appeared in three to six days (**Figure 3-2**). Supernatant of positive wells was collected, clarified to remove cell debris, and passaged on fresh Vero 76 cells for plaque purification. Picked plaques were collected into tubes containing DMEM with 10% FBS, incubated at 37°C for 1 hour with intermittent vortexing, and then the medium

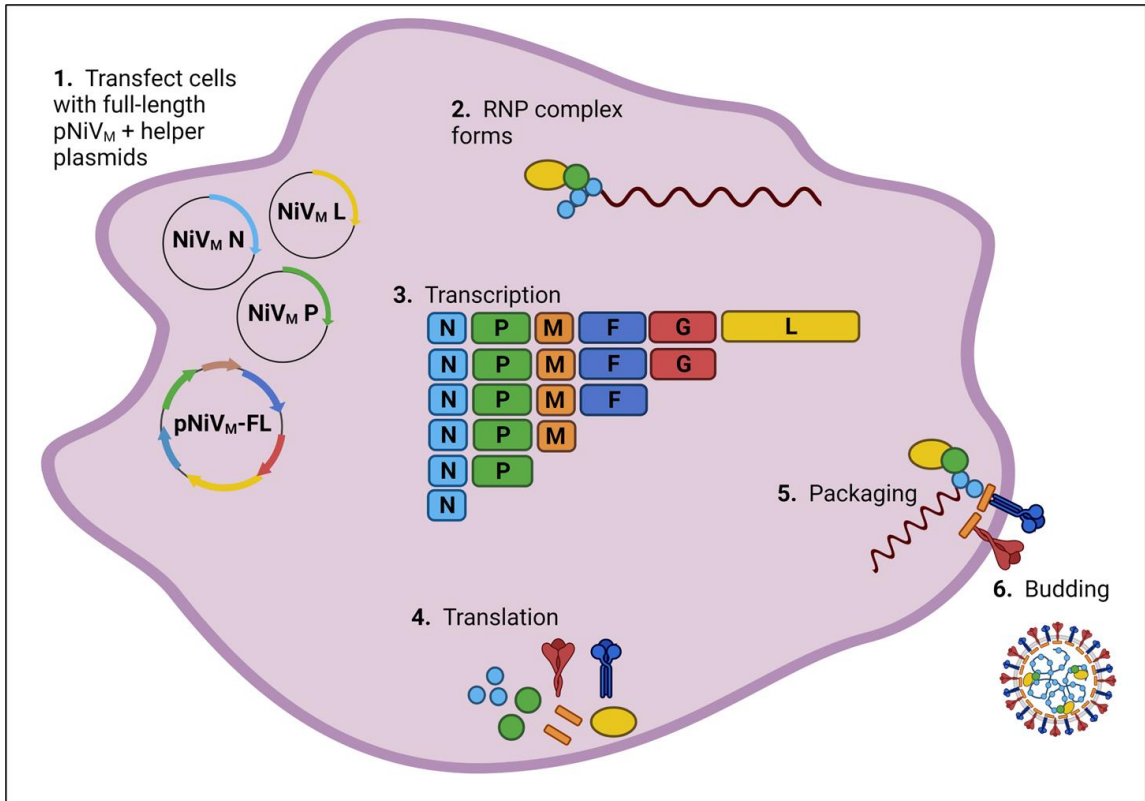


**Figure 3-1: Recovery of rNiV<sub>M</sub> full-length constructs**

Diagram of the process by which recovery of rNiV<sub>M</sub> virions occurred in BSR T7/5 cells expressing bacteriophage T7 polymerase. **1.** Cells were transfected with the full-length  $pNiV_M$  plasmid containing the mutations of interest and helper plasmids encoding NiV<sub>M</sub> N, P, and L (all under the control of the T7 promoter). **2.** The helper plasmids were transcribed and translated to produce NiV<sub>M</sub> N, P, and L protein; the full-length plasmid was transcribed to produce the RNA genome of the rNiV<sub>M</sub> construct. Together, they formed the RNP complex. **3.** The RNA genome was transcribed to produce mRNAs encoding NiV<sub>M</sub> N, P, M, F, G, and L. **4.** The mRNAs were translated to produce NiV<sub>M</sub> N, P, M, F, G and L proteins. **5.** The RNA genome and viral structural proteins were packaged into virions near the cell membrane. **6.** Live virions encoding designed mutations in the P ORF budded from the cell. Figure created using BioRender.com.

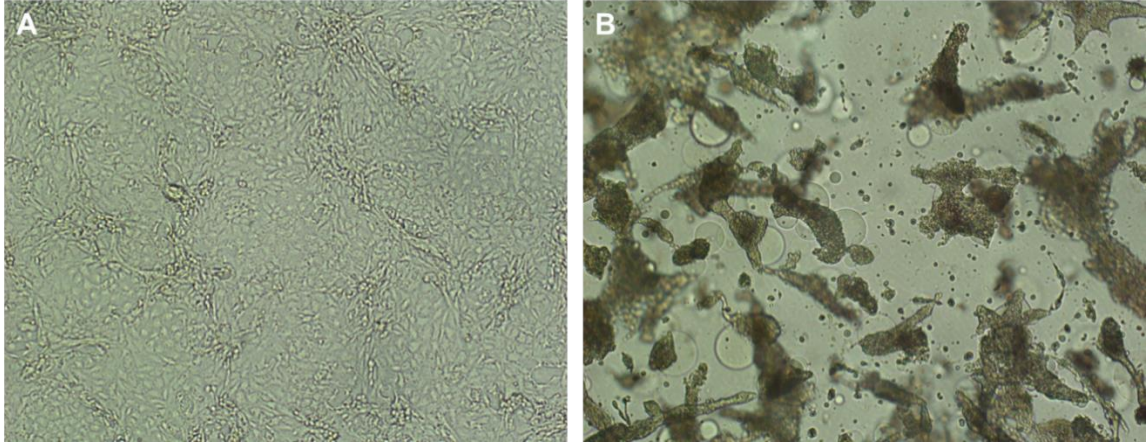


**Figure 3-2: rNiV<sub>M</sub>-induced CPE on Vero 76 cells**

Light micrographs showing Vero 76 cells at 72 hpi after (A) mock infection with cell culture medium or (B) infection with a representative rNiV<sub>M</sub> construct. The rNiV<sub>M</sub>-induced CPE visible in panel (B) shows large syncytia that have formed and floated off the flask and to the top of the culture medium.

was used to infect fresh Vero 76 cells for passage 1 (p1). A small amount of p1 supernatant was collected at around 48 hours post-infection (hpi), when 100% NiV CPE was observed. The supernatant was clarified to remove cell debris and used to infect T150 flasks of Vero 76 cells at a multiplicity of infection (MOI) of 0.01 for p2. At 48 hpi, 100% NiV CPE was observed, and the supernatant was collected, clarified, and aliquoted into 2-mL screwcap tubes with O-rings for storage of p2 seed stocks at -80°C.

Viral titers were determined using a standard plaque assay on Vero 76 cells in 6-well plates by inoculating duplicate wells with 200 µL per well of 10-fold serial dilutions of each sample. After one-hour adsorption at 37°C and 5% CO<sub>2</sub>, cells were overlaid with two mLs per well of medium containing final concentrations of 1X minimum essential medium (MEM; prepared from 2X; Thermo Fisher Gibco; Cat. No. 11935), 5% FBS, and 0.8% SeaKem® ME agarose (Lonza; Basel, Switzerland; Cat. No. 50014). At 48 hpi, plaques were stained with a solution of 5% neutral red (Sigma-Aldrich; St. Louis, Missouri, USA; Cat. No. N2889-100ML) and 5% FBS in PBS without calcium and magnesium, and plaques were visualized and counted at 72 hpi. All procedures involving transfection of full-length pNiV<sub>M</sub> clones into cells or using replicating rNiV<sub>M</sub> were carried out using approved protocols and under BSL-4 containment at the Galveston National Laboratory (GNL) at the University of Texas Medical Branch (UTMB) in Galveston, Texas, USA.

Viral RNA was isolated from p2 seed stock in TRIzol™ LS Reagent (Thermo Fisher Invitrogen; Cat. No. 10296028) using the Direct-zol RNA miniprep kit (Zymo Research; Cat. No. R2052) according to manufacturer instructions. Designed mutations were detected using Sanger sequencing of cDNA fragments that were created by RT-PCR using SuperScript™ IV Reverse Transcriptase (Thermo Fisher Invitrogen; Cat. No. 18090) and amplified using Platinum™ SuperFi™ DNA polymerase. Complete viral RNA genomes were sequenced with the NextSeq 550 system (Illumina; San Diego,

California, USA; Cat. No. SY-415-1002) with a depth of 130 million reads to confirm that each virus was complete and had the correct sequence.

### **Determination of rNiV<sub>M</sub> growth kinetics**

HEK293T and Vero 76 cells were seeded in 6-well plates for infection with wild-type and mutant rNiV<sub>M</sub>. Twelve hours prior to infection, half of the Vero 76 wells were treated with 1,000 units per mL of human IFN- $\alpha$  2a (PBL Assay Science; Piscataway, New Jersey, USA; Cat. No. 11100-1). In the BSL-4, cells were infected at either an MOI of 0.0001 or 0.00001 with rNiV<sub>M</sub>-wt, rNiV<sub>M</sub> V I414A, rNiV<sub>M</sub> V E411A+I414A, or rNiV<sub>M</sub> V Y116E+E411A+I414A. Briefly, cells were infected with 200  $\mu$ L of inoculum per well for one hour at 37°C and 5% CO<sub>2</sub>, the inoculum was removed and cells were washed four times with clean growth medium, and then two mLs of fresh growth medium was added to each well and cells were returned to the incubator. Supernatants were collected at 1, 24, 36, 48, 60, 72, 84, and 96 hpi. At each timepoint, supernatants were collected into 2-mL screwcap tubes, clarified by centrifugation, and stored at -80°C. Triplicate infections were performed for each virus at each MOI and in each cell line (with and without IFN). Samples were quantified by plaque assay on Vero 76 cells, as detailed in the previous section.

### **Animal Studies**

#### ***ANIMAL HANDLING AND PROCEDURES***

Protocols for animal studies were approved by UTMB's Institutional Animal Care and Use Committee (IACUC) and complied with the Animal Welfare Act and the *Guide for the Care and Use of Laboratory Animals*, National Research Council. Animal studies were performed under BSL-4 biocontainment in the UTMB GNL, which is fully accredited by the Association for Assessment and Accreditation of Laboratory Animal Care (AAALAC) International.

Female ferrets (*Mustela putorius furo*) that were five to six months old were obtained, quarantined per institutional guidelines, and determined to be healthy before beginning experiments. Animals had transponder chips implanted under the skin for identification and monitoring of their temperature during the study. Groups of four ferrets were inoculated with each virus and were housed in pairs within their virus cohorts. For all procedures, including virus challenge, ferrets were anesthetized with inhaled isoflurane before manipulation. Each animal received approximately 50,000 PFU of wild-type or mutant rNiV<sub>M</sub> (determined by back titration of inoculum) in one mL of Hank's Balanced Salt Solution (HBSS; Thermo Fisher Gibco; Cat. No. 14175) with 10% FBS. The virus inoculum was administered i.n., with 0.5 mL administered to each nostril. On days 0, 3, 6, 15, and 35 after challenge and at terminal endpoint, ferrets were examined for clinical signs, and blood was collected after anesthesia with inhaled isoflurane. Subjects were assessed for weight, temperature, and clinical score daily after challenge. Clinical observations were scored on a scale from 0 to 22 based on appearance, body condition, respiration, and behavior; animals scoring 8 or greater were humanely euthanized by lethal injection of a solution containing pentobarbital sodium and phenytoin sodium.

#### ***BLOOD COLLECTION, PROCESSING, AND HEMATOLOGY***

At each timepoint and at terminal endpoint, about one mL of blood each was collected into one EDTA and one serum separator MiniCollect® tube (Greiner Bio-One; Kremsmünster, Austria; Cat. Nos. 450480 and 450470, respectively) for each animal and processed immediately after collection. From the EDTA tube, 100 µL of whole blood was added to 600 µL of AVL Viral Lysis Buffer with carrier RNA (Qiagen; Hilden, Germany; Cat. No. 19073) and incubated for at least ten minutes to inactivate virus. Inactivated material was transferred to a 1.8-mL Nunc™ cryovial (Thermo Scientific;

Cat. No. 363401) and removed from the BSL-4. RNA was extracted using the QIAamp Viral RNA Mini Kit (Qiagen; Cat. No. 52906) according to manufacturer instructions.

Another 150  $\mu$ L of whole blood was removed from the EDTA tube and placed into a 0.5-mL screwcap tube for hematology analysis using the VetScan<sup>®</sup> HM5 Hematology Analyzer (Abaxis, Inc.; Union City, California, USA). Complete blood counts, including numbers of white blood cells, lymphocytes, monocytes, red blood cells, and platelets and measures of hematocrit and total hemoglobin, were obtained using a protocol optimized for ferrets according to manufacturer instructions. About 150  $\mu$ L of whole blood was removed from the EDTA tube and stored at -80°C in 2-mL screwcap tubes for later virus enumeration in whole blood by plaque assay.

The serum separator tubes and EDTA tubes were spun in a microcentrifuge at 4,000 revolutions per minute (RPM) for 10 minutes at 4°C to separate serum and plasma from cellular material. The serum was transferred to a 2-mL screwcap tube and stored at -80°C for later clinical chemistry analysis (see below). EDTA plasma was transferred to a 2-mL screwcap tube and stored at -80°C.

Analysis of clinical chemistry was performed using serum, Piccolo<sup>®</sup> BioChemistry Panel Plus reagent discs (Abaxis, Inc.; Cat. No. 400-7182-1), and the Piccolo<sup>®</sup> Xpress chemistry analyzer (Abaxis, Inc.). The BioChemistry Panel Plus measures levels of alanine aminotransferase (ALT), albumin, alkaline phosphatase (ALP), amylase, aspartate aminotransferase (AST), blood urea nitrogen (BUN), C-reactive protein (CRP), calcium, creatinine (CRE), gamma glutamyltransferase (GGT), glucose, total protein, and uric acid in serum.

#### ***TISSUE COLLECTION AND PROCESSING***

At terminal or study endpoint, the following tissues were collected from each ferret for histopathology analysis, virus enumeration by plaque assay, and RNA extraction: liver, spleen, kidney, lung, and brain (frontal lobe).

For virus enumeration, tissue samples were stored at -80°C for later processing. Tissues were homogenized in cell culture medium in 2-mL screwcap tubes containing 1.4-millimeter ceramic beads (Omni International; Kennesaw, Georgia, USA; Cat. No. 19-627) using the TissueLyser II (Qiagen; Cat. No. 85300) to create 10% w/v homogenate. Samples were spun in a microcentrifuge at 4°C to pellet beads and debris, and supernatants were transferred to new 2-mL screwcap tubes and stored at -80°C until titration (see next section).

For RNA extraction, approximately 100 mg of tissue was stored in one mL of RNAlater reagent (Qiagen; Cat. No. 76106) for later processing. RNAlater reagent was removed, and tissues were homogenized in 600 µL of RLT lysis buffer (Qiagen; Cat. No. 79216) in 2-mL screwcap tubes containing ceramic beads using the TissueLyser II. Samples were spun in a microcentrifuge to pellet beads and debris, and supernatants were transferred to 1.8-mL cryovials and removed from the BSL-4. RNA was extracted using the RNeasy Mini Kit (Qiagen; Cat. No. 74106) according to manufacturer instructions.

#### ***DETERMINATION OF VIRAL LOAD BY PLAQUE ASSAY AND RT-qPCR***

Isolated RNA from blood and tissues was subjected to RT-quantitative PCR (qPCR) using primers and probes specific to NiV<sub>M</sub> targeting the N gene and the N-P intergenic region. Inclusion of the intergenic region prevented detection of viral mRNA by the assay. The probe was ordered from Thermo Fisher Invitrogen and featured 6-carboxyfluorescein (6FAM) fluorescent reporter dye at the 5' end and tetramethylrhodamine (TAMRA) quencher at the 3' end, with a nucleotide sequence of 5' CGT CAC ACA TCA GCT CTG ACG A 3'. NiV<sub>M</sub> viral RNA was detected using the OneStep RT-PCR kit (Qiagen; Cat. No. 210215) and the CFX96 Touch Real-Time PCR Detection System (Bio-Rad Laboratories). CFX Manager<sup>TM</sup> software (Bio-Rad Laboratories) was used to evaluate threshold cycle values, and results are reported in genome equivalents (GEq)/mL for blood or GEq/gram (g) for tissues, determined from a

plasmid standard using Avogadro's number and the molecular weight of the NiV<sub>M</sub> genome.

Viral titers from whole blood were determined using a standard plaque assay on Vero 76 cells. Briefly, duplicate wells of 6-well plates were inoculated with 200  $\mu$ L each of 10-fold serial dilutions of each sample, adsorbed for one hour at 37°C and 5% CO<sub>2</sub>, and then overlaid with two mLs per well of medium containing final concentrations of 1X MEM, 5% FBS, and 0.8% SeaKem® ME agarose. At 48 hpi, plates were stained with a solution of 5% neutral red and 5% FBS in PBS without calcium and magnesium, and plaques were visualized and counted at 72 hpi. The limit of detection (LOD) of the assay was 25 PFU/mL.

## Statistics

Due to the nature of research in the BSL-4, the total number of biological samples for *in vitro* and *in vivo* studies was limited, as was the ability to repeat assays. Statistical differences in survival were calculated using GraphPad Prism software using the Log-Rank (Mantel-Cox) Test for Kaplan-Meier survival curves.

## RESULTS

### Full-length rNiV<sub>M</sub> containing MDA5- and STAT1-binding mutations were rescued by reverse genetics

Full-length antigenomic plasmids encoding rNiV<sub>M</sub> with MDA5- and STAT1-binding mutations in the +1 frame of the P ORF were cloned as described above and contained the mutations shown in **Table 3-1**. Replication-competent rNiV were rescued, purified, and amplified to create p2 seed stocks as described above and shown in **Figure 3-1**. In addition to mutations designed to inhibit binding to MDA5 by NiV<sub>M</sub> V that were covered in detail in Chapter 2, a mutation designed to inhibit the binding of NiV<sub>M</sub> P/V/W to STAT1, Y116E, was added. This mutation was characterized previously<sup>158</sup>, and it is

present in the NTD of the P/V/W proteins, so its binding site is shared among the three proteins. Importantly, this mutation has not yet been tested with the minigenome reporter assay. However, in a luciferase reporter assay using the ISG54 promoter to assess IFN signaling, the Y116E mutation was the single point mutation that most lost its ability to inhibit the IFN response compared to wild-type NiV<sub>M</sub> P and wild-type NiV<sub>M</sub> V proteins<sup>158</sup>.

The CPE of NiV replicating on Vero 76 cells was striking (**Figure 3-2**). These cells fused into large rafts that detached from the culture flask and floated to the top of the growth medium. All of the rescued constructs grew similarly to wild-type rNiV<sub>M</sub> by p2. Virus was collected at 48 hpi, as soon as the NiV-induced CPE had affected about 100% of cells. Notably, the constructs containing the Y116E mutations produced much smaller plaques on Vero 76 cells than the other constructs and wild-type rNiV<sub>M</sub>. Y116E-containing constructs also took an extra day to grow at earlier passages and grew to approximately one log lower peak titers by p2 (**Table 3-1**). Based on these observations and on previous studies investigating the impacts of mutations to NiV P on viral replication and characterizing the Y116E mutation<sup>66,158</sup>, the Y116E mutation causes a growth defect in Vero cells compared to wild-type rNiV<sub>M</sub>, which will be discussed in detail in the next section. The complete sequences of viral RNA for each of the mutant rNiV<sub>M</sub> were obtained through next-generation sequencing using the NextSeq 550 system and were found to match the expected sequences and contain the designed point mutations.

#### **Rescued rNiV<sub>M</sub> containing MDA5-binding mutations grew to slightly lower peak titers in IFN-competent cells and IFN-incompetent cells pretreated with IFN**

Having recovered and characterized rNiV<sub>M</sub> containing mutations designed to inhibit binding to MDA5 and STAT1, the impacts of these mutations on IFN sensitivity and viral growth kinetics were next evaluated in IFN-competent cells. Based on the site at

which NiV<sub>M</sub> V was found to bind to MDA5 in Chapter 2, I414, constructs containing the I414A mutation were chosen for further characterization.

**Figure 3-3** shows the results of assays to determine viral growth kinetics in Vero 76 and HEK293T cells. Cells were infected with rNiV<sub>M</sub> containing mutations designed to inhibit MDA5 and STAT1 binding at two extremely low MOIs, 0.0001 and 0.00001. These low MOIs were chosen because NiV can cause 100% CPE in Vero 76 cells after just 48 hours even at the relatively low MOI of 0.01, so lower MOIs were needed to see any differences between the wild-type and mutant rNiV<sub>M</sub>.

In Chapter 2, the MDA5-binding mutations were tested with a minigenome luciferase reporter assay (**Figure 2-16**) and determined to be unlikely to negatively affect viral replication. However, the Y116E STAT1-binding mutation was not tested using the minigenome system, and the minigenome results for the MDA5-binding mutants needed to be confirmed. Therefore, a growth curve was carried out in Vero 76 cells, which are incapable of producing type-I IFN<sup>224</sup>. The results of growth curves in these cells thus demonstrated the ability of each rNiV<sub>M</sub> to grow based only on the efficiency of its viral replication machinery, without confounding effects from innate immune induction. As seen in **Figure 3-3**, panels **A** and **D**, the rNiV<sub>M</sub> containing the I414A mutation but not the Y116E mutation, rNiV<sub>M</sub> V I414A and rNiV<sub>M</sub> V E411A+I414A, grew nearly identically to each other and to rNiV<sub>M</sub>-wt at both MOIs in Vero 76 cells with no IFN pretreatment. However, rNiV<sub>M</sub> Y116E+E411A+I414A demonstrated a growth defect in these cells of about one to 1.5 logs throughout the timecourse, as predicted based on observations during virus recovery and previous experiments with the P protein and with the Y116E mutation<sup>66,158</sup>. Therefore, the results in Vero 76 cells without IFN pretreatment corroborate the minigenome luciferase reporter assays in Chapter 2, as well as previously published results.

Having confirmed that the E411A and I414A mutations did not affect viral replication due to changes to the NiV<sub>M</sub> P protein sequence, whether the MDA5-binding

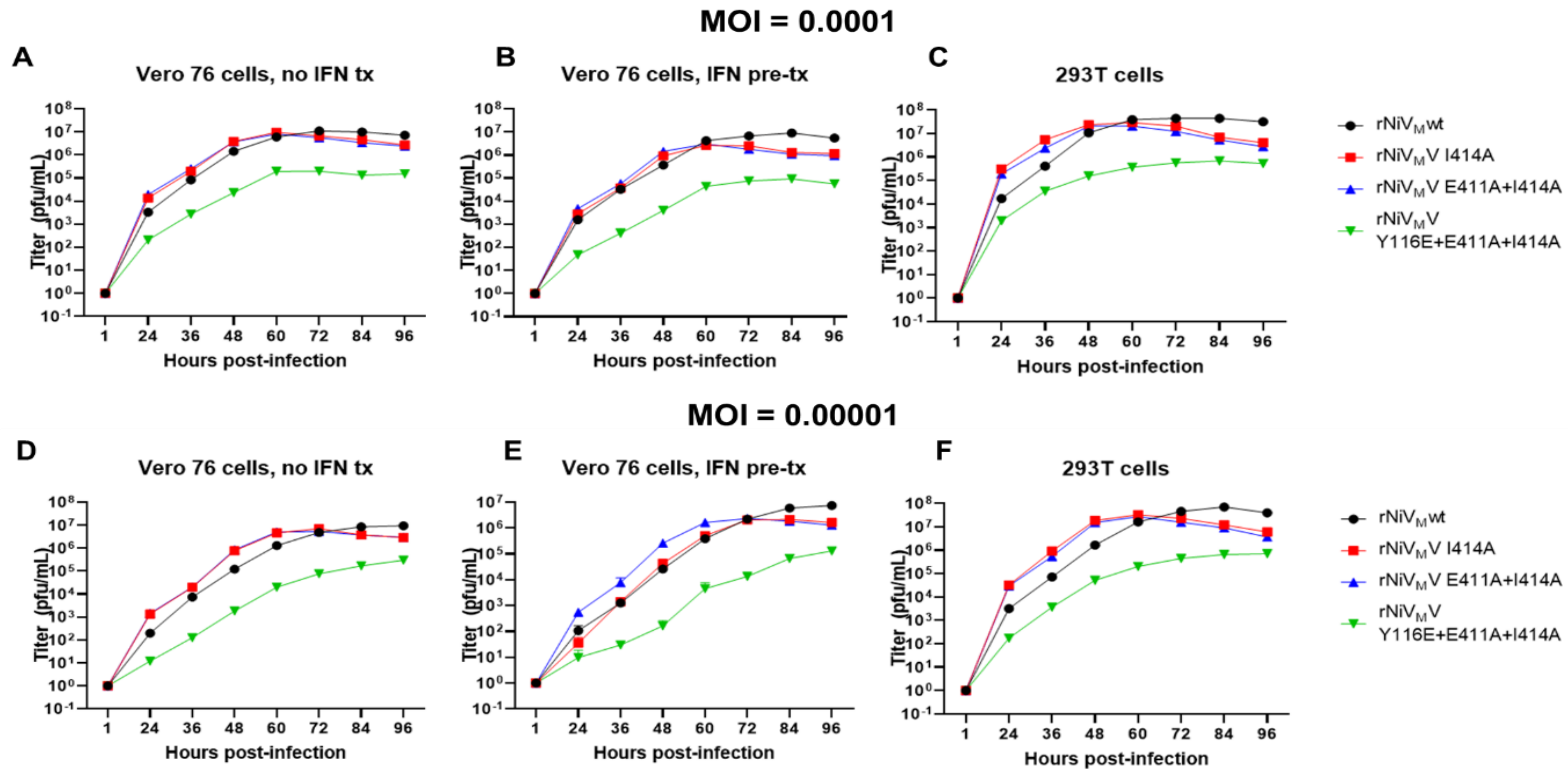


**Figure 3-3: Viral growth kinetics of rNiV<sub>M</sub> with MDA5- and STAT1-binding mutations in Vero 76 cells and HEK293T cells**

Results of growth curve assays (**panels A and D**) in Vero 76 cells without IFN pretreatment, (**panels B and E**) in Vero 76 cells with pretreatment with 1,000 units per mL of human IFN- $\alpha$  2a, and (**panels C and F**) in IFN-competent HEK293T cells. Cells were infected at an MOI of (**panels A through C**) 0.0001 or (**panels D through F**) 0.00001. Titters are shown in PFU/mL as black circles (rNiV<sub>M</sub>-wt), red squares (rNiV<sub>M</sub> V I414A), blue triangles (rNiV<sub>M</sub> V E411A+I414A), and green inverted triangles (rNiV<sub>M</sub> V Y116E+E411A+I414A).

mutants were inhibited in the presence of IFN compared to wild-type rNiV<sub>M</sub> was investigated. Vero 76 cells were pretreated with 1,000 units per mL of recombinant human IFN- $\alpha$  2a at 12 hours prior to infection, and the results of the growth curves at both MOIs are shown in **Figure 3-3**, panels **B** and **E**. In this case, rNiV<sub>M</sub> V I414A and rNiV<sub>M</sub> V E411A+I414A grew similarly to rNiV<sub>M</sub>-wt through 60 hpi, at which point they failed to reach the peak titers that rNiV<sub>M</sub>-wt reached at 84 hpi at MOI 0.0001 and 96 hpi at MOI 0.00001. Again, the rNiV<sub>M</sub> V Y116E+E411A+I414A mutant exhibited a growth defect, so comparisons to rNiV<sub>M</sub>-wt were difficult; differences due to lack of innate immune inhibition could not be distinguished from differences due to an inherent viral replication defect based on these results.

The Vero 76 cells were treated with IFN at just one timepoint and with one dose, so the ability of the rNiV<sub>M</sub> to grow in an IFN-competent cell line was also assessed to evaluate the impacts of intact IFN production and signaling throughout infection. HEK293T cells have a functional type-I IFN system and can produce IFN in response to a stimulus, as shown with MDA5 in Chapter 2. Therefore, any failure of the MDA5- and STAT1-binding mutants to control the IFN response compared to rNiV<sub>M</sub>-wt should be visible as slower growth and/or growth to a lower peak titer in HEK293T cells. The results of these growth curves are shown in **Figure 3-3**, panels **C** and **F**. Growth of the rNiV<sub>M</sub> was nearly identical to growth in Vero 76 cells pretreated with IFN. The rNiV<sub>M</sub> V I414A and rNiV<sub>M</sub> V E411A+I414A mutants grew similarly to rNiV<sub>M</sub>-wt through 60 hpi, at which point they failed to reach the same peak titer as rNiV<sub>M</sub>-wt. As seen in Vero 76 cells, the rNiV<sub>M</sub> V Y116E+E411A+I414A mutant had a replication defect that prevented distinguishing innate immune functional differences from viral polymerase machinery differences.

In summary, viral growth kinetics assays in Vero 76 cells and HEK293T cells demonstrated small differences between the MDA5-binding mutant rNiV<sub>M</sub> and rNiV<sub>M</sub>-wt at extremely low MOIs. The rNiV<sub>M</sub> Y116E+E411A+I414A construct, which contained a

mutation designed to inhibit binding to STAT1 as well as two mutations designed to inhibit binding to MDA5, replicated poorly compared to the other constructs in Vero 76 cells without IFN pretreatment. Therefore, definitive conclusions about the ability of this virus to inhibit IFN induction or response *in vitro* could not be drawn based on these results.

### **A rNiV<sub>M</sub> encoding mutations designed to prevent binding to MDA5 and STAT1 exhibited reduced lethality in the ferret model**

Because continuous cell lines are artificial systems lacking the complex immune systems and cell types present in a living organism, the impact of the MDA5-binding mutations on virulence in the ferret model was investigated next. Although the differences observed in cell culture viral kinetics assays were modest, rNiV that have replicated well in continuous cell lines, even in the presence of IFN (such as rNiV<sub>M</sub> V<sup>ko</sup>), have been non-lethal in ferrets at 5,000 PFU i.n.<sup>67</sup>. Furthermore, CDV engineered to be unable to bind MDA5 was non-lethal in ferrets, providing *in vivo* data in a similar model for a related virus<sup>194</sup>.

The design for the ferret study is shown in **Figure 3-4**. In addition to the three rNiV<sub>M</sub> encoding mutations designed to inhibit MDA5 and STAT1 binding examined in the last section and the rNiV<sub>M</sub>-wt control group, a group of ferrets receiving rNiV<sub>M</sub> V<sup>ko</sup>, which was previously shown to be non-lethal at a dose of 5,000 PFU i.n., was added as an additional control<sup>67</sup>.

Although the goal was to give a dose of 5,000 PFU i.n., as in previous studies using this model, back titration of the inoculum revealed that animals received closer to 50,000 PFU. The back titration results for the five groups were as follows: rNiV<sub>M</sub>-wt, 65,750 PFU; rNiV<sub>M</sub> V<sup>ko</sup>, 92,500 PFU; rNiV<sub>M</sub> V I414A, 58,000 PFU; rNiV<sub>M</sub> V E411A+I414A, 46,750 PFU; and rNiV<sub>M</sub> V Y116E+E411A+I414A, 27,500 PFU.

The survival curve for the ferret study is shown in **Figure 3-5**. There were no statistically significant differences between groups according to the Log-Rank (Mantel-

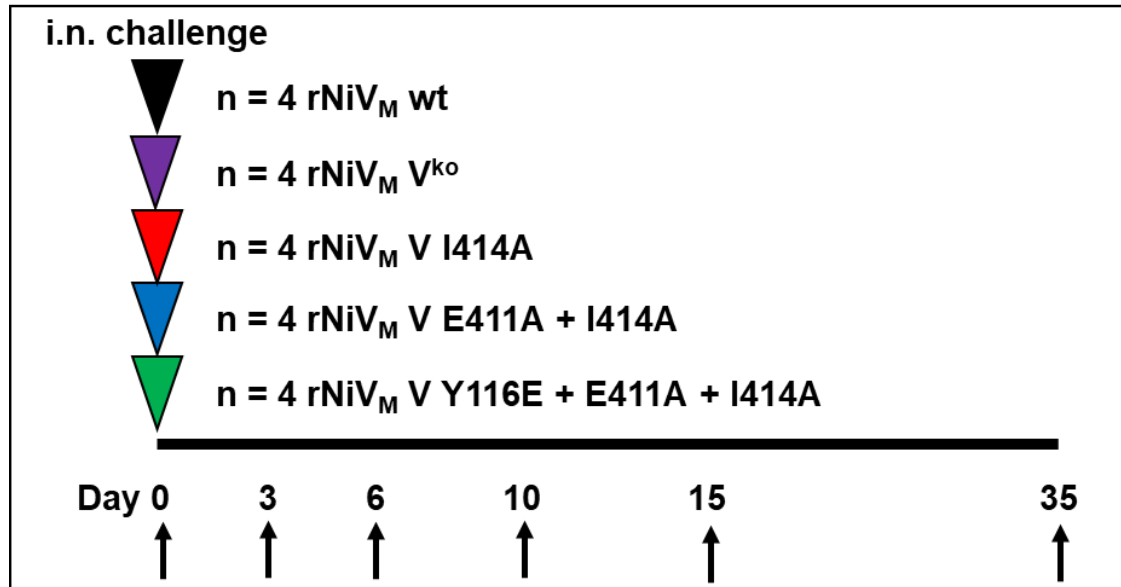


**Figure 3-4: Study design for ferrets challenged with rNiV<sub>M</sub>**

Study design for challenge study in which ferrets were experimentally infected via the i.n. route with each of the listed rNiV<sub>M</sub>. On day 0, four ferrets per group were challenged with rNiV<sub>M</sub>-wt (black triangle), rNiV<sub>M</sub> V<sup>ko</sup> (purple triangle), rNiV<sub>M</sub> V I414A (red triangle), rNiV<sub>M</sub> V E411A+I414A (blue triangle), or rNiV<sub>M</sub> V Y116E+E411A+I414A (green triangle). Study days in relation to challenge (day 0) are listed below the horizontal line, and arrows represent days on which blood samples were collected.

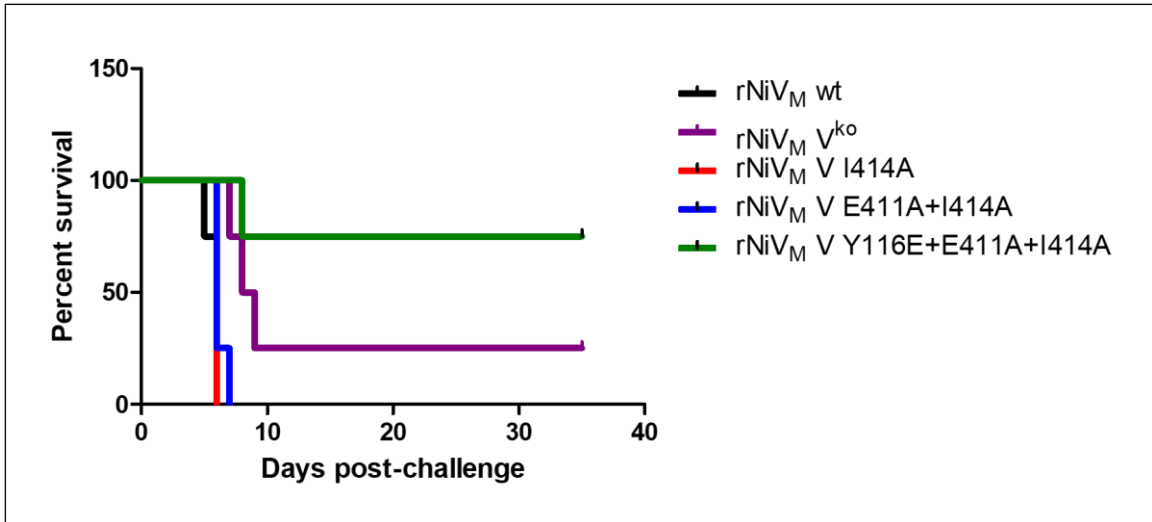


**Figure 3-5: Survival curve for ferrets challenged with rNiV<sub>M</sub>**

Kaplan-Meier survival curve for ferrets challenged with rNiV<sub>M</sub> containing mutations designed to inhibit binding to MDA5 and STAT1. Survival after challenge with about 50,000 PFU of rNiV<sub>M</sub>-wt (black line), rNiV<sub>M</sub> V<sup>ko</sup> (purple line), rNiV<sub>M</sub> V I414A (red line), rNiV<sub>M</sub> V E411A+I414A (blue line), and rNiV<sub>M</sub> V Y116E+E411A+I414A (green line) is shown. Survival was not determined to be significantly different between groups according to the Log-Rank (Mantel-Cox) test.

Cox) test, although the P value was 0.0657. The ferrets in the rNiV<sub>M</sub>-wt control group succumbed to NiV disease between five and seven days post-challenge. Death of a ferret infected with NiV at five dpi is uncommon but not unprecedented; subjects usually succumb to NiV disease between seven and eight dpi when given 5,000 PFU i.n.<sup>67,68,158</sup>. Similarly, the ferrets in the rNiV<sub>M</sub> V I414A group and the rNiV<sub>M</sub> V E411A+I414A group succumbed to NiV disease at six and seven dpi. These animals had a similar disease course in comparison to the control animals, and they received similar doses of virus according to the back titration; there did not appear to be a difference in virulence at this dose between wild-type rNiV<sub>M</sub> and rNiV<sub>M</sub> lacking the ability to bind to MDA5.

At the back-titrated dose of almost 100,000 PFU i.n., the rNiV<sub>M</sub> V<sup>ko</sup> virus was no longer non-lethal in ferrets. In this study, three ferrets in the group succumbed to NiV disease between seven and nine dpi, while the remaining animal survived to the study endpoint. The surviving animal had clinical signs of NiV disease at the same time as the other animals (**Table 3-2**) but recovered and had no further episodes of clinical illness.

At the back-titrated dose of around 30,000 PFU i.n., 75% of the animals in the rNiV<sub>M</sub> V Y116E+E411A+I414A group survived to the study endpoint. The last animal in the group succumbed to NiV disease on day eight post-challenge, in the same window as the animals in the other groups. One of the surviving animals had clinical signs of NiV disease during this window but recovered and had no further episodes of clinical illness up the study endpoint. The other two animals in this group remained well throughout the study but had mild changes in hematology and clinical chemistry (**Table 3-2**). In a previous study using the using the rNiV<sub>M</sub> P Y116E single mutant virus at a dose of about 5,000 PFU i.n., 100% of ferrets succumbed to NiV disease at eight or nine dpi<sup>158</sup>. Therefore, at a dose about six times higher in this study, the addition of the MDA5-binding mutations was sufficient to protect 75% of the animals from lethal outcome, although animals in this group exhibited hematological changes and/or signs of NiV disease.

<b>Ferret Group and Number</b>	<b>Clinical Signs/Outcome</b>	<b>Hematology/Clinical Pathology Findings</b>
rNiV <sub>M</sub> V I414A-1	Tachypnea (d6); dyspnea (d6); depression (d6). Subject euthanized (d6).	Lymphopenia (d6); monocytosis (d3, 6); neutrophilia (d3, 6); thrombocytopenia (d3, 6); ↓ CRE (d6); hypoalbuminemia (d6).
rNiV <sub>M</sub> V I414A-2	Tachypnea (d6); severe depression (d6). Subject euthanized (d6).	Lymphopenia (d3, 6); monocytosis (d3, 6); neutrophilia (d3, 6); thrombocytopenia (d6); hyperglycemia (d6); ↑ BUN (d6); ↓ CRE (d3); hypoalbuminemia (d6); ↓ AST (d3); hyperamylasemia (d3, 6).
rNiV <sub>M</sub> V I414A-3	Dyspnea (d6); depression (d6). Subject euthanized (d6).	Leukocytosis (d6); lymphopenia (d6); monocytosis (d3, 6); neutrophilia (d3, 6); thrombocytopenia (d3, 6); ↓ CRE (d3, 6); hypoalbuminemia (d6); ↓ ALP (d3, 6); hypoamylasemia (d6).
rNiV <sub>M</sub> V I414A-4	Tachypnea (d6); dyspnea (d6); severe depression (d6). Subject euthanized (d6).	Lymphopenia (d6); monocytosis (d3, 6); neutrophilia (d3, 6); thrombocytosis (d3); ↓ CRE (d3, 6); hypoalbuminemia (d3, 6); ↓ ALT (d3, 6); ↓ AST (d3, 6); ↓ ALP (d6); hypoamylasemia (d6).
rNiV <sub>M</sub> V E411A+I414A-1	Tachypnea (d6, 7); depression (d7). Subject euthanized (d7).	Lymphopenia (d3, 6, 7); monocytosis (d3, 6, 7); neutrophilia (d3, 6, 7); thrombocytopenia (d3); hypocalcemia (d7); hypoalbuminemia (d6, 7); ↑ ALT (d7); ↑ AST (d7); ↓ ALP (d6, 7); hypoamylasemia (d7).
rNiV <sub>M</sub> V E411A+I414A-2	Dyspnea (d6); severe depression (d6). Subject euthanized (d6).	Leukocytosis (d3, 6); lymphopenia (d6); monocytosis (d3, 6); neutrophilia (d3, 6); thrombocytosis (d3); ↑ CRE (d3, 6); hypoalbuminemia (d6); ↓ AST (d3); ↓ ALP (d6).
rNiV <sub>M</sub> V E411A+I414A-3	Dyspnea (d6); seizures (d6). Subject euthanized (d6).	Lymphopenia (d3, 6); monocytosis (d3, 6); neutrophilia (d3, 6); ↓ CRE (d3); hypoalbuminemia (d6); ↓ AST (d3); ↓ ALP (d6); ↓ GGT (d6); hypoamylasemia (d6).
rNiV <sub>M</sub> V E411A+I414A-4	Dyspnea (d6); severe depression (d6). Subject euthanized (d6).	Lymphopenia (d6); monocytosis (d6); neutrophilia (d3, 6); thrombocytopenia (d3, 6); ↓ CRE (d3, 6); hypoalbuminemia (d6); ↓ ALP (d6); hypoamylasemia (d6).
rNiV <sub>M</sub> V Y116E+E411A+I414A-1	None. Subject survived to study endpoint (d35).	Lymphopenia (d6, 35); monocytosis (d3, 6, 10, 15); neutrophilia (d6); ↑ BUN (d15); ↑ CRE (d3); ↓ CRE (d6); ↓ ALT (d6, 10, 35); ↓ AST (d10, 35); ↓ ALP (d6, 10, 35); ↓ GGT (d35); hypoamylasemia (d6, 35).
rNiV <sub>M</sub> V Y116E+E411A+I414A-2	None. Subject survived to study endpoint (d35).	Lymphopenia (d6); monocytopenia (d3); monocytosis (d15); neutrophilia (d6); ↓ CRE (d3, 6, 10, 15); hypoalbuminemia (d10); ↓ ALT (d3, 10, 15, 35); ↓ AST (d10, 15); ↓ ALP (d6, 10); hypoamylasemia (d3, 6, 10, 15, 35).
rNiV <sub>M</sub> V	Tachypnea (d7); dyspnea (d8);	Lymphopenia (d6, 8); monocytosis (d6); neutrophilia (d3, 6, 8);

Y116E+E411A+I414A-3	depression (d7); severe depression (d8). Subject euthanized (d8).	thrombocytosis (d3, 6, 8), ↑ CRE (d6, 8); hypoalbuminemia (d6, 8); ↓ AST (d3); ↓ ALP (d6).
rNiV <sub>M</sub> V Y116E+E411A+I414A-4	None. Subject survived to study endpoint (d35).	Leukocytosis (d15); lymphopenia (d6, 10); lymphocytosis (d15); monocytosis (d6, 10, 15, 35); neutrophilia (d6, 10); thrombocytopenia (d6); ↑ CRE (d3, 6, 10, 15, 35); hypoalbuminemia (d10); ↓ ALT (d6, 10, 15, 35); ↓ AST (d3, 6, 10, 15, 35); ↑ ALP (d3, 6, 10, 15, 35).
rNiV <sub>M</sub> V <sup>ko</sup> -1	Tachypnea (d8, 9). Subject survived to study endpoint (d35).	Leukocytosis (d6); monocytosis (d3, 6, 10, 35); neutrophilia (d6, 10); ↑ BUN (d6); ↑ CRE (d3, 6, 10, 15); hypoalbuminemia (d10); ↓ ALT (d15); ↓ AST (d15, 35); ↓ ALP (d35); hypoamylasemia (d35).
rNiV <sub>M</sub> V <sup>ko</sup> -2	Fever (d6, 7); tachypnea (d7, 8); dyspnea (d9); depression (d9); hind limb paresis (d9). Subject euthanized (d9).	Leukocytosis (d6, 9); lymphopenia (d6, 9); monocytopenia (d3); monocytosis (d6, 9); neutrophilia (d6, 9); thrombocytopenia (d9); ↑ BUN (d3, 9); ↑ CRE (d3, 6); ↓ CRE (d9); hypoalbuminemia (d6, 9); ↑ ALT (d9); ↓ ALP (d3, 6); ↑ ALP (d9); hypoamylasemia (d3, 6); loss of >10% body weight.
rNiV <sub>M</sub> V <sup>ko</sup> -3	Tachypnea (d7); seizures (d7). Subject euthanized (d7).	Lymphopenia (d6, 7); monocytopenia (d3); neutrophilia (d3, 6, 7); ↑ BUN (d3); ↓ CRE (d7); hypoalbuminemia (d7); ↓ ALP (d6, 7); ↓ GGT (d3, 6, 7); hypoamylasemia (d7).
rNiV <sub>M</sub> V <sup>ko</sup> -4	Dyspnea (d8); severe depression (d8). Subject euthanized (d8).	Leukocytosis (d6, 8); lymphopenia (d6, 8); monocytopenia (d3); monocytosis (d6, 8); neutrophilia (d6, 8); thrombocytopenia (d8); ↑ CRE (d6); ↓ CRE (d8); hypoalbuminemia (d8); ↓ ALT (d6); ↑ ALT (d8); ↓ AST (d3); ↓ ALP (d3, 6, 8); hypoamylasemia (d8).
rNiV <sub>M</sub> -wt-1	Nasal discharge (d5); mild depression (d5). Subject succumbed to infection (d6).	Lymphopenia (d6); neutrophilia (d3, 6); thrombocytopenia (d6); hypoglycemia (d6); ↑ BUN (d6); ↑ CRE (d3, 6); hyperuricemia (d6); hypoalbuminemia (d6); ↑ AST (d6); ↑ ALP (d6).
rNiV <sub>M</sub> -wt-2	Tachypnea (d6); mild depression (d6). Subject succumbed to infection (d7).	Lymphopenia (d3, 6); monocytosis (d3, 6); neutrophilia (d6); thrombocytopenia (d6); ↑ BUN (d6); ↑ CRE (d3); ↓ CRE (d6); hypoalbuminemia (d6); ↓ ALP (d6); hypoamylasemia (d6).
rNiV <sub>M</sub> -wt-3	Dyspnea (d6); depression (d5); severe depression (d6). Subject euthanized (d6).	Leukocytosis (d6); lymphopenia (d3, 6); neutrophilia (d3, 6); thrombocytopenia (d6); ↑ BUN (d6); ↑ CRE (d3, 6); hypoalbuminemia (d6); ↑ ALT (d6); ↑ AST (d6).
rNiV <sub>M</sub> -wt-4	Dyspnea (d5); depression (d5). Subject euthanized (d5).	Lymphopenia (d3, 5); monocytosis (d3, 5); neutrophilia (d3, 5); thrombocytopenia (d5); ↑ ALT (d5); ↓ ALP (d5); hypoamylasemia (d5).

Days after rNiV<sub>M</sub> challenge are in parentheses. All reported findings are in comparison to baseline (d0) values. Fever is defined as a temperature more than 2.5 °F over baseline. Lymphopenia, monocytopenia, neutropenia, and thrombocytopenia are defined by a  $\geq 35\%$  drop in numbers of lymphocytes, monocytes, neutrophils, or platelets, respectively. Leukocytosis, lymphocytosis, monocytosis, neutrophilia, and thrombocytosis are defined by a 100% or greater increase in numbers of white blood cells, lymphocytes, monocytes, neutrophils, or platelets, respectively. Hyperuricemia, hyperglycemia, and hyperamylasemia are defined by a 100% or greater increase in levels of uric acid, glucose, or amylase, respectively. Hypoglycemia, hypocalcemia, hypoalbuminemia, and hypoamylasemia are defined by a  $\geq 25\%$  decrease in levels of serum glucose, calcium, albumin, or amylase, respectively. Increases and decreases in BUN, CRE, ALT, AST, ALP, and CRP were graded on the following scale:  $\uparrow$  = 1- to 5-fold increase,  $\downarrow$  =  $\geq 25\%$  decrease.

**Table 3-2: Clinical disease and findings in ferrets after experimental infection with rNiV<sub>M</sub>**

**Table 3-2** details the clinical signs of NiV disease, clinical outcome, and hematological and clinical chemistry values observed for each subject in the ferret study. Animals exhibited systemic signs of NiV disease such as fever and depression, respiratory signs such as tachypnea and dyspnea, and neurological signs such as seizures and hind limb paresis one to two days prior to reaching euthanasia criteria. These clinical signs were accompanied by clinical findings such as lymphopenia, neutrophilia, thrombocytopenia, hypoalbuminemia, and hypoamylasemia within one to three days of euthanasia. Increased neutrophils and decreased serum albumin are generalized signs of inflammation, while the other clinical markers indicate systemic dysfunction due to severe illness. Animals that survived to the study endpoint developed similar clinical findings from around six to 10 dpi, which is the same time window in which the animals that succumbed to NiV disease were clinically ill. Surviving animals developed clinical signs to a lower severity than those that reached euthanasia criteria, although the signs and hematological changes were similar.

RT-qPCR with primers specific to the NiV<sub>M</sub> genome was carried out on samples of whole blood that were collected throughout the study and from which RNA was extracted, as well as from tissues collected at necropsy. The results of RT-qPCR on EDTA whole blood samples are shown in **Figure 3-6A** and are expressed in GEq/mL of blood. Viral RNA was detectable beginning at 3 dpi for two subjects, one in the rNiV<sub>M</sub> V E411A+I414A group and one in the rNiV<sub>M</sub> V<sup>ko</sup> group. All subjects were positive for NiV<sub>M</sub> genomic RNA by 6 dpi. For animals that succumbed to NiV disease, the highest levels of viral RNA were detected on the day of humane euthanasia. Interestingly, while viral RNA was undetectable after 10 dpi in the surviving subject within the rNiV<sub>M</sub> V<sup>ko</sup> cohort, RNA was detectable in two of the surviving rNiV<sub>M</sub> V Y116E+E411A+I414A animals at the study endpoint at 35 dpi. Previously, viremia resolved in ferret and AGM survivors of NiV challenge by around 10 dpi<sup>68,172,175</sup>, so the persistence of NiV<sub>M</sub> genomic RNA in the blood of surviving animals in the rNiV<sub>M</sub> V Y116E+E411A+I414A group will

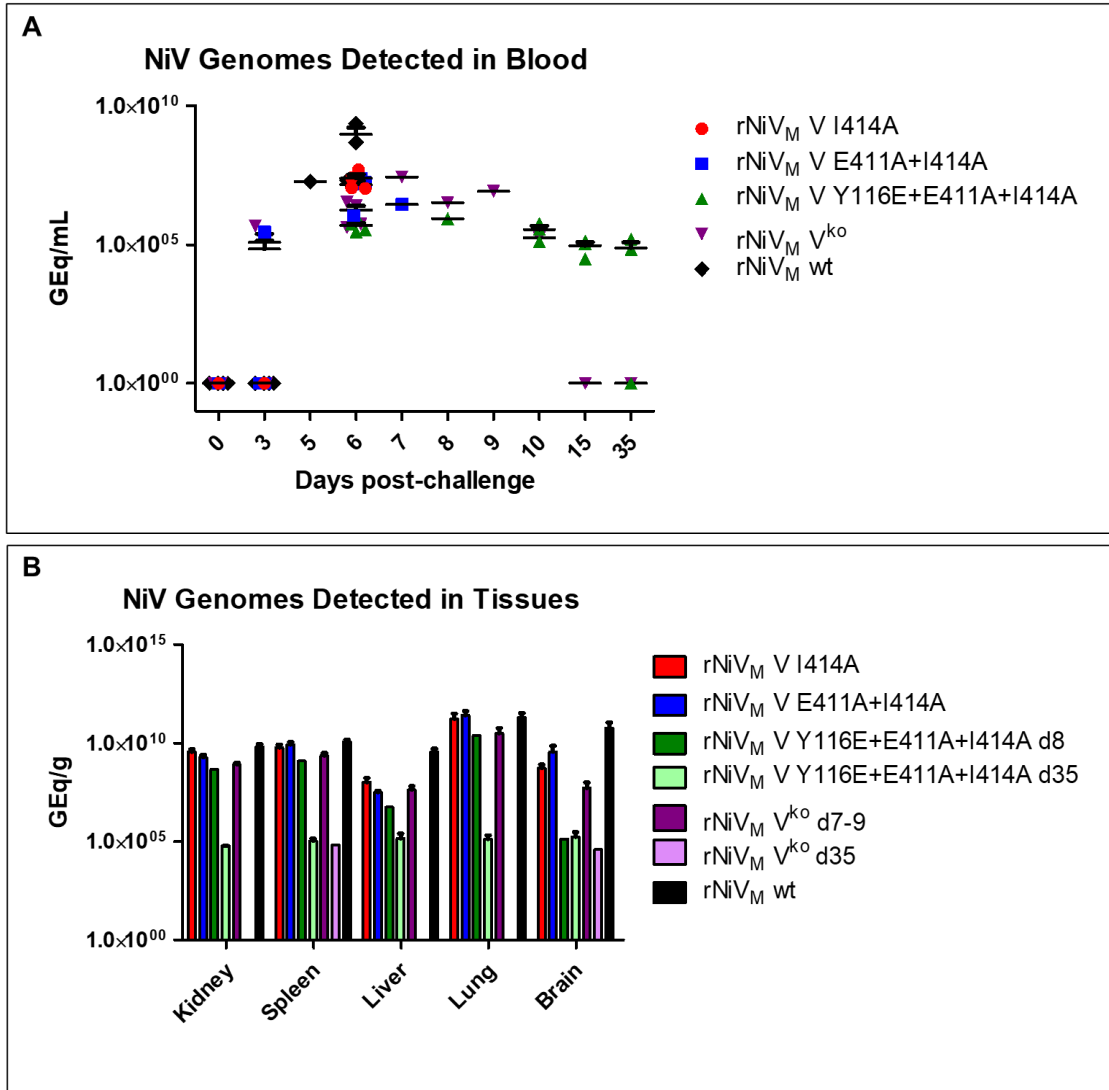


**Figure 3-6: NiV<sub>M</sub> genomes detected by RT-qPCR in ferrets challenged with rNiV<sub>M</sub>**

Results of RT-qPCR targeting the NiV<sub>M</sub> genome in the (A) blood and (B) tissues of ferrets challenged with rNiV<sub>M</sub> in the designated cohorts. For panel (A), results are expressed in GEq/mL of blood, and each subject is represented by a point, as indicated in the figure legend. The mean value for each group at each timepoint is represented by a horizontal line. For panel (B), results are expressed in GEq/g of tissue, and the mean value for each cohort is shown in the bar graph. For the rNiV<sub>M</sub> V Y116E+E411A+I414A and rNiV<sub>M</sub> V<sup>ko</sup> cohorts, animals are split based on survival status. The animal in the rNiV<sub>M</sub> V Y116E+E411A+I414A group that succumbed to NiV disease at 8 dpi is shown in dark green, while the surviving members of the cohort euthanized on day 35 are shown in light green. The subjects that succumbed to NiV disease within the rNiV<sub>M</sub> V<sup>ko</sup> cohort on days seven through nine post-challenge are shown in dark purple, while the surviving animal in that cohort is shown in lavender. For all other groups, all animals succumbed to NiV infection, so all animals are grouped together on the bar graph. Error bars represent the SEM. Colors represent the same groups across the two panels.

be further investigated by sequencing the isolated RNA to determine if the point mutations reverted to wild-type or whether other mutations that could promote persistence are present.

The results of RT-qPCR for NiV genomic RNA on sections of kidney, spleen, liver, lung, and frontal lobe collected at necropsy for each animal in the ferret study are shown in **Figure 3-6B** and are expressed in GEq/g of tissue. NiV<sub>M</sub> genomic RNA was detected in all collected tissues for all animals that succumbed to NiV disease. Animals that survived to the study endpoint had lower levels of detectable viral RNA in tissues than ferrets that succumbed to NiV disease. For the surviving ferret challenged with rNiV<sub>M</sub> V<sup>ko</sup>, NiV<sub>M</sub> RNA was detected only in the spleen and brain; this result corroborates previous ferret studies in which RNA was detectable in the spleen and brain of some survivors of rNiV challenge at study endpoint<sup>67,68,165</sup>. Surviving animals in the rNiV<sub>M</sub> V Y116E+E411A+I414A group had either three, four, or five tissues positive for viral RNA. Combined with the results from whole blood at the day 35 study endpoint, these results are indicative of increased persistence of NiV in the surviving rNiV<sub>M</sub> V Y116E+E411A+I414A animals compared to the surviving rNiV<sub>M</sub> V<sup>ko</sup> subject. However, additional experiments, including viral deep sequencing and plaque assays to quantify infectious virus, are needed to investigate this hypothesis further, as presence of viral RNA is common in tissues at the end of NiV animal studies and does not necessarily indicate the presence of infectious virus<sup>67,68,165</sup>.

Further analysis of this animal study is currently in progress. Quantification of culturable virus in blood and tissues will be an important step to determine whether infectious rNiV<sub>M</sub> is present at 35 dpi. Furthermore, examination of tissues for gross and histopathological lesions, as well as immunohistochemistry to assess the presence of NiV antigen in tissues, is underway. However, taken together, these results indicate that MDA5 and STAT1 may mediate NiV virulence, although the virus can overcome the inability to inhibit either one alone in the ferret model. Attempts to distinguish the unique

contributions of MDA5 inhibition and STAT1 inhibition to growth of rNiV<sub>M</sub> in cell culture in the presence of IFN were complicated by the growth defect in the virus containing the Y116E mutation. However, differences in virulence were observed *in vivo*, although additional studies will be needed for direct comparisons to previous results.

## DISCUSSION

Numerous experiments have investigated the impact of the NiV V protein on the innate immune response using expression plasmids under BSL-2 conditions; however, the experiments and results presented here add further analysis and depth to those earlier observations because they are some of the first to examine such mutations in rNiV<sub>M</sub> in BSL-4 biocontainment. Recognizing that plasmid-based protein overexpression studies are a first step and that findings do need to be validated in virus infection models and also with *in vivo* studies, the experiments and data presented here represent an important step forward in understanding the factors driving NiV pathogenesis.

The MOIs used in the growth curves covered in this chapter were extremely low. These MOIs offered the best chance of ensuring that NiV did not overwhelm the cells before the innate immune system had a chance to respond and also provided a better chance to see small differences between wild-type and mutant rNiV<sub>M</sub>. However, smaller differences than expected were seen in these assays; previous experiments with rNiV<sub>M</sub> V<sup>ko</sup> and rNiV<sub>M</sub> P Y116E at an MOI of 0.01 revealed growth defects of about one log compared to wild-type rNiV<sub>M</sub> in the presence of IFN<sup>67,158</sup>. Therefore, one possible explanation is that the low MOIs used in the study did not provide enough viral RNA to strongly induce the IFN production pathway soon enough to see differences. Another growth curve at an MOI of 0.01 is in progress, which will allow direct comparison of the newly generated rNiV<sub>M</sub> to previous results; rNiV<sub>M</sub> V<sup>ko</sup> and rNiV<sub>M</sub> P Y116E have been added as additional controls.

Another explanation for the small differences observed between wild-type and mutant rNiV<sub>M</sub> in these experiments could be that the IFN production pathway was not induced despite lack of MDA5 inhibition because NiV retains the ability to inhibit an upstream regulator of the pathway. For instance, the phosphatase PP1 is responsible for activating MDA5 by removing a phosphate group from a serine residue<sup>210,213</sup>. This hypothesis was discussed in detail in Chapter 2. The binding site for PP1 by NiV V has not been identified and is not the same as the one identified for MeV V<sup>210</sup>, so further investigation is needed to identify this binding site and determine whether blocking of binding to both MDA5 and PP1 by NiV V allows the IFN production pathway to function properly and transduce an antiviral signal.

These samples were treated with IFN just once prior to viral kinetics experiments, at a timepoint and dose previously optimized<sup>67,158</sup>. However, these experiments were carried out to 96 hpi while previous experiments ended at 48 or 72 hpi due to cell death because of the use of a higher MOI. Optimization is needed to determine whether additional and/or higher doses of exogenous IFN are needed for effective induction of the IFN pathway and to determine the kinetics of the IFN response during the course of NiV infection. Alternatively, it would be interesting to repeat these experiments with a specific agonist of RIG-I<sup>225</sup> or MDA5.

Although the *in vitro* experiments presented here showed smaller differences than expected between wild-type and mutant rNiV<sub>M</sub>, the *in vivo* experiments presented were still informative. The rNiV<sub>M</sub> V<sup>ko</sup> virus that was previously shown to be non-lethal in ferrets at 5,000 PFU still grew to high titers in continuous cell lines<sup>67</sup>, which lack the complex immune system and interplay between cell types of a living organism. Furthermore, previous *in vivo* data indicated that these experiments were worthwhile. An MDA5-blind recombinant CDV was non-lethal in ferrets despite causing transient viremia and clinical signs<sup>194</sup>, and delayed time to death was observed in ferrets infected with a rNiV<sub>M</sub> incapable of binding to STAT1<sup>158</sup>. Therefore, data from a closely related

virus and similar model indicated that MDA5 could be an important mediator of paramyxovirus virulence, and data from the same virus and model indicated that STAT1 plays a role in virulence. Inclusion of a virus incapable of binding both MDA5 and STAT1 allowed comparison of the individual contributions of MDA5 and STAT1 to their combined contributions to NiV virulence.

The ferrets in the study discussed here received significantly more virus than the 5,000 PFU per animal previously established as the minimum lethal dose for this model<sup>81</sup>. Therefore, it is impossible to compare the rNiV<sub>M</sub> V I414A and rNiV<sub>M</sub> V E411A+I414A groups from this study to previous work. However, the inclusion of a rNiV<sub>M</sub> V<sup>ko</sup> group and a group with a virus lacking the ability to bind to STAT1 allows comparisons between these groups and to prior results.

At 5,000 PFU, animals infected with rNiV<sub>M</sub> V<sup>ko</sup> developed mild clinical signs of NiV disease, changes in hematology and clinical pathology, and detectable viral RNA in blood and tissues<sup>67</sup>. Therefore, this virus was not avirulent but rather non-lethal at this dose. The results of the present study make clear that the rNiV<sub>M</sub> V<sup>ko</sup> virus is not benign, as three out of the four animals succumbed to the infection. However, the recovery and survival to the study endpoint of one animal without apparent lingering effects is encouraging, as this group received the highest dose of virus out of all the groups in the study according to back titration of the inoculum. Therefore, the observation of reduced virulence of a rNiV lacking the V CTD in the ferret model was replicated in this study.

Previous studies with a challenge dose of 5,000 PFU of rNiV<sub>M</sub> resulted in death of 100% of ferrets during the normal NiV window for animals receiving rNiV<sub>M</sub> P Y116E and delayed time to death for 100% of ferrets receiving rNiV<sub>M</sub> P Δ116-135<sup>158</sup>. Therefore, the results presented here for ferrets given about six times more virus in the rNiV<sub>M</sub> V Y116E+E411A+I414A group are illuminating. There are three possible explanations for the survival of 75% of the animals in this cohort without apparent lingering effects of NiV disease: lower initial viral dose, slower replication of this virus *in vivo*, or combined

lack of inhibition of innate sensing and innate signaling by this virus. While it is true that, according to back titration of the inoculum, these animals received less virus than animals in the other groups, they received several times higher doses than ferrets that succumbed to rNiV<sub>M</sub> designed to inhibit STAT1 binding<sup>158</sup>. Therefore, it is not likely that lower initial dose explains the survival result in this cohort.

In the viral kinetics assays presented in this chapter, a growth defect inherent to the Y116E mutation was demonstrated in cell culture. However, the rNiV<sub>M</sub> containing this mutation alone was still 100% lethal in ferrets at 5,000 PFU i.n., and viral RNA was detected in blood and tissues at similar timepoints and concentrations as rNiV<sub>M</sub>-wt and rNiV<sub>M</sub> P Δ116-135<sup>158</sup>. Therefore, the difference in survival between the rNiV<sub>M</sub> V I414A and rNiV<sub>M</sub> V E411A+I414A groups and the rNiV<sub>M</sub> V Y116E+E411A+I414A group was not likely to be due to slower replication of the virus in these animals. In fact, animals in the rNiV<sub>M</sub> V Y116E+E411A+I414A group had similar levels of NiV<sub>M</sub> genome in the blood as compared to subjects in the rNiV<sub>M</sub> V E411A+I414A and rNiV<sub>M</sub> V<sup>ko</sup> groups during acute NiV disease (**Figure 3-6A**). Instead, the most probable explanation is that combined prevention of STAT1 and MDA5 inhibition by NiV was enough for these animals to mount an adaptive immune response and recover from NiV disease. Therefore, blocking of binding to both MDA5 and STAT1 by NiV P gene products appears to reduce virulence in the ferret model, which supports the hypothesis that inhibition of both host molecules contributes to NiV virulence. Interestingly, CDV lacking the ability to bind to STAT1 was not less virulent in ferrets, but CDV lacking the ability to bind to STAT2 was<sup>194</sup>. Since NiV and CDV have distinct mechanisms and binding sites for inhibition of STAT1/STAT2 (see Chapter 1), it makes sense that different virulence strategies may be important for these two pathogens.

These experiments involved point mutations designed to prevent binding to MDA5 and STAT1. Point mutations were chosen to minimize changes to the essential P protein that could affect viral replication and confound the results, but they also make

reversion to wild-type NiV a possibility. Tissues were collected from these animals at terminal or study endpoint, and RNA was isolated from them. An important future direction would be to sequence viral RNA isolated from tissues and determine whether it has retained the point mutations present in the original inoculum. If the point mutations tend to revert in infected animals, that would have implications for analyzing these results and making conclusions about NiV virulence.

Taken together, the experiments and data presented in this chapter characterized the impact of the V-MDA5 interaction on viral replication and *in vivo* virulence using rNiV<sub>M</sub> constructs under BSL-4 containment. Indeed, these mutant rNiV<sub>M</sub> constructs grew to lower peak titers in continuous cell lines in the presence of IFN at very low MOI. Furthermore, and of significance, a rNiV<sub>M</sub> designed to prevent binding to both MDA5 and STAT1 resulted in significant attenuation and a 75% survival result in challenged ferrets, clearly indicating the importance of both of these viral-host cell interactions as virulence factors for NiV<sub>M</sub>. Future studies at lower doses of rNiV<sub>M</sub> and with prevention of binding to additional regulators of the MDA5 pathway are needed to determine the specific contributions that MDA5 inhibition alone may have on NiV virulence.

# **Chapter 4: A Single-Dose, Single-Cycle, VSV-Vectored Vaccine Protects African Green Monkeys when Given Shortly Prior to Nipah Virus Bangladesh Challenge**

## **INTRODUCTION**

NiV<sub>B</sub> causes small, sporadic outbreaks of NiV disease with high CFRs in Bangladesh and India<sup>226</sup>. During an outbreak in the state of Kerala, India, in 2018, NiV<sub>B</sub> spread to family and hospital caregivers through close contact and led to 23 identified cases and 21 deaths<sup>19</sup>. Most recently, six cases were identified in Bangladesh in 2020 that led to four reported deaths<sup>227</sup>. Person-to-person transmission is a common feature of outbreaks of NiV<sub>B</sub><sup>16,32</sup>. A human mAb, m102.4, was identified within an antigen-binding fragment antibody library from naïve healthy donors and prevents viral entry by binding to the receptor-binding domain of the G protein; it has potent cross-neutralizing activity against HeV, NiV<sub>M</sub>, and NiV<sub>B</sub><sup>159,160</sup>. The m102.4 mAb is currently available for compassionate use to treat symptomatic patients or prevent infection after laboratory exposures, and it has been used after 13 exposures to HeV in Australia and one exposure to NiV in the United States<sup>161</sup>. However, no licensed active immunization is available for prevention of NiV infection<sup>180</sup>. A vaccine that works rapidly is urgently needed to prevent spread during outbreaks of this highly lethal pathogen.

As discussed in Chapter 1, NiV vaccine candidates using rVSV as a vector have been in development for years<sup>187</sup>. Replication-incompetent vectors encoding either NiV F or G effectively protected Syrian hamsters, ferrets, and AGMs from challenge with NiV when given at least 28 days prior to challenge<sup>151,165,191</sup>. Replication-competent constructs encoding NiV<sub>M</sub> F or G along with EBOV GP protected 100% of Syrian hamsters as well as AGMs when given 28 days (hamsters) or 29 days (AGMs) prior to challenge with NiV<sub>M</sub>, and protection could be passively transferred to naïve hamsters<sup>152,176</sup>. In short,

rVSV- $\Delta$ G-NiV F and G constructs have been shown to protect ferrets, Syrian hamsters, and AGMs from lethal challenge with either NiV<sub>M</sub> or NiV<sub>B</sub> in a single dose, whether replication-competent or -incompetent.

Although previous studies compared constructs encoding NiV F, NiV G, and both NiV surface proteins from both NiV<sub>M</sub> and NiV<sub>B</sub>, NiV<sub>B</sub> G alone was chosen as the immunogen for the development and testing of the rVSV- $\Delta$ G vaccine described here. NiV<sub>B</sub> appeared to be more virulent than NiV<sub>M</sub> in the AGM model and had a shorter therapeutic window for treatment with m102.4 mAb, and NiV<sub>B</sub> has more recently and consistently caused outbreaks of NiV disease<sup>172,173,226</sup>. Previous studies demonstrated the most consistent and robust neutralizing antibody responses to rVSV expressing the NiV<sub>B</sub> G antigen alone (as opposed to expression of NiV<sub>B</sub> F or both NiV<sub>B</sub> F and G)<sup>191</sup>. Furthermore, the rVSV-NiV constructs used previously encoded the fluorescent reporter GFP, which was previously shown to generate robust immune responses in mice and interfered with tumor immune responses; GFP could thus be a confounding additional immunogen<sup>228</sup>. Therefore, the work presented here describes the development of an updated version of the G\*-rVSV- $\Delta$ G-NiV<sub>B</sub> G vaccine construct encoding NiV<sub>B</sub> G and lacking GFP. The rVSV vaccine vector has been previously demonstrated to induce rapid protection against EBOV in a single dose in NHPs, with 100% of animals vaccinated seven days prior to challenge and 67% of animals vaccinated three days prior to challenge surviving to the study endpoint<sup>229</sup>. The feasibility of rapid protection induced by rVSV vaccines is thus established, and such a vaccine with demonstrated rapid efficacy in relevant animal models would be invaluable for deployment in an outbreak scenario to prevent further spread of NiV.

This chapter describes the generation and characterization of an updated G\*-rVSV- $\Delta$ G-NiV<sub>B</sub> G vaccine lacking GFP and rescued using an established reverse genetics system. The vaccine was tested in AGMs challenged with NiV<sub>B</sub> seven or three days after a single dose of vaccine, and NiV-specific humoral immune responses were

interrogated. Efforts to define a survivor phenotype and to evaluate cellular NiV-specific immune responses are underway and will be discussed.

## **METHODS**

### **Cell culture**

BHK-21 clone WI-2 cells were a generous gift from Dr. Michael A. Whitt (currently at The University of Tennessee Health Science Center; Memphis, Tennessee, USA)<sup>230</sup>. BHK-21 clone WI-2 cells were maintained in high-glucose DMEM supplemented with 5% heat-inactivated FBS, 1% penicillin/streptomycin solution (10,000 units/mL penicillin and 10,000 µg/mL streptomycin), and 1% GlutaMAX™ Supplement.

Vero 76 monkey kidney cells were maintained as described in Chapter 3.

### **Cloning to produce the full-length pVSV-ΔG-NiV<sub>B</sub> G plasmid**

The pVSV-ΔG-NiV<sub>B</sub> G plasmid was made by Gibson assembly of fragments encoding the NiV<sub>B</sub> G gene and the remainder of the pVSV-ΔG backbone<sup>223</sup>. To generate vector material for Gibson assembly, a previously constructed pVSV-ΔG plasmid was digested with MluI-HF and AvrII restriction enzymes (NEB; Cat. Nos. R3198 and R0174, respectively) and purified by SDS-PAGE electroelution. Oligonucleotide PCR primers designed with large overhangs for Gibson assembly were ordered from IDT. Inserts were generated by using the primers to amplify the NiV<sub>B</sub> G gene from the previous pVSV-ΔG-NiV<sub>B</sub> G-GFP construct by PCR using Platinum™ SuperFi™ DNA polymerase according to manufacturer instructions. The full-length pVSV-ΔG-NiV<sub>B</sub> G construct, encoding rVSV-ΔG with NiV<sub>B</sub> G in place of VSV G in the pBluescript (pBS) plasmid backbone, was assembled using the NEBuilder® HiFi DNA Assembly Cloning Kit according to manufacturer instructions. Presence of the NiV<sub>B</sub> G gene was confirmed and cloning borders checked by Sanger sequencing and diagnostic restriction digest. A

large culture of *E. coli* transformed with the construct was grown, and plasmid was purified by alkaline lysis cesium chloride plasmid prep as previously described<sup>230</sup>.

### **Recovery, amplification, and characterization of the G\*-rVSV-ΔG-NiV<sub>B</sub> G vaccine**

The G\*-rVSV-ΔG-NiV<sub>B</sub> G vaccine construct was recovered using a protocol modified from Dr. Michael A. Whitt<sup>230</sup>. A schematic outlining the process for recovery of the construct in BHK-21 clone WI-2 cells is shown in **Figure 4-1**. Cells were seeded in 6-well plates to be 70 to 80% confluent for infection and transfection the next day. First, the cells were infected with modified vaccinia virus expressing bacteriophage T7 polymerase (vTF7-3; ATCC; Cat. No. VR-2153) at an MOI of 5. Immediately afterward, cells were transfected with pBS-VSV G, pBS-VSV N, pBS-VSV P, pBS-VSV L, and the full-length pVSV-ΔG-NiV<sub>B</sub> G plasmid (all under the control of the T7 promoter) in a ratio of 8:3:5:1:5 using TransfectACE reagent<sup>230</sup> at a ratio of 3.5 μL per μg of plasmid DNA. Control wells were transfected with pVSV-ΔG-GFP or pVSV-ΔL-GFP and the helper plasmids. Plates were incubated at 37°C and 5% CO<sub>2</sub> for four to five hours, at which point the growth medium was changed. Plates were returned to the incubator for 48 hours to allow production of infectious virions.

Because the G\*-rVSV-ΔG-NiV<sub>B</sub> G vaccine encodes only one of the two NiV surface proteins, it requires complementation with VSV G provided in *trans* for propagation in cells. BHK-21 clone WI-2 cells were seeded in 6-well plates to be 70 to 80% confluent for transfection the next day. Cells were transfected with 1 μg of pCAGGS-VSV G plasmid per well with 3 μL per well of Lipofectamine<sup>TM</sup> 2000 Transfection Reagent (Thermo Fisher Scientific; Cat. No. 11668019). Plates were incubated at 37°C and 5% CO<sub>2</sub> for four hours, the growth medium was changed, and the plates were returned to the incubator overnight to allow expression of VSV G and formation of syncytia. These cells are hereafter called G-complemented (G\*) BHK cells.

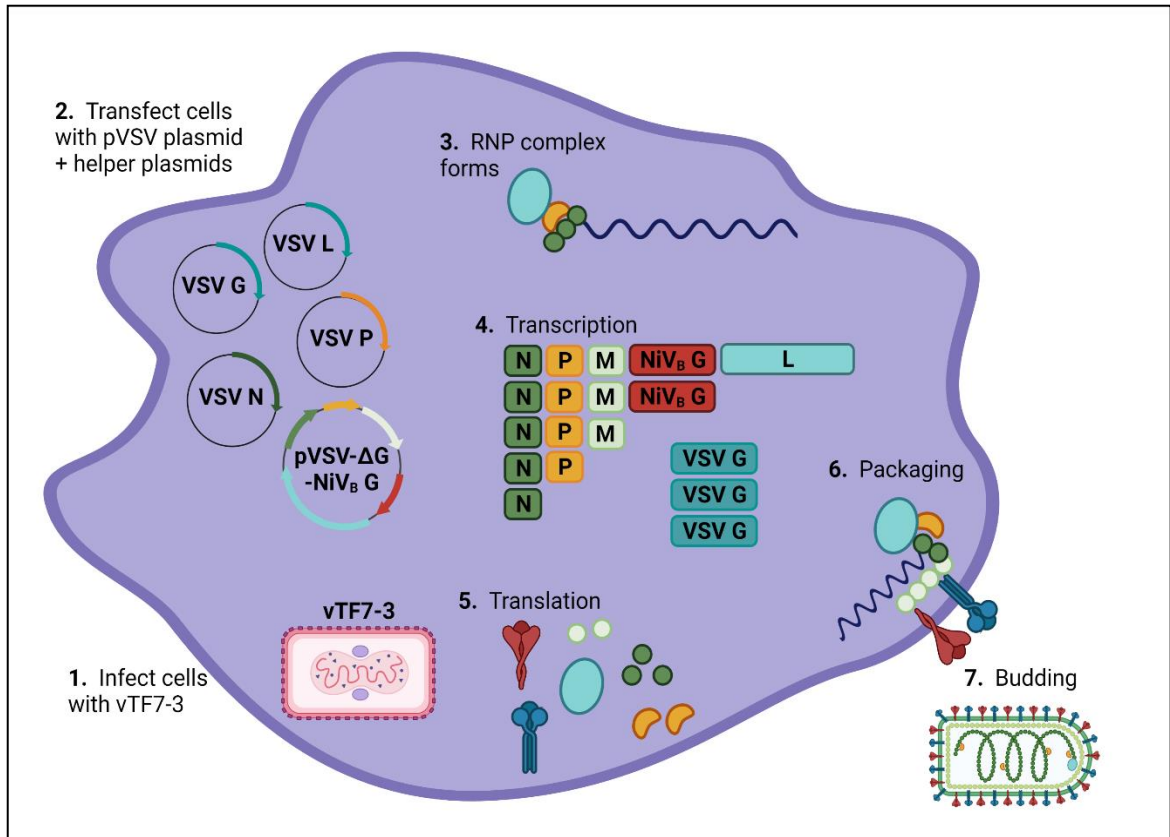


**Figure 4-1: Recovery of rVSV-ΔG-NiV<sub>B</sub> G virions**

Diagram of the process by which recovery of rVSV-ΔG-NiV<sub>B</sub> G virions occurred in BHK-21 clone WI-2 cells. **1.** Cells were infected with vTF7-3 to produce bacteriophage T7 polymerase. **2.** Cells were transfected with the full-length pVSV-ΔG-NiV<sub>B</sub> G plasmid and helper plasmids encoding VSV G, VSV N, VSV P, and VSV L (all under the control of the T7 promoter). **3.** The N, P, and L helper plasmids were transcribed and translated to produce VSV N, P, and L protein; the full-length plasmid was transcribed to produce the RNA genome of rVSV-ΔG-NiV<sub>B</sub> G. Together, they formed the RNP complex. The G helper plasmid was transcribed and translated to produce VSV G protein (transcripts shown under (4) and protein shown under (5)). **4.** The RNA genome was transcribed to produce mRNAs encoding VSV N, P, M, and L and NiV<sub>B</sub> G. **5.** The mRNAs were translated to produce VSV N, P, M and L and NiV<sub>B</sub> G proteins. **6.** The RNA genome and viral structural proteins were packaged into virions near the cell membrane. **7.** Live virions budded out from the cell with NiV<sub>B</sub> G and VSV G proteins on their surface. VSV G was not encoded in the genome but was provided in *trans*. Figure created using BioRender.com.

After the 48-hour incubation, supernatant was removed from the pVSV- $\Delta$ G-NiV<sub>B</sub> G transfection wells and filtered through a 0.22-micrometer Millex-GS syringe filter (Millipore; Burlington, Massachusetts, USA; Cat. No. SLGSM33SS) to remove vTF7-3. The filtered supernatant was then used to infect the G\* BHK cells by incubating 500  $\mu$ L per well for one hour at 37°C and 5% CO<sub>2</sub>. After adsorption, 2 mLs per well of complete DMEM with 5% FBS was added to the cells. Plates were incubated at 37°C and 5% CO<sub>2</sub> for 48 to 72 hours to allow VSV-specific CPE to develop. Once cells exhibited 40 to 100% VSV-specific CPE, supernatants were collected, clarified, aliquoted into 2-mL externally threaded screwcap tubes with O-rings, and frozen at -80°C.

Next, recovery supernatants were passaged on fresh G\* BHK cells for plaque purification. Picked plaques were collected into 2-mL screwcap tubes containing DMEM with 5% FBS, incubated at 37°C for 1 hour with intermittent vortexing, and then the medium was used to infect fresh G\* BHK cells for passage 1 (p1). Positive p1 supernatants were collected when VSV-specific CPE was observed (about 24 hpi), clarified to remove cell debris, and used to infect 10-centimeter cell culture dishes of G\* BHK cells at an MOI of 1 for p2. At 24 hpi, VSV-specific CPE was observed, and the supernatant was collected, clarified, and aliquoted into 2-mL screwcap tubes for storage of p2 G\*-rVSV- $\Delta$ G-NiV<sub>B</sub> G seed stocks at -80°C.

Viral titers were determined using a standard plaque assay by infecting duplicate wells of G\* BHK cells in 6-well plates with 200  $\mu$ L each of 10-fold serial dilutions of viral stocks. After one-hour adsorption, plates were overlaid with two mLs per well of medium containing final concentrations of 1X MEM, 5% FBS, and 0.8% SeaKem® ME agarose. At 24 hpi, plaques were stained with a solution of 5% neutral red and 5% FBS in PBS without calcium and magnesium, and plaques were visualized and counted four hours later.

Viral RNA was isolated from p2 seed stock in TRIzol™ LS Reagent using the Direct-zol RNA miniprep kit according to manufacturer instructions. The complete viral

RNA genome was sequenced with the NextSeq 550 system with a depth of 130 million reads. DNA was extracted from p2 seed stock in TRIzol™ LS according to manufacturer instructions for *Mycoplasma* testing with the e-Myc™ plus Mycoplasma PCR Detection Kit (LiliF Diagnostics; Burlington, Massachusetts, USA; Cat. No. 25238). The p2 seed stock was subjected to endotoxin testing using Endosafe®-PTS™ Limulus Amebocyte Lysate cartridges (Charles River Laboratories; Wilmington, Massachusetts, USA; Cat. No. PTS2001).

### **Immunofluorescence assays**

For immunofluorescence assays (IFAs) to check for expression of NiV<sub>B</sub> G in rVSV-ΔG-NiV<sub>B</sub> G-infected cells, BHK-21 clone WI-2 cells and Vero 76 cells were seeded in 6-well plates at a density of  $2 \times 10^5$  cells per well to be 50 to 70% confluent for infection the next day. Cells were infected with G\*-rVSV-ΔG-NiV<sub>B</sub> G at an MOI of 3 or mock-infected with growth media only. At eight hpi, cells were fixed with a solution of 4% paraformaldehyde (made from 16% stock; Electron Microscopy Sciences; Hatfield, Pennsylvania, USA; Cat. No. 15710) in water and then quenched overnight in PBS with 100 mM glycine (PBS-glycine; made from Dulbecco's PBS with calcium and magnesium, Thermo Fisher Gibco, Cat. No. 14040; and glycine powder, Amresco, Dallas, Texas, USA, Cat. No. 0167-5KG). Half of the wells for each cell line were permeabilized with 0.5% Triton™ X-100 (Sigma-Aldrich; Cat. No. T8787-100ML) in PBS-glycine, while the remaining wells were processed without permeabilization. All wells were blocked for one hour in 3% sterile BSA (Thermo Fisher Gibco; Cat. No. 15260-037) in PBS (hereafter known as blocking buffer). Conditions receiving m102.4 primary antibody for the detection of the NiV<sub>B</sub> G attachment glycoprotein were incubated with 50 μg/mL antibody in blocking buffer at 4°C overnight, while secondary-only infected wells were incubated in blocking buffer only at 4°C overnight.

All wells were washed three times with blocking buffer and then incubated with secondary antibody solution comprising goat anti-human IgG conjugated to Alexa Fluor™ 488 (dilution 1:5,000; Thermo Fisher Invitrogen; Cat. No. A11013) in blocking buffer for one hour, protected from light. Wells were then washed three times with blocking buffer and stored under PBS-glycine for imaging on a Nikon Eclipse Ti inverted fluorescent microscope (Nikon; Minato City, Tokyo, Japan). Images were obtained using the fluorescein isothiocyanate filter and were exposed for 300 milliseconds at 20% power. Magnification from eyepiece and objectives totaled 100X.

## **Animal Studies**

### ***ANIMAL HANDLING AND PROCEDURES***

Protocols for animal studies were approved by UTMB's IACUC and complied with the Animal Welfare Act and the *Guide for the Care and Use of Laboratory Animals*, National Research Council. Animal studies were performed under BSL-4 biocontainment in the UTMB GNL, which is fully accredited by AAALAC International.

For each study, nine adult AGMs (three to eight kilograms in weight) were randomized to the rVSV-ΔG EBOV 76 nonspecific vaccine control group or the G\*-rVSV-ΔG-NiV<sub>B</sub> G specifically vaccinated group (three females and three males in the NiV-vaccinated group and two of one sex and one of the other in the nonspecifically vaccinated control group). Animals were anesthetized with ketamine according to body weight for each procedure and received  $1 \times 10^7$  PFU of the appropriate vaccine via the intramuscular (i.m.) route either seven (Study 1) or three (Study 2) days prior to inoculation with  $5 \times 10^5$  PFU of NiV<sub>B</sub>, split equally between the i.n. and i.t. routes. On days 0, 4, 7, 10, 14 (Study 2) or 15 (Study 1), 21, 28, and 35 after challenge and at terminal endpoint, subjects were anesthetized and examined, body temperature and weight were measured, and blood was collected. Subjects were assessed for clinical signs and respiration speed and quality daily after challenge. Clinical observations were scored

on a scale from 0 to 29 based on respiration, appetite, activity/appearance, and neurologic signs; animals scoring 9 or greater were humanely euthanized by lethal injection of a solution containing pentobarbital sodium and phenytoin sodium.

#### ***BLOOD COLLECTION AND PROCESSING***

At each timepoint and at terminal endpoint, blood was collected into a 4-mL Vacutainer® serum separator tube (BD; Franklin Lakes, New Jersey, USA; Cat. No. 367812), a 3-mL Vacutainer® EDTA tube (BD; Cat. No. 367856), and a 4-mL Vacutainer® lithium heparin tube (BD; Cat. No. 367884) for each animal and processed immediately after collection. From the EDTA tube, 100 µL of whole blood was added to 600 µL of AVL Viral Lysis Buffer with carrier RNA and incubated for at least ten minutes to inactivate virus. Inactivated material was transferred to a 1.8-mL Nunc™ cryovial and removed from the BSL-4. RNA was extracted using the QIAamp Viral RNA Mini Kit according to manufacturer instructions.

Another 150 µL of whole blood was removed from the EDTA tube and placed into a 0.5-mL screwcap tube for hematology analysis using the VetScan® HM5 Hematology Analyzer. Complete blood counts, including numbers of white blood cells, lymphocytes, monocytes, eosinophils, basophils, red blood cells, and platelets and measures of hematocrit and total hemoglobin, were obtained using a protocol optimized for NHPs according to manufacturer instructions.

The serum separator tubes and EDTA tubes were spun in a tabletop centrifuge at 2,500 RPM for 10 minutes at 4°C to separate serum and plasma from cellular material. Serum was transferred to a 2-mL screwcap tube, used for clinical chemistry analysis (see below), and stored at -80°C. EDTA plasma was transferred to a 2-mL screwcap tube and stored at -80°C for later use in immunological assays.

Analysis of clinical chemistry was performed using serum, Piccolo® BioChemistry Panel Plus reagent discs, and the Piccolo® Xpress chemistry analyzer. The

BioChemistry Panel Plus measures levels of ALT, albumin, ALP, amylase, AST, BUN, CRP, calcium, CRE, GGT, glucose, total protein, and uric acid in serum.

The lithium heparin tubes and cell pellets from the EDTA tubes (resuspended in HBSS) were used for isolation of peripheral blood mononuclear cells (PBMCs) for downstream immunological analysis. Briefly, the buffy coat was isolated by centrifugation using 12-mL sterile ACCUSPIN™ tubes (Sigma-Aldrich; Cat. No. A1805) containing Histopaque®-1077 reagent (Sigma-Aldrich; Cat. No. 1077-1). Cells were washed, treated with Ammonium-Chloride-Potassium Lysing Buffer (Thermo Fisher Gibco; Cat. No. A1049201) to remove red blood cells, and enumerated using a TC20 Automated Cell Counter (Bio-Rad Laboratories; Cat. No. 1450102). PBMCs were resuspended in freezing medium comprising 10% dimethyl sulfoxide (Fisher Scientific; Cat. No. BP231-100) in FBS and were dispensed evenly across five 1.8-mL cryovials and frozen in a Mr. Frosty™ controlled-rate freezing device (Thermo Scientific; Cat. No. 5100-0001) and stored at -80°C.

#### ***TISSUE COLLECTION AND PROCESSING***

At terminal or study endpoint, the following tissues were collected from each AGM for histopathology analysis, virus enumeration by plaque assay, and RNA extraction: axial lymph node, inguinal lymph node, liver, spleen, kidney, adrenal gland, lung (right upper, right middle, right lower, left upper, left middle, and left lower lobes), brain (frontal lobe, brain stem, and cervical spinal cord), pancreas, urinary bladder, ovary or testis, uterus or prostate, nasal mucosa, conjunctiva, and eye.

For virus enumeration, tissue samples were stored at -80°C for later processing. Tissues were homogenized in cell culture medium in 2-mL screwcap tubes containing 1.4-millimeter ceramic beads using the TissueLyser II to create 10% w/v homogenate. Samples were spun in a microcentrifuge at 4°C to pellet beads and debris, and

supernatants were transferred to new 2-mL screwcap tubes and stored at -80°C until titration (see below).

For RNA extraction, approximately 100 mg of tissue was stored in 1 mL of RNAprotect reagent for later processing. RNAprotect reagent was removed, and tissues were homogenized in 600 µL of RLT lysis buffer in 2-mL screwcap tubes containing ceramic beads using the TissueLyser II. Samples were spun in a microcentrifuge to pellet beads and debris, and supernatants were transferred to 1.8-mL cryovials and removed from the BSL-4. RNA was extracted using the RNeasy Mini Kit according to manufacturer instructions.

#### ***DETERMINATION OF VIRAL LOAD BY PLAQUE ASSAY AND RT-qPCR***

Isolated RNA from blood and tissues was subjected to RT-qPCR using primers and probes specific to NiV<sub>B</sub> targeting the N gene and the N-P intergenic region. Inclusion of the intergenic region prevented detection of viral mRNA by the assay. The probe was ordered from Thermo Fisher Invitrogen and featured 6FAM fluorescent reporter dye at the 5' end and TAMRA quencher at the 3' end, with a nucleotide sequence of 5' CGT CAC ACA TCA GCT CTG AGA A 3'. NiV<sub>B</sub> viral RNA was detected using the OneStep RT-PCR kit and the CFX96 Touch Real-Time PCR Detection System. CFX Manager™ software was used to evaluate threshold cycle values, and results are reported in GEq/mL (blood) or GEq/g (tissues), determined from a plasmid standard using Avogadro's number and the molecular weight of the NiV<sub>B</sub> genome.

Viral titers from blood were determined using a standard plaque assay on Vero 76 cells. Briefly, duplicate wells of 6-well plates were inoculated with 200 µL each of 10-fold serial dilutions of each sample, adsorbed for one hour at 37°C and 5% CO<sub>2</sub>, and then overlaid with two mLs per well of medium containing final concentrations of 1X MEM, 5% FBS, and 0.8% SeaKem® ME agarose. At 48 hpi, plates were stained with a solution

of 5% neutral red and 5% FBS in PBS without calcium and magnesium, and plaques were visualized and counted at 72 hpi. The LOD for the assay was 25 PFU/mL.

#### ***NiV<sub>B</sub> PLAQUE REDUCTION NEUTRALIZATION TESTS***

Plaque reduction neutralization tests (PRNTs) were performed using EDTA plasma saved from each timepoint to give an estimate of neutralizing antibodies present in the blood at timepoints following vaccination/challenge. Plasma samples were heat-inactivated and serially diluted two-fold. They were then incubated with about 100 PFU per sample of wild-type NiV<sub>B</sub> for one hour at 37°C and 5% CO<sub>2</sub>. Following incubation, virus/plasma mixes were plated on duplicate wells of Vero 76 cells and quantified by plaque assay with neutral red staining as described in previous sections. The PRNT<sub>50</sub> for each sample is reported as the reciprocal dilution at which plaque counts are 50% lower than control wells containing virus but no plasma.

#### ***NiV-SPECIFIC ENZYME-LINKED IMMUNOSORBENT ASSAYS***

Enzyme-linked immunosorbent assays (ELISAs) using plates coated with NiV G and secondary antibodies specific for monkey IgM or IgG were carried out using kits from Alpha Diagnostic International (San Antonio, Texas, USA; Cat. Nos. NIV-020 and NIV-015, respectively) according to the manufacturer protocol. Banked serum collected throughout the two studies was used to measure the magnitude of antibody responses during the acute and convalescent phases of NiV disease.

## **RESULTS**

### **The G\*-rVSV-ΔG-NiV<sub>B</sub> G vaccine grew to high titers in cell culture and expressed the NiV<sub>B</sub> G protein**

The previous version of the VSV-vectored NiV<sub>B</sub> G vaccine encoded GFP downstream of the NiV<sub>B</sub> G protein (**Figure 4-2A**). This vaccine protected 100% of ferrets and AGMs from NiV<sub>M</sub> and NiV<sub>B</sub> when given 28 days prior to challenge<sup>165,191</sup>, but the

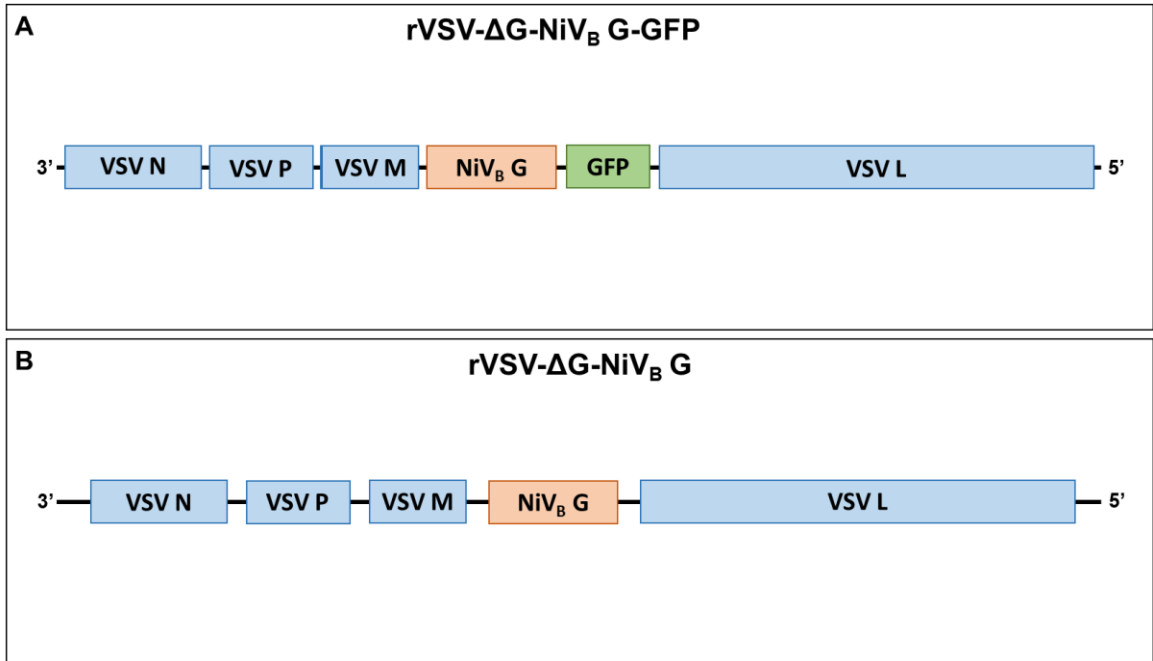


**Figure 4-2: The rVSV-ΔG-NiV<sub>B</sub> G-GFP and rVSV-ΔG-NiV<sub>B</sub> G genomes**

**(A)** Schematic of the rVSV-ΔG-NiV<sub>B</sub> G-GFP RNA genome with the name of each gene indicated (VSV N, VSV P, VSV M, NiV<sub>B</sub> G, GFP, and VSV L). **(B)** Schematic of the rVSV-ΔG-NiV<sub>B</sub> G RNA genome with the name of each gene indicated (VSV N, VSV P, VSV M, NiV<sub>B</sub> G, and VSV L). For both panels, the genes are shown as boxes, while the intergenic regions and 3' and 5' untranslated regions are shown as black lines. VSV genes are shown in blue, the NiV<sub>B</sub> G gene is shown in pink, and the GFP gene is shown in green. The 3' and 5' ends of the negative-sense viruses are indicated.

presence of a fluorescent marker would have been an obstacle to clinical trials and applications for licensure in the future. Therefore, a version of the construct lacking GFP was created (**Figure 4-2B**). A full-length antigenomic plasmid encoding the new vaccine construct was cloned as described above. G\*-rVSV-ΔG-NiV<sub>B</sub> G was recovered, purified, and amplified to create a large stock of vaccine as discussed above and shown in **Figure 4-1**. The viral RNA genomes of the previous G\*-rVSV-ΔG-NiV<sub>B</sub> G-GFP and new G\*-rVSV-ΔG-NiV<sub>B</sub> G constructs are shown in **Figure 4-2**. Quantification of the virus by standard plaque assay on G\* BHK cells gave a calculated titer of  $4.25 \times 10^8$  PFU/mL, confirming that the vaccine grows to similarly high titers in cell culture as other VSV constructs. The vaccine was tested and found to be negative for *Mycoplasma* and endotoxin contamination, and cloning borders and the NiV<sub>B</sub> G gene were sequenced using Sanger sequencing. The complete sequences of viral RNA and full-length plasmid were obtained through next-generation sequencing using the NextSeq 550 system and were found to match the expected sequences.

To confirm that the vaccine construct was expressing NiV<sub>B</sub> G protein in cells, an IFA was performed in Vero 76 and BHK-21 clone WI-2 cells. As shown in **Figure 4-3**, NiV<sub>B</sub> G protein was strongly expressed in cells infected with G\*-rVSV-ΔG-NiV<sub>B</sub> G. Mock-infected wells, as well as infected wells treated with secondary antibody only as controls, were included as confirmation that the fluorescence observed was not due to autofluorescence. The high concentration of m102.4 primary antibody used contributed to some background fluorescence, as seen in the mock-infected wells in **Figure 4-3**, panels **C**, **F**, and **I**. However, this background fluorescence disappeared in the secondary-only controls (**Figure 4-3**, panels **A**, **D**, **G**, and **J**), which were infected with G\*-rVSV-ΔG-NiV<sub>B</sub> G. The much brighter fluorescent signal in the G\*-rVSV-ΔG-NiV<sub>B</sub> G-infected wells that were incubated with both primary and secondary antibodies (**Figure 4-3**, panels **B**, **E**, **H**, and **K**) confirmed that the construct produces NiV<sub>B</sub> G protein. The results were similar between BHK-21 clone WI-2 and Vero 76 cells, although the cell number of the

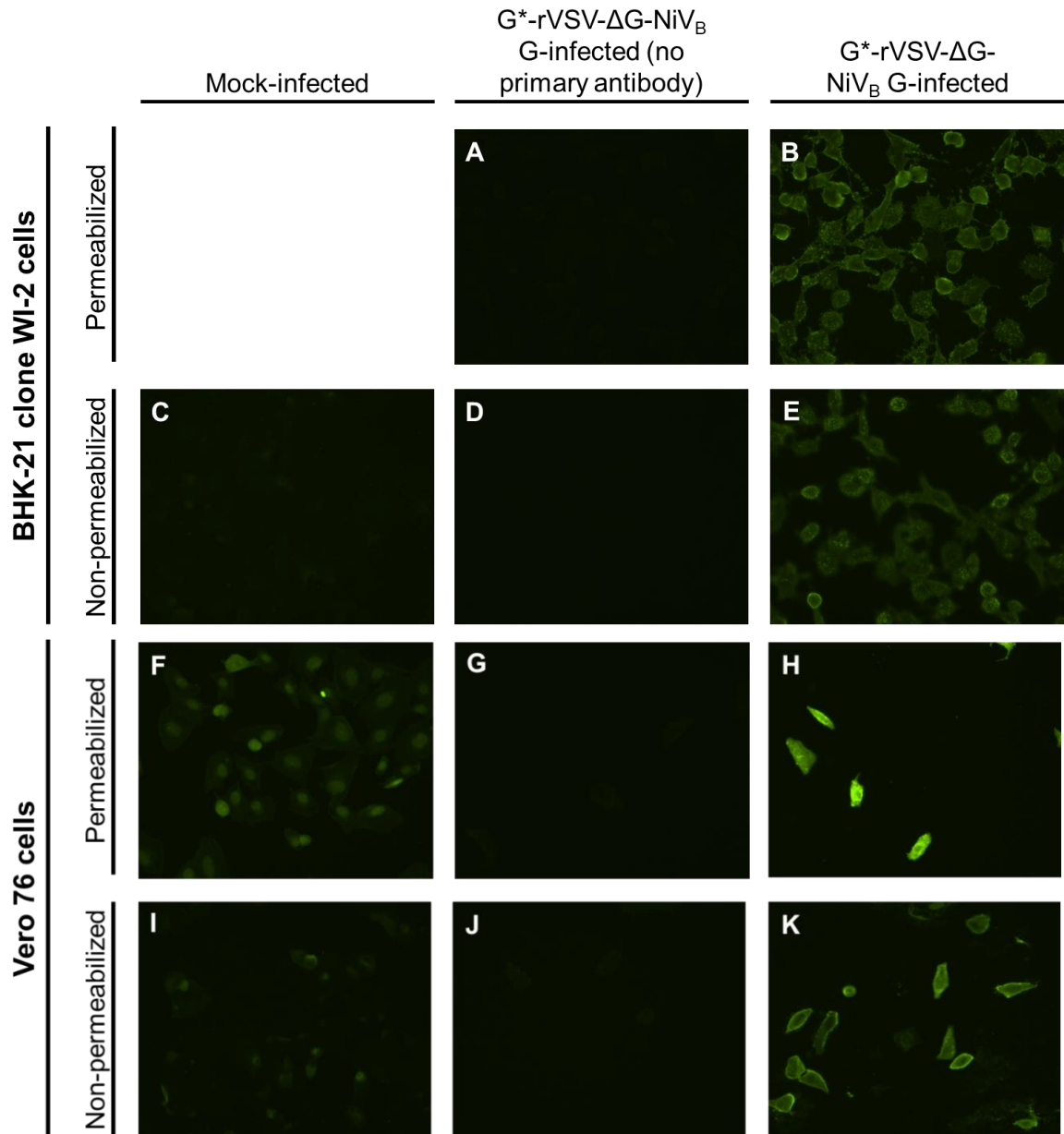


**Figure 4-3: The G\*-rVSV-ΔG-NiV<sub>B</sub> G construct expresses NiV<sub>B</sub> G protein**

Results of an IFA in BHK-21 clone WI-2 (panels **A through E**) and Vero 76 cells (panels **F through K**) infected with G\*-rVSV-ΔG-NiV<sub>B</sub> G (panels **A, B, D, E, G, H, J, and K**) or mock-infected with growth medium only (panels **C, F, and I**). Cells were permeabilized with 0.5% Triton<sup>TM</sup> X-100 (panels **A and B** and **F through H**) or not permeabilized (panels **C through E** and **I through K**) and then incubated with human m102.4 primary antibody (panels **B, C, E, F, H, I, and K**) followed by a secondary antibody against human IgG conjugated to a green fluorescent fluorophore (all panels).

76 cells was lower overall. While the subcellular localization of the NiV<sub>B</sub> G protein could not be confirmed using these images, the results were similar for permeabilized and non-permeabilized cells, suggesting that the NiV<sub>B</sub> G protein traffics to the cell surface for budding of G\*-rVSV-ΔG-NiV<sub>B</sub> G virions.

### **The G\*-rVSV-ΔG-NiV<sub>B</sub> G vaccine protected AGMs from lethal NiV disease when given shortly prior to challenge with NiV<sub>B</sub>**

Having recovered and characterized the G\*-rVSV-ΔG-NiV<sub>B</sub> G vaccine lacking GFP, the next step was to test its ability to protect AGMs from lethal challenge with NiV. It had been previously shown that NiV<sub>B</sub> is uniformly lethal in the AGM model, causes more severe lung and spleen histopathology than NiV<sub>M</sub>, and has a shorter therapeutic window for treatment with m102.4<sup>172</sup>. Therefore, the studies presented here focused on the ability of the vaccine to protect from NiV<sub>B</sub>, which is also the strain that has caused the vast majority of outbreaks with regularity in Bangladesh and India. Previous studies showed that the earlier version of the vaccine protected AGMs from NiV<sub>B</sub> with one dose given 28 days prior to challenge<sup>191</sup>, but shorter periods of time between vaccination and challenge were evaluated here because rapid protection is vital for controlling an ongoing outbreak.

The study designs for two studies with nine AGMs each are shown in **Figure 4-4**. Animals in Study 1 were given  $1 \times 10^7$  PFU of G\*-rVSV-ΔG-NiV<sub>B</sub> G (six AGMs) or  $1 \times 10^7$  PFU of rVSV-ΔG-EBOV 76 (three AGMs) i.m. seven days prior to challenge with  $5 \times 10^5$  PFU of NiV<sub>B</sub> given i.n./i.t. Animals in Study 2 were given the same doses of vaccine three days prior to challenge with the same dose of NiV<sub>B</sub>. The animals receiving the nonspecific EBOV vaccine served as controls and succumbed to NiV disease by day nine post-challenge. Survival curves are shown in **Figure 4-5**. When given G\*-rVSV-ΔG-NiV<sub>B</sub> G seven days prior to NiV<sub>B</sub> challenge, 100% of the animals survived to the study endpoint. Encouragingly, 67% of the animals receiving G\*-rVSV-ΔG-NiV<sub>B</sub> G three days prior to NiV<sub>B</sub> challenge also survived. Therefore, the G\*-rVSV-ΔG-NiV<sub>B</sub> G

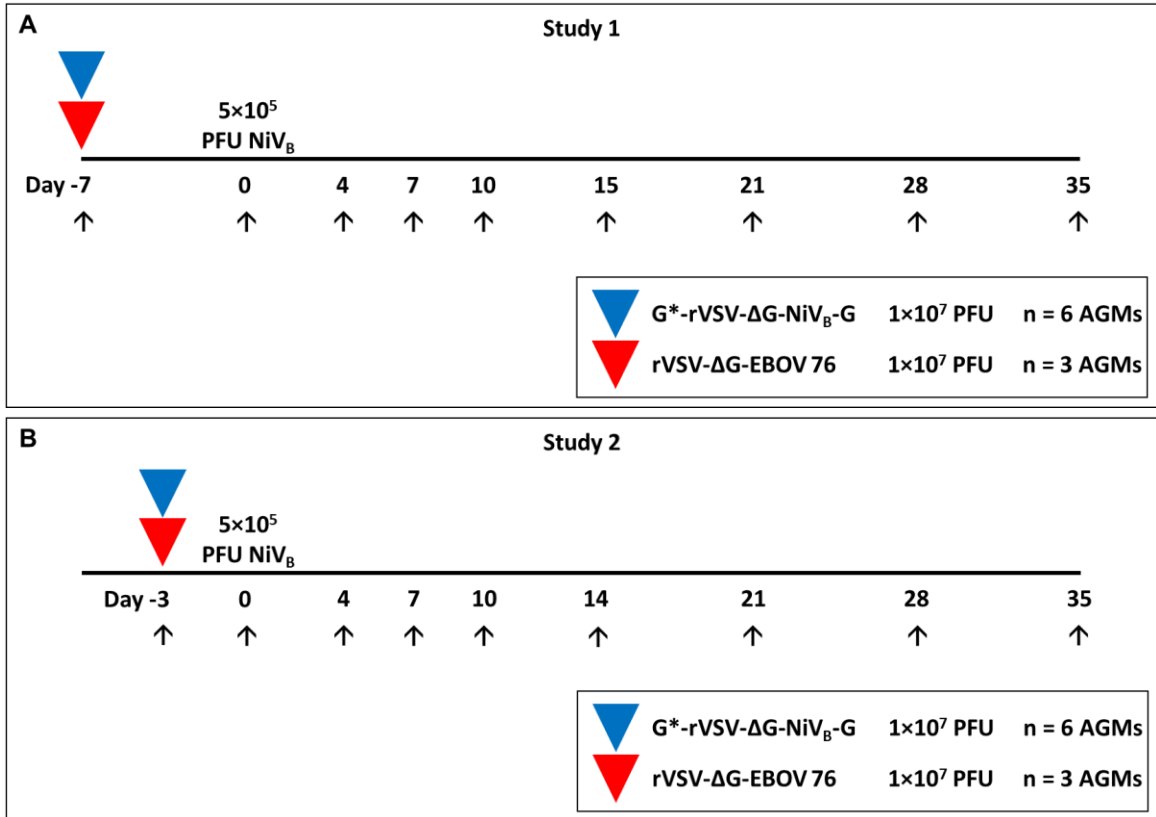


**Figure 4-4: Study designs for experimental challenge studies in AGMs**

Experimental design for **(A)** Study 1, in which AGMs were vaccinated seven days prior to challenge with NiV<sub>B</sub>, and **(B)** Study 2, in which AGMs were vaccinated three days prior to challenge. The red triangle indicates vaccination with the nonspecific rVSV-ΔG-EBOV 76 vector, while the blue triangle denotes vaccination with the G\*-rVSV-ΔG-NiV<sub>B</sub> G vector developed for these studies. Study days relative to challenge with 5×10<sup>5</sup> PFU of NiV<sub>B</sub> are shown below the horizontal black line, with days of blood collection indicated with arrows.

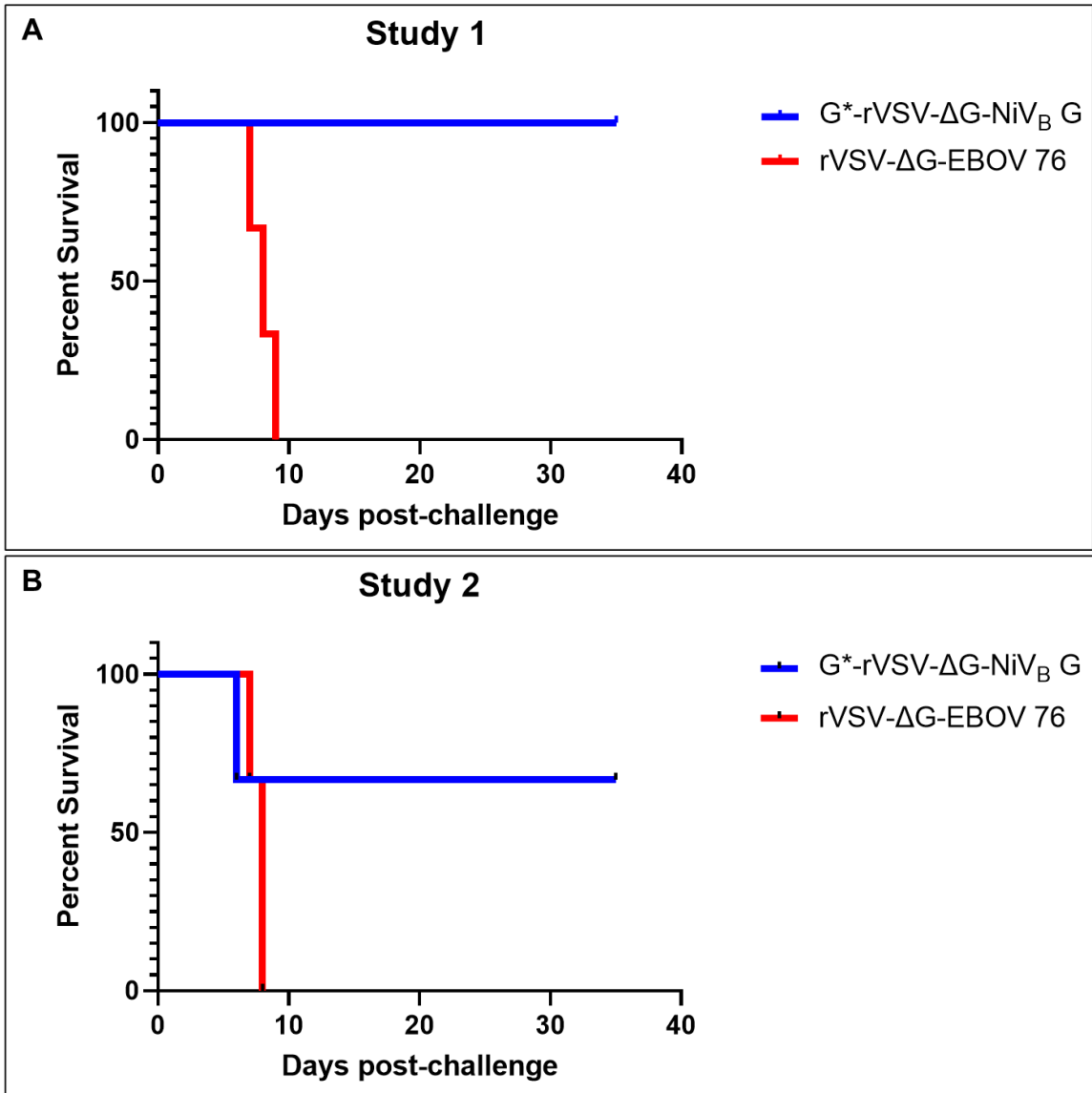


**Figure 4-5: Survival curves following challenge of vaccinated AGMs with NiV<sub>B</sub>**

Kaplan-Meier survival curves for AGMs vaccinated with rVSV-ΔG-NiV<sub>B</sub> G (blue line; n=6 animals for each study) or rVSV-ΔG-EBOV 76 (red line; n=3 animals for each study) (A) seven days or (B) three days prior to challenge with NiV<sub>B</sub>.

vaccine protected AGMs from NiV disease when given shortly before exposure. These results demonstrate rapid protection in one dose in a robust, 100% lethal animal model that faithfully recapitulates human NiV disease, and a vaccine that works quickly is essential for controlling an ongoing outbreak of NiV disease.

Clinical signs and observations for Study 1 are shown in **Table 4-1**. Importantly, animals that received the G\*-rVSV-ΔG-NiV<sub>B</sub> G vaccine seven days prior to challenge exhibited no clinical signs other than decreased appetite throughout the study. Clinical pathology was minimal, although some subjects had transient increases in CRP, indicating inflammation, and some changes to blood counts outside of their baseline values (**Table 4-1**). Conversely, animals that received the rVSV-ΔG-EBOV 76 vaccine seven days prior to challenge developed dyspnea and depression prior to reaching humane euthanasia criteria between seven and nine dpi. Their respiratory rates increased sharply just prior to euthanasia, and significantly increased respiratory rates were a reliable marker of rapid clinical decline in infected animals (**Figure 4-6**). These animals had decreased levels of white blood cells, lymphocytes, and thrombocytes, indicating immune suppression associated with hemorrhagic disease. They also had increased levels of neutrophils and CRP, which are hallmarks of inflammation. In short, animals in the rVSV-ΔG-EBOV 76 nonspecific vaccine control group were unable to control their NiV infection and succumbed to NiV disease with its trademark clinical markers, while subjects in the G\*-rVSV-ΔG-NiV<sub>B</sub> G specifically vaccinated group effectively controlled the NiV infection and survived to the study endpoint without noticeable clinical signs.

Clinical signs and observations for Study 2 are shown in **Table 4-2**. As in Study 1, animals receiving the rVSV-ΔG-EBOV 76 vaccine developed respiratory and systemic signs consistent with NiV disease, such as tachypnea, dyspnea, and depression, and reached euthanasia criteria at seven or eight dpi. However, two of the animals vaccinated with G\*-rVSV-ΔG-NiV<sub>B</sub> G three days prior to challenge reached euthanasia criteria at six dpi. The four remaining animals receiving the NiV<sub>B</sub>-specific vaccine in Study 2

NHP	Sex	Vaccine	Clinical Signs/Outcome	Hematology/Clinical Pathology Findings
C7-1	Female	rVSV-ΔG-EBOV 76	Tachypnea (d7); dyspnea (d7); anorexia (d7); depression (d7); hypothermia (d7). Subject euthanized (d7).	Leukopenia (d0); lymphopenia (d0, 7); monocytopenia (d0, 4, 7); eosinopenia (d0, 4); basopenia (d0, 4, 7); thrombocytopenia (d7); neutrophilia (d7); ↑ CRP (d7).
C7-2	Female	rVSV-ΔG-EBOV 76	Dyspnea (d7); shallow breathing (d8); severe depression (d8); fever (d7); hypothermia (d8). Subject euthanized (d8).	Leukopenia (d8); lymphopenia (d0, 7, 8); eosinopenia (d0, 4, 7, 8); basopenia (d0, 4, 7, 8); thrombocytopenia (d7, 8); hyperglycemia (d8); ↑ BUN (d8); ↓ CRE (d0); ↑ ALT (d7, 8); ↑ AST (d8); ↑ CRP (d7); ↑↑ CRP (d8).
C7-3	Male	rVSV-ΔG-EBOV 76	Tachypnea (d9); shallow breathing (d9); dyspnea (d9); decreased appetite (d8, 9); depression (d9). Subject euthanized (d9).	Lymphopenia (d9); eosinopenia (d0, 4, 7); basopenia (d0, 4, 7, 9); thrombocytopenia (d9); monocytosis (d9); neutrophilia (d0, 9); ↓ CRE (d4); ↑ CRP (d9).
V7-1	Female	G*-rVSV-ΔG-NiV <sub>B</sub> G	Decreased appetite (d1, 5-11, 20, 22); hypothermia (d35). Subject survived to study endpoint (d35).	Leukopenia (d35); lymphopenia (d35); monocytopenia (d35); neutropenia (d4); eosinopenia (d0, 7); basopenia (d0, 7); thrombocytopenia (d4); monocytosis (d4); eosinophilia (d4); basophilia (d4, 15); ↑ CRE (d7); ↓ CRE (d15, 35).
V7-2	Female	G*-rVSV-ΔG-NiV <sub>B</sub> G	Decreased appetite (d16); fever (d4); hypothermia (d35). Subject survived to study endpoint (d35).	Leukopenia (d28, 35); monocytopenia (d0, 4, 7, 10, 15, 21, 28, 35); neutropenia (d28, 35); eosinopenia (d0, 4, 7, 10, 15, 21, 28, 35); basopenia (d28, 35); neutrophilia (d4); thrombocytosis (d10); ↓ CRE (d35); ↑ CRP (d4).
V7-3	Female	G*-rVSV-ΔG-NiV <sub>B</sub> G	Decreased appetite (d1, 5, 8, 11, 16, 18-24, 27-32, 34, 35); hypothermia (d35). Subject survived to study endpoint (d35).	Leukocytosis (d7, 10); monocytosis (d4, 7, 10, 15, 21, 35); neutrophilia (d4, 7, 10); eosinophilia (d4, 7, 10, 15); basophilia (d4, 7, 10, 15); ↓ CRE (d35).
V7-4	Male	G*-rVSV-ΔG-NiV <sub>B</sub> G	None. Subject survived to study endpoint (d35).	Leukocytosis (d4, 7, 10, 15); lymphocytosis (d0, 7, 10, 15); neutrophilia (d0, 4, 7, 10, 15, 21, 28, 35); basophilia (d15); monocytopenia (d0, 4, 7, 10, 15, 21, 28, 35); eosinopenia (d28); basopenia (d21, 28).
V7-5	Male	G*-rVSV-ΔG-NiV <sub>B</sub> G	Hypothermia (d35). Subject survived to study endpoint (d35).	Monocytopenia (d0, 4, 7, 10, 15, 28, 35); neutrophilia (d0, 4, 7, 10, 15, 21, 28, 35); ↑ CRP (d4).
V7-6	Male	G*-rVSV-ΔG-NiV <sub>B</sub> G	None. Subject survived to study endpoint (d35).	Monocytopenia (d0, 4, 7, 10, 15, 21, 28, 35); eosinopenia (d7); neutrophilia (d0, 4, 7, 10, 15, 21, 28, 35); basophilia (d0, 21, 35); ↓ CRE (d0, 10, 15, 21); ↑ CRP (d4).

Days after NiV<sub>B</sub> challenge are in parentheses. All reported findings are in comparison to baseline (d-7) values. Decreased appetite is defined as some

food but not all food consumed from the previous day. Anorexia is defined as no food consumed from the previous day. Fever is defined as a temperature more than 2.5 °F over baseline, or at least 1.5 °F over baseline and  $\geq 103.5$  °F. Hypothermia is defined as a temperature  $\leq 3.5$ °F below baseline. Leukopenia, lymphopenia, monocytopenia, neutropenia, eosinopenia, basopenia, and thrombocytopenia are defined by a  $\geq 35\%$  drop in numbers of white blood cells, lymphocytes, monocytes, neutrophils, eosinophils, basophils, or platelets, respectively. Leukocytosis, lymphocytosis, monocytosis, neutrophilia, eosinophilia, basophilia, and thrombocytosis are defined by a 100% or greater increase in numbers of white blood cells, lymphocytes, monocytes, neutrophils, eosinophils, basophils, or thrombocytes, respectively. Hyperglycemia is defined as a 100% or greater increase in levels of glucose. Increases and decreases in BUN, CRE, ALT, AST, and CRP were graded on the following scale:  $\uparrow$  = 1- to 5-fold increase,  $\uparrow\uparrow$  =  $>5$ - to 10-fold increase,  $\uparrow\uparrow\uparrow$  =  $>10$ - to 20-fold increase,  $\uparrow\uparrow\uparrow\uparrow$  =  $>20$ -fold increase,  $\downarrow$  =  $\geq 50\%$  decrease.

**Table 4-1: Clinical disease and findings in AGMs vaccinated seven days prior to experimental infection with NiV<sub>B</sub>**

NHP	Sex	Vaccine	Clinical Signs/Outcome	Hematology/Clinical Pathology Findings
C3-1	Female	rVSV- $\Delta$ G-EBOV 76	Dyspnea (d7, 8); anorexia (d8); depression (d8); fever (d7); hypothermia (d8). Subject euthanized (d8).	Leukocytosis (d8); monocytosis (d0, 4, 8); neutrophilia (d7, 8); lymphocytopenia (d7, 8); neutropenia (d4); eosinopenia (d0, 4, 7); basopenia (d4, 7); thrombocytopenia (d8); $\uparrow$ CRE (d8); $\uparrow$ ALT (d8); $\uparrow$ CRP (d7); $\uparrow\uparrow$ CRP (d8).
C3-2	Male	rVSV- $\Delta$ G-EBOV 76	Tachypnea (d8); dyspnea (d8); decreased appetite (d5-7); anorexia (d8); depression (d8). Subject euthanized (d8).	Lymphopenia (d8); monocytopenia (d7); eosinopenia (d0, 4, 7, 8); basopenia (d0, 8); neutrophilia (d8); hypoalbuminemia (d8); $\uparrow\uparrow$ ALT (d0, 4, 7, 8); $\uparrow$ AST (d8); hypoamylasemia (d8); $\uparrow$ CRP (d7); $\uparrow\uparrow$ CRP (d8).
C3-3	Male	rVSV- $\Delta$ G-EBOV 76	Tachypnea (d7); dyspnea (d7); decreased appetite (d5-7); depression (d7). Subject euthanized (d7).	Lymphopenia (d7); eosinopenia (d0, 4, 7); basopenia (d0, 4, 7); thrombocytopenia (d7); monocytosis (d7); $\uparrow$ CRP (d7).
V3-1	Female	G*-rVSV- $\Delta$ G-NiV <sub>B</sub> G	Tachypnea (d5, 6); dyspnea (d6); anorexia (d5, 6); depression (d6); fever (d4); hypothermia (d6). Subject euthanized (d6).	Leukocytosis (d6); monocytosis (d0, 4, 6); neutrophilia (d6); eosinophilia (d6); lymphocytopenia (d4); eosinopenia (d4); basopenia (d4); thrombocytopenia (d4, 6); hyperglycemia (d6); $\uparrow$ CRE (d6); hypoalbuminemia (d6); $\uparrow\uparrow$ ALT (d6); $\uparrow\uparrow$ AST (d6); $\uparrow\uparrow\uparrow$ CRP (d6).
V3-2	Female	G*-rVSV- $\Delta$ G-NiV <sub>B</sub> G	Tachypnea (d6); dyspnea (d6); decreased appetite (d5, 6); depression (d6); fever (d4); hypothermia (d6); seizures (d6); epistaxis (d6). Subject euthanized (d6).	Leukocytosis (d6); monocytosis (d0, 6); neutrophilia (d6); eosinophilia (d6); lymphocytopenia (d4); basopenia (d4, 6); thrombocytopenia (d6); hyperglycemia (d6); $\downarrow$ CRE (d4); $\uparrow$ CRE (d6); hypoalbuminemia (d6); hypoproteinemia (d6); $\uparrow$ CRP (d4,

				6).
V3-3	Female	G*-rVSV- ΔG-NiV <sub>B</sub> G	Tachypnea (d5, 6, 7); decreased appetite (d5-9, 11, 12). Subject survived to study endpoint (d35).	Leukopenia (d0); lymphopenia (d4, 35); monocytopenia (d0, 21, 35); neutropenia (d0, 21); eosinopenia (d0, 7, 14, 21, 28); basopenia (d7, 28); monocytosis (d14); neutrophilia (d4); eosinophilia (d10); basophilia (d10); hypoglycemia (d35); hypoalbuminemia (d7); ↑ ALT (d35); ↑ AST (d7); hypoamylasemia (d4); ↑ CRP (d4, 7).
V3-4	Male	G*-rVSV- ΔG-NiV <sub>B</sub> G	Tachypnea (d8); dyspnea (d7); decreased appetite (d5-11); fever (d7). Subject survived to study endpoint (d35).	Leukocytosis (d10, 14); lymphocytosis (d14); neutrophilia (d4, 7, 10, 14, 21); basophilia (d14); eosinopenia (d0, 4, 10, 35); basopenia (d4, 7, 10); thrombocytopenia (d7); ↑ AST (d10); hypoamylasemia (d4, 7, 14, 21, 28, 35); ↑↑↑ CRP (d7).
V3-5	Male	G*-rVSV- ΔG-NiV <sub>B</sub> G	Decreased appetite (d5-8; 11, 15, 22, 29, 30, 33, 35); fever (d4, 7). Subject survived to study endpoint (d35).	Monocytosis (d7, 10, 14); neutrophilia (d10); eosinophilia (d35); eosinopenia (d0, 4, 10, 21); basopenia (d0, 4, 7, 10, 21); thrombocytopenia (d7, 35); ↑ ALT (d0, 35); ↑↑ AST (d35); hypoamylasemia (d4); ↑ CRP (d7).
V3-6	Male	G*-rVSV- ΔG-NiV <sub>B</sub> G	Tachypnea (d6, 7); dyspnea (d8); decreased appetite (d5-7, 9-11, 15, 22, 24, 25, 29, 30, 32-34); anorexia (d8); hypothermia (d10). Subject survived to study endpoint (d35).	Leukocytosis (d10, 14); lymphocytosis (d14); monocytosis (d10); neutrophilia (d7, 10, 14); lymphocytopenia (d7); monocytopenia (d0, 4, 35); eosinopenia (d7); basopenia (d4, 7); thrombocytopenia (d4, 7); ↑ CRP (d7).
<p>Days after NiV<sub>B</sub> challenge are in parentheses. All reported findings are in comparison to baseline (d-3) values. Decreased appetite is defined as some food but not all food consumed from the previous day. Anorexia is defined as no food consumed from the previous day. Fever is defined as a temperature more than 2.5 °F over baseline, or at least 1.5 °F over baseline and ≥ 103.5 °F. Hypothermia is defined as a temperature ≤3.5°F below baseline. Leukopenia, lymphopenia, monocytopenia, neutropenia, eosinopenia, basopenia, and thrombocytopenia are defined by a ≥35% drop in numbers of white blood cells, lymphocytes, monocytes, neutrophils, eosinophils, basophils, or platelets, respectively. Leukocytosis, lymphocytosis, monocytosis, neutrophilia, eosinophilia, and basophilia are defined by a 100% or greater increase in numbers of white blood cells, lymphocytes, monocytes, neutrophils, eosinophils, or basophils, respectively. Hyperglycemia is defined as a 100% or greater increase in levels of serum glucose. Hypoglycemia, hypoalbuminemia, hypoproteinemia, and hypoamylasemia are defined by a ≥25% decrease in levels of serum glucose, albumin, total protein, or amylase, respectively. Increases and decreases in CRE, ALT, AST, and CRP were graded on the following scale: ↑ = 1- to 5-fold increase, ↑↑ = &gt;5- to 10-fold increase, ↑↑↑ = &gt;10- to 20-fold increase, ↑↑↑↑ = &gt;20-fold increase, ↓ = ≥50% decrease.</p>				

**Table 4-2: Clinical disease and findings in AGMs vaccinated three days prior to experimental infection with NiV<sub>B</sub>**

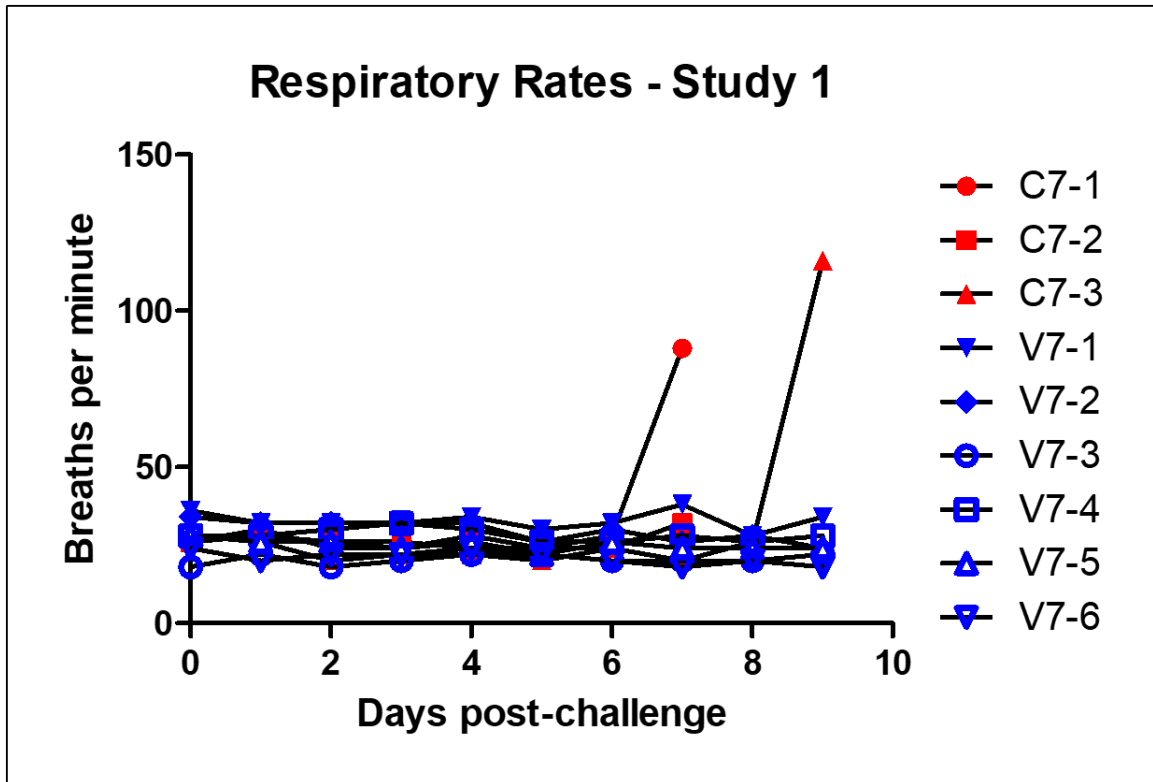


**Figure 4-6: Respiratory rates following challenge of AGMs with NiV<sub>B</sub>**

Line graph of respiratory rates in breaths per minute tracked daily throughout Study 1 for animals vaccinated with rVSV-ΔG-NiV<sub>B</sub> G (blue symbols) or rVSV-ΔG-EBOV 76 (red symbols) seven days prior to challenge with NiV<sub>B</sub>. Animal IDs are shown in the legend to the right of the graph.

developed respiratory signs and transiently elevated CRP but recovered and survived to the study endpoint at 35 dpi. These subjects also had temporary increases in inflammatory immune cells, such as neutrophils, and temporary decreases in thrombocytes. These clinical findings were similar to those observed in the animals that succumbed to NiV<sub>B</sub> infection, although they were less severe, and these animals recovered (**Table 4-2**). Unlike Study 1, in which animals vaccinated with G\*-rVSV-ΔG-NiV<sub>B</sub> G did not develop clinical signs of NiV disease, all AGMs in Study 2 developed clinical signs consistent with NiV disease. However, the severity was lower in four out of the six animals in the NiV<sub>B</sub>-vaccinated group, and these animals recovered, with their clinical pathology values returning to normal by around 10 dpi (**Table 4-2**).

Viremia at timepoints at which blood was collected during each study, as measured as replicative virus by plaque assay and as GEq by RT-qPCR, is shown in **Figure 4-7**. During Study 1, no animals vaccinated with G\*-rVSV-ΔG-NiV<sub>B</sub> G developed viremia detectable by either method. Conversely, nonspecifically vaccinated control animals administered rVSV-ΔG-EBOV 76 developed detectable viremia (two animals by plaque assay and all three animals by RT-qPCR) shortly prior to terminal endpoint (**Figure 4-7A and B**). Results were similar for Study 2. All animals that succumbed to NiV disease in either vaccination group developed detectable viremia by plaque assay and RT-qPCR shortly prior to euthanasia (**Figure 4-7C and D**). Additionally, two of the four survivors vaccinated with G\*-rVSV-ΔG-NiV<sub>B</sub> G developed viremia detectable by RT-qPCR, although it resolved by 10 dpi (**Figure 4-7D**). No virus was detected by either method prior to day six or after day eight post-challenge.

Detectable NiV<sub>B</sub> genomic RNA in tissues on necropsy, measured as GEq by RT-qPCR, is shown in **Figure 4-8**. NiV<sub>B</sub> genomic RNA was detected in all tissues tested in AGMs vaccinated with nonspecific rVSV-ΔG-EBOV 76 at time of death (**Figure 4-8A and B**). In Study 1, genomic RNA was also detected in most tissues collected at 35 dpi from surviving animals that had been vaccinated with G\*-rVSV-ΔG-NiV<sub>B</sub> G; however,

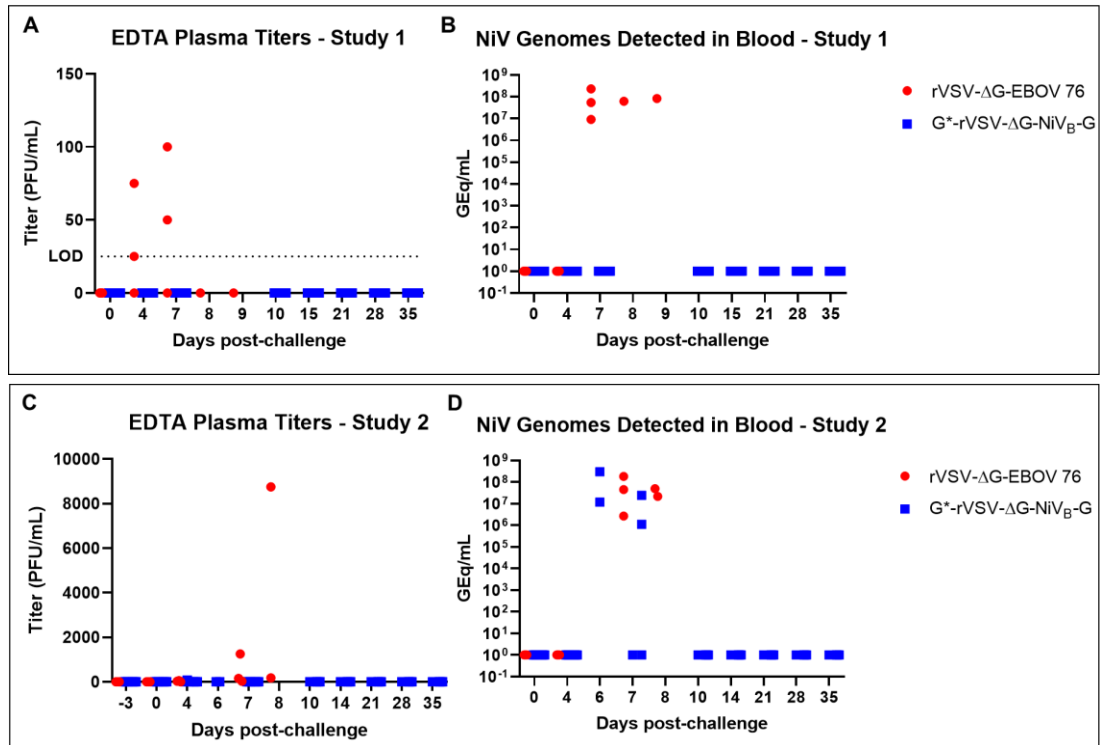


**Figure 4-7: Viremia in vaccinated AGMs after challenge with NiV<sub>B</sub>**

NiV<sub>B</sub> isolated from EDTA plasma by plaque assay (**panels A and C**) or genomic RNA detected in whole blood by RT-qPCR specific for NiV<sub>B</sub> (**panels B and D**) for AGMs challenged with NiV<sub>B</sub> seven days after vaccination (**panels A and B**) or three days after vaccination (**panels C and D**). Subjects nonspecifically vaccinated with rVSV-ΔG-EBOV 76 are represented by red circles, and subjects specifically vaccinated with G\*-rVSV-ΔG-NiV<sub>B</sub>-G against NiV are represented by blue squares. The LOD for the plaque assays was 25 PFU, represented by a horizontal line in (**A**). RT-qPCR values are reported as 1 GEq/mL if they were below the LOD.

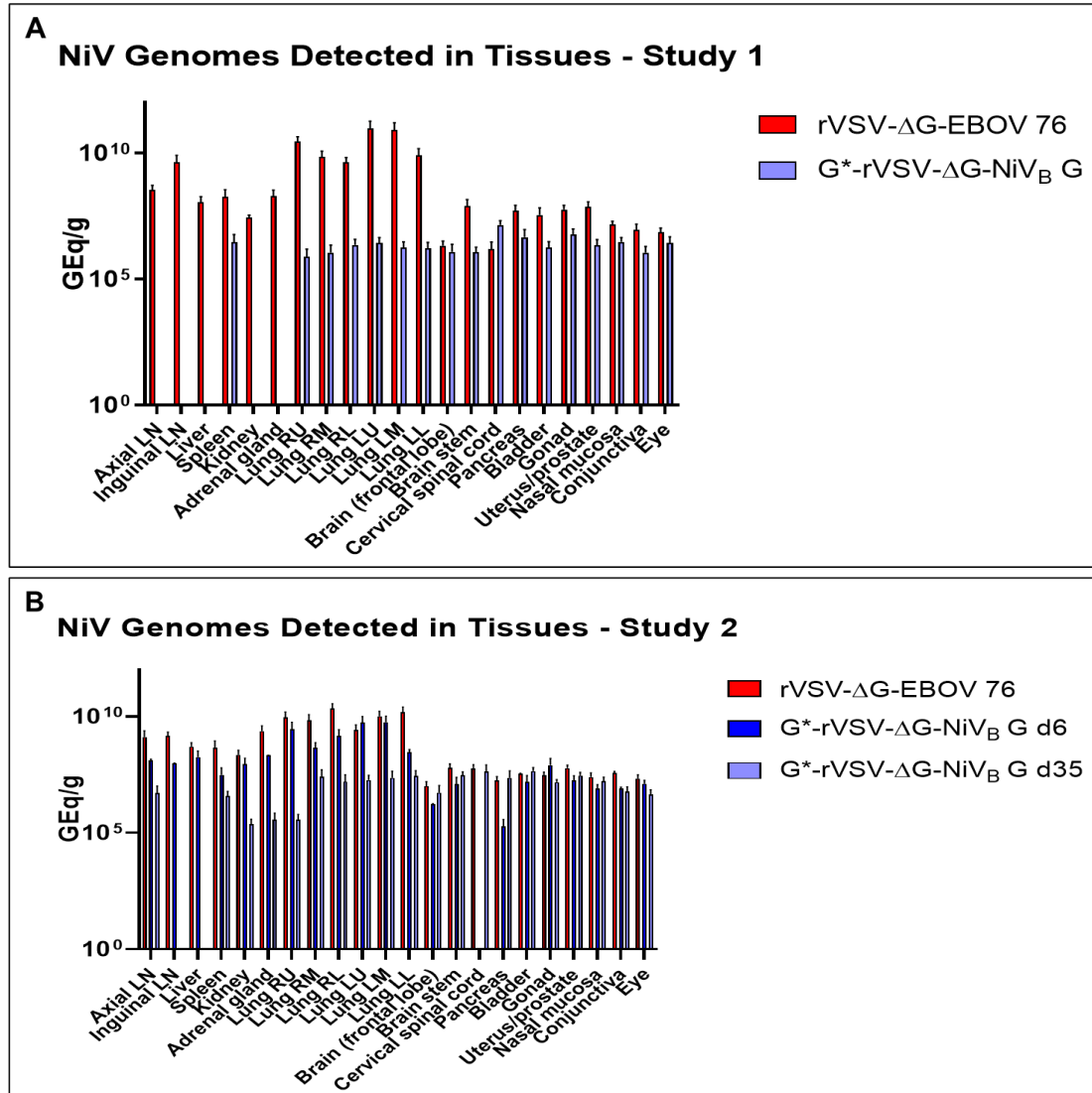


**Figure 4-8: NiV<sub>B</sub> genomic RNA detected in vaccinated AGMs after challenge with NiV<sub>B</sub>**

Genomic RNA detected in tissues by RT-qPCR specific for NiV<sub>B</sub> for AGMs challenged with NiV<sub>B</sub> seven days after vaccination (**A**) or three days after vaccination (**B**). Control animals nonspecifically vaccinated with rVSV-ΔG-EBOV 76, which all succumbed to NiV disease, are shown in red. Animals that survived to the study endpoint of 35 dpi and were specifically vaccinated with G\*-rVSV-ΔG-NiV<sub>B</sub> G against NiV are shown in light blue (**panels A and B**). Animals vaccinated with G\*-rVSV-ΔG-NiV<sub>B</sub> G that succumbed to NiV disease are shown in dark blue (**B**). Height of bars represents the mean GEq for all subjects in each group, and error bars represent the SEM. RT-qPCR values are reported as 1 GEq/mL if they were below the LOD.

RNA levels were lower than in the same tissues of animals vaccinated with rVSV- $\Delta$ G-EBOV 76 (**Figure 4-8A**). In Study 2, NiV<sub>B</sub> genomic RNA was detected from animals in both vaccination groups (**Figure 4-8B**). For many tissues, RNA levels were similar between control animals vaccinated nonspecifically with rVSV- $\Delta$ G-EBOV 76, animals specifically vaccinated with G\*-rVSV- $\Delta$ G-NiV<sub>B</sub> G that succumbed to NiV disease (dark blue), and survivors vaccinated with G\*-rVSV- $\Delta$ G-NiV<sub>B</sub> G (light blue). However, the amount of NiV<sub>B</sub> genomic RNA detected was lower in the lungs of survivors than of animals that succumbed to NiV disease (**Figure 4-8B**).

#### **Surviving AGMs vaccinated with the G\*-rVSV- $\Delta$ G-NiV<sub>B</sub> G vaccine developed NiV-specific humoral immune responses**

The G\*-rVSV- $\Delta$ G-NiV<sub>B</sub> G vaccine protected AGMs when given shortly prior to challenge with NiV<sub>B</sub>, so the next question of interest was what immunological factor(s) contributed to survival of animals vaccinated with the NiV-specific vaccine. First, NiV-specific humoral responses were investigated. **Figure 4-9** shows the results of PRNT assays to quantify neutralizing antibody to NiV<sub>B</sub> in the EDTA plasma of all subjects. All survivors in both Study 1 (animals V7-1 through V7-6) and Study 2 (animals V3-3 through V3-6) developed neutralizing antibodies that were detectable beginning at day seven post-challenge. Interestingly, animals in Study 2 developed higher neutralizing antibody titers than subjects in Study 1. This difference may be due to replication of the NiV<sub>B</sub> inoculum in these animals due to incomplete control of the viral infection because these subjects were vaccinated only three days prior to challenge instead of a full week (as in Study 1), so NiV-specific immunological responses may have taken a few days after challenge to develop. However, early replication in tissues could not be confirmed in these studies because animals were not sacrificed prior to humane endpoint or the end of the study. None of the animals that succumbed to NiV disease developed detectable neutralizing antibodies, regardless of vaccine group.

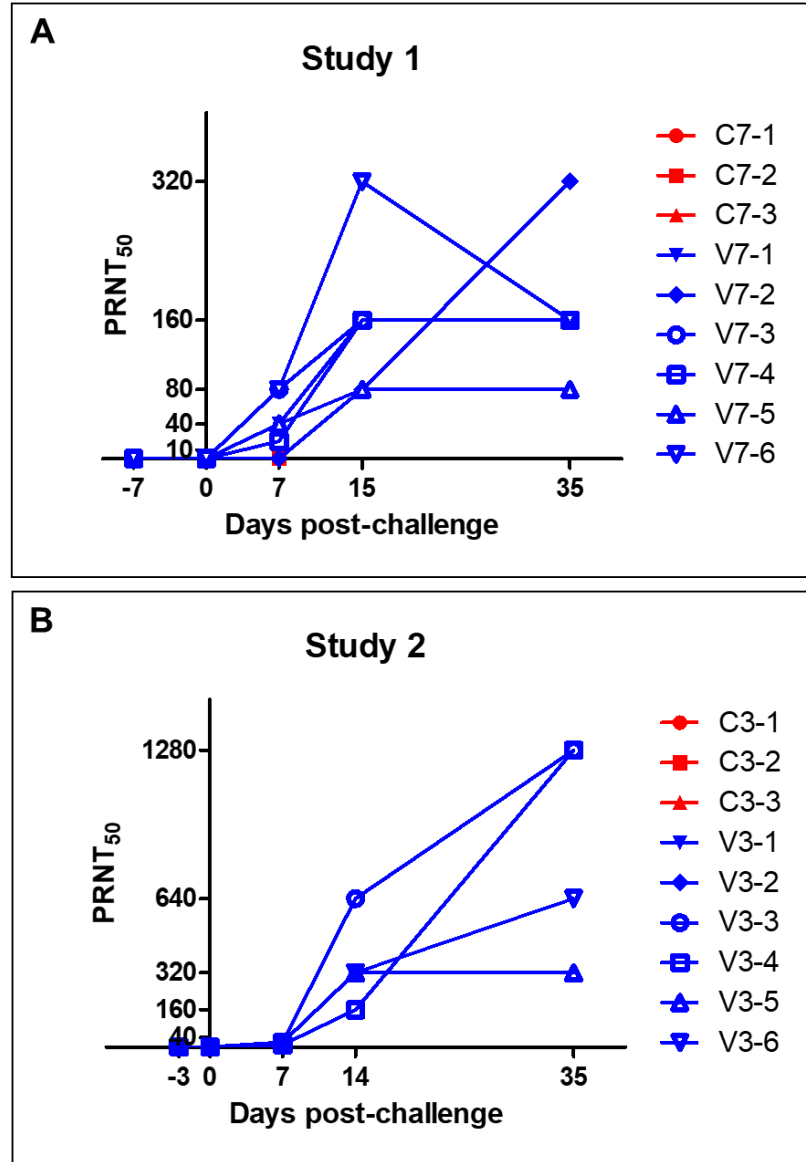


**Figure 4-9: PRNT<sub>50</sub> results for AGMs vaccinated prior to challenge with NiV<sub>B</sub>**

PRNT<sub>50</sub> values from EDTA plasma, reported as reciprocal dilutions at which plaque counts were reduced by 50% compared to control wells, for animals vaccinated with G\*-rVSV-ΔG-NiV<sub>B</sub> G (blue symbols) or rVSV-ΔG-EBOV 76 (red symbols) (A) seven days or (B) three days prior to challenge with NiV<sub>B</sub>. Animal IDs are shown in the legend to the right of the graph.

**Figure 4-10** shows the results of ELISAs for the detection of NiV-specific binding antibodies in the serum of vaccinated AGMs. Results for Study 1 are shown in **Figure 4-10A** (IgM) and **Figure 4-10C** (IgG). Animals in both vaccine groups had similar antibody titers at baseline, but survivors developed strong IgM and especially IgG responses by around 11 days post-vaccination. As expected, IgM titers waned by the study endpoint. Non-survivors did not develop IgG antibodies above baseline. Results for Study 2 are shown in **Figure 4-10B** (IgM) and **Figure 4-10D** (IgG). Like Study 1, animals in both vaccination groups had similar antibody titers at baseline. Survivors developed strong IgM and IgG responses by around 10 days post-vaccination. Non-survivors, regardless of vaccination group, did not develop IgM nor IgG titers higher than baseline. Since high antibody titers were not detectable until around 10 days post-vaccination, at which point non-survivors were beginning to succumb to the infection (especially in Study 2), it is not likely that these responses were protective on their own. The additional T-cell experiments in progress will help to further define a survivor phenotype.

In summary, the experiments described here have shown that the G\*-rVSV-ΔG-NiV<sub>B</sub> G vaccine is highly effective at protecting AGMs, an excellent model of NiV disease in humans, from a dose of  $5 \times 10^5$  PFU of NiV<sub>B</sub> given by a biologically plausible route either seven days or three days after vaccination. Clinical signs of NiV disease, inflammatory and hematological markers, and viremia were transient in survivors, and no lingering nor late-onset neurological signs were observed. All surviving animals developed neutralizing antibodies to NiV<sub>B</sub>, as well as NiV-specific IgM and IgG binding antibodies. However, these antibodies were not detectable until the window during which non-survivors were beginning to succumb to NiV disease. Further analyses of specific immune responses to the G\*-rVSV-ΔG-NiV<sub>B</sub> G vaccine and to NiV<sub>B</sub> itself are in progress, including cytotoxic T-lymphocyte assays using a NiV<sub>B</sub>-specific peptide pool and NanoString nCounter® immunology and inflammation panels for targeted

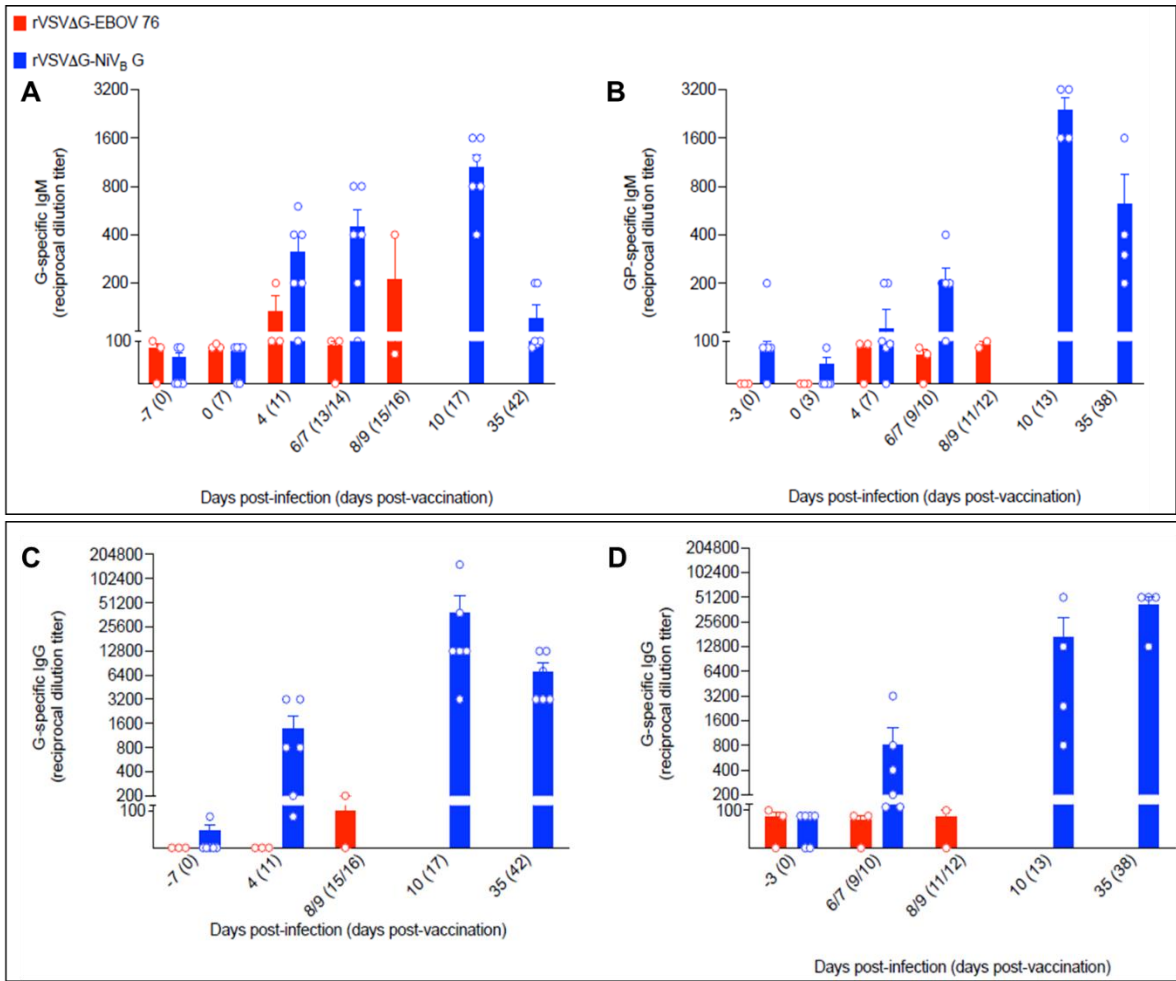


**Figure 4-10: Detection of NiV-specific IgM and IgG binding antibodies in AGMs vaccinated prior to challenge with NiV<sub>B</sub>**

ELISA results from gamma-irradiated serum, reported as reciprocal dilutions, for animals vaccinated with G\*-rVSV-ΔG-NiV<sub>B</sub> G (blue) or rVSV-ΔG-EBOV 76 (red) (**A and C**) seven days or (**B and D**) three days prior to challenge with NiV<sub>B</sub>. Bars and error bars represent the mean and SEM across vaccination groups, and individual values are visible as dots with each bar. The x-axis indicates dpi, followed by equivalent days post-vaccination in parentheses. Values are provided for (**A and B**) IgM and (**C and D**) IgG antibody isotypes.

transcriptomics to compare upregulated genes in survivors with non-surviving G\*-rVSV- $\Delta$ G-NiV<sub>B</sub> G-vaccinated and rVSV- $\Delta$ G-EBOV 76-vaccinated animal subjects. These assays will help to define a survivor phenotype and to elucidate the innate, humoral, and cellular immune factors that are important for creating a vaccine-induced, protective immune response to NiV<sub>B</sub>.

## DISCUSSION

This chapter detailed the process of rescuing the G\*-rVSV- $\Delta$ G-NiV<sub>B</sub> G vaccine and testing its protective efficacy in AGMs in two studies in which it was given shortly before challenge with a lethal dose of NiV<sub>B</sub>. The rVSV-based NiV vaccine replicated to high titers in cell culture when complemented with VSV G and strongly expressed NiV<sub>B</sub> G (**Figure 4-3**). When administered i.m. to AGMs seven days prior to challenge, G\*-rVSV- $\Delta$ G-NiV<sub>B</sub> G protected 100% of the animals from NiV disease, while 67% of vaccinated animals survived NiV<sub>B</sub> challenge three days after vaccination. Therefore, the G\*-rVSV- $\Delta$ G-NiV<sub>B</sub> G vaccine induced rapid protection against NiV disease, as would be critical in an emergency response to a NiV outbreak.

The G\*-rVSV- $\Delta$ G-NiV<sub>B</sub> G vaccine has an ideal profile for licensure and deployment during an outbreak of NiV disease. Firstly, it is expected to be safe for use in humans because VSV-based vaccines have been shown to be safe and effective in the past, as evidenced by the licensure of Ervebo, Merck's VSV-vectored Ebola vaccine<sup>188</sup>. A ring vaccination trial in Guinea and Sierra Leone resulted in 100% efficacy, calculated based on zero confirmed EBOV cases at greater than 10 days post-vaccination<sup>189</sup>, and rapid protective efficacy of rVSV-EBOV vectors has also been demonstrated in NHP models of EBOV disease<sup>229</sup>. VSV has mild pathogenicity in humans, and because the G\*-rVSV- $\Delta$ G-NiV<sub>B</sub> G construct encodes only NiV<sub>B</sub> G and is not an attenuated NiV, it cannot revert to virulent NiV<sub>B</sub>. As a negative-sense, single-stranded RNA virus, it cannot

reassort and cannot integrate into the host genome. Furthermore, the fact that G\*-rVSV- $\Delta$ G-NiV<sub>B</sub> G is a single-cycle vaccine which cannot replicate without complementation and yet is still immunogenic, as evidenced by the development of binding and neutralizing antibodies to NiV<sub>B</sub> in surviving AGMs here and by previous studies with replication-incompetent rVSV constructs<sup>231</sup>, enhances its safety profile.

While G\*-rVSV- $\Delta$ G-NiV<sub>B</sub> G requires storage at -80°C and maintenance of cold chain to ensure efficacy, Ervebo has the same storage and transportation constraints and has been used effectively in recent outbreaks of Ebola in the Democratic Republic of the Congo. Multiple technologies have been developed to transport the vaccine to remote, resource-limited areas while maintaining cold chain, and stability studies could be undertaken to determine how long the vaccine could be stored at, for example, 4°C while retaining its potency. Studies are underway to determine the dose of G\*-rVSV- $\Delta$ G-NiV<sub>B</sub> G vaccine needed to protect AGMs from lethal NiV<sub>B</sub> challenge, but the construct easily grows to titers exceeding  $1 \times 10^8$  PFU per mL in just 24 hours, so manufacturing of many doses in a short timeframe is achievable. Importantly, however, complementation with VSV G is necessary with each passaging step, so certified cell lines that stably express VSV G will need to be developed in order to facilitate scalable manufacturing and quality control.

The nonspecific control vaccine used in these studies was also a VSV-vectored vaccine, although it is fully replicative because the EBOV GP glycoprotein is the only protein required for entry of EBOV into cells. A non-replicating, nonspecific rVSV vector could have been used as a more direct control instead, or the control group could have been administered PBS instead of a vaccine. However, the replicating VSV-vectored vaccine provided a more robust control group than a non-replicating rVSV or saline control group. A previous study showed that 100% of hamsters vaccinated one day prior to challenge with a replicating rVSV-vectored NiV vaccine survived challenge with NiV<sub>M</sub>; partial survival was observed in additional groups that were vaccinated on the day

of challenge (four out of six animals) or one day after challenge (one out of six animals)<sup>192</sup>. However, the authors attributed this protection to innate responses or responses to the rVSV-ΔG vector itself rather than specific responses to the NiV component of the vaccines, as animals vaccinated with a nonspecific rVSV-ΔG-EBOV GP control vector survived challenge with NiV<sub>M</sub> when vaccinated one day prior to challenge (three out of six animals) or day of challenge (two out of six animals)<sup>192</sup>. The studies discussed here used a very similar nonspecific control vector but a more relevant model of NiV disease in humans (AGMs) and more virulent strain of NiV in that model (NiV<sub>B</sub>), and 100% of the animals vaccinated with the nonspecific rVSV-ΔG-EBOV 76 control vector succumbed to NiV disease. Therefore, it is likely that survival was not based solely on innate nor vector-specific immunity. However, VSV G was present on the surface of the G\*-rVSV-ΔG-NiV<sub>B</sub> G vaccine, so effects of immunity to VSV G cannot be ruled out based on the results of these studies, as VSV G was not present in the nonspecific rVSV-ΔG-EBOV 76 vector. Although all animals vaccinated with rVSV-ΔG-EBOV 76 succumbed to NiV disease during the normal window for this model and dose, ELISAs to detect antibodies specific to VSV G are necessary in order to determine the level of immunity to the VSV G protein present in G\*-rVSV-ΔG-NiV<sub>B</sub> G-vaccinated AGMs.

Late-onset encephalitis and lingering neurological deficits are a concern in NiV patients, and neurovirulence is a possibility with wild-type VSV and has been investigated for other VSV-vectored constructs. Ensuring that these concerns are not likely to be exacerbated by the G\*-rVSV-ΔG-NiV<sub>B</sub> G construct is critical for continuing studies with the rVSV-NiV vaccine construct described here. None of the animals in either of the studies presented in this chapter developed late-onset neurological signs, which have occurred between 28 and 35 dpi in previous AGM NiV challenge studies. While these were short-term studies, lasting only five weeks, this is an encouraging sign that the vaccine is not just suppressing viral replication to a low level and then allowing it

to begin replicating later. However, more and longer studies are needed to confirm these results. A previous study found that other rVSV- $\Delta$ G constructs did not cause neurovirulence in NHPs when administered directly to the thalamus, in contrast to wild-type rVSV encoding VSV G<sup>232</sup>. The G\*-rVSV- $\Delta$ G-NiV<sub>B</sub> G construct does not encode the gene that allows VSV neurovirulence (VSV G), but it does have VSV G protein present on its surface from the G-complemented cells from which the viral envelope was derived. While only one of the two proteins necessary for NiV viral entry and therefore NiV-mediated neurovirulence is present in the construct, further investigation is needed to ensure the safety of the vaccine. Nonetheless, based on previous studies and on results of the two studies in AGMs described here, the G\*-rVSV- $\Delta$ G-NiV<sub>B</sub> G vaccine is expected to be safe.

The NiV vaccine candidate that has been most extensively studied and is most advanced along the path toward licensure for human use is the HeV-sG vaccine, with a phase 1 clinical trial to assess safety in human volunteers currently underway (Clinical Trial #NCT04199169). This vaccine candidate has been shown to be safe, immunogenic, and highly effective at preventing NiV disease in ferrets, cats, and AGMs<sup>135,164,174</sup>. Previous experiments evaluating HeV-sG as a vaccine candidate employed two doses, with the second dose given at least 20 days prior to challenge with NiV. However, a recent study demonstrated that a single dose of the vaccine was effective at preventing NiV disease in AGMs as close as seven days prior to challenge<sup>175</sup>. As a recombinant protein subunit vaccine, the HeV-sG vaccine is also inherently extremely safe. However, times between vaccination and challenge shorter than seven days have not been tested, and the HeV-sG vaccine is formulated with an adjuvant to boost its immunogenicity. Given its rapid efficacy in a single, adjuvant-free dose, ability to be grown to very high titers quickly in cell lines expressing VSV G, and apparently strong safety profile, continued characterization of the G\*-rVSV- $\Delta$ G-NiV<sub>B</sub> G vaccine as an additional tool for controlling spread of NiV disease in emergency settings is worthwhile. However,

manufacturing of the G\*-rVSV- $\Delta$ G-NiV<sub>B</sub> G construct is complicated by the need for VSV G complementation for growth in cell culture, and cell lines approved for vaccine manufacture and stably expressing VSV G will need to be developed and certified.

In conclusion, G\*-rVSV- $\Delta$ G-NiV<sub>B</sub> G is a safe, immunogenic, and effective vaccine which protected AGMs from a high dose of NiV<sub>B</sub> given shortly after vaccination. These studies are an encouraging first step in showing the potential safety and efficacy of the vaccine in an outbreak scenario. Studies are ongoing to evaluate protective immune responses to the vaccine, minimum dose needed for efficacy, and durability of vaccine-induced immune responses. Future studies will focus on standardizing manufacturing with an eye towards licensure. A fast-acting and effective vaccine is urgently needed for NiV, which continues to emerge and cause outbreaks in India and Bangladesh on nearly an annual basis with high CFRs, and G\*-rVSV- $\Delta$ G-NiV<sub>B</sub> G could be an invaluable tool in the control of this deadly pathogen.

## Chapter 5: Conclusions

### PREVIOUS UNDERSTANDING OF NiV INHIBITION OF RLRs

As discussed in Chapter 1, interactions of NiV V with RLRs have been well-characterized at BSL-2 using plasmid overexpression experiments. Interaction with MDA5 and LGP2 had been isolated to the CTD of NiV V and the helicase domain of the RLRs, although an exact binding site had not been determined<sup>121,131,195</sup>. Interaction with RIG-I had been isolated to the CTD of NiV V and the N-terminal CARDs of RIG-I and had been shown to inhibit TRIM25-mediated activation of RIG-I signaling<sup>111</sup>. However, none of these interactions had been examined with replicating virus under BSL-4 conditions, nor had the contributions of MDA5 evasion to virulence *in vivo* been investigated. The closest *in vivo* evidence of the importance of MDA5 to paramyxovirus virulence was that CDV lacking the ability to bind to MDA5 caused clinical signs and transient viremia in ferrets but was otherwise non-lethal<sup>194</sup>.

### CONTRIBUTIONS TO UNDERSTANDING OF NiV INHIBITION OF RLRs MADE HERE

#### 1. The single amino acid I414 is necessary for NiV V binding to MDA5, but additional amino acids are likely involved in binding to LGP2

Chapter 2 detailed the process of determining the specific binding site of NiV V to MDA5 through alanine scanning mutations in a NiV<sub>M</sub> V expression plasmid using co-IP/western blot assays. As shown in **Figure 2-10**, alanine scanning over the first fifteen amino acids of the NiV<sub>M</sub> V CTD identified I414 as a key residue in binding to MDA5. Creation of a NiV<sub>M</sub> V expression plasmid containing the I414A point mutant confirmed these results (**Figure 2-13**). Interestingly, this binding site is unique among paramyxoviruses whose specific binding sites have so far been identified; other paramyxoviruses use different nearby residues, including the glutamic acid at position 411 in NiV<sub>M</sub>, to mediate their interactions with MDA5<sup>193,194</sup>. Further research is needed

to determine the structural basis of binding between I414 and the helicase domain of MDA5, but the fact that all known paramyxovirus V-MDA5 binding sites are within a few amino acids of each other indicates that a  $\beta$ -sheet within the NiV<sub>M</sub> V CTD likely interleaves with a  $\beta$ -sheet within the MDA5 helicase domain, as it does in the case of PIV5<sup>193</sup>.

A single arginine residue shared by MDA5 and LGP2 within their helicase domains is thought to mediate interaction with paramyxovirus V proteins<sup>193,195</sup>. Therefore, the binding site for MDA5 and LGP2 by V is thought to be shared. The shared MDA5/LGP2 binding site was confirmed for MeV V as the glutamic acid residue at position 235<sup>193,195</sup>. However, PIV5 V had additional amino acid requirements for binding to LGP2<sup>195</sup>. Interestingly, preliminary co-IP/western blot results showed that NiV V also has additional amino acid requirements for binding to LGP2, as I414A alone was not sufficient to completely abrogate binding to LGP2 (**Figure 2-15**). Additional experiments are needed to further characterize the NiV V-LGP2 interaction and to assess its functional importance. Most known paramyxoviruses, including NiV, can bind to LGP2 and inhibit its helicase activity<sup>233</sup>. However, whether this interaction is incidental due to structural and sequence similarity with MDA5 or is a separate immune evasion mechanism in the context of LGP2 regulation of RLR signaling needs to be investigated.

## **2. Blocking of viral inhibition of MDA5 alone was not sufficient to attenuate rNiV<sub>M</sub> *in vitro* or *in vivo***

The wild-type NiV V protein is a strong inhibitor of type-I IFN induction in plasmid overexpression assays with IFN- $\beta$  luciferase reporters<sup>121,196</sup>. Prevention of binding to MDA5 by NiV would theoretically reverse this inhibition of the IFN production pathway. However, NiV V likely has another way to inhibit IFN production when MDA5 binding is blocked, as NiV<sub>M</sub> V expression plasmids containing the I414A mutation only partially lose the ability to inhibit IFN- $\beta$  induction at relatively low

concentrations of expression plasmid (**Figure 2-14**). Other interactions between NiV V and components of the IFN production pathway have been previously identified; NiV V can bind to (and inhibit the activity of) RIG-I as well as an upstream activator of MDA5, PP1<sup>111,210</sup>. The ability of NiV to inhibit an upstream regulator of MDA5 and another inducer of the IFN production pathway when binding to MDA5 is blocked helps to explain the results of the reporter experiments presented in **Figure 2-11** and **Figure 2-14**.

Previously, all work with NiV V inhibition of MDA5 had been done at BSL-2 with expression plasmids. In Chapter 3, however, *in vitro* and *in vivo* data with replicative rNiV<sub>M</sub> lacking the ability to bind to MDA5 was presented. As in Chapter 2, *in vitro* results were modest. Full-length rNiV<sub>M</sub> containing the I414A mutation were not growth-inhibited compared to rNiV<sub>M</sub>-wt at very low MOIs at early timepoints after IFN pretreatment, but they did replicate to a lower final peak titer than wild-type rNiV<sub>M</sub> (**Figure 3-3**, panels **B** and **D**). These results were corroborated in IFN-competent HEK293T cells (**Figure 3-3**, panels **C** and **F**). The viral kinetics results confirm those seen with expression plasmids in Chapter 2—NiV V has additional ways of inhibiting IFN production when unable to bind to MDA5. These results were further corroborated when ferrets infected with rNiV<sub>M</sub> containing the I414A mutation succumbed to NiV disease six to seven days after challenge (**Figure 3-5**), although these results were confounded by the higher challenge dose than previous studies given to these animals. Additional studies are needed to determine whether the I414A mutation is sufficient to attenuate NiV *in vivo* at lower doses. However, the myriad protein-protein interactions in which NiV<sub>M</sub> V is involved and the additional regulators of the RLR signaling pathways that NiV V can inhibit indicate that simultaneous inhibition of multiple components of these pathways, such as MDA5 and PP1, will likely be necessary for viral attenuation<sup>210</sup>.

### **3. Together, MDA5 and STAT1 are important mediators of NiV virulence**

Knockout of the entire CTD of the NiV V protein rendered the virus non-lethal at a dose of approximately 5,000 PFU given to ferrets *i.n*.<sup>67</sup>. Although the *in vivo* results of prevention of binding to MDA5 alone by NiV did not recapitulate this phenotype at the dose tested, a rNiV<sub>M</sub> containing the MDA5-binding mutations as well as a previously characterized mutation designed to prevent binding to STAT1, Y116E, was also recovered. In ferrets, the Y116E mutation was not sufficient to attenuate the virus at a dose of 5,000 PFU, as all animals succumbed to infection by day nine post-challenge<sup>158</sup>. However, a virus containing a deletion of a slightly larger region of the P ORF, rNiV<sub>M</sub> P Δ116-135, resulted in delayed time to death at around 12 to 13 dpi in ferrets given 5,000 PFU<sup>158</sup>. Interestingly, combining the Y116E STAT1-binding mutation with the MDA5-binding mutations resulted in 75% survival of infected ferrets, despite administration of a dose closer to 30,000 PFU (**Figure 3-5**). These results indicated that while neither MDA5 nor STAT1 is a determinant of NiV virulence on its own, prevention of binding to both MDA5 and STAT1 by NiV was sufficient to attenuate the virus at the dose tested. Surviving animals had clinical signs of NiV disease and/or hematological changes, but values returned to normal by 10 dpi, and subjects had no apparent lingering effects.

#### **PREVIOUS PROGRESS TOWARD A NiV VACCINE FOR EMERGENCY USE**

As discussed in Chapter 1, no vaccine is currently approved for the prevention of NiV infection and disease in humans. Since NiV continues to cause recurrent outbreaks nearly every year with high CFRs, a vaccine that is efficacious early following administration and suitable for an emergency response setting to stop the spread of NiV during outbreaks is urgently needed. The most advanced vaccine candidate is HeV-sG, a recombinant, soluble version of the HeV G attachment glycoprotein, which is considered a subunit vaccine<sup>163</sup>. A version of the HeV-sG vaccine, known as Equivac® HeV and marketed by Zoetis, Inc., has been approved for use in Australia for prevention of HeV in

horses<sup>162</sup>. The same recombinant HeV-sG antigen, formulated for use in humans, is currently in a phase I clinical trial<sup>162</sup>. This vaccine has been shown to be highly effective in AGMs within seven days of administration of a single dose<sup>175</sup>, and it protects ferrets from NiV challenge more than a year following two doses<sup>164</sup>. However, the vaccine requires an adjuvant to enhance its immunogenicity, and durability of responses to a single dose has not yet been investigated.

Like the HeV-sG vaccine, rVSV-vectored NiV vaccines encoding one of the two NiV surface proteins instead of VSV G have been in preclinical development for several years<sup>187</sup>. Most recently, a version encoding GFP and NiV<sub>B</sub> G has been shown to be 100% effective at protecting ferrets and AGMs from lethal challenge with NiV<sub>M</sub> and NiV<sub>B</sub> in a single dose when given 28 days prior to challenge<sup>165,191</sup>. The construct does not require an adjuvant and is a single-cycle vector because it only encodes one of the two NiV surface proteins, which enhances its safety. However, it has not been tested at shorter intervals between vaccination and challenge, as might be necessary during an active outbreak.

## CONTRIBUTIONS TOWARD A RAPID-ACTING NiV VACCINE

### **1. The G\*-rVSV-ΔG-NiV<sub>B</sub> G vaccine protected 100% of AGMs from NiV<sub>B</sub> when given seven days prior to challenge and 67% of AGMs when given three days prior to challenge**

As discussed in Chapter 4, a rVSV-vectored NiV vaccine lacking the fluorescent reporter present in the previous version of the construct was rescued, purified, and characterized. The G\*-rVSV-ΔG-NiV<sub>B</sub> G vaccine grew quickly to high titers in cells complemented with VSV G, and it strongly expressed NiV<sub>B</sub> G in infected cells (**Figure 4-3**). The vaccine was used to vaccinate AGMs seven days or three days prior to a lethal dose of NiV<sub>B</sub>. 100% of animals vaccinated with rVSV-ΔG-NiV<sub>B</sub> G seven days prior to challenge survived to the study endpoint, while 67% of animals vaccinated three days

prior to challenge survived (**Figure 4-5**). These results constitute the first demonstration of protective efficacy this close to challenge with NiV<sub>B</sub> for any NiV vaccine; previous vaccine candidates were tested with NiV<sub>M</sub>, but NiV<sub>B</sub> is more pathogenic in AGMs than NiV<sub>M</sub><sup>172</sup>. Furthermore, 100% of control animals receiving the nonspecific, replication-competent rVSV-ΔG-EBOV 76 vector succumbed to NiV disease between seven and nine days post-challenge, demonstrating that the G\*-rVSV-ΔG-NiV<sub>B</sub> G vaccine specifically mediated protection from challenge, not innate immunity or immunity directed against the VSV backbone (**Figure 4-5**).

## **2. Survivors vaccinated with G\*-rVSV-ΔG-NiV<sub>B</sub> G mounted a NiV-specific humoral response**

The fact that control animals vaccinated with a different rVSV-ΔG vaccine succumbed to NiV disease strongly indicates that vaccination close to challenge did not simply upregulate generalized inflammation and elicit an innate immune response that protected survivors from NiV<sub>B</sub> challenge. PRNT<sub>50</sub> assays and NiV-specific IgM and IgG ELISAs were performed on each of the animals in both studies. All animals lacked NiV-specific neutralizing antibodies prior to vaccination and at time of challenge, but all surviving animals developed NiV-specific neutralizing antibodies that were detectable as a reduction in plaques by at least 50% compared to control wells by seven dpi (**Figure 4-8**). Furthermore, all surviving animals developed NiV-specific IgM and IgG responses by 10 to 11 days post-vaccination (**Figure 4-9**). Therefore, all surviving animals mounted a NiV-specific humoral response, either to the vaccine itself or to the challenge virus or both. Additional assays to further characterize the NiV-specific immune response are underway, including cytotoxic T-lymphocyte assays using a NiV peptide pool to assess NiV-specific T-cell responses and NanoString nCounter® inflammation and immunity panels to identify genes upregulated at the transcriptional level in response to vaccination and challenge. ELISAs to evaluate binding antibodies specific to VSV G will be carried out, as well. The goal is to identify components of a protective immune response that

contribute to a survivor phenotype following vaccination with the G\*-rVSV- $\Delta$ G-NiV<sub>B</sub> G vaccine. Previous investigations in experimentally infected AGMs and in NiV-infected humans indicate that T-cell immunity may be an important contributor to a survivor phenotype in these animals<sup>19,168</sup>.

In conclusion, the experiments and data derived and detailed here have furthered understanding of the mechanisms of immunity to and protection against NiV infection and disease by identifying the specific binding site of MDA5 by NiV<sub>M</sub> V, determining that MDA5 inhibition alone is not a major determinant of virulence for NiV<sub>M</sub> but that it can work with inhibition of STAT1 to contribute to virulence in a lethal ferret model, and generating a new G\*-rVSV- $\Delta$ G-NiV<sub>B</sub> G construct that worked quickly and induced NiV-specific humoral responses in vaccinated NHPs that survived NiV<sub>B</sub> challenge. The protective efficacy of this vaccine when given shortly prior to virus challenge is an important first step toward demonstrating its potential utility as an emergency response vaccine in an outbreak setting to stop the spread of NiV infection and disease in people.

## References

1. Chua, K. B. *et al.* Nipah Virus: A Recently Emergent Deadly Paramyxovirus. *Science* **288**, 1432–1435 (2000).
2. Paton, N. I. *et al.* Outbreak of Nipah-virus infection among abattoir workers in Singapore. *Lancet* **354**, 1253–1256 (1999).
3. Harcourt, B. H. *et al.* Molecular characterization of Nipah virus, a newly emergent paramyxovirus. *Virology* **271**, 334–349 (2000).
4. Centers for Disease Control and Prevention (CDC). Outbreak of Hendra-like virus--Malaysia and Singapore, 1998-1999. *MMWR Morb Mortal Wkly Rep* **48**, 265–269 (1999).
5. Selvey, L. A. *et al.* Infection of humans and horses by a newly described morbillivirus. *Medical Journal of Australia* **162**, 642–645 (1995).
6. Wang, L.-F. *et al.* The Exceptionally Large Genome of Hendra Virus: Support for Creation of a New Genus within the Family Paramyxoviridae. *Journal of Virology* **74**, 9972–9979 (2000).
7. Murray, K. *et al.* A Morbillivirus That Caused Fatal Disease in Horses and Humans. *Science* **268**, 94–97 (1995).
8. Marsh, G. A. *et al.* Cedar Virus: A Novel Henipavirus Isolated from Australian Bats. *PLoS Pathogens* **8**, (2012).
9. Wu, Z. *et al.* Novel Henipa-like Virus, Mojiang Paramyxovirus, in Rats, China, 2012. *Emerging Infectious Diseases* **20**, 1062–1064 (2014).
10. Drexler, J. F. *et al.* Bats host major mammalian paramyxoviruses. *Nature Communications* **3**, (2012).
11. Chua, K. B. *et al.* Fatal encephalitis due to Nipah virus among pig-farmers in Malaysia. *Lancet* **354**, 1257–1259 (1999).
12. Chua, K. B. Nipah virus outbreak in Malaysia. *Journal of Clinical Virology* **26**, 265–275 (2003).
13. Hsu, V. P. *et al.* Nipah Virus Encephalitis Reemergence, Bangladesh. *Emerging Infectious Diseases* **10**, 2082–2087 (2004).
14. Luby, S. P. *et al.* Foodborne Transmission of Nipah Virus, Bangladesh. *Emerging Infectious Diseases* **12**, 1888–1894 (2006).
15. Rahman, M. A. *et al.* Date Palm Sap Linked to Nipah Virus Outbreak in Bangladesh, 2008. *Vector-Borne and Zoonotic Diseases* **12**, 65–72 (2012).
16. Gurley, E. S. *et al.* Person-to-Person Transmission of Nipah Virus in a Bangladeshi Community. *Emerging Infectious Diseases* **13**, 1031–1037 (2007).
17. Ching, P. K. G. *et al.* Outbreak of henipavirus infection, Philippines, 2014. *Emerging Infectious Diseases* **21**, 328–331 (2015).
18. Harcourt, B. H. *et al.* Genetic Characterization of Nipah Virus, Bangladesh, 2004. *Emerging Infectious Diseases* **11**, 1594–1597 (2005).
19. Arunkumar, G. *et al.* Outbreak Investigation of Nipah Virus Disease in Kerala, India, 2018. *Journal of Infectious Diseases* **219**, 1867–1878 (2019).
20. Chua, K. B. *et al.* Isolation of Nipah virus from Malaysian Island flying-foxes. *Microbes and Infection* **4**, 145–151 (2002).

21. Johara, M. Y. *et al.* Nipah Virus Infection in Bats (Order Chiroptera) in Peninsular Malaysia. *Emerging Infectious Diseases* **7**, 439–441 (2001).
22. Plowright, R. K. *et al.* Prioritizing surveillance of nipah virus in India. *PLoS Neglected Tropical Diseases* **13**, (2019).
23. Reynes, J.-M. *et al.* Nipah Virus in Lyle’s Flying Foxes, Cambodia. *Emerging Infectious Diseases* **11**, 1042–1047 (2005).
24. Gaudino, M. *et al.* High Pathogenicity of Nipah Virus from Pteropus lylei Fruit Bats, Cambodia. *Emerging Infectious Diseases* **26**, 104–113 (2020).
25. Tan, C. T. & Tan, K. S. Nosocomial Transmissibility of Nipah Virus. *Journal of Infectious Diseases* **184**, 1367- (2001).
26. de Wit, E., Bushmaker, T., Scott, D., Feldmann, H. & Munster, V. J. Nipah virus transmission in a hamster model. *PLoS Neglected Tropical Diseases* **5**, (2011).
27. Clayton, B. A. *et al.* The Nature of Exposure Drives Transmission of Nipah Viruses from Malaysia and Bangladesh in Ferrets. *PLoS Neglected Tropical Diseases* **10**, (2016).
28. Khan, S. U. *et al.* A randomized controlled trial of interventions to impede date palm sap contamination by bats to prevent Nipah virus transmission in Bangladesh. *PLoS ONE* **7**, (2012).
29. Pallivalappil, B. *et al.* Dissecting an outbreak: A clinico-epidemiological study of Nipah virus infection in Kerala, India, 2018. *Journal of Global Infectious Diseases* **12**, 21–27 (2020).
30. Wong, K. T. *et al.* Nipah Virus Infection: Pathology and Pathogenesis of an Emerging Paramyxoviral Zoonosis. *American Journal of Pathology* **161**, 2153–2167 (2002).
31. Goh, K. J. *et al.* Clinical Features of Nipah Virus Encephalitis among Pig Farmers in Malaysia. *The New England Journal of Medicine* **342**, 1229–1235 (2000).
32. Luby, S. P., Gurley, E. S. & Hossain, M. J. Transmission of Human Infection with Nipah Virus. *Clinical Infectious Diseases* vol. 49 1743–1748 (2009).
33. Clayton, B. A. *et al.* Transmission routes for Nipah virus from Malaysia and Bangladesh. *Emerging Infectious Diseases* **18**, 1983–1993 (2012).
34. Chew, M. H. L. *et al.* Risk Factors for Nipah Virus Infection among Abattoir Workers in Singapore. *The Journal of Infectious Diseases* **181**, 1760–1763 (2000).
35. Tan, C. T. *et al.* Relapsed and Late-Onset Nipah Encephalitis. *Annals of Neurology* **51**, 703–708 (2002).
36. Wong, S. C. *et al.* Late presentation of Nipah virus encephalitis and kinetics of the humoral immune response. *Journal of Neurology Neurosurgery and Psychiatry* **71**, 552–554 (2001).
37. Chong, H. T. & Tan, C. T. Relapsed and late-onset Nipah encephalitis, a report of three cases. *Neurol J Southeast Asia* **8**, 109–112 (2003).
38. Tan, C. T. & Wong, K. T. Nipah encephalitis outbreak in Malaysia. *Annals of the Academy of Medicine, Singapore* **32**, 112–117 (2003).
39. Abdullah, S., Chang, L.-Y., Rahmat, K., Goh, K. J. & Tan, C. T. Late-onset Nipah virus encephalitis 11 years after the initial outbreak: A case report. *Neurology Asia* **17**, 71–74 (2012).
40. O’Sullivan, J. D. *et al.* Fatal encephalitis due to novel paramyxovirus transmitted from horses. *The Lancet* **349**, 93–95 (1997).

41. Wong, K. T. *et al.* Human Hendra virus infection causes acute and relapsing encephalitis. *Neuropathology and Applied Neurobiology* **35**, 296–305 (2009).
42. Sejvar, J. J. *et al.* Long-term neurological and functional outcome in Nipah virus infection. *Annals of Neurology* **62**, 235–242 (2007).
43. Ng, B.-Y., Lim, C. C. T., Yeoh, A. & Lee, W. L. Neuropsychiatric Sequelae of Nipah Virus Encephalitis. *Journal of Neuropsychiatry and Clinical Neurosciences* **16**, 500–504 (2004).
44. Amarasinghe, G. K. *et al.* Taxonomy of the order Mononegavirales: update 2018. *Archives of Virology* **163**, 2283–2294 (2018).
45. Halpin, K., Bankamp, B., Harcourt, B. H., Bellini, W. J. & Rota, P. A. Nipah virus conforms to the rule of six in a minigenome replication assay. *Journal of General Virology* **85**, 701–707 (2004).
46. Sugai, A., Sato, H., Yoneda, M. & Kai, C. Gene end-like sequences within the 3' non-coding region of the Nipah virus genome attenuate viral gene transcription. *Virology* **508**, 36–44 (2017).
47. Takimoto, T. & Portner, A. Molecular mechanism of paramyxovirus budding. *Virus Research* **106**, 133–145 (2004).
48. Ciancanelli, M. J. & Basler, C. F. Mutation of YMYL in the Nipah Virus Matrix Protein Abrogates Budding and Alters Subcellular Localization. *Journal of Virology* **80**, 12070–12078 (2006).
49. Wang, Y. E. *et al.* Ubiquitin-regulated nuclear-cytoplasmic trafficking of the Nipah virus matrix protein is important for viral budding. *PLoS Pathogens* **6**, (2010).
50. Aguilar, H. C. & Iorio, R. M. Henipavirus Membrane Fusion and Viral Entry. in *Henipavirus: Ecology, Molecular Virology, and Pathogenesis* (eds. Lee, B. & Rota, P. A.) 79–94 (2012). doi:10.1007/82\_2012\_200.
51. Lee, B. & Ataman, Z. A. Modes of paramyxovirus fusion: A Henipavirus perspective. *Trends in Microbiology* vol. 19 389–399 (2011).
52. Steffen, D. L., Xu, K., Nikolov, D. B. & Broder, C. C. Henipavirus mediated membrane fusion, virus entry and targeted therapeutics. *Viruses* vol. 4 280–309 (2012).
53. Bossart, K. N., Fusco, D. L. & Broder, C. C. Paramyxovirus Entry. in *Viral Entry into Host Cells* (eds. Pöhlmann, S. & Simmons, G.) (2013). doi:10.1007/978-1-4614-7651-1\_6.
54. Bonaparte, M. I. *et al.* Ephrin-B2 ligand is a functional receptor for Hendra virus and Nipah virus. *Proceedings of the National Academy of Sciences* **102**, 10652–10657 (2005).
55. Negrete, O. A. *et al.* EphrinB2 is the entry receptor for Nipah virus, an emergent deadly paramyxovirus. *Nature* **436**, 401–405 (2005).
56. Negrete, O. A. *et al.* Two key residues in EphrinB3 are critical for its use as an alternative receptor for Nipah virus. *PLoS Pathogens* **2**, 0078–0086 (2006).
57. Bowden, T. A. *et al.* Structural basis of Nipah and Hendra virus attachment to their cell-surface receptor ephrin-B2. *Nature Structural and Molecular Biology* **15**, 567–572 (2008).

58. Xu, K. *et al.* Host cell recognition by the henipaviruses: Crystal structures of the Nipah G attachment glycoprotein and its complex with ephrin-B3. *Proceedings of the National Academy of Sciences* **105**, 9953–9958 (2008).
59. Xu, K., Broder, C. C. & Nikolov, D. B. Ephrin-B2 and ephrin-B3 as functional henipavirus receptors. *Seminars in Cell and Developmental Biology* vol. 23 116–123 (2012).
60. Hyatt, A. D., Zaki, S. R., Goldsmith, C. S., Wise, T. G. & Hengstberger, S. G. Ultrastructure of Hendra virus and Nipah virus within cultured cells and host animals. *Microbes and Infection* **3**, 297–306 (2001).
61. Park, M.-S. *et al.* Newcastle Disease Virus (NDV)-Based Assay Demonstrates Interferon-Antagonist Activity for the NDV V Protein and the Nipah Virus V, W, and C Proteins. *Journal of Virology* **77**, 1501–1511 (2003).
62. Vidal, S., Curran, J. & Kolakofsky, D. A stuttering model for paramyxovirus P mRNA editing. *EMBO Journal* **9**, 2017–2022 (1990).
63. Kolakofsky, D., Roux, L., Garcin, D. & Ruigrok, R. W. H. Paramyxovirus mRNA editing, the “rule of six” and error catastrophe: A hypothesis. *Journal of General Virology* vol. 86 1869–1877 (2005).
64. Kulkarni, S. *et al.* Nipah Virus Edits Its P Gene at High Frequency To Express the V and W Proteins. *Journal of Virology* **83**, 3982–3987 (2009).
65. Lo, M. K. *et al.* Determination of the henipavirus phosphoprotein gene mRNA editing frequencies and detection of the C, V and W proteins of Nipah virus in virus-infected cells. *Journal of General Virology* **90**, 398–404 (2009).
66. Ciancanelli, M. J., Volchkova, V. A., Shaw, M. L., Volchkov, V. E. & Basler, C. F. Nipah Virus Sequesters Inactive STAT1 in the Nucleus via a P Gene-Encoded Mechanism. *Journal of Virology* **83**, 7828–7841 (2009).
67. Satterfield, B. A. *et al.* The immunomodulating V and W proteins of Nipah virus determine disease course. *Nature Communications* **6**, (2015).
68. Satterfield, B. A. *et al.* Nipah Virus C and W Proteins Contribute to Respiratory Disease in Ferrets. *Journal of Virology* **90**, 6326–6343 (2016).
69. Yoneda, M. *et al.* The nonstructural proteins of Nipah virus play a key role in pathogenicity in experimentally infected animals. *PLoS ONE* **5**, 1–8 (2010).
70. Mathieu, C. *et al.* Nonstructural Nipah Virus C Protein Regulates both the Early Host Proinflammatory Response and Viral Virulence. *Journal of Virology* **86**, 10766–10775 (2012).
71. Pasquale, E. B. Eph-Ephrin Bidirectional Signaling in Physiology and Disease. *Cell* vol. 133 38–52 (2008).
72. Lee, B. Envelope-receptor interactions in Nipah virus pathobiology. in *Annals of the New York Academy of Sciences* vol. 1102 51–65 (Blackwell Publishing Inc., 2007).
73. Pernet, O., Wang, Y. E. & Lee, B. Henipavirus Receptor Usage and Tropism. in *Henipavirus: Ecology, Molecular Virology, and Pathogenesis* (eds. Lee, B. & Rota, P. A.) 59–78 (2012). doi:10.1007/82\_2012\_222.
74. Bossart, K. N. *et al.* Functional studies of host-specific ephrin-B ligands as Henipavirus receptors. *Virology* **372**, 357–371 (2008).
75. Wong, K. T. *et al.* A Golden Hamster Model for Human Acute Nipah Virus Infection. *American Journal of Pathology* **163**, 2127–2137 (2003).

76. Al-Obaidi, J. M. M. *et al.* Disruption of the blood brain barrier is vital property of neurotropic viral infection of the central nervous system. *Acta Virologica* vol. 62 16–27 (2018).
77. Mungall, B. A. *et al.* Vertical transmission and fetal replication of Nipah virus in an experimentally infected cat. *Journal of Infectious Diseases* **196**, 812–816 (2007).
78. Mathieu, C. *et al.* Nipah Virus Uses Leukocytes for Efficient Dissemination within a Host. *Journal of Virology* **85**, 7863–7871 (2011).
79. Geisbert, T. W. *et al.* Development of an acute and highly pathogenic nonhuman primate model of nipah virus infection. *PLoS ONE* **5**, (2010).
80. Mungall, B. A. *et al.* Feline Model of Acute Nipah Virus Infection and Protection with a Soluble Glycoprotein-Based Subunit Vaccine. *Journal of Virology* **80**, 12293–12302 (2006).
81. Bossart, K. N. *et al.* A neutralizing human monoclonal antibody protects against lethal disease in a new ferret model of acute Nipah virus infection. *PLoS Pathogens* **5**, (2009).
82. Middleton, D. J. *et al.* Experimental Nipah Virus Infection in Pteropid Bats (*Pteropus poliocephalus*). *Journal of Comparative Pathology* **136**, 266–272 (2007).
83. Weingartl, H. *et al.* Invasion of the Central Nervous System in a Porcine Host by Nipah Virus. *Journal of Virology* **79**, 7528–7534 (2005).
84. Middleton, D. J. *et al.* Experimental Nipah Virus Infection in Pigs and Cats. *Journal of Comparative Pathology* **126**, 124–136 (2002).
85. Marianneau, P. *et al.* Experimental infection of squirrel monkeys with Nipah virus. *Emerging Infectious Diseases* **16**, 507–510 (2010).
86. Prasad, A. N. *et al.* Resistance of Cynomolgus Monkeys to Nipah and Hendra Virus Disease Is Associated with Cell-Mediated and Humoral Immunity. *Journal of Infectious Diseases* **221**, S436–S447 (2020).
87. Dups, J. *et al.* Subclinical infection without encephalitis in mice following intranasal exposure to Nipah virus-Malaysia and Nipah virus-Bangladesh. *Virology Journal* **11**, (2014).
88. Dhondt, K. P. *et al.* Type I interferon signaling protects mice from lethal henipavirus infection. *Journal of Infectious Diseases* **207**, 142–151 (2013).
89. Chan, Y. K. & Gack, M. U. RIG-I-like receptor regulation in virus infection and immunity. *Current Opinion in Virology* vol. 12 7–14 (2015).
90. Takeuchi, O. & Akira, S. Pattern Recognition Receptors and Inflammation. *Cell* vol. 140 805–820 (2010).
91. Yoneyama, M. & Fujita, T. Structural Mechanism of RNA Recognition by the RIG-I-like Receptors. *Immunity* vol. 29 178–181 (2008).
92. Yoneyama, M. *et al.* The RNA helicase RIG-I has an essential function in double-stranded RNA-induced innate antiviral responses. *Nature Immunology* **5**, 730–737 (2004).
93. Kang, D.-C. *et al.* mda-5: An interferon-inducible putative RNA helicase with double-stranded RNA-dependent ATPase activity and melanoma growth-suppressive properties. *Proceedings of the National Academy of Sciences* **99**, 637–642 (2002).

94. Cui, Y. *et al.* The Stat3/5 locus encodes novel endoplasmic reticulum and helicase-like proteins that are preferentially expressed in normal and neoplastic mammary tissue. *Genomics* **78**, 129–134 (2001).
95. Tanner, N. K. & Linder, P. DExD/H Box RNA Helicases: From Generic Motors to Specific Dissociation Functions. *Molecular Cell* **8**, 251–262 (2001).
96. Yoneyama, M., Onomoto, K., Jogi, M., Akaboshi, T. & Fujita, T. Viral RNA detection by RIG-I-like receptors. *Current Opinion in Immunology* vol. 32 48–53 (2015).
97. Seth, R. B., Sun, L., Ea, C. K. & Chen, Z. J. Identification and characterization of MAVS, a mitochondrial antiviral signaling protein that activates NF- $\kappa$ B and IRF3. *Cell* **122**, 669–682 (2005).
98. Kawai, T. *et al.* IPS-1, an adaptor triggering RIG-I- and Mda5-mediated type I interferon induction. *Nature Immunology* **6**, 981–988 (2005).
99. Meylan, E. *et al.* Cardif is an adaptor protein in the RIG-I antiviral pathway and is targeted by hepatitis C virus. *Nature* **437**, 1167–1172 (2005).
100. Xu, L. G. *et al.* VISA is an adapter protein required for virus-triggered IFN- $\beta$  signaling. *Molecular Cell* **19**, 727–740 (2005).
101. Jensen, S. & Thomsen, A. R. Sensing of RNA Viruses: a Review of Innate Immune Receptors Involved in Recognizing RNA Virus Invasion. *Journal of Virology* **86**, 2900–2910 (2012).
102. Basler, C. F. Nipah and Hendra Virus Interactions with the Innate Immune System. in *Henipavirus: Ecology, Molecular Virology, and Pathogenesis* (eds. Lee, B. & Rota, P. A.) 123–152 (2012). doi:10.1007/82\_2012\_209.
103. Hiscott, J. Convergence of the NF- $\kappa$ B and IRF pathways in the regulation of the innate antiviral response. *Cytokine and Growth Factor Reviews* **18**, 483–490 (2007).
104. Yoneyama, M. *et al.* Shared and Unique Functions of the DExD/H-Box Helicases RIG-I, MDA5, and LGP2 in Antiviral Innate Immunity. *The Journal of Immunology* **175**, 2851–2858 (2005).
105. Kato, H. *et al.* Differential roles of MDA5 and RIG-I helicases in the recognition of RNA viruses. *Nature* **441**, 101–105 (2006).
106. Kato, H. *et al.* Length-dependent recognition of double-stranded ribonucleic acids by retinoic acid-inducible gene-I and melanoma differentiation-associated gene 5. *Journal of Experimental Medicine* **205**, 1601–1610 (2008).
107. Rodriguez, K. R., Bruns, A. M. & Horvath, C. M. MDA5 and LGP2: Accomplices and Antagonists of Antiviral Signal Transduction. *Journal of Virology* **88**, 8194–8200 (2014).
108. Venkataraman, T. *et al.* Loss of DExD/H Box RNA Helicase LGP2 Manifests Disparate Antiviral Responses. *The Journal of Immunology* **178**, 6444–6455 (2007).
109. Rodriguez, K. R. & Horvath, C. M. Paramyxovirus V Protein Interaction with the Antiviral Sensor LGP2 Disrupts MDA5 Signaling Enhancement but Is Not Relevant to LGP2-Mediated RLR Signaling Inhibition. *Journal of Virology* **88**, 8180–8188 (2014).
110. Quicke, K. M., Kim, K. Y., Horvath, C. M. & Suthar, M. S. RNA Helicase LGP2 Negatively Regulates RIG-I Signaling by Preventing TRIM25-Mediated Caspase

- Activation and Recruitment Domain Ubiquitination. *Journal of Interferon and Cytokine Research* **39**, 669–683 (2019).
111. Sánchez-Aparicio, M. T., Feinman, L. J., García-Sastre, A. & Shaw, M. L. Paramyxovirus V Proteins Interact with the RIG-I/TRIM25 Regulatory Complex and Inhibit RIG-I Signaling. *Journal of Virology* **92**, (2018).
  112. McNab, F., Mayer-Barber, K., Sher, A., Wack, A. & O’Garra, A. Type I interferons in infectious disease. *Nature Reviews Immunology* vol. 15 87–103 (2015).
  113. Horvath, C. M. Weapons of STAT destruction: Interferon evasion by paramyxovirus V proteins. *European Journal of Biochemistry* vol. 271 4621–4628 (2004).
  114. Plataniias, L. C. Mechanisms of type-I- and type-II-interferon-mediated signalling. *Nature Reviews Immunology* vol. 5 375–386 (2005).
  115. Yang, K. *et al.* Interferons, Double-stranded RNA, and RNA Degradation: Isolation and Characterization of Homogeneous Human (2’-5’) (A)n Synthetase. *The Journal of Biological Chemistry* **256**, 9324–9328 (1981).
  116. Pichlmair, A. *et al.* IFIT1 is an antiviral protein that recognizes 5’-triphosphate RNA. *Nature Immunology* **12**, 624–630 (2011).
  117. Perng, Y. C. & Lenschow, D. J. ISG15 in antiviral immunity and beyond. *Nature Reviews Microbiology* vol. 16 423–439 (2018).
  118. Stawowczyk, M., van Scoy, S., Kumar, K. P. & Reich, N. C. The Interferon Stimulated Gene 54 Promotes Apoptosis. *Journal of Biological Chemistry* **286**, 7257–7266 (2011).
  119. Gotoh, B., Komatsu, T., Takeuchi, K. & Yokoo, J. *Paramyxovirus Accessory Proteins as Interferon Antagonists*. *Microbiol. Immunol* vol. 45 (2001).
  120. Andrejeva, J. *et al.* The V proteins of paramyxoviruses bind the IFN-inducible RNA helicase, mda-5, and inhibit its activation of the IFN-promoter. *PNAS* **101**, (2004).
  121. Childs, K. *et al.* mda-5, but not RIG-I, is a common target for paramyxovirus V proteins. *Virology* **359**, 190–200 (2007).
  122. Bharaj, P. *et al.* The Matrix Protein of Nipah Virus Targets the E3-Ubiquitin Ligase TRIM6 to Inhibit the IKK $\epsilon$  Kinase-Mediated Type-I IFN Antiviral Response. *PLoS Pathogens* **12**, (2016).
  123. Shaw, M. L., Cardenas, W. B., Zamarin, D., Palese, P. & Basler, C. F. Nuclear Localization of the Nipah Virus W Protein Allows for Inhibition of both Virus- and Toll-Like Receptor 3-Triggered Signaling Pathways. *Journal of Virology* **79**, 6078–6088 (2005).
  124. Ulane, C. M. & Horvath, C. M. Paramyxoviruses SV5 and HPIV2 assemble STAT protein ubiquitin ligase complexes from cellular components. *Virology* **304**, 160–166 (2002).
  125. Palosaari, H., Parisien, J.-P., Rodriguez, J. J., Ulane, C. M. & Horvath, C. M. STAT Protein Interference and Suppression of Cytokine Signal Transduction by Measles Virus V Protein. *Journal of Virology* **77**, 7635–7644 (2003).
  126. Rodriguez, J. J., Parisien, J.-P. & Horvath, C. M. Nipah Virus V Protein Evades Alpha and Gamma Interferons by Preventing STAT1 and STAT2 Activation and Nuclear Accumulation. *Journal of Virology* **76**, 11476–11483 (2002).

127. Rodriguez, J. J., Wang, L.-F. & Horvath, C. M. Hendra Virus V Protein Inhibits Interferon Signaling by Preventing STAT1 and STAT2 Nuclear Accumulation. *Journal of Virology* **77**, 11842–11845 (2003).
128. Rodriguez, J. J., Cruz, C. D. & Horvath, C. M. Identification of the Nuclear Export Signal and STAT-Binding Domains of the Nipah Virus V Protein Reveals Mechanisms Underlying Interferon Evasion. *Journal of Virology* **78**, 5358–5367 (2004).
129. Sugai, A., Sato, H., Takayama, I., Yoneda, M. & Kai, C. Nipah and Hendra Virus Nucleoproteins Inhibit Nuclear Accumulation of Signal Transducer and Activator of Transcription 1 (STAT1) and STAT2 by Interfering with Their Complex Formation. *Journal of Virology* **91**, (2017).
130. Parisien, J.-P. *et al.* A Shared Interface Mediates Paramyxovirus Interference with Antiviral RNA Helicases MDA5 and LGP2. *Journal of Virology* **83**, 7252–7260 (2009).
131. Childs, K., Randall, R. & Goodbourn, S. Paramyxovirus V Proteins Interact with the RNA Helicase LGP2 To Inhibit RIG-I-Dependent Interferon Induction. *Journal of Virology* **86**, 3411–3421 (2012).
132. Shaw, M. L., García-Sastre, A., Palese, P. & Basler, C. F. Nipah Virus V and W Proteins Have a Common STAT1-Binding Domain yet Inhibit STAT1 Activation from the Cytoplasmic and Nuclear Compartments, Respectively. *Journal of Virology* **78**, 5633–5641 (2004).
133. Lo, M. K. *et al.* Characterization of the antiviral and inflammatory responses against Nipah virus in endothelial cells and neurons. *Virology* **404**, 78–88 (2010).
134. Geisbert, T. W., Feldmann, H. & Broder, C. C. Animal Challenge Models of Henipavirus Infection and Pathogenesis. in *Nipah and Hendra Virus Interactions with the Innate Immune System* (eds. Lee, B. & Rota, P. A.) 153–177 (2012). doi:10.1007/82\_2012\_208.
135. McEachern, J. A. *et al.* A recombinant subunit vaccine formulation protects against lethal Nipah virus challenge in cats. *Vaccine* **26**, 3842–3852 (2008).
136. Geisbert, J. B. *et al.* An Intranasal Exposure Model of Lethal Nipah Virus Infection in African Green Monkeys. *Journal of Infectious Diseases* **221**, S414–S418 (2020).
137. Rockx, B. *et al.* Clinical Outcome of Henipavirus Infection in Hamsters Is Determined by the Route and Dose of Infection. *Journal of Virology* **85**, 7658–7671 (2011).
138. Genzer, S. C. *et al.* Alterations in Blood Chemistry Levels Associated with Nipah Virus Disease in the Syrian Hamster Model. *Journal of Infectious Diseases* **221**, S454–S459 (2020).
139. DeBuysscher, B. L. *et al.* Comparison of the Pathogenicity of Nipah Virus Isolates from Bangladesh and Malaysia in the Syrian Hamster. *PLoS Neglected Tropical Diseases* **7**, (2013).
140. Baseler, L., de Wit, E., Scott, D. P., Munster, V. J. & Feldmann, H. Syrian Hamsters (*Mesocricetus auratus*) Oronasally Inoculated With a Nipah Virus Isolate From Bangladesh or Malaysia Develop Similar Respiratory Tract Lesions. *Veterinary Pathology* **52**, 38–45 (2015).

141. Munster, V. J. *et al.* Rapid Nipah virus entry into the central nervous system of hamsters via the olfactory route. *Scientific Reports* **2**, (2012).
142. de Wit, E. *et al.* Foodborne Transmission of Nipah Virus in Syrian Hamsters. *PLoS Pathogens* **10**, (2014).
143. Georges-Courbot, M. C. *et al.* Poly(I)-poly(C12U) but not ribavirin prevents death in a hamster model of Nipah virus infection. *Antimicrobial Agents and Chemotherapy* **50**, 1768–1772 (2006).
144. Mathieu, C. *et al.* Heparan sulfate-dependent enhancement of henipavirus infection. *mBio* **6**, (2015).
145. Dawes, B. E. *et al.* Favipiravir (T-705) protects against Nipah virus infection in the hamster model. *Scientific Reports* **8**, (2018).
146. Lo, M. K. *et al.* Griffithsin Inhibits Nipah Virus Entry and Fusion and Can Protect Syrian Golden Hamsters from Lethal Nipah Virus Challenge. *Journal of Infectious Diseases* **221**, S480–S492 (2020).
147. Guillaume, V. *et al.* Nipah Virus: Vaccination and Passive Protection Studies in a Hamster Model. *Journal of Virology* **78**, 834–840 (2004).
148. Ploquin, A. *et al.* Protection against henipavirus infection by use of recombinant adeno-associated virus-vector vaccines. *Journal of Infectious Diseases* **207**, 469–478 (2013).
149. Yoneda, M. *et al.* Recombinant Measles Virus Vaccine Expressing the Nipah Virus Glycoprotein Protects against Lethal Nipah Virus Challenge. *PLoS ONE* **8**, (2013).
150. van Doremalen, N. *et al.* A single-dose ChAdOx1-vectored vaccine provides complete protection against Nipah Bangladesh and Malaysia in Syrian golden hamsters. *PLoS Neglected Tropical Diseases* **13**, (2019).
151. Lo, M. K. *et al.* Single-dose replication-defective VSV-based Nipah virus vaccines provide protection from lethal challenge in Syrian hamsters. *Antiviral Research* **101**, 26–29 (2014).
152. DeBuysscher, B. L., Scott, D., Marzi, A., Prescott, J. & Feldmann, H. Single-dose live-attenuated Nipah virus vaccines confer complete protection by eliciting antibodies directed against surface glycoproteins. *Vaccine* **32**, 2637–2644 (2014).
153. Walpita, P. *et al.* A VLP-based vaccine provides complete protection against Nipah virus challenge following multiple-dose or single-dose vaccination schedules in a hamster model. *npj Vaccines* **2**, (2017).
154. Lo, M. K. *et al.* Evaluation of a Single-Dose Nucleoside-Modified Messenger RNA Vaccine Encoding Hendra Virus-Soluble Glycoprotein Against Lethal Nipah virus Challenge in Syrian Hamsters. *Journal of Infectious Diseases* **221**, S493–S498 (2020).
155. Peng, X. *et al.* The draft genome sequence of the ferret (*Mustela putorius furo*) facilitates study of human respiratory disease. *Nature Biotechnology* **32**, 1250–1255 (2014).
156. Belser, J. A., Katz, J. M. & Tumpey, T. M. The ferret as a model organism to study influenza A virus infection. *Disease Models and Mechanisms* **4**, 575–579 (2011).
157. Pallister, J. *et al.* Chloroquine Administration Does Not Prevent Nipah Virus Infection and Disease in Ferrets. *Journal of Virology* **83**, 11979–11982 (2009).

158. Satterfield, B. A. *et al.* Antagonism of STAT1 by Nipah virus P gene products modulates disease course but not lethal outcome in the ferret model. *Scientific Reports* **9**, (2019).
159. Zhu, Z. *et al.* Potent Neutralization of Hendra and Nipah Viruses by Human Monoclonal Antibodies. *Journal of Virology* **80**, 891–899 (2006).
160. Zhu, Z. *et al.* Exceptionally potent cross-reactive neutralization of Nipah and Hendra viruses by a human monoclonal antibody. *Journal of Infectious Diseases* **197**, 846–853 (2008).
161. Playford, E. G. *et al.* Safety, tolerability, pharmacokinetics, and immunogenicity of a human monoclonal antibody targeting the G glycoprotein of henipaviruses in healthy adults: a first-in-human, randomised, controlled, phase 1 study. *The Lancet Infectious Diseases* **20**, 445–454 (2020).
162. Middleton, D. *et al.* Hendra virus vaccine, a one health approach to protecting horse, human, and environmental health. *Emerging Infectious Diseases* **20**, 372–379 (2014).
163. Eldridge, J. H. *et al.* A Brighton Collaboration standardized template with key considerations for a benefit/risk assessment for a soluble glycoprotein vaccine to prevent disease caused by Nipah or Hendra viruses. *Vaccine* vol. 39 5436–5441 (2021).
164. Pallister, J. A. *et al.* Vaccination of ferrets with a recombinant G glycoprotein subunit vaccine provides protection against Nipah virus disease for over 12 months. *Virology Journal* **10**, (2013).
165. Mire, C. E. *et al.* Single injection recombinant vesicular stomatitis virus vaccines protect ferrets against lethal Nipah virus disease. *Virology Journal* **10**, 353-undefined (2013).
166. Prasad, A. N. *et al.* A Lethal Aerosol Exposure Model of Nipah Virus Strain Bangladesh in African Green Monkeys. *Journal of Infectious Diseases* **221**, S431–S435 (2020).
167. Lee, J. H. *et al.* The Use of Large-Particle Aerosol Exposure to Nipah Virus to Mimic Human Neurological Disease Manifestations in the African Green Monkey. *Journal of Infectious Diseases* **221**, S419–S430 (2020).
168. Lara, A. *et al.* Peripheral immune response in the African green monkey model following Nipah-Malaysia virus exposure by intermediate-size particle aerosol. *PLoS Neglected Tropical Diseases* **13**, (2019).
169. Hammoud, D. A. *et al.* Aerosol exposure to intermediate size Nipah virus particles induces neurological disease in African green monkeys. *PLoS Neglected Tropical Diseases* **12**, (2018).
170. Cong, Y. *et al.* Loss in lung volume and changes in the immune response demonstrate disease progression in African green monkeys infected by small-particle aerosol and intratracheal exposure to Nipah virus. *PLoS Neglected Tropical Diseases* **11**, (2017).
171. Johnston, S. C. *et al.* Detailed analysis of the african green monkey model of nipah virus disease. *PLoS ONE* **10**, (2015).
172. Mire, C. E. *et al.* Pathogenic Differences between Nipah Virus Bangladesh and Malaysia Strains in Primates: Implications for Antibody Therapy. *Scientific Reports* **6**, (2016).

173. Geisbert, T. W. *et al.* Therapeutic Treatment of Nipah Virus Infection in Nonhuman Primates with a Neutralizing Human Monoclonal Antibody. *Science Translational Medicine* **6**, (2014).
174. Bossart, K. N. *et al.* A Hendra Virus G Glycoprotein Subunit Vaccine Protects African Green Monkeys from Nipah Virus Challenge. *Science Translational Medicine* **4**, (2012).
175. Geisbert, T. W. *et al.* A single dose investigational subunit vaccine for human use against Nipah virus and Hendra virus. *npj Vaccines* **6**, (2021).
176. Prescott, J. *et al.* Single-dose live-attenuated vesicular stomatitis virus-based vaccine protects African green monkeys from Nipah virus disease. *Vaccine* **33**, 2823–2829 (2015).
177. Mire, C. E. *et al.* Use of single-injection recombinant vesicular stomatitis virus vaccine to protect nonhuman primates against lethal nipah virus disease. *Emerging Infectious Diseases* **25**, 1144–1152 (2019).
178. Walpita, P., Barr, J., Sherman, M., Basler, C. F. & Wang, L. Vaccine Potential of Nipah Virus-Like Particles. *PLoS ONE* **6**, (2011).
179. Chackerian, B. Virus-like particles: flexible platforms for vaccine development. *Expert Review of Vaccines* **6**, (2007).
180. Amaya, M. & Broder, C. C. Annual Review of Virology Vaccines to Emerging Viruses: Nipah and Hendra. *Annu. Rev. Virol* **7**, 447–473 (2020).
181. Weingartl, H. M. *et al.* Recombinant Nipah Virus Vaccines Protect Pigs against Challenge. *Journal of Virology* **80**, 7929–7938 (2006).
182. Kalodimou, G. *et al.* A Soluble Version of Nipah Virus Glycoprotein G Delivered by Vaccinia Virus MVA Activates Specific CD8 and CD4 T Cells in Mice. *Viruses* **12**, (2019).
183. Kurup, D., Wirblich, C., Feldmann, H., Marzi, A. & Schnell, M. J. Rhabdovirus-Based Vaccine Platforms against Henipaviruses. *Journal of Virology* **89**, 144–154 (2015).
184. Keshwara, R. *et al.* Rabies-based vaccine induces potent immune responses against Nipah virus. *npj Vaccines* **4**, (2019).
185. Shuai, L. *et al.* Immune responses in mice and pigs after oral vaccination with rabies virus vectored Nipah disease vaccines. *Veterinary Microbiology* **241**, (2020).
186. Bossart, K. N. *et al.* Receptor Binding, Fusion Inhibition, and Induction of Cross-Reactive Neutralizing Antibodies by a Soluble G Glycoprotein of Hendra Virus. *Journal of Virology* **79**, 6690–6702 (2005).
187. Fathi, A., Dahlke, C. & Addo, M. M. Recombinant vesicular stomatitis virus vector vaccines for WHO blueprint priority pathogens. *Human Vaccines and Immunotherapeutics* **15**, 2269–2285 (2019).
188. Wolf, J. *et al.* Development of pandemic vaccines: ERVEBO case study. *Vaccines* **9**, 1–25 (2021).
189. Henao-Restrepo, A. M. *et al.* Efficacy and effectiveness of an rVSV-vectored vaccine in preventing Ebola virus disease: final results from the Guinea ring vaccination, open-label, cluster-randomised trial (Ebola Ça Suffit!). *The Lancet* **389**, 505–518 (2017).

190. Chattopadhyay, A. & Rose, J. K. Complementing Defective Viruses That Express Separate Paramyxovirus Glycoproteins Provide a New Vaccine Vector Approach. *Journal of Virology* **85**, 2004–2011 (2011).
191. Mire, C. E. *et al.* Use of single-injection recombinant vesicular stomatitis virus vaccine to protect nonhuman primates against lethal nipah virus disease. *Emerging Infectious Diseases* **25**, 1144–1152 (2019).
192. Debuysscher, B. L., Scott, D., Thomas, T., Feldmann, H. & Prescott, J. Peri-exposure protection against Nipah virus disease using a single-dose recombinant vesicular stomatitis virus-based vaccine. *npj Vaccines* **1**, (2016).
193. Motz, C. *et al.* Paramyxovirus V Proteins Disrupt the Fold of the RNA Sensor MDA5 to Inhibit Antiviral Signaling. *Science* **339**, 690–693 (2013).
194. Svitek, N. *et al.* Morbillivirus Control of the Interferon Response: Relevance of STAT2 and mda5 but Not STAT1 for Canine Distemper Virus Virulence in Ferrets. *Journal of Virology* **88**, 2941–2950 (2014).
195. Rodriguez, K. R. & Horvath, C. M. Amino Acid Requirements for MDA5 and LGP2 Recognition by Paramyxovirus V Proteins: a Single Arginine Distinguishes MDA5 from RIG-I. *Journal of Virology* **87**, 2974–2978 (2013).
196. Uchida, S., Horie, R., Sato, H., Kai, C. & Yoneda, M. Possible role of the Nipah virus v protein in the regulation of the interferon beta induction by interacting with UBX domain-containing protein1. *Scientific Reports* **8**, (2018).
197. von Messling, V., Springfield, C., Devaux, P. & Cattaneo, R. A Ferret Model of Canine Distemper Virus Virulence and Immunosuppression. *Journal of Virology* **77**, 12579–12591 (2003).
198. Audsley, M. D. *et al.* The immune evasion function of J and beilong virus V proteins is distinct from that of other paramyxoviruses, consistent with their inclusion in the proposed genus Jeilongvirus. *Journal of General Virology* **97**, 581–592 (2016).
199. Niwa, H., Yamamura, K.-I. & Miyazaki, J.-I. Efficient selection for high-expression transfectants with a novel eukaryotic vector (Recombinant DNA; B-actin promoter; bovine papilloma virus; transfection; interleukin-2; G418 selection; copy number). *Gene* **108**, 193–200 (1991).
200. Bamming, D. & Horvath, C. M. Regulation of signal transduction by enzymatically inactive antiviral RNA helicase proteins MDA5, RIG-I, and LGP2. *Journal of Biological Chemistry* **284**, 9700–9712 (2009).
201. Yoneyama, M. *et al.* Autocrine Amplification of Type I Interferon Gene Expression Mediated by Interferon Stimulated Gene Factor 3 (ISGF3)1. *Journal of Biochemistry* **120**, 160–169 (1996).
202. Dubridge, R. B. *et al.* Analysis of Mutation in Human Cells by Using an Epstein-Barr Virus Shuttle System. *Molecular and Cellular Biology* **7**, 379–387 (1987).
203. Buchholz, U. J., Finke, S. & Conzelmann, K.-K. Generation of Bovine Respiratory Syncytial Virus (BRSV) from cDNA: BRSV NS2 Is Not Essential for Virus Replication in Tissue Culture, and the Human RSV Leader Region Acts as a Functional BRSV Genome Promoter. *Journal of Virology* **73**, 251–259 (1999).
204. Guito, J. C., Albariño, C. G., Chakrabarti, A. K. & Towner, J. S. Novel activities by ebolavirus and marburgvirus interferon antagonists revealed using a standardized in vitro reporter system. *Virology* **501**, 147–165 (2017).

205. Li, T., Chen, X., Garbutt, K. C., Zhou, P. & Zheng, N. Structure of DDB1 in complex with a paramyxovirus V protein: Viral Hijack of a propeller cluster in ubiquitin ligase. *Cell* **124**, 105–117 (2006).
206. Salladini, E., Delauzun, V. & Longhi, S. The Henipavirus V protein is a prevalently unfolded protein with a zinc-finger domain involved in binding to DDB1. *Molecular BioSystems* **13**, 2254–2267 (2017).
207. Martinez-Gil, L., Vera-Velasco, N. M. & Mingarro, I. Exploring the Human-Nipah Virus Protein-Protein Interactome. *Journal of Virology* **91**, (2017).
208. Keiffer, T. R., Ciancanelli, M. J., Edwards, M. R. & Basler, C. F. Interactions of the Nipah Virus P, V, and W Proteins across the STAT Family of Transcription Factors Downloaded from. *mSphere* **5**, (2020).
209. Ludlow, L. E., Lo, M. K., Rodriguez, J. J., Rota, P. A. & Horvath, C. M. Henipavirus V Protein Association with Polo-Like Kinase Reveals Functional Overlap with STAT1 Binding and Interferon Evasion. *Journal of Virology* **82**, 6259–6271 (2008).
210. Davis, M. E. *et al.* Antagonism of the phosphatase PP1 by the measles virus v protein is required for innate immune escape of MDA5. *Cell Host and Microbe* **16**, 19–30 (2014).
211. Schountz, T. *et al.* Differential Innate Immune Responses Elicited by Nipah Virus and Cedar Virus Correlate with Disparate In Vivo Pathogenesis in Hamsters. *Viruses* **11**, (2019).
212. Laing, E. D. *et al.* Structural and functional analyses reveal promiscuous and species specific use of ephrin receptors by Cedar virus. *Proceedings of the National Academy of Sciences of the United States of America* **116**, 20707–20715 (2019).
213. Wies, E. *et al.* Dephosphorylation of the RNA Sensors RIG-I and MDA5 by the Phosphatase PP1 Is Essential for Innate Immune Signaling. *Immunity* **38**, 437–449 (2013).
214. Habjan, M. *et al.* Processing of genome 5' termini as a strategy of negative-strand RNA viruses to avoid RIG-I-dependent interferon induction. *PLoS ONE* **3**, (2008).
215. Gitlin, L. *et al.* Melanoma differentiation-associated gene 5 (MDA5) is involved in the innate immune response to Paramyxoviridae infection in vivo. *PLoS Pathogens* **6**, (2010).
216. Ikegame, S. *et al.* Both RIG-I and MDA5 RNA Helicases Contribute to the Induction of Alpha/Beta Interferon in Measles Virus-Infected Human Cells. *Journal of Virology* **84**, 372–379 (2010).
217. Errett, J. S., Suthar, M. S., McMillan, A., Diamond, M. S. & Gale, M. The Essential, Nonredundant Roles of RIG-I and MDA5 in Detecting and Controlling West Nile Virus Infection. *Journal of Virology* **87**, 11416–11425 (2013).
218. Sauerhering, L. *et al.* Variability of interferon- $\lambda$  induction and antiviral activity in nipah virus infected differentiated human bronchial epithelial cells of two human donors. *Journal of General Virology* **98**, 2447–2453 (2017).
219. Elvert, M., Sauerhering, L. & Maisner, A. Cytokine Induction in Nipah Virus-Infected Primary Human and Porcine Bronchial Epithelial Cells. *Journal of Infectious Diseases* **221**, S395–S400 (2020).

220. He, B. *et al.* Recovery of Paramyxovirus simian virus 5 with a V protein lacking the conserved cysteine-rich domain: The multifunctional V protein blocks both interferon- $\beta$  induction and interferon signaling. *Virology* **303**, 15–32 (2002).
221. Patterson, J. B., Thomas, D., Lewicki, H., Billeter, M. A. & Oldstone, M. B. A. V and C proteins of measles virus function as virulence factors in vivo. *Virology* **267**, 80–89 (2000).
222. Tober, C. *et al.* Expression of Measles Virus V Protein Is Associated with Pathogenicity and Control of Viral RNA Synthesis. *Journal of Virology* **72**, 8124–8132 (1998).
223. Gibson, D. G. *et al.* Enzymatic assembly of DNA molecules up to several hundred kilobases. *Nature Methods* **6**, 343–345 (2009).
224. Emeny, J. M. & Morgan, M. J. Regulation of the Interferon System: Evidence that Vero Cells have a Genetic Defect in Interferon Production. *Journal of General Virology* **43**, 247–252 (1979).
225. Bowen, J. R. *et al.* Zika Virus Antagonizes Type I Interferon Responses during Infection of Human Dendritic Cells. *PLoS Pathogens* **13**, (2017).
226. Pillai, V. S., Krishna, G. & Veetil, M. V. Nipah virus: Past outbreaks and future containment. *Viruses* vol. 12 (2020).
227. News Desk. Nipah virus: Bangladesh IEDCR reports 6 cases, 4 deaths. *Outbreak News Today* (2020).
228. Stripecke, R. *et al.* Immune response to green fluorescent protein: implications for gene therapy. *Gene Therapy* vol. 6 <http://www.stockton-press.co.uk/gt> (1999).
229. Marzi, A. *et al.* VSV-EBOV rapidly protects macaques against infection with the 2014/15 Ebola virus outbreak strain. *Science* **349**, 739–742 (2015).
230. Whitt, M. A. Generation of VSV pseudotypes using recombinant  $\Delta$ G-VSV for studies on virus entry, identification of entry inhibitors, and immune responses to vaccines. *Journal of Virological Methods* **169**, 365–374 (2010).
231. Publicover, J., Ramsburg, E. & Rose, J. K. A Single-Cycle Vaccine Vector Based on Vesicular Stomatitis Virus Can Induce Immune Responses Comparable to Those Generated by a Replication-Competent Vector. *Journal of Virology* **79**, 13231–13238 (2005).
232. Mire, C. E. *et al.* Recombinant vesicular stomatitis virus vaccine vectors expressing filovirus glycoproteins lack neurovirulence in nonhuman primates. *PLoS Neglected Tropical Diseases* **6**, (2012).
233. Childs, K. S., Randall, R. E. & Goodbourn, S. LGP2 Plays a Critical Role in Sensitizing mda-5 to Activation by Double-Stranded RNA. *PLoS ONE* **8**, (2013).

## Vita

Stephanie Leigh Foster was born on February 16, 1990, in Greenville, South Carolina, to Ron and Julia Foster. She has a younger brother named Tim Foster. The Fosters moved to a suburb of Cincinnati, Ohio, when Stephanie was eight years old, where she graduated from Milford High School in 2008 as the salutatorian of her class. Stephanie attended the University of Georgia in Athens, Georgia, where she earned her Bachelor of Science in Microbiology in 2011 and was active in the Redcoat Marching Band as a member of the percussion section. She worked as a research technician in Dr. Biao He's lab at the University of Georgia from 2011 to 2013, a continuation of her final year of her undergraduate degree performing research in Dr. He's lab on respiratory syncytial virus. In 2013, Stephanie took a job with the Centers for Disease Control and Prevention in Atlanta, Georgia, developing quality control materials for molecular newborn screening tests. In 2015, Stephanie matriculated into the Microbiology and Immunology Ph.D. program at UTMB and moved to Galveston, Texas, with her miniature dachshund, Leo.

### Peer-Reviewed Publications in Reverse Chronological Order

- Fontes C.M., Lipes B.D., Liu J., Agans K.N., Cruz D.F., Kelly G., Luginbuhl K., Joh D.Y., Foster S.L., Heggstad J, Hucknall A., Mikkelsen M.H., Pieper C.F., Horstmeyer R.W., Geisbert T.W., Gunn M., and Chilkoti A (2021). Ultrasensitive point-of-care immunoassay for secreted glycoprotein detects Ebola infection earlier than PCR. *Science Translational Medicine* **13**(588): eabd9696.
- Woolsey C., Borisevich V., Prasad A.N., Agans K.N., Deer D.J., Dobias N.S., Heymann J.C., Foster S.L., Levine C.B., Medina L., Melody K., Geisbert J.B., Fenton K.A., Geisbert T.W., and Cross R.W (2021). Establishment of an African green monkey model for COVID-19 and demonstration of protection against reinfection. *Nature Immunology* **22**(1): 86-98.
- Geisbert J.B., Borisevich V., Prasad A.N., Agans K.N., Foster S.L., Deer D.J., Cross R.W., Mire C.E., Geisbert T.W., and Fenton K.A (2020). An intranasal exposure model of lethal Nipah virus infection in African green monkeys. *Journal of Infectious Diseases* **221**(Suppl 4): S414-S418.
- Satterfield B.A., Borisevich V., Foster S.L., Rodriguez S.E., Cross R.W., Fenton K.A., Agans K.N., Basler C.F., Geisbert T.W., and Mire C.E (2019). Antagonism of

STAT1 by Nipah virus P gene products modulates disease course but not lethal outcome in the ferret model. *Scientific Reports* **9**(1): 16710.

Hendrix M.M., Foster S.L., and Cordovado S.K (2016). Newborn Screening Quality Assurance Program for CFTR Mutation Detection and Gene Sequencing to Identify Cystic Fibrosis. *Journal of Inborn Errors of Metabolism & Screening* **4**: 1-11.

Phan S.I., Chen Z., Xu P., Li Z., Gao X., Foster S.L., Teng M.N., Tripp R.A., Sakamoto K., and He B (2014). A respiratory syncytial virus (RSV) vaccine based on parainfluenza virus 5 (PIV5). *Vaccine* **32**(25): 3050-3057.

Permanent address: 6424 Central City Blvd., Apt. 923, Galveston, TX 77551

This dissertation was typed by Stephanie Leigh Foster.

All figures in this dissertation were created by Stephanie Leigh Foster (unless otherwise noted).